Powder Processing Parameters and Their Influence on the Electrical Performance of ZnO Varistor

Shahida Begum

Ph.D **1996**

DUBLIN CITY UNIVERSITY

Powder Processing Parameters and Their Influence on the Electrical Performance of ZnO Varistor

A thesis submitted to Dublin City University in Fulfilment
of the Requirements for the Degree of
Doctor of Philosophy

by

Shahida Begum, BSc (Eng)

Name of Supervisors Prof M S J Hashmi
Dr Ramon Puyane

Collaborating Establishment Harris Corporation,
Semiconductor Division
Dundalk, Ireland

August, 1996

To

my parents and son

DECLARATION

I hereby certify that this material, which I now submit for assessment on the programme of study leading to the award of ***Doctor of Philosophy*** is entirely my own work and has not been taken from the works of others save and to the extent that such work has been cited and acknowledged within the text of my work

Signed Shahida Begum **ID No** 93700067
Shahida Begum

Date August, 1996

ACKNOWLEDGEMENT

The author would like to express her sincere appreciation and gratitude to Prof M S J Hashmi, D Sc , Head of the School of Mechanical and Manufacturing Engineering for his supervision, guidance, constructive suggestions and encouragement during the course of this study and in compilation of the thesis Moreover, the financial support arranged by him will always be gratefully acknowledged

The author would also like to express her sincere gratitude to Dr Ramon Puyane of Harris Ireland Limited, for his supervision, support throughout the period of work in the project and valuable input into the thesis

The author would like to thank Prof Ben Mills for giving his time to be the external examiner

My appreciation is due to Pat Bellew of Harris Ireland for his help at various stages of the experiment and to James Blaney for helping with various drawings Sincere thanks are also extended to Sean Moynihan for his guidance in computer applications and to Peter O'Connell, Liam Cravan for their help in conducting the experiments

I must remember the names of the BRITE team members, in Harris Ireland, with whom I have spent nearly three years In this regard I would like to express my sincere thanks to B Daly for his help during the production of powder in the pilot line I would also like to extend my thanks to M Lambe for her co-operation

The works contained in the thesis have been performed as a part of the DOCERPO project under BRITE/EURAM programme I am indebted to Harris Ireland Ltd for providing me the opportunity to work with their facilities

I would like to express my sincere thanks to my relatives back at home for their good wishes The name of my eldest sister Dr Fatima will always be remembered for her encouragement and mental support to go ahead with the tedious process

I would like to offer my sincere thanks to all the Bangladeshi friends and families, specially Suraiya and her family for their love and good wishes I am also grateful to Patricia Hayes, Ursula Hughes, and Mr and Mrs Hughes for their love and care for my son Rafid

Last but not least, the support and encouragement from my husband, M Karim at different phases will always be remembered gratefully

Powder Processing Parameters and Their Influence on the Electrical Performance of ZnO Varistor

Shahida Begum

ABSTRACT

The preparation of pressing grade electronic ceramic demands powder with a high degree of reliability in terms of compositional and microstructural homogeneity, having proper particle size and shape. The study was mainly concerned with the powder processing parameters such as the spray drying, the type and concentration of organic binder, and the distribution of particles.

Experiments with the spray drying variables were conducted in the laboratory and in the pilot scale dryer. Factorial analysis was carried out to estimate the main and interacting effects of the independent variables on the response. A mathematical model for the mean particle size of the spray dried granules was also developed to optimize the operating condition of the dryer. The adequacy of the model was verified by statistical analysis. Improved powder characteristics were achieved by optimizing the spray drying variables. Varistor performance and powder characteristics had shown significant correlation. Optimum spray drying conditions were identified depending on the electrical characteristics of the varistor.

The influence of different latex binders and their blends for a fixed concentration of binder and solid in the slurry was initially evaluated. Among the various binders including the conventional PVA, the latex binder, Ltx C was found to be superior. The slurry with a low level of the new binder and a high solid content produced powder with further enhancement in powder properties.

The fracture strength of the green and sintered body made from the powder with different binder systems were analyzed by Weibull approach. The estimation of the Weibull parameters indicated that a more reliable green and sintered body can be generated by using a lower level of Ltx C and a higher level of solid in the slurry. However, the best binder, its level and solid concentration were selected on the basis of the performance characteristics of the varistor.

Regarding the particle size fraction, the physical and electrical properties were not very different for the coarse, medium and wide distribution of powder. However, the green and the fired density of the discs produced from the fine fraction of powder were higher. Though

the varistor with fine fractions exhibited higher nominal voltage but was poor in terms of energy absorption capability

In addition to the powder processing, an investigation was conducted to assess the effect of passivation thickness on the performance of the varistor The energy absorption capability of the varistor was found to be highly sensitive to this thickness Neither too thin nor too a thick coating of glassing was found to be favourable Failure mode was also changed with the passivation thickness Thicker passivation generated pinholes as a result of higher insulation, whereas, thinner passivation led to flashover due to dielectric breakdown The analysis of variance also showed the significance of the glass thickness on varistor performance

TABLE OF CONTENTS

Chapter 1 **Introduction**

Chapter 2 **Experimental Equipment, Materials and Procedure Ceramic Powder Processing and Characterization**

Chapter 3 Experimental Procedure, Equipment and Testing Varistor Preparation

Chapter 4 Data Analysis and Model Formulation

Chapter 5 Results and Discussions

Chapter 6 Conclusions and Recommendations

Appendices

Chapter 1

INTRODUCTION

1.1 GENERAL BACKGROUND

Ceramic materials have been produced and used for centuries and have become very important in modern industrial and consumer technology These are compounds of metallic and non-metallic elements often in the form of oxides, carbides and nitrides A wide variety of ceramic materials with large variations in their physical, mechanical, and electrical properties are produced by different elemental combinations and structural arrangements[1 2] Most of them have a crystal structure and strong ionic or covalent bonds The unique properties of low electrical conductivity, refractoriness, hardness, wear resistance, high compressive strength are exhibited by ceramic materials because of the strong bonding and structural arrangements

Depending upon the use and nature of the product ceramics can be classified as traditional or advanced ceramics Traditional ceramics refer to the product commonly used as building materials or within home and the industry They can be fine (having particles under 0 2 mm) or coarse (particles as large as 8 0 mm) which in turn produce dense or porous fired bodies[3] The oldest ceramic product is pottery and it was originated from clay materials Bricks, fire clay bricks, glass, cements, enamel, glassware, tableware, sanitary goods, porcelain etc can be categorized as traditional ceramics Traditional approaches lack a clear methodology for controlling microstructural heterogeneity and uniformity of the product

Advanced ceramics refer to the ceramic materials which exhibit superior mechanical properties, corrosion and oxidation resistance, or electrical, optical and magnetic properties[4] Dielectric, semiconductors, insulators, transducers, lasers, emission control, sensors etc can be classified as advanced ceramics The material used to produce these include monolithic ceramics as well as particular whisker, fibre reinforced glass, glass ceramic and ceramic matrix composites The material should have resistance to temperature, stress and environment Though the engineering implementation of advanced ceramic is still hindered by their poor formability and brittle nature, the pressing technology has advanced in comparison to the traditional ceramic production techniques Pressing grade advanced ceramic powders require a high degree of compositional and microstructural homogeneity, as well as a high degree of purity and reliability[2 5] Performance and reliability of electronic ceramic depends on the grain and the grain boundary phenomena[2 6 10] Hence in the development and production of more advanced ceramic materials, extra-ordinary control of the materials and processing parameters is a requisite to minimize microstructural defects

The use of ceramic as transient over-voltage suppression device is a recent development of electronic ceramics There are two major categories of transient over voltage suppression device which are used for voltage stabilization or transient surge suppression in electronic power systems One is based on the principle of attenuating the transient signal and the other on diverging the sensitive load and so limiting the residual voltages The first category suppressor is a filter (capacitor) which is inserted in series within the circuit and attenuates the transient (high frequency) and allows the signal and power flow (low frequency) to continue undisturbed The second type of suppressor is a crowbar type device which short circuits a high voltage to ground The short circuit will continue until the current is brought to a low level

The zinc oxide varistor is a high transient over-voltage suppppressor This is characterized by its excellent non-ohmic properties[11] in current voltage as shown in the I-V curve in Figure 1 1 It has very large suppression capabilities, which are considered a combination of both the feature of silicon-zener diodes and silicon carbide varistor The feature of zinc oxide varistor is a grain boundary phenomenon and this is the *intrinsic property* of the ceramic material

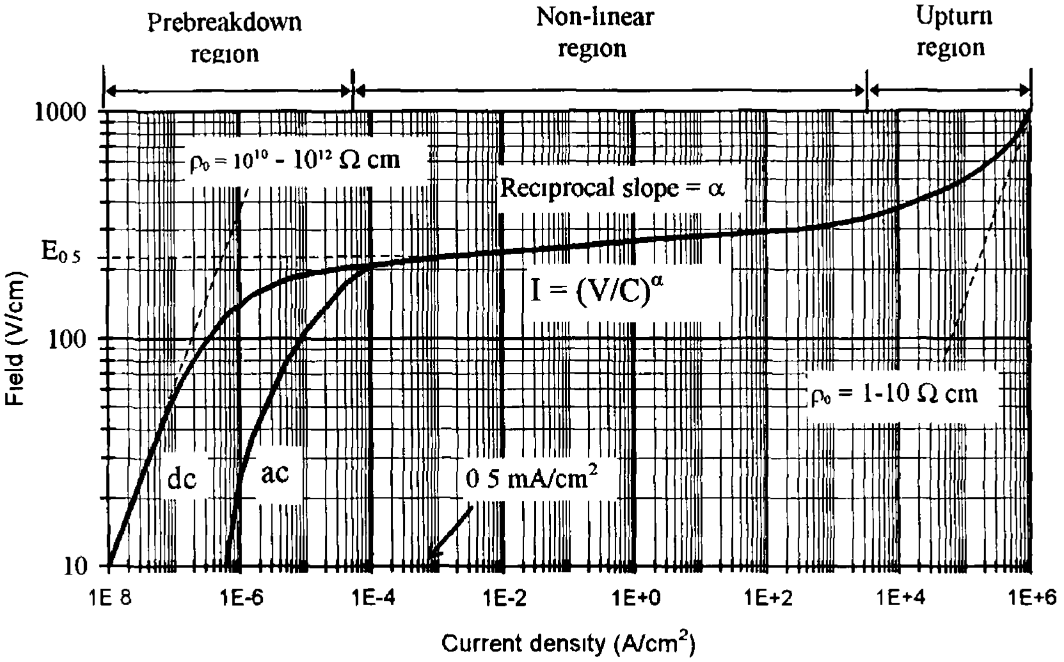

Figure 1 1 Current-voltage characteristics of ZnO varistor plotted on log-log scale (adapted from reference 6)

The non-ohmic relationship of zinc oxide varistor can be mathematically expressed in the non-linear region as

$$I = KV^{\alpha} \qquad (1\ 1)$$

where α is the non-linear coefficient, defined as the ratio of $\log(I_2/I_1)$ and $\log(V_2/V_1)$ and K is a proportional constant related to its non-ohmic behaviour

The I-V relationship of zinc oxide varistor has three distinct regions a low current linear region (ohmic, $<10^{4}$ A/cm^2), an intermediate non-linear region (non-ohmic) and a high current upturn region (ohmic, usually above 10^3 A/cm^2) All of these three regions serve important functions in the design and operation of the surge protector The low current linear or the pre-breakdown region determines the wattloss under normal steady state voltage The non-linear region determines the clamping voltage upon the application of transient surge This region is the heart of the varistor and the degree of non-linearity is determined by the flatness of the region The high current region ($>10^3$ A/cm^2) provides protection from high current surges Hence to characterize the device, it is necessary to determine the I-V curve for all the three regions of the varistors

Pure zinc oxide is a non-stoichiometric n-type semiconductor with a linear I-V behaviour The addition of Bi_2O_3 is essential to form a non-linear *region* However, multiple dopants (additives) such as a combination of Bi_2O_3, Sb_2O_3, MnO_2, SiO_2 Cr_2O_3 and Co_3O_4 etc are added to produce greater non-linearity than a single dopant[6 7 12 25] The high current non-linearity can be enhanced by decreasing the grain boundary resistivity which is usually achieved by doping with aluminium or gallium oxide[26-30] Transition metal oxide Co_3O_4 and MnO_2 are used to improve the non-ohmic property and NiO, Cr_2O_3, or a small amount of glass frit are included to improve the reliability and peak pulse stability The major processing steps for the fabrication of zinc oxide varistor is illustrated schematically in Figure 1 2

The zinc oxide varistor is formed by sintering the pressed body of mixed powder containing zinc oxide and the additives The formation of the microstructure of the varistor is dependent on the sintering time, temperature and environment The presence of different phases and their composition[31] are diagramatically presented in Figure 1 3

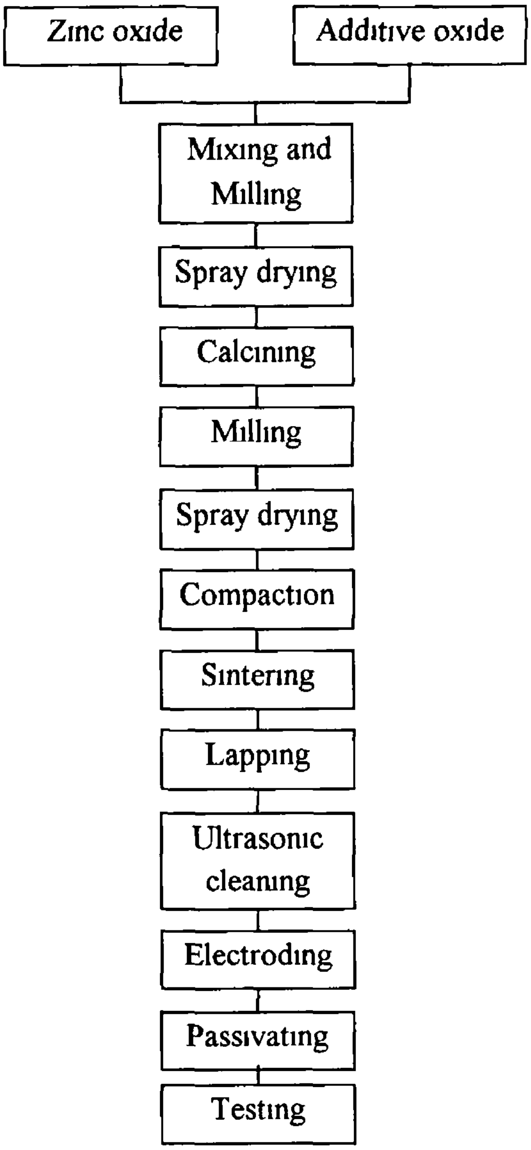

Figure 1 2 Schematic flow diagram for the fabrication of zinc oxide varistor

Zinc oxide, spinel, pyrochlore, and several Bi rich phases are the four basic compounds found in the microstructure[31,33] Zinc oxide and additives react with each other during the sintering process, forming intermediate compounds such as pyrochlore and spinel phases Low temperature is favourable for the formation of pyrochlore phase, whereas, high temperature is for the spinel phase The increase of sintering time and temperature leads to an increase in grain size and results in fewer grain boundaries The typical grain size of commercial zinc oxide varistor is between 15-20 µm and the grains for this type of varistor composition show crystal twinnings[6,34]

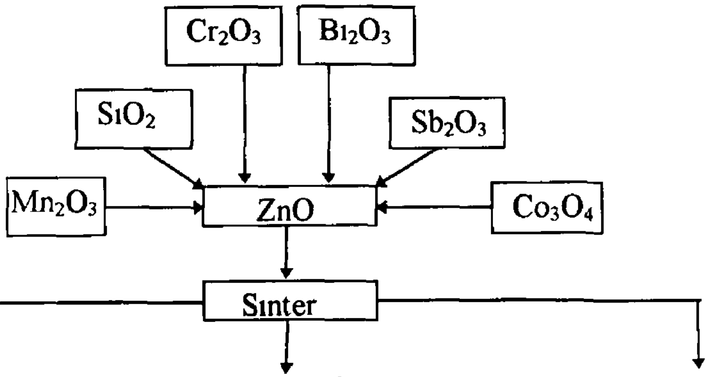

Compound	Chemical formulation	Doped elements and their locations	
		Symbol	Location
Zinc oxide	ZnO	Co,Mn	Grains
Spinel	$Zn_7Sb_2O_{12}$	Co,Mn,Cr	Intergranular phase
Pyrochlore	$Bi_2(Zn_{4/3}Sb_{2/3})O_6$	Co,Mn,Cr	Intergranular phase
Bi-rich glassy phases	$12Bi_2O_3\ \ Cr_2O_3$ $14Bi_2O_3\ \ Cr_2O_3$ β-Bi_2O_3 ∂-Bi_2O_3 $12Bi_2O_3\ \ SiO_2$	Zn,Sb	Triple point

Figure 1.3 Microstructure of ZnO varistor, crystalline phases, their chemical formulation and location, and dopants in various phases (adapted from reference 31)

During sintering the non-stoichiometric nature of zinc oxide produces excess zinc ions The excess ions are accommodated at the interstitial sites in the lattice and are “frozen in” at room temperature during cooling Of the frozen interstitials some will be trapped in the depletion layer[31 34] which is 50-100 nm from the grain boundary to the grain The varistor action and stability are very much dependent on the charge characteristics of the depletion layer within the grains

The application of zinc oxide varistor is selected on the basis of some critical parameters such as non-linear coefficient, nominal voltage, leakage current, and energy absorption capability etc The material and processing parameters like the density of the green and the fired body, homogeneity, grain size, porosity, varistor chemistry, and peak firing temperature affect the energy absorption capability remarkably[35-40] The life of varistor is largely dependent on the leakage current and energy absorption capability

Various models have been developed to describe the conduction mechanism, life, and stability of zinc oxide varistors These are ‘‘Space charge-limited current’’ (Matsuoka)[11], ‘‘Hole-assisted tunneling through Schottky barriers’’ (Mahan, Levinson and Philipp)[41], ‘‘Tunneling through Schottky barriers’’ (Levine)[42], ‘‘Tunneling through Schottky barriers with heterojunctions’’ (Eda)[43], ‘‘Tunneling through Schottky barriers’’ (Hower and Gupta)[44], “Hole-induced breakdown” (Pike)[45] Of all barriers the Schottky barrier is considered to be the most likely barrier at the grain boundary of zinc oxide varistor A model of two back-to-back Schottky barriers at each interface can explain the non-ohmic properties, the temperature dependence of the I-V curve, effect of additives, dielectric properties and degradation phenomena

1 2 SPECIFIC LITERATURE REVIEW

1.2.1 Spray Drying

Thermal drying is used throughout the chemical and process industries for various requirements Some involve the removal of moisture or volatile materials such as pigments, clays and synthetic rubbers Others involve the drying of solution or liquid suspensions Depending upon the purpose different types of drying processes are adopted The preparation of the pressing grade electronic ceramic material demands powders with a high degree of compositional and microstructural homogeneity, high purity and reliability Spray drying is recognized as an excellent method to generate this kind of ceramic powder Relatively uniform spheres can be formed by this method[46 47] The feed slurry is in the form of solution, suspension or paste and the dried product conforms to powders, granules, or agglomerates

Spray drying is a single step unit operation and an almost instantaneous mean of production of dried products from solution or slurry When contact between the spraying and drying medium (hot air) is made, evaporation of moisture takes place and this continues until the desired level of moisture is obtained in the dried product The elapsed time is only a few milliseconds due to high surface to mass ratio[47 48] In spray drying of electronic and other ceramics, the feed slurry contains different additives of certain amount The slurry should be free of air bubble to increase the density of the resultant granules All of the organic additives used in ceramics are soluble in water, so each droplet produced by the atomizer consists of insoluble ceramic and soluble organic additives When the water evaporates the soluble materials coat themselves evenly onto each ceramic particle and hold the submicron particles together

Process stages of spray drying

Spray drying consists of the following four process stages

(i) Atomization of feed
(ii) Spray air contact
(iii) Drying of spray
(iv) Separation of the dried product

Atomization of feed

Atomization of the feed into spray is the heart of the drying operation It produces a spray with high surface to mass ratio from a bulk of liquid and thus rapid evaporation of moisture is possible There are three main types of atomization processes These are (i) Centrifugal atomization (ii) Pressure atomization and (iii) Pneumatic atomization

Centrifugal atomization

In this process the feed slurry is centrifugally accelerated to a high velocity before being discharged into an air or gas atmosphere The liquid is distributed centrally on a wheel and extends over the rotating surface as a thin film The degree of atomization depends upon the peripheral speed, feed rate, liquid properties and atomizer design[47] Maximum centrifugal energy is imparted to the liquid when the liquid acquires peripheral speed of the wheel prior to discharge

The wheel usually rotates at linear peripheral speed of 300 to 700 ft/sec (91 to 213 m/sec) to whirl a drop horizontally under centrifugal force A chamber with large diameter is required for higher capacity The centrifugal atomizer is usually selected for higher capacity This can produce a narrower particle size distribution than that of two fluid nozzles Capacities up to a level of 60,000 lb/hr (27,273 kg/hr) of feed can be reached from a single atomizer

The droplet size can be varied by changing the atomizer design (wheel diameter, number and geometry of the vanes), speed of rotation, feed rate, viscosity of the feed and the air, density and surface tension of the feed[47] However, the effect of the feed rate and surface tension are less important

A centrifugal atomizer has three main components (i) the atomizer drive (ii) the liquid distributor and (iii) the atomizer wheel The atomizer has a spindle rotating in a heavy duty, high speed and fully lubricated bearing The wheel is mounted on the spindle and is securely fastened As the spindle and the wheel rotate, the feed material is fed to the centre of the wheel through the pipe line and the liquid distributor The atomizer can be of fixed or variable speed type

Pressure atomization

The principle of pressure atomization is the conversion of pressure energy to kinetic energy within the liquid bulk to form a thin sheet The break up of the liquid depends on the properties of the feed and frictional effects of the medium into which the sheet is discharged The pressure applied is within the range of 1968-27487 KN/m^2 and only 0 5% of the applied energy is used for liquid break up[47] Virtually the whole amount is imparted in the liquid as the kinetic energy The motion of the liquid is rotary and this permits greater transfer of energy to improve atomization For rotary motion within the nozzle various inserts are used spiral grooved inserts, inclined slotted inserts, swirl inserts or simple use of tangential flow entry The slotted insert has multiple feed inlet but of smaller cross section and is prone to clogging The swirl insert has a single feed inlet but the channel has large flow passages, so it can handle high solid feed without wear and clogging

The spray as discharge from the orifice has a well defined spray angle assuming a regular spray pattern which can be a hollow cone or a solid cone The hollow cone has an air core at the centre which results from the rotation of liquid within the nozzle The greater the rotation the larger is the air core By balancing the rotational motion with an axial velocity, a solid cone can be obtained For equal feed rate and feed pressures, the droplet size distribution is more homogenous for a hollow cone than for a solid one Though the spray has a well defined spray pattern, it becomes distorted due to the effect of ambient air condition in relation to the momentum of each droplet The performance of the nozzle is influenced by pressure, density and viscosity of the feed slurry The approximate relationship at two operating flow rates and corresponding operating pressure and density of liquid is given by the following equation

$$Q_2/Q_1 = (P_2/P_1)^{1/2} = (\rho_2/\rho_1)^{1/2} \qquad (1\ 2)$$

where Q = volumetric flow rate of liquid
P = pressure of liquid
ρ = density of liquid

Any change in the liquid density is associated with the change of other liquid properties and thus the above relationship cannot be applied in all cases A minimum pressure is required to develop any spray angle The effect of viscosity is more prominent At very high viscosity the spray angle is so reduced that the plug flow results and atomization ceases

Capacity, feed pressure, viscosity, surface tension and nozzle size have a significant effect on the droplet size However, the effect of surface tension is less significant than that of the viscosity because the feed liquids that are nozzle atomized vary over a small range of surface tension The droplet size increases with the square root of orifice diameter when other parameters are constant[47]

Pneumatic nozzle atomization

In the pneumatic nozzle atomization a high velocity gas, usually air or steam, (but inert gas is chosen for specialized close cycle) creates high frictional forces over the liquid surfaces causing liquid disintegration into spray droplets Though the overall process is complex, it can be simplified into two general phases The first phase involves the tearing of the liquid into filaments and larger droplets The second phase completes atomization by breaking the liquid of the first phase into smaller droplets The entire process is influenced by the magnitude of liquid properties such as surface tension, density, viscosity, and gaseous properties A high relative velocity between the liquid and air must be generated so that the liquid is subjected to optimum frictional conditions Liquid break up is very rapid and both low and high viscous liquid can be handled

Various design techniques are available to produce optimum conditions of liquid air contact for atomization The designs available can be featured as (i) internal mixing (ii) external mixing and (iii) combination of internal and external mixing

Internal mixing offers higher energy transfer than external mixing But external mixing permits greater control of atomization by independent control of both the liquid and air streams Moreover, as it is abrasive resistant, it is suitable for ceramic and other abrasive products The combined internal and external mixing has the advantages of both the internal and external designs, hence suitable for liquids of higher viscosity

Dittman and Cook[49] have developed different equations to calculate the droplet sizes within the adiabatic spray drying process for different atomizer and correlated the overall heat and mass transfer of the process Several publications from Bowen Engineering Inc [46 48 50] have described different types of spray dryer, their use and advantage, powder properties and control of the properties The dryer handbook from APV[51] has explained the use of different types of dryer in different chemical process industries, the importance of spray drying for electronic ceramic, the cost analysis and the advancement in spray drying

Drying of atomized slurry and air flows

The design of drying chamber depends on the direction and degree of atomization, air flow pattern, product discharge, inherent and desired product characteristics, retention time and air flow rate[46 47] It is necessary that the drying chamber is properly designed so that the water is removed from the feed to the extent that the resulting solid is completely or nearly moisture free

The mechanism of water flow through a droplet during drying is diffusional supplemented by capillary flow As soon as a droplet comes in contact with the drying air evaporation takes place The temperature of the surface of the agglomerates is the wet bulb temperature of the drying air

The rate of heat and mass transfer is a function of temperature, humidity, and the transport properties of the air surrounding each droplet It is also a function of the diameter and relative velocity between the droplet and the air As long as there is unbound water, the rate is constant as diffusion within the spray droplet is fast enough to maintain a saturated condition When diffusion and capillary flow cannot maintain a saturated condition, the critical point is reached and a dried shell is formed at the droplet surface Evaporation is then dependent on the diffusion through the dried shell The thickness of the shell increases and the rate of evaporation decreases The rate will continue to decrease until the equilibrium moisture is attained

A substantial amount of moisture is removed from the droplet when it is saturated and cool[47] The drying chamber design and air flow pattern prevent deposition of partially dried product at the wall and on the atomizer Wall deposits are caused when the droplet travels too rapidly towards the wall Air enters the drying chamber through the air disperser The functions of the air disperser are to provide the required heat of drying, to control the droplet travel and to remove the vaporized moisture rapidly away from the atomization zone The air disperser and atomizer can influence the droplet size distribution of the spray In centrifugal atomizers the air disperser can create rotational flow around the atomizer and local flow around the wheel edge in order to form an air umbrella cloud In the case of nozzle atomization, air disperser creates rotary or nonrotary flow in the drying chamber, depending upon the dryer design

Belchen et al[52] have demonstrated the significance of psychrometric chart for design of the spray dryer Smith[53] has studied the influence of the slurry viscosity on the thermal efficiency of the dryer and the effect of the input operating variables on the powder characteristics in case of traditional ceramic The operating manual[54] of the Yamato Spray dryer has provided the general guidelines for the operation of the spray dryer and the maximum allowable limit of the slurry viscosity Nakamura et al[55] have concluded that materials with excellent superconducting properties can be manufactured from powder produced through spray drying Chen et al[56] compared different powder synthesis routes for the processing of high thermal conductivity aluminium nitride powder They concluded that optimum spray drying condition could produce solid sphere with non-sticky surface and good flow behaviour

Product separation

Several types of separators are used to separate the dried product from the conveying air Maintaining a steady pressure is of prime importance because fluctuation will upset the balance of feed and air flow[47] The separation stage must meet two important requirements (i) an economic recovery of the dried solid and (ii) an exhaust free of the air borne particles To find the optimum condition of spray drying is a matter of finding the point at which the drying chamber has less accumulation on the drying chamber wall and the percent yield is a maximum

The separation of the dried product can be carried out first at the chamber base (primary product separation) followed by the recovery of fine particles in the collecting equipment (secondary product separation) This is a two point discharge design In single point discharge or total product separation, all products can be conveyed to the collecting equipment The amount of primary product separation depends on the chamber design, atomization of the product and the drying air flow[47] The product is separated from the air by a cyclonic air flow set up at the conical chamber base or by the ability of the particles to fall out of the air flow to a flat chamber base

Though there are different types of separators (dry or wet), the dry type separator is most ideal for ceramic oxide powders In the laboratory type spray dryer, the separator can have one or two points of collection. Generally 60-70% can be collected in the primary collector vessel by adjusting the slurry rheology and the spray drying operating conditions, very little pulverulent body adheres to the cyclone.

1.2.2 Binder Systems

The processing of electronic ceramic starts with one or more ceramic materials, liquids and special processing aid known as organic additives. The organic additives include binders, plasticizer, dispersant and lubricating agent etc. These are critical for slurry rheology and powder characteristics which eventually affect the green as well as the fired (sintered) properties of the ceramics[57].

In spray drying higher solid content enhances the efficiency of the spray dryer. A deflocculant is added to lower the viscosity making it possible to increase the solid content in the slurry. Sodium salts of phosphates, silicates and carbonates are usually used as deflocculant which act as electrolytes[58]. Low viscosity slurry produces finer atomization, with a sharp homogenous spray profile. However, too low viscosity also shifts the cloud of drops to the side wall and cone resulting in great reduction in the thermal efficiency of the dryer[53]. As the slurry viscosity is increased, larger drops are formed which do not dry quickly and produce powder with higher moisture content.

Besides the deflocculants, binder is also added to the slurry to hold ceramic particles together as spray dried granules and to impart high compact density and strength[59,60] .

Plasticizer is added to the slurry to improve the flexibility of the binder films and to promote plastic deformation of granules during pressing.

Lubricant is added in the powder to reduce the pressure required in the press and to increase the life of the pressing tool It also reduces the ejection force and thus helps to release the pressed body from the die The amount of lubricant is usually less than 1 percent[61]

Of all the additives mentioned above, the binder plays the most significant role in the processing of electronic ceramic The use of binder in the ceramic processing i e, pressing, extrusion, thick film printing, tape casting, roll forming, slip casting, injection moulding and compression moulding is very important Though different binders are used for different processes, the ideal binder for a particular process has to meet the following general functional requirements

(i) The binder must be soluble, dispersible or emulsifiable in water

(ii) It should impart adequate bonding strength for both the granules and the compacts

(iii) The binder should assist in formability

(iv) It should not be tacky in order to avoid sticking to die and punch faces and abrasion of the die materials

(v) It should be nonfoaming, nonhygroscopic and easily blendable with the batch

(vi) The binder should be burnt out before the maturation temperature and should not leave any detrimental residue

(vii) The binder should be nontoxic, reproducible, reasonably inexpensive and effective in low concentration

Types of binders

Different varieties of binders are used for the processing of electronic ceramic, which are made of natural and synthetic materials They are mostly available as water soluble, water dispersible or water emulsifiable materials Levine[62] has classified the binders according to their origin and use The classification of the binders is presented in Table 1 1

Table 1.1 Classifications of binders (reference 62)

Generic name	Solvent	Commercial name
Gums	Water	Gum Arabic Gum Tragacanth Gum Guar Locust Bean Gum Algin
Starches	Water	Starches Starch derivatives Dextrin
Resins	Water	Polyvinyl alcohol polymer Acrylics Sodium carboxymethylcellulose Methylcellulose
Resins	Water emulsion	Acrylics
Lignosulphates	Water dispersible	Sodium lignin sulfonate Ammonium lignin sulfonate Calcium lignin sulfonate
Organic solvent binders	-	Synthetic waxes (amides)
Wax emulsions	Water emulsion	Petroleum waxes (paraffin waxes, microcrystalline waxes) Synthetic waxes (stearates)

Glass transition temperature of binders

The published literature shows the extensive work that has been carried out at different levels of polyvinyl alcohol, its glass transition temperature and the effect of plasticizer on glass transition temperature and the compaction behaviour of the spray dried ceramic powder The glass transition temperature (T_g) is defined as the temperature or the range of temperatures below which the amorphous polymer is glassy and rigid and above which it is flexible and deformable The compressibility of the powder is dependent on the glass transition temperature, if all other factors, such as granule density, particle size and its distribution, flowability, frictional effect among the particles remain the same To achieve better compressibility, the pressing temperature should be higher than T_g The hard binder not only reduces the compressibility but also imparts elastic strain, known as, springback The release of this stress can cause dimensional distortion accompanied by lamination or capping defects

Brewer et al[63] have studied the use of polyvinyl alcohol for the processing of barium titanate and manganese zinc ferrite agglomerates and have concluded that higher green strength can be achieved by increasing the density and this is obtainable when the agglomerates are stored in a more humid atmosphere Dimilia and Reed[64] have shown the dependence of compaction on glass transition temperature for alumina powder containing polyvinyl alcohol They have observed that the increased percentage of absorbed moisture can lower the glass transition temperature and the apparent yield point of the granules Nies and Messing[65] have investigated the effect of addition of PEG in polyvinyl alcohol and its consequential effect on glass transition temperature and physical properties of alumina powder

Chemical structure of binders

The soluble organic binders are usually long chain organic molecules, consisting of covalently bonded atoms, such as carbon, oxygen and nitrogen They are the backbone of the molecules where the side groups are attached at regular intervals along the length of the molecules The solvent type and the solubility of the binder are dependent on the side groups

The binders from the starch group have a ring type structure The ring has five carbon atoms as shown in Figure 1 4 Each of the carbon atoms could be identified by the numbers such as C-1 or C-2 etc according to the position In between C-1 of one monomer and C-4 of another, there will be one ether (-O-) bond The other three carbon atoms positions are available for the side group, of which C-5 is the most favourable

The binders from resin group are of vinyls, acrylics or polyethylene oxide type The vinyl group is characterized by the linear backbone consisting of carbon to carbon linkage with a side group attached to every other carbon atom Polyvinyl alcohol is from vinyl origin It has two side groups, H and OH The polar side group OH is hydrophilic The hydrophilic side group promotes initial wetting and dissolving in a polar liquid Hydrogen bonding of the OH side group to the surface of a particle provides adhesion, and the dipolar attraction of the OH group produces intermolecular bonding

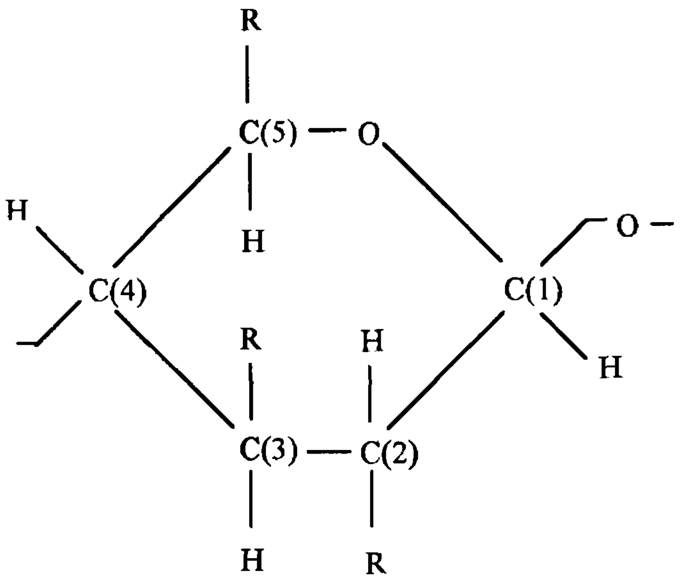

Figure 1 4 The structure of starch derivatives binder (modified α-glucose monomer)

Acrylic binders have the same backbone structure like vinyl, but some acrylic binders have two side groups attached to the same carbon atom They are available in water soluble solid form or in the emulsion form An emulsion is a two phase system consisting of 0 05 to 0 5 micron diameter polymer particles dispersed in water As they are dispersed and not dissolved in water, the viscosity is much lower than a polymer solution of equivalent molecular weight and concentration Many emulsion polymers are extremely hydrophobic and making themselves insensitive to the change of humidity Nyberg et al[66] have studied the advantage of acrylic latex in the processing of homogeneous granules of alumina by spray drying More uniform green and fired body can be obtained by the use of acrylic latex Wu and McAnany[67] have concluded that the acrylic binder can produce green compacts of very high green strength because of strong interactions of carboxylic acid group with ceramic powder and polymer to polymer interaction by hydrogen bonding within the carboxylic group The green machining can thus be facilitated without any chipping problem

Polyethylene glycol (PEG) is another type of organic additive, which can be used as binder or plasticizer depending on its molecular weight It is a water soluble polymer, with a low level of toxicity and is commercially available in molecular weights ranging from 200 to 8000 The higher molecular weights are waxy solids with a high degree of crystallinity[68] By compounding PEG of molecular weight 8000 with a di-epoxy linking group L, Verma et al[69] have produced a new amorphous material of molecular weight 15-20,000 and designated it as PEG compound 20M This new amorphous polymer degrades at lower temperature and produces agglomerated alumina powder of better quality

Rheology of the binders

The molecules and colloids are constantly in motion, because of thermal vibration and impact by the liquid molecules The solute molecules tumble and rotate and the time average volume swept by the molecules or the colloids is defined as their ''sphere of influence'' The effectiveness of a molecule or colloid for increasing the viscosity is dependent on the ''sphere of influence'' Usually the binder molecules have a large ''sphere of influence'' relative to their size The random orientation of the dispersed binder molecules due to Brownian motion is offset by the shear forces in the liquid The molecules tend to line up in such a way that the resistance to flow reduces Thus the viscosity decreases with the increase of shear stress and the binder solution exhibit pseudoplastic behaviour

When the binder solution is added in the slurries containing different particle sizes, a complex interaction occurs and the rheological behaviour of the slurry changes and it behaves like a dilatant fluid The onset of the dilatant behaviour for a particular solid loading can be improved by enhancing packing efficiency As the packing efficiency increases the viscosity of the slurry rises less abruptly with increasing solid content This type of rheological behaviour is very important in pumping and spraying of slurries

1 2 3 Particle Size Distribution

The processing of electronic ceramics starts with the powders, hence to understand the process, it is necessary to have a clear idea of the powder characteristics The characteristics of powder is mainly influenced by the particle size and shape The electronic ceramic powder is usually prepared by spray drying which produces powder of uniform spherical shape Therefore, the distribution pattern, as well as, the fraction percentage of each size influence significantly the particle arrangement and packing density, the size and the shape of the pore interstices, the deformation nature, sintering behaviour, and the microstructure developed during firing

Huffine and Bonilla[70] studied the effect of particle size on the compressibility for non-metallic powders They concluded that compressibility is dependent on pressing modules which is defined as the absolute value of slope of log P vs V_0 of Bal'shin equation and is a simple exponential function of the particle size The volume change accompanying a given pressure increase is greater for smaller particles Evans[71] investigated the effect of inhomogeneity of the powder particle size and packing The creation of stress by differential shrinkage due to the accumulation of fine particles within coarse particles is explained in his work The stresses are capable to generate defects which will ultimately lead to the formation of large voids

Uniform spheres having only one size can arrange themselves in five different ways cubical, orthorhombic, tetragonal, pyramidal, or tetrahedral The fraction and the percent of the bulk volume occupied by the spheres are referred to as the packing fraction and the packing density respectively The packing density can be varied from 52% for simple cubic packing to 74% for tetrahedral and pyramidal close packing and is independent on the size of the spheres The interstitial pore fraction (ø), or the interstitial porosity (ø%), indicates the portion of pore volume present at interstices among the nonporous spheres The pore size is a function of both the size of the spheres and the packing arrangement By introducing smaller particles into the interstices of packed larger particles, pore size and porosity can be reduced This is well known Furnas model for particle packing[2] This type of blending is commonly practiced in formulating coarse grained refractories and concrete which have very little dimensional change on firing

The distribution pattern of powder for technical ceramics are assumed to be log normal and the particle size range between some maximum to a finite minimum The maximum packing density can be increased from 65% to 69% The size distribution to achieve higher packing density can be explained by Andreasen[72] or Dinger and Funk[2] equation which suggest that the packing density can be increased by increasing the distribution modules and the range of sizes

The effect of the particle size distribution on sintering was observed by Yeh and Sacks[73] They concluded that green alumina compacts prepared from powders containing both narrow and wide size distribution can be sintered to high fired density without any exaggerated grain growth However, the use of broad distribution will enhance the green density of compacts, and therefore, the shrinkage will be reduced to achieve the theoretical density Lange and Kellett[74] described the kinetics and transport theory for pore shrinkage with different packing arrangements and their dependence on the co-ordination number, ratio of the external surface energy to the grain boundary energy, short range and long range mass transport phenomena The significant influence of the particle size on the tensile stress of compacts made of aluminium and copper powders are observed by German[75] Duffield and Grootenhuis[76] concluded that for the optimal strength the fine powder with narrow distribution is necessary Rumpf's theory[77] explains the effect of the particle size and packing on the green strength of the compacts, the influence of flaws on green strength, describes the variability of strength, and interprets the effect of powder mixing, of environment and of sintering

The movement of particles into the minimum porosity configuration during processing is hindered by both the internal and external factors The external factor is mostly determined by the particle size and shape, which make the powder free flowing or cohesive and nonfree flowing mixtures The free flow mixture will have a nominal diameter >50 μm and the gravitational force of particles will be much larger than the restraining interparticle force The free flowing nature of particles can also be hindered by the presence of binder molecules As the molecular weight of binder increases, the bridging between the particles increases, due to the formation of coating on the larger particles by the fine ones

1 3 TERMINOLOGY

This section describes the different terminology used for feed slurry and spray dried powder

Flocs

These are cluster particles formed in a slurry or suspension By altering the solution chemistry the flocs can be dispersed The additive known as deflocculant is added to the slurry to deflocculate the suspension by applying a small charge (i e positive or negative) to all particles causing them mutually repulsive and so destroying the flocs

Colloids

If the particles are so finite that inertial forces of a particle are insignificant but surface force is dominating their behaviour, then they are known as colloids Usually particles smaller than 1 μm are termed as colloids They are dispersed in low viscosity liquid and show Brownian motion at around 20°C[2 78]

Primary particle

It is a discrete unit of solid material and may be single or multiple phase in composition If there are any pores, they are isolated from each other and therefore, the primary particle is impervious to fluids[78]

Agglomerate

An agglomerate is composed of two or more particles adhering to each other Agglomeration is often desired in spray drying operation as agglomerates show improved dispersibility characteristics However, if the bond between the particles is strong, the agglomerates cannot be dispersed easily and it is referred to as hard agglomerates Bonds in hard agglomerate are generally chemical bonds formed by chemical reaction or sintering The soft agglomerates are formed through two or more droplets coalescing in the proximity of the atomizer and drying in that state Also partially dried droplets may adhere to one another at the lower region of the chamber, because of their sticky nature Electrostatic, magnetic, van der Waals or capillary adhesion type weak bonds can act on soft agglomerates

1 4 POWDER CHARACTERISTICS AND MEASURING TECHNIQUE

All powder processing starts with a powder, consequently the understanding of the process can be no better than the understanding of the powder The characteristics of the powder are very important in this regard Here a general overview of the powder characteristics, their measurement techniques and effects of powder properties on subsequent processing steps are discussed Powders are characterized by the qualitative data on the following parameters

(i) Particle size and its distribution
(ii) Particle shape and its variation with particle size
(iii) Surface area
(iv) Powder density
(v) Inter particle friction

1 4 1 Particle Size and Its Distribution

The size of a particle/droplet/agglomerate is the representative dimension that expresses the degree of communition The diameter represents the size for spherical particle, while the apparent diameter represents the size for nonspherical particles

The particle size and its distribution is critical for dry pressing of the powder Usually spherical particles or granules with smooth and non-sticky surfaces which are coarser than 40 μm have good flow behaviour Under this condition the gravitational effect is greater than the interparticle forces and particles retained their freedom of movement[2 79] A broad distribution of particles with a small amount of fine particles show better compressibility[80] The presence of more than 5% of fines may sometimes stop the flow altogether and the fine particles may enter the annulus between the punch and the die wall, causing friction and reducing the escape of the air The size distribution also indicates the porosity, pore distribution and flowability of the powder

In subsequent processing stages such as sintering, the particle size plays an important role It is already established that the rate of densification in sintering is inversely proportional to the particle size[81] This is because of the fact that higher free energy enhances the sintering process and the surface free energy increase as the specific surface area of the particle increases

There are a number of methods to measure the particle size of the powders A brief description of each technique is given below

Microscopy

Microscopy technique can quickly show the nominal size and shape of the particles in a sample Using an automatic image analyzer the diameter, height, length and area can be counted and the frequency of distribution data can be generated However, for statistical accuracy, it is necessary to measure at least 700 particles in a plane[2 72] Difficulty in distinguishing the fine particles may cause a skewing of the particle size distribution towards more coarse sizes

Screening and sieving

Sieving is the most common technique to measure the particle size and its distribution The powder is loaded onto a stack of sieves with successively fine apertures from top to bottom The particles are agitated to induce translation until they are blocked by an aperture smaller than their size The screening technique is usually applied for spherical particles larger than 38 μm It is commonly used for particle size measurement of ceramic powders When powder is produced from the same slurry and the same dryer, the possibility of variation of particle size is minimized and more accurate results are achieved

Sedimentation technique

Particle size analysis by sedimentation technique can be applied to particles in the range of 0 05 to 60 μm This is based on Stoke's law where the free falling of a spherical particle in a fluid under laminar flow (Reynold's number <0 2) condition is considered The diameter of the particle having the same settling characteristics can be calculated as follows

$$d = (18Hv/gt(\rho_m-\rho_f))^{1/2} \qquad (1\ 3)$$

where d = diameter of the particles
h = settling height
v = viscosity of the fluid
g = aceleration due to gravity
ρ_m = particle density
ρ_f = fluid density

As the technique assumes that the particles are spherical, the less spherical the powder, the less accurate the technique is Smaller particles (smaller than 1 µm) with slow settling and turbulence can make the size distribution data unreliable

Light scattering

This is a versatile screening technique available for particle size analysis Monochromatic light and dispersed particles provide a basis for automatic size analysis The particle size affects both the intensity and the angular extent of scattering With coherent light the angle of scattering varies with the particle diameter and the extent of scattering varies with the square of particle diameter Computer analysis of the intensity and angular data of the streaming particles can be applied for particles size of 1 to 200 µm The limitation of this technique is that it assumes spherical particles and agglomeration detection by this technique is also difficult

Electrical conductivity

In this technique the particles are well dispersed in an electrolyte (1% salt water) and are passed through a narrow aperture in a non-conductive glass tube under a small pressure differential An electric current is maintained between the electrodes When ceramic particles pass through the orifice, the resistance between the two electrodes increases The pulse resistance is proportional to the volume of the electrolyte displaced The aperture of the orifice should be large enough (about 1 6 times of the largest particle) so that no plugging occurs The dispersion of the particle should be high, otherwise the assumption of one particle at a time in the orifice is not valid Undercounting of fine particles and overcounting of large particles can cause skewing of data to finer or coarser particle size

1 4 2 Particle Shape

The shape of the particle is an important parameter which can influence packing, flow and compressibility of the powder Particle shape varies with particle size and the technique by which powder is manufactured The simple way to describe the particle shape is the aspect ratio It is the ratio of maximum and minimum dimensions of the particle For a spherical particle the aspect ratio is one, and there is only one point of contact Agglomeration and attraction due to van der Waals forces are reduced in spherical particles due to one point of contact As particles deviate from spherical shape, there are more points of contact between the particles, and therefore, there is an increase in friction which in turn decrease the flowability of the powder The shape and the surface area of particles define thermodynamic densification during sintering The driving force for sintering is the reduction in total free energy Optical electron microscope and transmission electron microscopy technique provide much information about the size and the shape of the particles

1.4 3 Specific Surface Area

The surface area is an average measure of the external surface of a large number of particles and is measured by BET isotherm technique It is developed by Brauner, Emmet, and Teller in 1938 In this technique, the specific surface area is measured by absorption of adsorbate from a flowing mixture of an adsorbate and an inert nonadsorbate gas The process of adsorption and desorption is monitored by measuring the change of thermal conductivity of the mixture BET isotherm technique determines the volume of gases necessary to cover the surface of powder with a monolayer of adsorbed gas The molecular diameter and the molecular weight of the adsorbate adsorbed at a coverage of one monolayer are used to calculate the surface area of the powder Though there are many other methods e g Harkin and Jura relative method, Harkin and Jura absolute method and Permeatry method, BET isotherm is mostly used to measure the specific surface area of the particles[82] Multilayer assumption has made this method more reliable than any other method Specific surface area affects both the compressibility and sintering of ceramic powders Too high specific surface area of particles reduces the green compact density with subsequent higher shrinkage on sintering which often leads to nonuniform fired body Conversely, surface activity available for sintering is insufficient if specific surface area is too low[83]

1 4 4 Powder Density

The density of the powder influences significantly the green properties of the compact There are various methods for measuring density, the most common of which are discussed

Bulk density(D_b)

The powder mass when divided by the volume occupied by the solid plus the volume of the voids yields bulk or fill density The voids include open and close pores within the particles and between the particles Here no external force of vibration or tapping is applied The powder is simply poured in a graduated cylinder up to a mark and its weight is taken

Tap density(D_t)

The tap density is another form of bulk density obtained by tapping or vibrating the container in a specified manner to achieve more efficient packing The typical number of taps is usually 1000 and it is performed in a tapping machine The tap density is usually greater than the bulk density The ratio of tap to bulk density is known as the Hausner ratio The ratio is slightly higher than unity for spherical particle

Apparent density(D_a)

Apparent density is the measure of basic particle density which includes basic particle volume and the volume of trapped and closed pores It is usually measured by fluid immersion technique When densities are measured by liquid displacement the apparent density can differ according to the liquid used because of their different capacity to penetrate the pores The average apparent density for a population of particles can be measured by Stereo Pycnometer Here a dry powder can be used, so it is advantageous for ceramic powder containing additives

1 4 5 Interparticle Friction

The interparticle friction plays an important role in powder compaction The main feature of friction is resistance to flow The density and the packing properties decrease because of poor flow There are three indicators to measure the friction of powder These are (i) the angle of repose (ii) Hausner ratio and (iii) shear resistance

The angle of repose

This is the angle formed by pouring a powder mass into a pile where the tangent of angle equals the height divided by the radius of the base of the loose powder pile

Hausner ratio

Hausner ratio is defined as the ratio of tap to bulk density The ratio is slightly higher than unity for spherical particles and increases rapidly for particles of irregular shape Hausner ratio very close to unity is desirable as it indicates little interparticle friction and good fill properties of the powder

Shear resistance

This depends on the particle size and its distribution, shape, surface condition and specific surface area Friction occurs at the point of contact As fine particles will have more points of contact than the coarse particles per unit volume, there will be more points of contacts and therefore, there will be an increase in friction Usually friction increases with surface roughness Specific surface area is related to particle size, shape and surface condition When the particle size is smaller than 1 μm, specific surface area increases exponentially and friction increases as well

1 5 SCOPE OF WORK

The processing of zinc oxide varistor is accompanied by an enormously large number of variables - arising from the composition to the finishing operation like passivation and electroding Even for a fixed chemical composition, the scope of input parameters at various stages of the manufacturing route is quite vast The present work, however, is confined primarily with the variables concerned with the powder preparation The main areas of focus of this study are

(i) the analysis of the influence of spray drying parameters
(ii) the evaluation of a new binder system, and

(iii) the study of the effect of particle size fractions

In addition, the passivation and its thickness, an important factor of varistor performance at high current, was evaluated depending on the effect on energy handling capability The study comprises of the characterization of powder, the evaluation of green body properties, and the determination of electrical characteristics of varistor, in particular the I-V characteristics and the energy absorption capability

1.5 1 Spray Drying

There are a number of parameters in the spray drying process which influences the powder characteristics However, the optimum characteristics in respect of bulk and tap density, flowability, compressibility etc do not necessarily lead to the best ceramic after sintering The aim of the present work was to produce homogenous powder with the necessary green properties which would eventually ensure the maximum energy absorption capability and the optimum level of other critical electrical parameters The work was carried out in a laboratory as well as a pilot scale spray dryer to trace the optimum condition for the production of powder The following variables were considered to carry out the experiment

(i) atomizing air pressure
(ii) feed slurry flow rate
(iii) outlet drying air temperature and
(iv) drying air flow rate

Atomizing air pressure, feed slurry and drying air flow rates were the parameters considered for the laboratory scale whereas, atomizing air pressure, feed slurry flow rate, and outlet drying air temperature were the parameters for the pilot scale spray dryer All of the individual above mentioned parameters and their interactions are expected to affect the basic powder characteristics Experiments were conducted by changing the three operating variables at different levels A two level factorial analysis was performed to identify the significant individual and interactive parametric effects

Powder is characterized generally by the parameters based on the green properties But it is not yet established whether a powder with good green qualities ultimately leads to a varistor of better performance A complete analysis was, therefore, undertaken and depending upon the electrical performance characteristics of varistor, the operating conditions of the spray dryer was optimized for the production of metal oxide varistor (MOV) powder

1 5 2 Binder Systems

Plasticized polyvinyl alcohol is commonly used as a binder in the electronic ceramic industry This binder is available in solid form and the hygroscopic nature of the binder causes the characteristics of powder to change with the variation of environmental humidity Moreover, gelating is associated with the polyvinyl alcohol which is attributable to generate pinholes in the varistor block during the sintering process This seriously confines the electrical performance of the disc The objective of the present work was to evaluate an alternative binder in the processing of varistor powder The variables considered are as follows

(i) different types of binders
(ii) level of binder content and
(iii) level of solid content in the slurry

The investigation includes the study of slurry rheology, the evaluation of powder characteristics, physical properties of green and sintered body, I-V characteristics and energy absorption capability of the varistor The effect of the individual parameter and their interactions was evaluated on the basis of the impact on the critical varistor properties

1.5.3 Particle Size Distribution

The main objective of this work was to evaluate the performance of the zinc oxide varistor produced from different narrow size fraction The standard ''as produced'' powder was fractionated to coarse, medium and fine particles by sieving The performance of varistors from different narrow fractions was compared with the varistor from standard powder to identify the best distribution of powder in terms of the improved performance of the varistor Energy absorption capability, being a very important factor in the context of the reduction in size with higher rated capability, was given the maximum priority Other characteristics of varistor such as the non-linear coefficient, clamping efficiency, nominal voltage, degradation behaviour were also investigated

In chapter 2, titled experimental equipment, materials and procedure ceramic powder processing and characterization, description of both the laboratory and the pilot scale spray dryer, slurry preparation and powder production for different spray drying parameters and binder systems is given Fractionating procedure of the standard "as produced" powder is also discussed in this chapter It also covers the powder characterization and the techniques used for all the processing conditions

Chapter 3, titled experimental procedure, equipment and testing varistor preparation, describes the general operations used in varistor manufacturing, specific techniques used for samples of different size, varistor characterization and the equipment used for the characterization

Statistical analysis of the results obtained under different processing conditions are discussed in chapter 4 The methods used for the analysis are "Two level factorial design", "Response surface methodology", and "Weibull theory for fracture strength" Two level factorial design was used to identify the main and interacting effects of several independent variables on the response of the process Response surface methodology generated the relationship between the measured mean particle size of the spray dried granules and the input spray drying parameters Weibull parameters were calculated for the green and the fired strength produced from the powder containing different latex binder systems to estimate *the scatterness*

Chapter 5 covers the experimental results based on the spray drying parameters, different latex binder systems, particle size fractions, and passivation thickness The effect of the processing parameters on the powder characteristics as well as on the electrical properties are discussed and compared with the results of the standard processing

Finally, in chapter 6, conclusions and recommendations for future work are presented They are based on the results obtained from different powder processing parameters and passivation thicknesses

Chapter 2

EXPERIMENTAL EQUIPMENT, MATERIALS AND PROCEDURE: CERAMIC POWDER PROCESSING AND CHARACTERIZATION

2 1 INTRODUCTION

Powder was prepared and characterized in order to optimize the spray drying parameters as well as to evaluate a suitable binder for the processing The work of powder processing and characterization was carried out at the laboratory and pilot scale Initially the study on the spray drying parameters was conducted extensively with a large number of experiments using a small laboratory type spray dryer The knowledge gained in optimization of the smaller dryer was utilized to design a two level half factorial experiment for a pilot scale dryer Several binders were evaluated with the powder processed through the pilot scale spray dryer The effect of the particle size distribution was evaluated by fractionating the standard production powder at different ranges The powder produced to carry out the experiments was fully chracterized

2.2 CERAMIC POWDER PROCESSING

There are several steps in the processing of varistor powder with changed spray drying parameters and different binders A schematic flow diagram of fabrication is illustrated in Figure 2 1 The description of powder processing and characterization is detailed in the subsequent sections

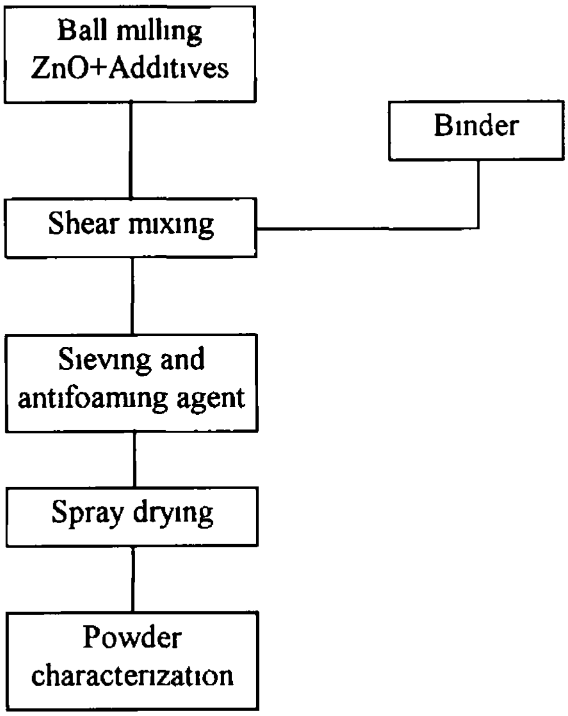

Figure 2 1 Schematic flow diagram of powder processing

2.3 DESCRIPTION OF SPRAY DRYER

The spray dryers used to undertake the study were (i) Yamato spray dryer, a laboratory scale dryer, model no DL-41, made by Yamato Scientific Company and (ii) Bowen #1 Tower spray dryer, a pilot scale spray dryer, made by Bowen Engineering Inc A brief description of each of the dryers is given in the following sections highlighting the salient features

2 3 1 Laboratory Scale Spray Dryer

This is a small spray dryer with spraying capacity of only about two kilograms of slurry per hour The external view of the spray dryer is given in Figure 2 2 A schematic flow diagram indicating the main components is shown in Figure 2 3

Spraying system

The spraying system of the dryer is a two fluid nozzle system The diameter of the orifice is approximately 0 7 µm and the nozzle system consists of inlets for drying air, atomizing air, and feed slurry as shown in Figure 2 4 The flow pattern of the slurry is downward parallel The feed slurry is broken into small droplets by atomizing air pressure just prior to the exit from the nozzle to the drying chamber The atomizing air pressure can be controlled by the air flow control valve and it can be adjusted between 0 to 6 Kg_f/cm^2 according to the indicator (Bourdon tube air pressure gauge) reading

Air heater

The heating source is an electric heater There are two stainless steel pipe heaters each with power of 2 0 kW The set temperature of the heater is 300 °C The inlet and outlet temperature of the drying air can be recorded by a sensor equipped with platinum thermoresistance The temperature recorder is graduated from 0 to 300 °C The inlet drying air temperature can be controlled between 40 °C to 300 °C with an accuracy of ±1 °C by controlling the drying air and feed flow rate, and the atomizing air pressure

Drying air flow and drying chamber

The inlet air is drawn away from the drying chamber by the aspirator The flow rate is controlled by a flow control valve and it is indicated by the drying air float system flow meter

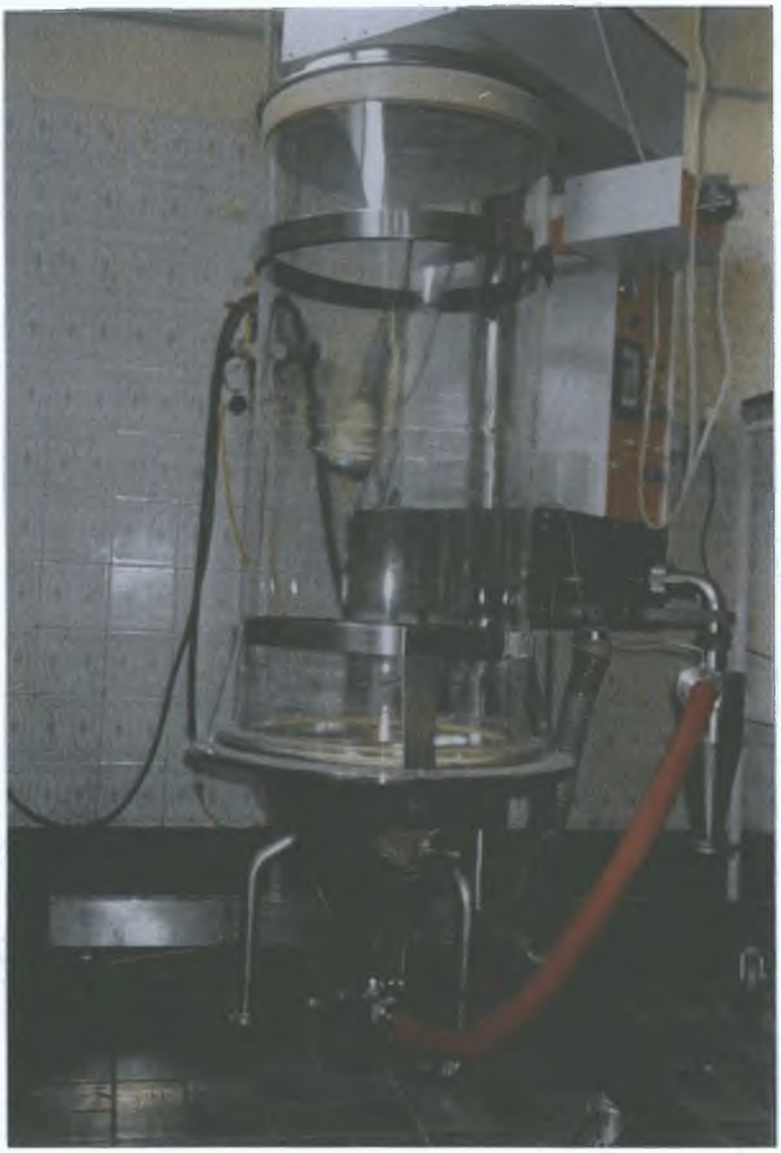

Figure 2.2 External view of the laboratory scale spray dryer

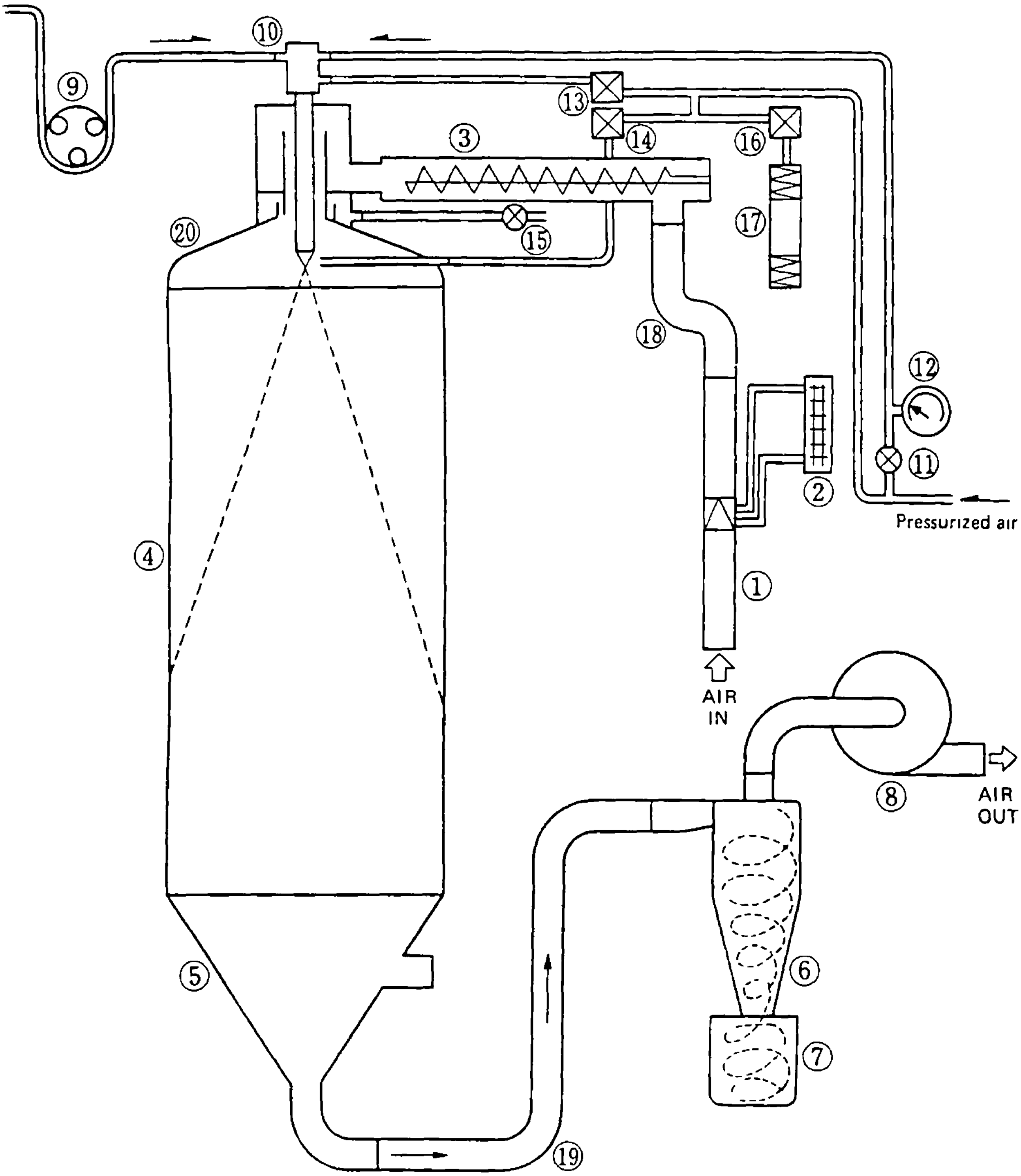

① Orifice tube
② Drying air flow meter
③ Heater
④ Drying chamber
⑤ Lower chamber
⑥ Cyclone
⑦ Product vessel
⑧ Aspirator
⑨ Sample liquid feed pump
⑩ Spray nozzle

⑪ Spraying air needle valve
⑫ Spraying air pressure gauge
⑬ Magnetic valve for needle knocker
⑭ Magnetic valve for nozzle blow
⑮ Cold air regulating valve
⑯ Magnetic valve for head elevating and lowering
⑰ Air cylinder
⑱ Connection duct
⑲ Connection hose
⑳ Upper chamber

Figure 2 3 Schematic flow diagram of the laboratory scale dryer

The hot air is forced into the drying chamber which is made of borosilicate glass and is cylindrical in shape with dimensions of 450 mm in diameter and 1000 mm in height

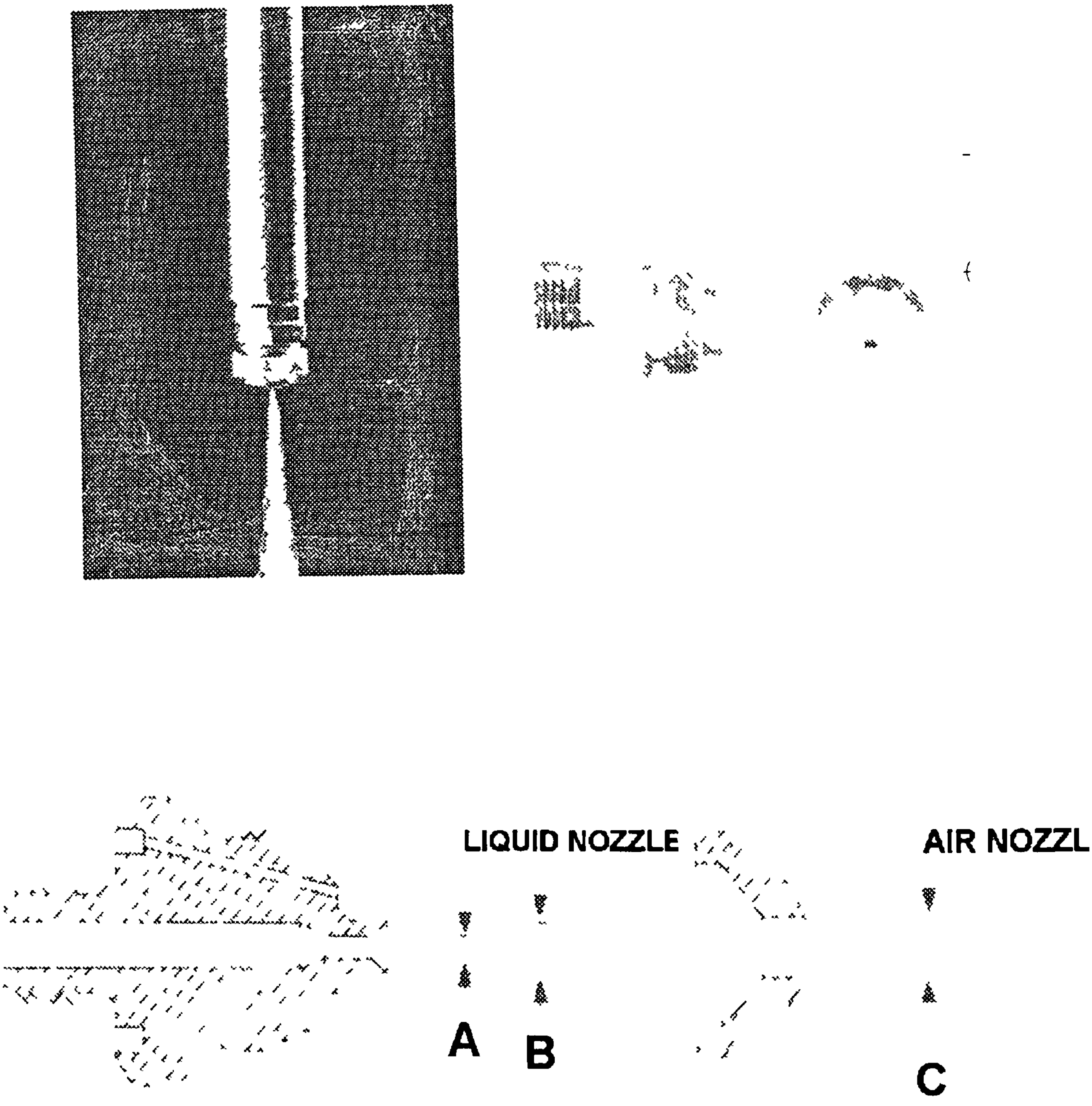

Figure 2 4 Diagram of spray nozzle of the laboratory scale dryer

Slurry feed pump

The slurry is fed by a quantitative peristaltic constant flow pump The feed flow meter has ten divisions The flow can be controlled at any desired rate between 0 to 80 ml/min by setting the pointer of meter at a particular division

Cyclone collector

The dried particles from the drying chamber are passed through the connection hose to the cyclone to be dried further and separated from any liquid The moisture is further extracted at the cyclone and the dried powder is collected in the product vessel The connection hose is made of silicone rubber tube, whereas, the cyclone and the product vessel are of stainless steel and borosilicate glass respectively

2 3 2 The Pilot Scale Spray Dryer

This is a larger spray dryer with an approximate processing capacity of about 25 kg of slurry per hour The external view and schematic flow diagram of the dryer are given in Figures 2 5 and 2 6 respectively The main components of the dryer are as follows

(i) Air heater
(ii) Slurry feed pump
(iii) Atomizing nozzle assembly
(iv) Drying chamber
(v) Product receptacles

Figure 2.5 External view of the pilot scale dryer

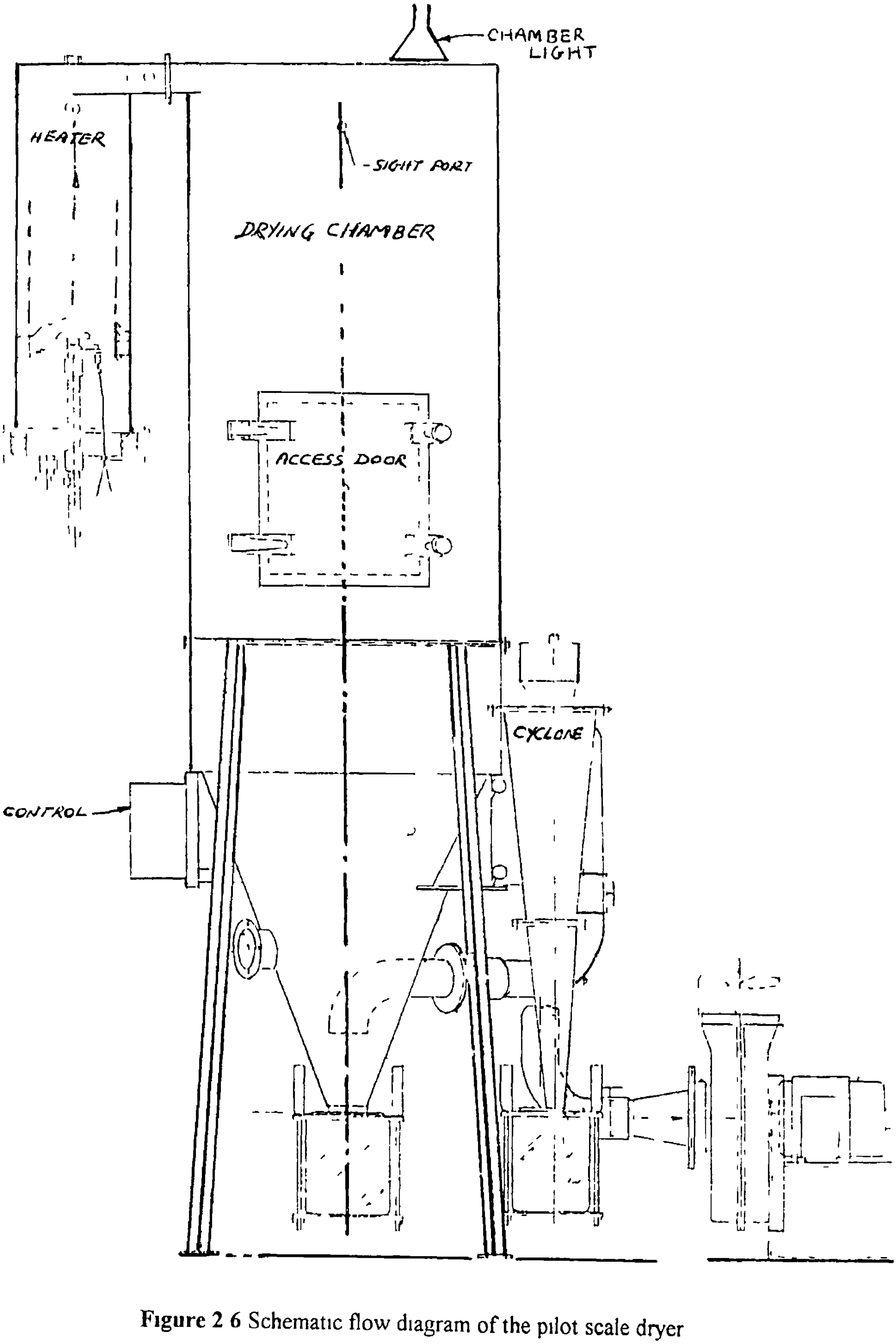

Figure 2 6 Schematic flow diagram of the pilot scale dryer

Air heater

The air heater is composed of heater shell, gas burner, temperature control, and flame safety unit The heater shell is made up of three parts outer shell of stainless steel, insulated jacket, and inner shell of stainless steel

The gas burner is a Vel-Air burner This can be used for various gases when equipped with the proper ancillary equipment The recommended maximum gas pressure to the burner is 8 inches (203 2 mm) of water for natural gas and 12 inches (304 8 mm) of water for propane gas

The temperature of the hot air entering the drying chamber is controlled by means of a partlow control It has a knob and dial system with which the temperature can be set

Safe operation of the gas burner is maintained with the Fenwal spark ignition system The Fenwal system is responsible for igniting the gas burner and monitoring the flame when the burner is in operation The air exhaust fan is interlocked with the burner power supply circuit to secure further safety The cyclone fan must be in operation before the ignition of the burner

Slurry feed pump

The feed is supplied to the dual fluid nozzle, by a variable speed positive displacement pump as shown in Figure 2 7 This is a single screw rotary pump and the pumping actions are created by the double threaded helix of the stator As the motor rotates, the rotor forms, in conjunction with the stator, a series of sealed cavities 180° apart and the cavities progress from suction to discharge As one cavity diminishes, the opposite cavity starts discharging exactly at the same rate and thus maintains a constant flow rate As a result, pulsationless positive displacement occurs without any flow valves

Atomizing nozzle assembly

The atomizing equipment consists of a double fluid type nozzle body as shown in Figure 2 8 For any particular nozzle assembly, the capacity and atomizing characteristics are altered by varying the feed and the atomizing air pressure The feed is delivered to the nozzle by a variable speed, positive displacement pump Atomizing characteristics may be modified by adjusting the atomizing air pressure up to 100 psig A maximum free air flow rate of approximately 15 cfm is required for the complete atomization

Drying chamber

Hot air enters the top of the drying chamber from the air heater via the hot air duct, the flow being induced by the main fan located after the cyclone stage The two fluid nozzle is centrally positioned near the bottom of the chamber in standard operation and fired upward A swirl is imparted to the hot air by the vane ring to provide proper contact between air and atomized droplets Heat is transferred from the hot air to the droplets, moisture is vaporized from the droplets and carried away by the flowing air The condition of the chamber wall is a prime indication of whether or not the dryer is operating properly The heavy impingement on the dryer wall can be avoided by decreasing the feed flow rate, whereas, the flow can be increased if the chamber is running very clean The dried product falls to the base of the chamber where it discharges into a sealed jar The cooled air with entrained finer particles leaves the chamber through a central downward-pointing gooseneck located just below the nozzle

Figure 2.7 External view of feed and pumping system of the pilot scale dryer

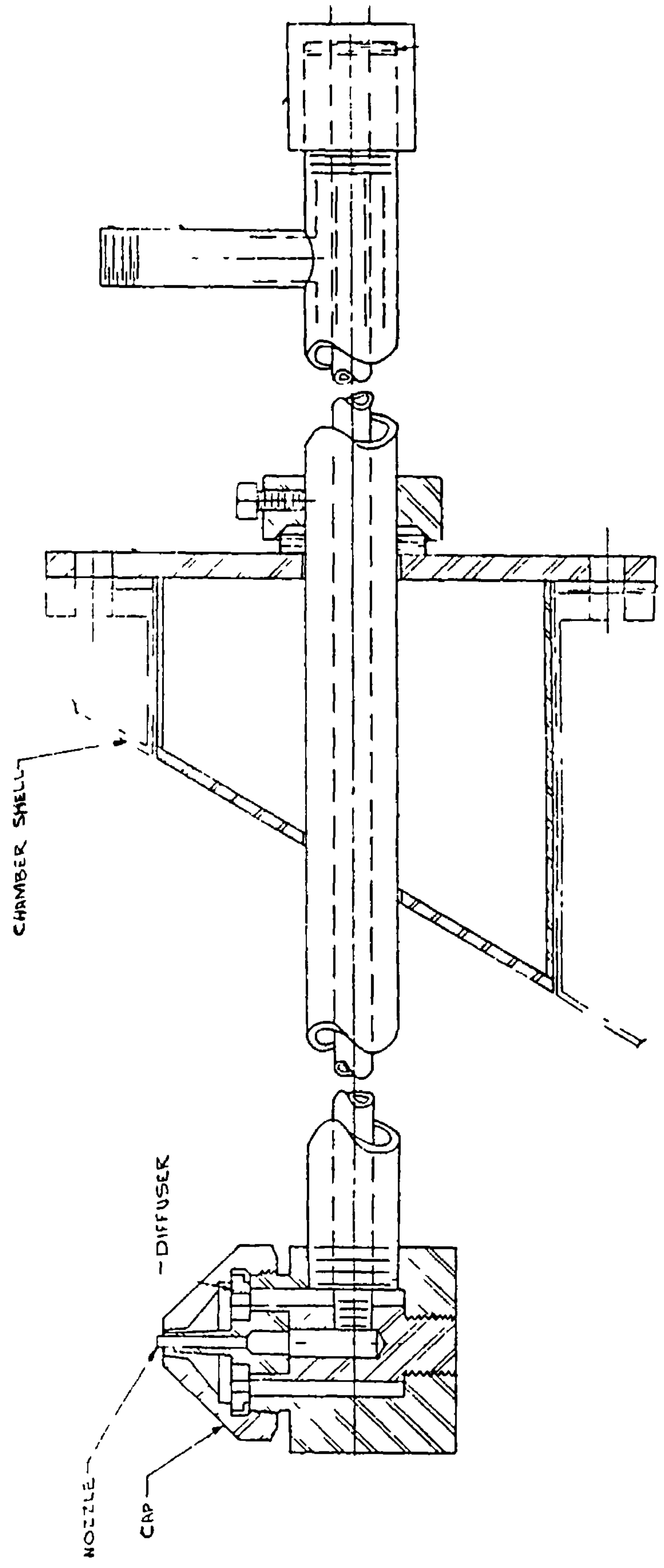

Figure 2 8 Dual fluid nozzle atomizer

Cyclone collector

The gas exits from the drying chamber through a duct to a high pressure drop cyclone where entrained particles are separated from the air by centrifugal acceleration The separated fine particles are collected from the cyclone base into a sealed jar Clean air leaves from the cyclone top and travels via the duct to the main fan which discharges it through a stack to the atmosphere

2 4 SPRAY DRYING PARAMETERS

The correct setting of the operating parameters of the spray dryer play an important role in the production of homogenous powder with spherical shape having the ideal physiochemical characteristics for shaping parts by uniaxial compaction However, the importance and the criticality of the slurry rheology must not be ignored Too low or too high viscosity influences the particle size, percent yield of powder and the evaporation capacity of the dryer To carry out this experiment, the slurry viscosity was maintained at a fixed level The main identifiable parameters affecting the performance of a spray dryer are drying air flow rate, atomizing air pressure, feed flow rate or feed pump pressure, and the inlet and outlet temperature of the drying air However, all of these parameters cannot be set independently The inlet and outlet temperatures are significantly influenced by other parameters in the case of small scale spray dryer, whereas, the outlet temperature could be fixed by controlling the inlet temperature and the cyclone pressure for the pilot scale dryer

Three independent parameters were selected for both the spray dryers The identification of different run conditions for the two dryers is given in Tables 2 1 and 2 2 respectively

2 4 1 Production of Powder

The process pertaining to the production of powder using various spray drying parameters has three major steps These are

(i) Slurry preparation
(ii) Spray drying and
(iii) Characterization of spray dried powder

Slurry preparation

The slurry of standard calcined varistor powder was collected from the production line A fixed amount of slurry was taken for each experiment Binder (PVA) was added at a concentration of 0 5% of the dry weight of the powder A 10% solution of the binder was prepared and shear mixed for about 15 minutes Before spraying, the solid content and viscosity of the slurry were measured and found to be 78 2% and 71 2 CP respectively

Spraying of the feed slurry

The spray dryer was ready to start-up once the chamber and the feed pipe system were completely cleaned and receptacles for the product and the fines were connected tightly The exhaust fan was started and the gas burner was ignited The inlet temperature was increased until the desired outlet temperature was reached The atomizing air pressure was set and the deionized water was fed slowly through the pumping system As the steady state operating conditions were reached, the flow was switched from water to feed slurry Small droplets are produced in the nozzle from the feed slurry by tearing first into filaments and then smaller droplets After completion of spraying the slurry for a particular set condition, only one parameter was changed to conduct the next experiment

The feed pump of pilot scale spray dryer was calibrated by using the standard slurry to be certain about the control of the input parameters The slurry was pumped at different set pressure of the feed pump and weight was taken at regular time intervals Density of the feed was measured at 22 5 °C Volumetric feed flow rate was calculated from the weight and density of the slurry collected Calibration plots of the feed pump are shown in Figures 2 9 and 2 10

Table 2 1 Settings of different operating conditions for the laboratory scale spray dryer for large nozzle (150-100-SS), the small nozzle (SU3-SS-64 5)* and replicated run

No of run	Drying air flow rate (m^3/min)	Atomizing air pressure (Kg_f/cm^2)	Feed flow rate (ml/min)	Drying air inlet temp (°C)	Drying air outlet temp (°C)
1	0 6	1 0	39 0	270 0	78 0
2	0 6	1 0	26 0	270 0	80 0
3	0 6	1 0	56 0	270 0	75 0
4	0 7	0 8	26 0	230 0	100 0
5	0 7	0 8	39 0	230 0	98 0
6	0 8	1 2	26 0	205 0	92 0
7	0 8	1 2	39 0	205 0	90 0
8	0 6	0 8	26 0	250 0	85 0
9	0 6	0 8	39 0	250 0	80 0
10	0 7	1 0	26 0	240 0	83 0
11	0 7	1 0	39 0	220 0	80 0
12	0 6	1 2	26 0	250 0	82 5
13	0 6	1 2	39 0	250 0	81 0
14	0 7	1 2	26 0	230 0	91 0
15	0 7	1 2	39 0	230 0	83 5
16	0 8	0 8	26 0	210 0	96 5
17	0 8	0 8	39 0	210 0	85 0
18	0 8	1 0	26 0	210 0	93 0
19	0 8	1 0	39 0	210 0	83 5
20	0 7	0 8	26 0	230 0	100 0
21	0 7	0 8	39 0	230 0	95 0
22	0 6	0 8	26 0	250 0	85 0
23	0 6	0 8	39 0	250 0	80 0
24*	0 6	0 8	26 0	250 0	95 0
25*	0 6	0 8	39 0	250 0	90 0
26*	0 7	0 8	26 0	230 0	100 0
27*	0 7	0 8	39 0	230 0	90 0

Table 2 2 Settings of different operating conditions for the pilot scale spray dryer

No of run	Atomizing air pressure (Psi)	Feed pump pressure (dial division)	Feed flow rate (ml/min)	Outlet drying air temp (°C)
1	10	3	71	130
2	10	6	258	115
3	40	6	258	130
4	40	3	71	115
5	10	4	172	127
Control	20	5	215	126

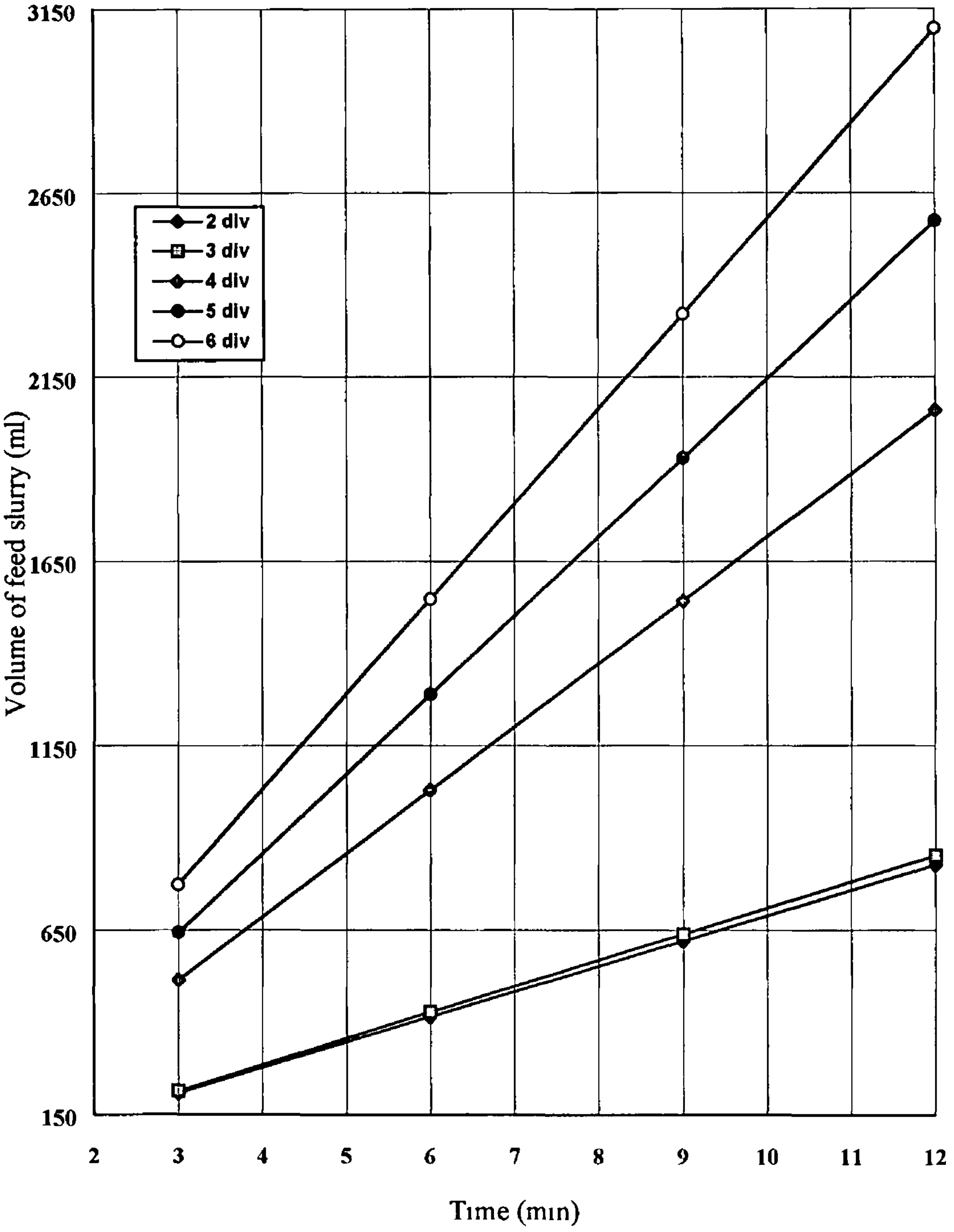

Figure 2 9 Volumetric flow of the feed slurry for different settings of pump pressure of the pilot scale spray dryer

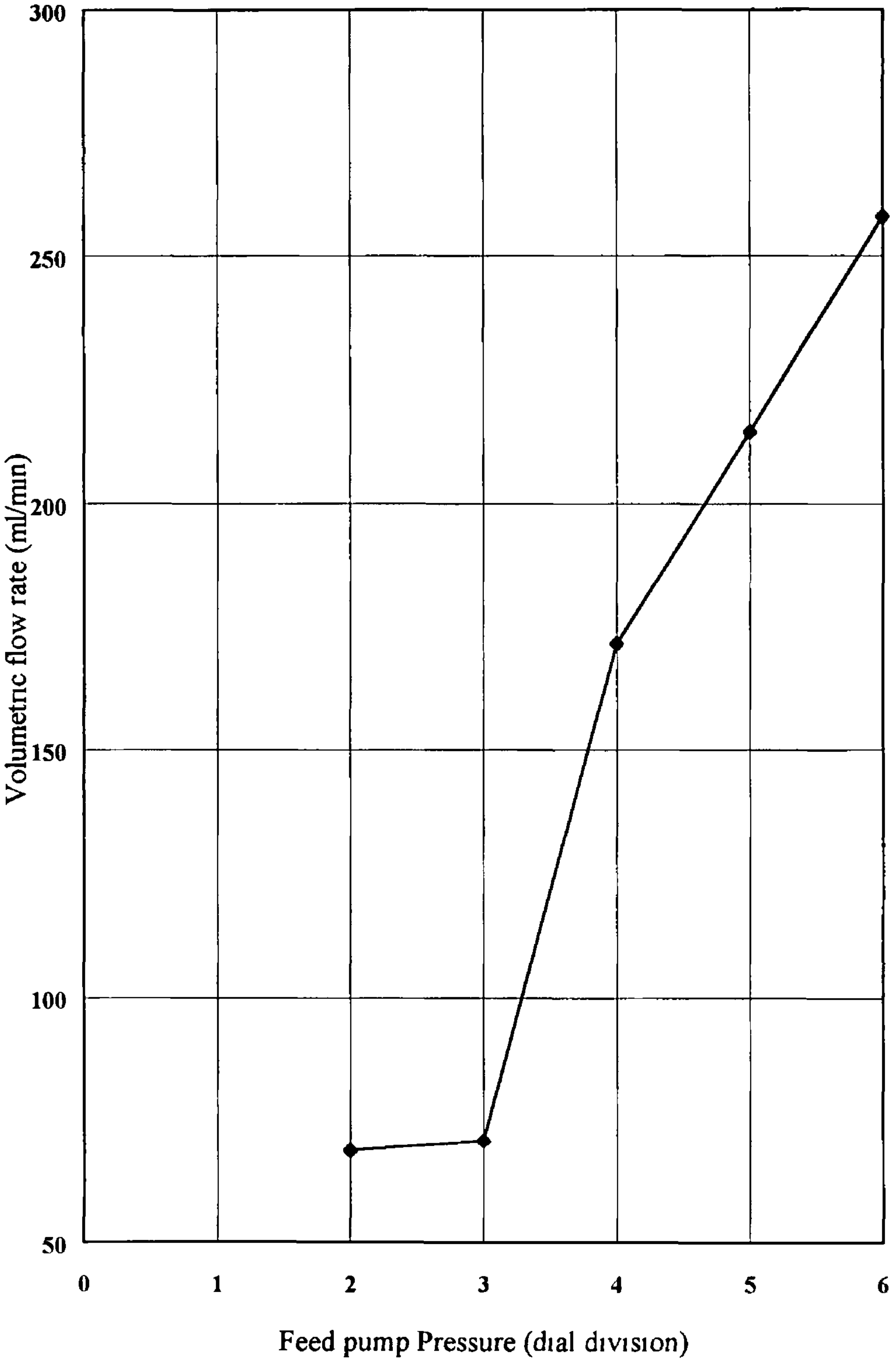

Figure 2 10 Calibration of the feed pump of the pilot scale spray dryer

Characterization of the spray dried powder

Conventional methods were used to characterize the spray dried powders The techniques are discussed in the subsequent section 2 7 The parameters measured are the percent yield of powder, moisture content, bulk, tap, and green density, mean particle size, particle shape, flowability, angle of repose, compressibility and green strength

2.5 EVALUATION OF BINDER

Different commercially available binders were selected to evaluate an alternative binder in the processing of varistor powder They were from the group of polyethylene glycol and emulsion acrylic latex Initially three PEG binders of high molecular weight and five latex binders and their blends were taken The total percentage of the binder was kept fixed for PEG, while the ratio of binder to plasticizer was varied at three levels Hence, nine different powders were planned to produce with PEG binders In the case of latex binders the percentage of the binder was fixed and therefore, only five types of powders were considered to produce as a trial run The processing steps involving to the production of powder using different binders are the same as discussed in section 2 4 1 and these are (i) slurry preparation, (ii) spraying of the slurry, and (iii) powder characterization

During spraying it was observed that the slurry prepared with PEG was not perfoming satisfactorily The droplets from the slurry containing different PEG binders with various ratios of binder to plasticizer were sticking heavily to the drying chamber base Whereas, the spray dryer was perfectly operational under standard spray drying conditions The powder collected by continuous tapping at the drying chamber base was very tacky in nature So considering the practical limitations of the powders produced with PEG, these were not evaluated any more The slurry with different latex binders and their blends could be sprayed conveniently without any problem Powder obtained using these binder systems was hand sieved through mesh 60 before characterization as a conventional procedure The best binder was selected on the basis of powder characteristics The level of that binder and the solid concentration in the slurry was varied at two levels for further evaluation The identification of different latex binders used in the experiment is presented in Table 2 3

Table 2 3 Identification of different binder systems depending on the type, binder and solid contents

Binder type	Ltx A	Ltx B	Ltx C	Ltx D	Ltx E	PVA	Ltx C1	Ltx C2	Ltx C3	Ltx C4	Ltx C5
Binder (%)	1 3	1 3	1 3	1 3	1 3	1 3	1 0	1 6	1 0	1 3	1 6
Solid (%)	72	72	72	72	72	72	72	72	80	80	80

2 5 1 Slurry Preparation

The slurry of varistor powder was prepared by ball milling which was carried out for six hours as it is conventionally practiced in the industry Organic additives such as deflocculant and plasticizer were added during milling Zirconia was the milling media After milling, the slurry was collected in a container and shear mixed with binder for about half an hour The percentage of the binder and solid in the slurry was kept at standard level The slurry was transferred to the feed tank of the dryer as the dispersion was completed The slurry viscosity was measured before spraying at room temperature by using a Brookfield viscometer with spindle #1 at 100 rpm

2 5.2 Spraying of the Feed Slurry

The spraying mechanism is the same as discussed in the previous section After spraying of one sample the dryer was washed thoroughly to conduct the next experiment

2 5 3 Characterization of Powders

The characteristics of powders are the primary indicators to choose a suitable binder, its level, and solid concentrations in the slurry Conventional methods were adopted to characterize the powder The measurement techniques are described under section 2 7 The properties evaluated were bulk, tap, and granule densities, flowability, angle of repose, green density, compressibility, fired density, shrinkage, green and fired strength

2.6 PARTICLE SIZE DISTRIBUTION

Investigation of the effect of particle size fractions on the varistor properties was performed by taking the standard ‘‘as produced’’ powder The powder was then fractionated to different narrow distributions containing large, medium and fine particles A stack of sieves with 150, 90, 75, and 45 μm apertures was arranged successively from top to bottom By placing the powder, the top most sieve was closed with a lid and secured tightly The sieves were agitated for about 30 minutes and the fraction of powders on each sieve was collected The effect of particle size fractions on the physical properties was evaluated by measuring the green density and strength The measurement techniques are the same as discussed in section 2 7 The identification of different fractions is given in Table 2 4

Table 2 4 Identification of different size fractions of powder

Type of powder	Size range (μm)
Cell A	150-90
Cell B	90-75
Cell C	75-45
Cell D	<45
Standard powder	150-45

2 7 CHARACTERIZATION OF POWDER

The powders produced with changed spray drying parameters, different binder systems and particle size fractions were characterized to determine the optimum operating conditions for the spray dryer and selecting the suitable binder and size distribution Conventional techniques were adopted to characterize the powder The properties such as the yield of powder, moisture content, bulk, tap, and granule densities, flowability, angle of repose, green density, compressibility, shrinkage, fired density, green and fired strength of the discs were measured

2 7 1 Percent Yield of Powder

This is the ratio of powder obtained by spray drying to that of the solid present in the slurry The efficiency of the spray dryer is primarily indicated by the yield of the powder However, the yield depends not only on the operating conditions of the dryer but also on the rheology of the slurry

2 7 2 Moisture Content

The moisture content was measured by taking a sample of 5 0 gm of powder and placing it in an oven at 110 °C for one hour After removing the sample from the oven, it was kept in a dessicator for about 10-15 minutes to cool it down and weighed again The difference in weight was considered as the moisture present in the powder This measurement is valid for comparison purposes since some PEG is also lost, but this is assumed to be the same quantity in every occasion

2 7 3 Bulk Density

The bulk or the fill density is the density when the powder is in a loose state and poured without any agitation This was measured by using a graduated cylinder and filling the sample powder to the 100 cc mark and weighing the powder mass Thus the bulk density was computed from the relation, D_b = weight of the powder/volume of the powder

2 7.4 Tap Density

The tap density is the highest density of the powder that can be achieved by vibration of a powder in a controlled way without applying any external pressure To obtain the tap density the cylinder of the powder mass was secured on a tapping machine (Quantchrome) and tapped for 1000 times and the reduced new volume was measured The tap density was calculated as D_t = weight of the powder/reduced volume

2.7 5 Granule Density

The powder was fractioned into two different narrow distributions by sieving in the range of (i) 150-90 µm and (ii) 90-53 µm The sample of powder from each fraction was taken in a graduated cylinder and then subjected to 1000 tapping using the same tapping machine The weight (W) and the volume (V) were measured The granule would fill 64% of the packing assuming cubic packing arrangement with perfect spherical shape[2 64] The granule density was calculated as follows

$$D_g = \frac{W}{0\,64V} \qquad (2\ 1)$$

The average density of the two fractions was considered as the granule density for a particular powder

2.7.6 Flowability

This is a measure of flow rate at which the powder flows under gravity through a small opening It was measured by a Hall flow meter An amount of powder of known weight was allowed to pass through the small opening and the total time required was measured using a timer The flowability was calculated as follows

$$\mathit{Flowability} = \mathit{Weight\ (gm)/Time\ (sec)} \qquad (2\ 2)$$

Usually spherical particles having suitable size distribution and high bulk density show good flow property In general if nominal particle size is greater than about 50 µm, the powder retains freedom of movement

2 7.7 Angle of Repose

This is a widely accepted measure of interparticle friction A particular amount of powder was allowed to flow through the Hall flow meter and collected on a piece of paper in the form of a pile The base (b) and the height (h) of the pile was measured with standard instrument The values of b and h were sufficient to calculate the angle of repose

$$Angle\ of\ repose = \tan^{-1}\left(\frac{2h}{b}\right) \qquad (2\ 3)$$

2 7 8 Particle Size and Its Distribution

A Sonic Sifter, ATM model L3, was used to measure the particle size and its distribution A 5 0 gm sample of powder was placed on mesh number 80 of nominal size 180 µm where successively fine apertures of nominal size in the range of 180-45 µm were arranged from top to bottom The powder was agitated ultrasonically for 5 minutes The weight fraction of powder on each mesh was measured in a laboratory type balance with an accuracy of ±0 1 mg The range of the particle size measurement was 45-180 µm

2.7.9 Particle Shape

The shape of the particles was observed by using a scanning electron microscope (JSM-840A) The powder sample was coated with gold palladium thin film by magnetron sputtering technique

2 7 10 Specific Surface Area

The specific surface area was measured by BET isotherm using Quantasorb Jr Integration count for desorption was taken at three levels of adsorbate concentration and the corresponding calculated volume and count were also evaluated The specific surface area was computed using the PC and Quantachrome software BET isotherm is valid when the following conditions are satisfied

(i) uppermost molecules in adsorbed stacks are in dynamic equilibrium with the vapor

(ii) vibrational frequency of adsorbate normal to the surface, adsorption energy, and condensation co-efficient remain constant for second and higher layer

(iii) BET isotherm can only be applied within the range of 0 05 < P/P_o < 0 35

The final formula of the BET isotherm is as follows

$$\frac{1}{X\left(\frac{P_o}{P}-1\right)}=\frac{1}{X_mC}+\frac{C-1}{X_mC}\frac{P}{P_o} \qquad (2\ 4)$$

where C = constant

P_o = saturated vapor pressure of adsorbate

P = partial pressure of adsorbate

X_m= weight of monolayer coverage of adsorbate

X = weight of adsorbate adsorbed at P/P_o

Using the above relationship the total surface area can be calculated as follows

$$S_t=\frac{X_mNA}{M} \qquad (2\ 5)$$

where N = Avogadro's number, 6 023x10^{23}

A = cross-sectional area of the adsorbed gas, the value of which is 16 2x10 ^{20} m^2 for nitrogen gas

M = molecular weight of the adsorbed gas

The specific surface area was calculated as S_t per unit weight of the powder This analysis complements the particle size distribution and provides information about the minor amount of internally fine particles In general the smaller the particle size the greater the specific surface area However, the specific surface area is also dependent on the particle shape, size and its distribution and surface conditions[2 78]

2 7 11 Green Density of Pressed Body

The green density of the powder produced under different processing conditions was measured A 10 0 gm sample of powder was taken and pressed into discs of 17 mm diameter and around 12 5 mm thickness using a Carver laboratory press, model M A 17 mm floating die was used and uniaxial double action compaction technique was adopted The maximum pressure applied was 130 MPa The green disc is assumed to be cylindrical shape, and its diameter (d_g) and height (h_g) are sufficient to calculate the volume (V_g)

2 7 12 Compressibility

The compressibility of the ceramic oxide powders produced under various spray drying conditions and with different binder systems was evaluated Uniaxial single action compaction was adopted to measure the compressibility of the powder A sample of 10 0 gm of powder was poured in a die of 17 mm and pressed by an Instron machine, model 4204, up to 110 MPa stress and with a pressing speed of 10 mm/min After the pressing operation, the diameter, height, and weight of the discs were measured with standard instrument The stress and corresponding green density were calculated from the load-displacement curve The compressibility is plotted as a continuous curve of density versus stress

2.7 13 Fired Density

During pressing frictional forces at the powder and die wall interfaces and at particle to particle contacts generate density gradients within the green body[84] As a consequence the disc does not remain perfectly cylindrical after sintering Moreover, during shrinkage the bottom face slides with the supporting powder or the liner material and ends up with a diameter different from that of the top or the middle[85] So the volume of the disc if calculated on the basis of the regular cylinder, will be inaccurate To overcome this difficulties the fired volume (V_f) was calculated considering two cylinders one above the other and using the following equation

$$V_f = \frac{\pi}{64} h_f \left[(d_t + d_b)^2 + 4d_m (d_t + d_b) + 4d^2{}_m \right] \qquad (2\ 6)$$

where h_f, d_t, d_b, and d_m indicate respectively the height, and the diameter at the top, bottom, and the middle of the fired disc

2.7 14 Shrinkage

During the process of firing the green disc shrinks both radially and axially Shrinkage is mainly influenced by the green density This occurs both in the radial and axial direction The radial shrinkage was calculated by using the following equation

$$Radial\ shrinkage = \frac{d_g - d_f}{d_g} \qquad (2\ 7)$$

where d_f is the average diameter of the fired disc The axial shrinkage was calculated as the reduction in height to that of the original height of the green state It was calculated by using the following equation

$$Axial\ shrinkage = \frac{h_g - h_f}{h_g} \qquad (2\ 8)$$

2.7 15 Green Strength

The green strength of the discs is a very important parameter A green body with higher strength facilitates the handling of the discs prior to sintering, thereby, reducing the possibility of mechanical damage such as edge chipping The compact green strength was determined by using diametral compression test The disc was placed on its cylindrical side between two flat plates and load was applied subsequently by an Instron with a cross-head speed of 5 mm/min until the fracture occurred The strength was calculated from the following relationship

$$\sigma_g = \frac{2P}{\pi dh} \qquad (2\ 9)$$

where P = load at fracture
d = diameter of disc
h = thickness of disc

2 7 16 Sintered Strength

The mechanical strength of the sintered disc is a very important property for the electronic ceramics to achieve better electrical performance It is envisaged that a disc with higher mechanical strength could be capable of withstanding more thermal stress due to temperature gradients The energy absorption capability as well as high current performance can thus be enhanced The strength was measured by diametral compression test as before, where the disc was placed in a fixture in between two flat plates and applying the load at a cross-head speed of 1 mm/min The load at fracture was recorded and the strength was calculated using equation 2 9 Dimensions of the fired discs were used to calculate the strength

Chapter 3

EXPERIMENTAL PROCEDURE, EQUIPMENT AND TESTING: VARISTOR PREPARATION

3.1 INTRODUCTION

The critical electrical parameters such as the I-V characteristics, wattloss, and energy absorption capability etc are the determinants of the performance of the ZnO varistor In this regard there can be a large number of input variables emerging from different sources such as the basic composition of the powder, organic systems, processing of powder, compaction, sintering and the finishing operations It is generally thought that the powder with improved characteristics will ensure better devices processed with the standard pressing condition and sintering cycle However, it is not yet established whether the powder with apparently good properties could guarantee the optimum characteristics of the device Therefore, the powder processing parameters are necessary to be optimized on the basis of the electrical performance The study is mainly focused on the evaluation of the effect of the spray drying conditions, various binder systems, and different narrow size fractions of powder A few spray dried samples were investigated if there was any influence on the microstructures In addition to that a separate study was carried out to observe the effect of passivation thickness on the energy absorption capability

3 2 PREPARATION OF SAMPLES

There are various operations in the varistor manufacturing The major processing steps have been schematically illustrated in Figure 1 2 in chapter 1 All of the major operations were performed for each type of varistor but the methods might be different in some cases depending upon the size of the varistor The general procedure of varistor fabrication is briefly discussed below and the specific methods adopted for different categories are elaborated in the respective sections

Cylindrical green bodies were produced from the powder by pressing, using the laboratory and the production press Uniaxial double action compaction technique was used for both the cases The compacted green discs were sintered in the pot as well as in the production line kiln with standard firing profile

Passivation or glassing of the fired blocks is critical to achieve the required high current characteristics It was done by (i) preheating of the discs (ii) spraying the glass slurry on the side surface and (iii) firing in the glass oven The main purpose of glassing is to prevent “flashover” from electrical transient surges at high voltage fields as well as to improve the long term stability of the block

The flat faces of the varistors are ground, with the purpose of (i) achieving dimensional accuracy (ii) having parallel faces with good edge quality (iii) removal of surface contamination and shallow pinholes, and (iv) providing a surface with adequate roughness for good adhesion of thermally sprayed aluminum electrode

Ultrasonic washing was performed to clean the discs by passing them through an automatic system The samples were vibrated ultrasonically during washing to clean them properly After drying, they were inspected visually to identify the defects such as pinholes or damaged edges The blocks with pinholes or chipped edges were usually ground again if the thickness is more than the lower limit of the specified value

Electroding was done on the flat faces of the cylindrical discs by spraying aluminum in an electric arc spray The area covered by the electrode and their adhesion are important in the context of electrical conduction

The electrode surface produced by the electric arc spray usually contains some loose particles and is not smooth So a buffing operation is performed to remove the loose particles Wool fiber is used as the buffing medium and the samples are held gently keeping the face against the rotating fiber medium Aluminum dust sticking loosely on the varistor body is removed by passing them through the ultrasonic washing system again

3.2.1 Varistor from Powder with Different Spray Drying Conditions

The powders produced under different spray drying conditions using both the spray dryers were pressed to produce compact discs A tableting press, Stokes model T4, was used for the powders from the laboratory scale dryer A target weight of 10 0 gm of powder was taken to produce green compacts of 17 mm in diameter and approximately 10 0 mm in thickness Eight 17 0 mm discs were produced for each laboratory type of powder, whereas powders from the pilot scale dryer were pressed using the production line machine (Hydramet Model HC-75EC Compacting Press) A target weight of 159 0 gm of powder was taken to produce green compacts of 38 mm in diameter A standard pressing cycle was used and uniaxial double action compaction technique was adopted The peak load applied for pressing three discs at a time was 25 ton leading to a pressure of about 74 MPa Twelve blocks were pressed for each type of powder They were sintered in a pot kiln with a peak temperature of 1120 °C But the total firing time was different for the two categories of discs It was 65 0 hours for the small and 70 0 hours for the large discs The fired dimensions were measured and the large blocks were processed through the standard procedure using the production line facilities whereas the small ones were processed according to the procedure as outlined in the following section The electrical properties evaluated to optimize the spray drying parameters are discussed in the subsequent sections

3.2.2 Varistor Processed with Different Binder Systems

In order to fabricate varistors from powder processed with different binder systems a target weight of 10 0 gm of powder was taken The powder was pressed in the laboratory type compacting machine (Carver press, model M), using a 17 0 mm floating die Uniaxial double action compaction technique was adopted and the maximum stress applied was 130 MPa Fifteen samples were pressed for each type of powder in this case The discs were sintered in the pot kiln using conventional firing profile of peak temperature 1120 °C and the total sintering time of about 65 0 hours The fired dimensions of the discs were measured by standard instrument Passivation was done by using standard process Grinding was performed manually in the laboratory type grinder (Rotary Pregrinder, Metaserv) using grinding paper of grit size 120 Ultrasonic washing was carried out in the ultrasonic cleaner (Hilsonic) Ground height of the discs was recorded A 14 mm screen-printer was used to deposit a thin layer of silver on both the faces of the varistor which was fired in the glass oven to secure sufficient adhesion The procedure of electrical characterization is discussed in the subsequent sections

3.2.3 Varistors with Powder of Different Size Fractions

Powder with different narrow size fractions (a description of separating powder into different size fractions is already given in section 2 6) was pressed into 38 mm cylindrical blocks in the Hydramet Hydraulic Press The blocks were processed following the procedure similar to that mentioned in section 3 2 1

3.2.4 Varistor Passivated with Different Glass Thickness

The arrester blocks are passivated with glass material to prevent dielectric breakdown when subjected to stresses due to transient electrical surges The material property and thickness of the coating are very critical in this respect In this study the effect of glass thickness was evaluated with standard glass material and usual glassing procedure Samples of 32 mm fired diameter were collected from the production line Forty five discs were randomly grouped into three cells, fifteen in each the glass thickness was varied by passing the discs through the glass spraying system Thus the first cell was sprayed once, the second cell twice, and the third cell thrice After firing, the measurement of dimensions was carried out to estimate the glass thickness All the blocks were processed according to the procedure mentioned earlier in order to appraise the energy absorption capability

3.3 TESTING EQUIPMENT

Once the processing of the varistors was complete, they were ready for electrical testing and characterization The testing requires a wide range of currents with pulses of different peak values and time duration to evaluate the I-V characteristics It is not possible to use the same equipment for all types of characterization Not only that, sometimes for the same characterization but of various geometry of discs, different equipment was necessary The pre-breakdown, non-linear, and upturn regions of the I-V curve were measured by dc and 60 Hz alternating current, and 8X20 and 4X10 μs peak pulse wave respectively The energy absorption capability was estimated by long wave of 2 ms duration Brief *description* of the *equipment* used for electrical characterization is given in the following sections

High Voltage Test System

The High Voltage Test System consists of two parts (i) Kepco power supply unit (model BOP 1000M) and (ii) Keithley data measurement unit (model 237 SMU) The power supply unit can be operated within the range of 0-5000 volt and 0-5 mA current in dc mode The system is capable of measuring the leakage current at 1200 volts, the value of rated voltage V_r at 10 µA, delta V at 50 µA, and the nominal voltage at 1 mA The varistor was placed one by one in the sample holder and the lid was closed to take the measurement The data measured were stored in the computer memory On completion of the test with all the samples, the stored data were retrieved in the printed form

Wattloss High Temperature Tester

The equipment (model LC-1201B) is composed of (i) High voltage control panel and (ii) Ambient test/Select panel The machine is operated in the ac mode and the current-voltage characteristics of up to 10 mA can be measured Of the available modes a set point of 10 mA at the ambient temperature is selected to measure the I-V characteristics at pre-breakdown region for arresters By placing the individual test sample in the holder, the powerstat knob in the control panel was rotated clockwise until the desired current level was attained The voltage for the particular current was recorded and the procedure was continued for all the test pieces

Classifier

The voltage of the non-linear region was measured at a current of 100 A and 5 KA by 8X20 μs peak pulse wave Haefely impulse generator (model no WO 4433-34) with capacity of 30 KV and 4KJ/27J was used The main components of the machine are (i) impulse current generator (ii) impulse peak voltage and (iii) trigatron

There are two parts of the impulse current generator test circuit consisting inductance, capacitance, and resistance in the circuit The values of them are different for 100 A and 5 KA test The Impulse peak voltmeter measures and stores the peak value of impulse voltages and currents The trigatron is used for automatic control of impulse generator which performs the following functions

(i) regulates the charging of the impulse generator with digitally adjustable charging time and voltage

(ii) automatic stabilization of charging voltage at preset value

(iii) automatic adjustment of the "sphere gap" of the generator in accordance with the selected charging voltage

HASD Tester

The voltage at the upturn region is measured by an impulse current test system (model WO 4924) The main components of the system are (i) impulse current generator (ii) charging rectifier (iii) control unit and (iv) resistive impulse voltage divider

The impulse generator is capable of measuring the high amplitude pulses of different duration Depending upon the type of ZnO varistors and the current, appropriate circuit is selected and the charging voltage of the generator is adjusted to obtain the required peak current

The charging rectifier of type (LGR 100/15) is designed for use in the S-series impulse voltage test system The control unit is used to co-ordinate and control the impulse generator, charging rectifier, safety system, and triggerable auxiliary equipment

Resistive impulse voltage dividers are used to measure the lightning impulse voltages, as well as, the high impulse voltages with the steep wave fronts

Strength Tester

The energy absorption capability of the varistors was performed in Haefely (model no WO 4435-36) impulse generator with capacity of 50 KV and 45 KJ The main components of the machine are (i) impulse generator (ii) impulse peak voltmeter and (iii) trigatron

The generator produces square waves which consists of LC network of capacitor and reactor coils in between the capacitors The shape of the square wave is given in Figure 3 1

The peak value of the impulse voltages are measured by type 64 M impulse peak voltmeter The peak value of high voltage is displayed by a built-in multiplier

The type 94 Trigatron is used as a semi-automatic control unit for the impulse generator The charging action is controlled by the trigatron through a solid state controller The transient current peaks are suppressed and the generator is charged with an approximately constant current level

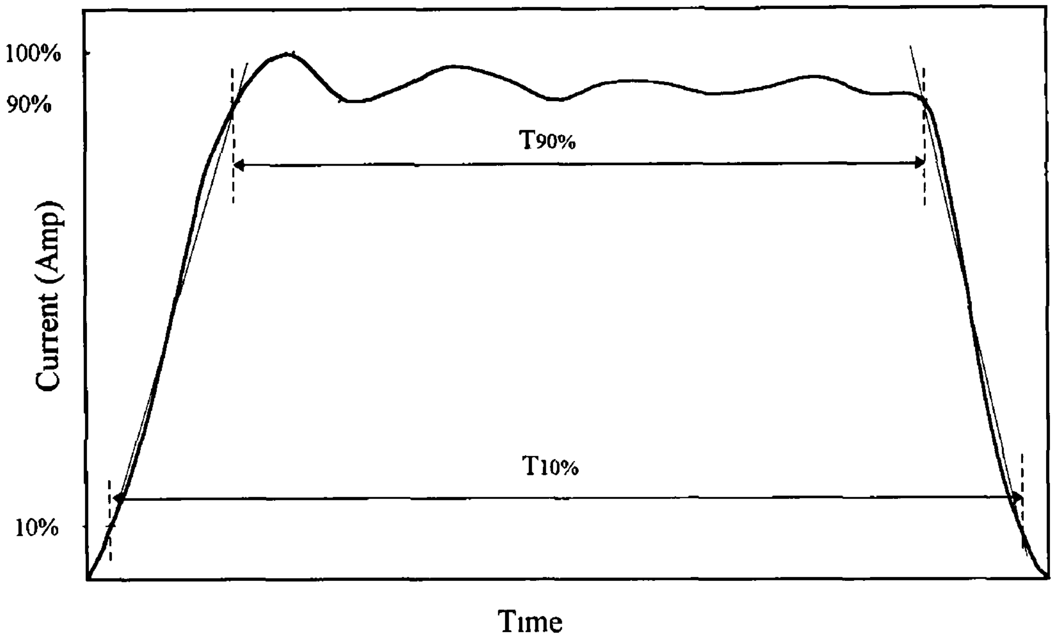

Figure 3 1 The shape of the square-wave current applied to evaluate the energy of varistor

3.4 ELECTRICAL CHARACTERISTIC PARAMETERS

Zinc oxide varistors are characterized by the I-V curve in low, medium, and high current regions The various regions associated with the I-V curve serves various functions in the design and operation of a surge protector The most suitable device should have a low value of clamping ratio and leakage current, a high value of non-linear co-efficient and energy absorption capability, and a longer life A brief description of the important parameters and their measuring techniques adopted for different categories of varistors are outlined below

3 4 1 Pre-breakdown Region

The pre-breakdown region determines the steady state joule heating and the nominal voltage of the varistors The current-voltage relationship is ohmic in this region and is controlled by the resistivity of the grain boundary It was calculated at the rated level for the small discs by the High Voltage Test System However, the voltage at a current of 0 1, 0 3, 1 0, and 5 0 mA were measured by the Wattloss High Temperature Tester at a set point of ambient temperature and 10 mA current for the arrester blocks

Wattloss

The degradation of a varistor is a complex phenomenon which is considered to be a function of barrier height, donor density, and breakdown voltage of the grains and their boundary[13 86 93] The gradual weakening of the barrier height due to the field assisted ion migration and/or current channeling through the high conductivity paths are responsible for degradation Varistors are required to sustain a constant bias voltage in normal operation without significant degradation Wattloss is the measure of degradation and this was measured at 80% of the voltage at 1 mA and 5 mA current respectively for small and large discs in the Wattloss High Temperature Tester This corresponds to $0\ 8E_{0\ 6}$ where the figure in subscript indicates the current density in mA/cm^2 After applying the high amplitude short duration pulse of peak current 10 KA and 65 KA for the small and for the large discs respectively, the wattloss was again measured at $0\ 8E_{0\ 6}$ for both polarity to estimate the degradation trend

Nominal voltage

Varistors are rated by a voltage at which the flow of current from linear to non-linear mode starts The rated voltage is designated as "threshold", "turn on", "non-linear", or "nominal" voltage The nominal voltage E is evaluated as the voltage per unit thickness for the specified current density As industrial practice, this is usually measured at 1 mA, neglecting the variation in the cross-section of the device The nominal voltage, when normalized, becomes 0 6 mA/cm^2 at 1 mA for small discs and at 5 mA for big discs This figure is very close to the recommended value of 0 5 mA/cm^2 The nominal voltage was evaluated by the following relationship

$$E_{0\,6} = \frac{V}{t} \tag{3 1}$$

where V is the voltage, t is the thickness of the device The value of $E_{0\,6}$ is controlled by the grain size and thus by the number of grains The parameter can be increased by the reduction of the grain size, thereby increasing the number of the grains Sintering parameters are very important in this regard The increase of the sintering time and temperature lead to the bigger grain size and consequently reduce the nominal voltage The High Voltage Test System and Wattloss High Temperature Tester were used to measure the nominal voltage for the small and large devices respectively

3.4 2 Non-linear Region

This region shows the non-linear properties of zinc oxide varistors This is the heart of varistor, wherein the device conducts a large amount of current for a small increase of voltage The degree of non-linearity is determined by the flatness of the region The clamping efficiency, and non-linear co-efficient indicate the flatness The voltages at a current of 100 A and 5 KA were measured by the classifier with pulses of 8X20 μs wave shape

Clamping efficiency

The clamping efficiency of the varistors is defined as the ratio of voltages in the non-linear region This is a very important parameter which affirms the ability of the varistor to limit the transient voltage and the level of protection The clamping ratio was calculated as follows

$$\text{Clamping ratio} = \frac{V_2}{V_1} \tag{3 2}$$

where V_2 is the voltage per unit length at a current density I_2 in the upturn region and V_1 is the voltage per unit length at a current density of I_1 at the onset of the non-linear region V_1 was computed at 1 or 5 mA and V_2 was taken at 1 or 5 KA depending on the discs size Basically the lower the clamp ratio, the better is the device

Non-linear co-efficient

The most critical parameter to characterize ZnO varistors is the non-linear co-efficient The coefficient, α is defined by the following formula

$$\alpha = \frac{d \ln I}{d \ln V} \tag{3 3}$$

The magnitude, therefore, varies with the current density It increases in the pre-breakdown region, attains a maximum value in the non-linear region, then diminishes sharply in the upturn region[13] Moreover, pressure and temperature of the test environment significantly affect the α value The value decreases with the increase of both the temperature[11] and pressure[94] In the non-linear region the higher value of α corresponds to the lower clamp ratio, thereby, providing better protection due to the lower increase of voltage at higher current level The values of the voltage and current were considered the same as the clamping efficiency to calculate α

3 4.3 Upturn Region

This is the high current region, where the I-V characteristics are again linear and the voltage rises faster with current It is controlled by the impedance of the grain and the decrease of grain resistivity can lead to an increase of high current non-linearity The current-voltage relationship was obtained by HASD Tester with peak pulse wave of 8X20 or 4X10 μs duration The peak value of current was considered to be 1 and 10 KA for the small and 65 KA for the large discs

3 4.4 Energy Absorption Capability

Energy absorption capability is considered to be the second most important parameter to judge the performance of zinc oxide varistor This can be calculated from the measured peak current and clamp voltage, and time duration by using the following relationship

$$E = \int_0^t vidt = CVIt \qquad (3\ 4)$$

where, C is a constant and it depends on the wave shape of testing The value of V is taken in volt/cm, I in amp/cm^2 , and t in seconds to calculate energy in J cm ^{3}

The energy absorption capability of the varistors was measured by selecting a charging voltage for a fixed charging time Three repeated shots of 2 ms square wave was applied for each cycle The charging voltage was chosen at a low level so that no failure occurs in the first cycle The injected energy within the varistor was increased by less than 10% for each of the next cycles by increasing the charging voltage The cycle of shots was continued until all of the discs failed The value of clamp voltage and peak current for each cycle was recorded The cumulative curve of energy absorption was plotted from the calculated energy and the number of discs failed at that energy level

Degradation with long pulse application

Conventionally the varistors are tested at a rated energy The rated energy can be increased by subjecting the varistors to screen test, thereby, weeding out the week devices To verify the degradation rate with the application of long wave, some of the varistors were tested to record the wattloss Measurement was performed on each of the samples in the Wattloss High Temperature Tester at 0 8$E_{0\ 6}$ for both polarity after every cycle of shots The testing was continued until all of the discs failed The calculated energy and the measured wattloss were plotted for each cycle to correlate energy absorption and degradation

3.4 5 Microstructure

The microstructure developed during sintering plays an important role in the electrical performance of the ZnO varistor Samples were prepared for microstructural analysis of the varistors produced from powder under different spray drying conditions The sample piece was prepared from the same relative position of each varistor and analyzed by Scanning Electron Microscopy (JEOL, JSM-840A) Photographs were taken using the secondary image and the backscattered electron mode For the first case, topographic features are more clearly seen whereas with the backscattered electron image it is easier to appreciate the chemical (elemental) difference of the sample under observation

3.5 EVALUATION OF DIFFERENT CATEGORIES OF DISCS

The varistors prepared with powders under different processing conditions were characterized electrically However, the properties evaluated were not the same for all categories A brief description of the test parameters corresponding to each category of samples is given below

3 5 1 Spray Dried Samples

The parameters evaluated to optimize the spray drying conditions of both the dryers are the I-V characteristics which include primarily pre-breakdown, non-linear and upturn region The energy absorption capability was estimated only with the larger samples The degradation of the varistors during energy testing, after each cycle of pulses was also measured with the standard samples A few samples were also evaluated microstructurally The measuring techniques adopted were the same as mentioned in the previous sections

3 5 2 Binder Samples

The critical parameters evaluated for the varistors with different binder systems are the I-V characteristics, and the energy absorption capability Due to the small size of the varistor, the current-voltage data at the pre-breakdown region was obtained by the High Voltage Test System The upturn region was determined at a current of 1 and 10 KA by HASD tester with peak pulse wave of 8X20 μs The calculation procedure of wattloss, clamping efficiency, non-linear co-efficient, and energy absorption capability were the same as discussed earlier

3.5.3 Different Particle Size Fraction Samples

The parameters evaluated were the I-V characteristics, wattloss, and energy absorption capability to assess the influence of particle size fractions on varistors Similar computing procedures were adopted to evaluate the different parameters

3.5.4 Samples with Various Glass Thickness

The effect of glass thickness on the varistor performance was investigated on the basis of energy absorption capability The values of peak current and corresponding voltage were collected in the same way as mentioned in the earlier section

Chapter 4

DATA ANALYSIS AND MODEL FORMULATION

4.1 INTRODUCTION

An experimental design technique was adopted to carry out the experiments so that the results could be analyzed by the standard methods Data are generally not exact, commonly subjected to errors emerging from the process variation and the measurement technique Therefore, the typical data do not exactly fit the model that is being developed, even when the model is adequate

Statistical methods are often considered to be useful tools to analyze the results They are easy and simple to design an experiment, to evaluate the data, and also to quantify their reliability on the responses for a process which is influenced by multiple input parameters In this regard factorial design, response surface methodology are very common Ceramic strength usually exhibits considerable scattering The Weibull distribution was adopted to analyze the green as well as the fired strength of the ceramic A brief description of the techniques such as factorial design, response surface methodology, and Weibull theory is given in the following sections

4.2 FACTORIAL DESIGN

Factorial designs are widely used in the experiments to estimate the main and interacting effects of several independent variables on the response[95 96] There are various special cases of factorial design of which 2^k is particularly very important in the early stage of the experimental work Only two levels are considered for each of the k factors and it is assumed that the response is linear over the range of the level chosen The variables are denoted as "-" and "+" or "-1" and "+1" This is entirely arbitrary but very effective for analyzing the results The 2^k factorial allows independent estimates of k (where k is the dimension of the design) main effects, ${}^kC_2$ two-factor interactions, ${}^kC_3$ three factor interactions, and one k-factor interaction That is, for a 2^k design the complete analysis will contain 2^k -1 effects

Fractional factorial design is another popular means of analyzing the data when the number of variables, k is large It is often true, that the main effects are larger than two-factor interactions, which in turn tends to be higher than three-factor interactions and so on The "effect" of a factor or a variable means the change in response due to the movement from the lower level to higher level and the average of the "effect" is called the "main effect" for a particular variable All of the variables in an experiment do not behave additively and are therefore, said to "interact" The interactive effect is measured from the difference of the "main effects" Usually the higher order interactions tend to become negligible and can be disregarded Not only that, under some experimental conditions, it is not possible to set all the variables using 2^k factorial design and hence redundancy is required The design for the factorial analysis is constructed in the following way

(i) If there are k number of variables, a full $2^{k\ 1}$ design will be written for the k-1 variables

(ii) The column of signs for the 1,2, k-1 interaction will be written and that will be used to define the levels of the kth variables

Thus with three variables by half factorial design, only four experiments are sufficient This is called resolution III design, where no main effects are confounded with any other main effect, but the main effects are confounded with two-factor interactions and two factor interactions are confounded with each other

4 3 RESPONSE SURFACE METHODOLOGY

Response surface methodology or RSM is a collection of mathematical and statistical techniques used in the empirical study of the relationships between the measured responses and a number of input variables[95,96] The ultimate goal of the use of RSM is to optimize the response The method is widely used because of some attractive features such as (i) it is a sequential approach, the result at each stage guiding the experimentation to be conducted at the next (ii) it casts the experimental problem in readily understandable geometric terms and (iii) it is applicable for any number of variables The independent variables are denoted by x_1, x_2, x_3, ,x_k and are assumed to be continuous and controllable by the experimenter, whereas, response, y, is assumed to be a random variable in response surface methodology

As the relationship between the response and the independent variables is unknown, the first step in RSM is to fix a true functional relationship between y and the set of independent variables Usually a low order polynomial is considered for the first-order model and a higher-order polynomial is assumed for the second-order model In the first-order model, $(y = \beta_o + \sum_{i=1}^{k} \beta_i x_i + \in)$, orthogonal first-order designs are adopted which includes the 2^k factorial The k factors are coded to the standardized levels ±1 But the 2^k design does not afford an estimate of the experimental error, until some runs are replicated Hence, a centre point is considered and replicated The addition of the centre point does not influence { β_i} for i ≥1, but the estimates of β_o becomes the grand average of all observations Furthermore, the addition of the centre point does not alter the orthogonal property

4.4 WEIBULL THEORY FOR FRACTURE STRENGTH

There are two classes of theories to predict the strength of the brittle materials The first is derived from Griffith's flaw theory[97], which assumes the presence of flaws of a specific shape, and there is always one with the least favourable orientation and the crack growth from this flaw causes failure The second class is statistical but it fails to specify the nature of the flaw But, in a ceramic, there are a range of flaw sizes which results in a corresponding variation in strength The most popular means of characterizing the flaw distribution is by the Weibull approach[98] The probability of failure in a structure is predicted by dividing the total volume into many volume elements, each element has a probability of failure The probability of survival of the part as a whole is obtained by multiplying the probabilities of survival of all the elements It is based on the weakest link theory[99], which assumes that a given volume of ceramic under a uniform stress will fail at the most severe flaw Thus the properties of the volume element as inferred from the statistics of fracture in the simple tension or bending play a major role in Weibull's theory

The theory states[100] that the probability that rupture will occur within a given volume subjected to any uniform stress is assumed to be completely determined by the quantity σ, which can be calculated from the three principal stresses In the case of a solid subjected to any load, the probability that the ultimate strength will not be reached is equal to the probability that the rupture does not occur in any parts of the solids If a solid is imagined to be divided into n volume elements for which the individual probability of rupture are S_1, S_2, S_n

respectively, the probability of rupture, S for the solid as a whole is, therefore, given by the equation

$$1-S=(1-S_1)(1-S_2)\quad(1-S_n) \tag{4 1}$$

This equation can be taken to be the fundamental formula for all regular materials If all individual element probabilities are equal to S_o, we have

$$1-S=(1-S_o)^n \tag{4 2}$$

For infinitely small elements S_o becomes infinitely small In this case we may omit the infinitely small quantities of higher order and thus obtain

$$S=nS_o \tag{4 3}$$

This equation means that the probability of rupture is proportional to the volume Consequently the distribution function for an infinitely small volume dV may be written as follows

$$S_o=f(\sigma)dV \tag{4 4}$$

The equation is valid only when $f(\sigma)$ is finite and dV is infinitely small By the use of equation (4 1) we obtain

$$\log(1-S)=\sum_{i=1}^{n}\log(1-S_i) \tag{4 5}$$

If n increases indefinitely, S_i converges towards zero and then equation (4 5) will have the following form

$$\log(1-S_i) = -S_i \tag{4 6}$$

By the use of equation (4 4) we have

$$\log(1-S) = -\int f(\sigma)dV \tag{4 7}$$

The function *"f"* is determined by the distribution constants of the material It varies from point to point in an anisotropic solid If these constants and the distribution of stress are known, the quantity "B" known as the "Risk of Rupture" may be computed from the following equation

$$B = \int f(\sigma)dV \tag{4 8}$$

According to equation (4 7) the distribution function takes the form

$$S = 1 - \exp^{-\int f(\sigma)dV} \tag{4 9}$$

For an isotropic solid subjected to uniform stress, the formula takes the simpler form

$$S = 1 - \exp^{-vf(\sigma)} \tag{4 10}$$

Thus the calculation of the strength of a solid starts with the calculation of risk of rupture "B" from equation (4 8) The stress distribution function *f(σ)* is assumed to have the following form to calculate the risk of rupture

$$f(\sigma) = \left(\frac{\sigma}{\sigma_o}\right)^m \tag{4 11}$$

where σ_o = normalizing parameter, selected as characteristic stress at which the probability of failure is 0 632

m = Weibull modulus, which describes the scattering of the data, the higher is the value the better is the uniformity

Thus by substituting equation (4 11) into equation (4 10) we have

$$S = 1 - \exp^{-v\frac{\sigma^m}{\sigma^m_o}} \qquad (4\ 12)$$

The values of σ_o and m are determined by the least square method from the following equation

$$\ln\left(\ln\frac{1}{1-S}\right) = \ln V - m\ln\sigma_o + m\ln\sigma \qquad (4\ 13)$$

where S is the probability of rupture This was calculated from the number of specimen under test, by giving each specimen a rank after sorting the stress values from the tests in an ascending order

$$S = \frac{i}{N+1} \qquad (4\ 14)$$

where i is the test rank and N is the number of the tested specimens

4 5 SPRAY DRYING PARAMETERS

The powder produced through the laboratory scale spray dryer was analyzed to find the main and interacting effects of the spray drying variables on the powder characteristics The analysis was carried out by considering feed flow rate, atomizing air pressure, and drying air flow rate as independent variables, while bulk and tap density, moisture content and mean particle size were taken as dependent variables A mathematical model was developed to describe the mean particle size of the spray dried granules in terms of three input variables The measured property of powder from the small spray dryer was used to develop the model The effect on the electrical properties of the arresters was investigated by characterizing the powder produced by the pilot scale dryer A two level half factorial design was adopted to evaluate the effect of the spray drying parameters For this purpose arresters were prepared from the powder produced under different spray drying run conditions The nominal voltage, wattloss, clamp ratio, non-linear co-efficient and energy absorption capability were measured to estimate the electrical properties of the varistor

4 5 1 Powder Characteristics

A two level full factorial design was applied to determine the main and interacting effects of the spray drying variables on the powder characteristics The three input variables, their codes, and the corresponding responses e g mean particle size, moisture content, bulk, and tap densities etc are presented in Table 4 1 The effects determined by the factorial design are summarized in Table 4 2

Table 4.1 Data for 2^3 full factorial design and the responses on the powder characteristics

No of run	Drying air flow rate (m^3/min)	Atomizing air pressure (Kg$_f$/cm^2)	Feed flow rate (ml/min)	Mean particle size (µm)	Moisture content (%)	Bulk density (gm/cc)	Tap density (gm/cc)
1	(-)0.6	(-)0.8	(-)26	57	0.24	1.97	2.29
2	(+)0.8	(-)0.8	(-)26	57	0.23	1.78	2.17
3	(-)0.6	(+)1.2	(-)26	46	0.30	1.77	2.10
4	(+)0.8	(+)1.2	(-)26	43	0.27	1.75	2.18
5	(-)0.6	(-)0.8	(+)39	60	0.33	1.99	2.33
6	(+)0.8	(-)0.8	(+)39	65	0.35	1.87	2.26
7	(-)0.6	(+)1.2	(+)39	54	0.35	1.81	2.15
8	(+)0.8	(+)1.2	(+)39	50	0.37	1.89	2.22

It is evident from the values in Table 4.2, that the feed flow rate and the atomizing air pressure have main significant effects on the mean particle size. The drying air flow rate has very insignificant individual effect on this parameter but its interactive effects with the atomizing air pressure is not negligible. Therefore, the influence of different variables can be summarized as follows:

(i) The effect of change of feed flow rate from the lower to a higher level has raised the mean particle size by 6.5 µm.

(ii) The increase of atomizing air pressure from the lower to a higher level has resulted to drop the mean particle size by 11.5 µm. Since the effect of atomizing air pressure and drying air flow rate cannot be interpreted separately because of their interaction, a two way table pictorially given in Figure 4.1 can be used to describe the interactive effects.

Table 4 2 Main and interactive effects of the spray drying variables on the powder characteristics

Main and interactive effects	Responses			
	Mean size (µm)	Moisture content (%)	Bulk density (gm/cc)	Tap density (gm/cc)
Drying air flow rate (1)	-0 50	0 00	-0 063	-0 010
Atm air pressure (2)	-11 5	0 035	-0 098	-0 100
Feed flow rate (3)	6 5	0 090	0 093	0 055
Interaction (12)	-3 0	-0 005	0 085	0 085
Interaction (13)	1 00	0 020	0 050	0 010
Interaction (23)	1 00	-0 015	0 025	-0 010
Interaction (123)	1 50	-0 075	0 000	0 015

At lower level of the drying air flow rate, the change of the atomizing air pressure from the lower to higher level has reduced the mean particle size by 8 5 µm, while at higher level, the change has reduced the size by 14 5 µm The sensitivity of the atomizing air pressure at higher level of the drying air flow rate is due to the fact that the dryer becomes thermally less efficient This leads to agglomeration owing to the presence of the binder in the feed slurry

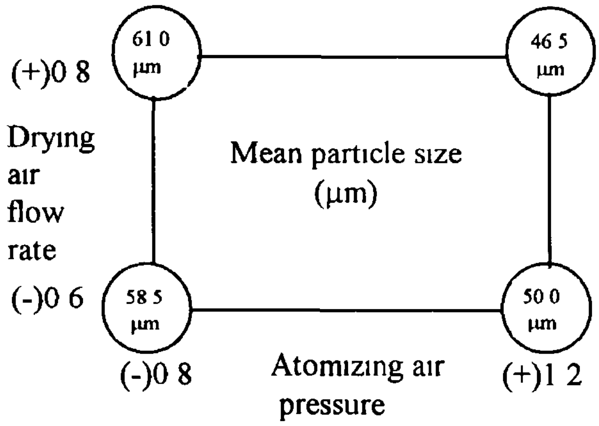

Figure 4.1 The interaction of the drying air flow rate and the atomizing air pressure on the mean particle size of powder

The feed flow rate was found to have a positive effect on the moisture content of the spray dried powder as it led to an increase in the moisture content by 33 5% when changed from lower to a higher level It is thought that for a set condition of other operating variables, the higher drying air flow rate will lower the moisture content in the powder However, the result of statistical analysis does not validate the assumption This may be due to the fact that the level at which the drying air flow rate has been varied had no significant influence on the moisture content of the powder

The bulk density was mainly influenced by the feed flow rate and the atomizing air pressure The interactive effect of the drying air flow rate and the atomizing air pressure was also found to be significant for the bulk density The influence of the atomizing air pressure and its interactive effect with the drying air flow rate are prominent on the tap density

4 5 2 Modelling for the Mean Particle Size

The mathematical model for the mean particle size of the spray dried granules was developed by using response surface methodology (RSM) It is a simple way to establish the relationship between the independent variables and the response The developed relationship is capable of predicting the mean particle size in terms of the drying air flow rate, the atomizing air pressure and the feed flow rate The method has been successfully used in various areas e g the chemical process industry[101], in predicting tool life[102 104], and the surface roughness analysis[105] amongst others

Experimental design and conditions

To develop the first order model, a design consisting of twelve experiments was carried out The first eight experiments formed the 2^3 factorial design and the rest were from the centre point which was replicated four times The added centre point was used to estimate the pure error Figure 4 2 shows the 2^3 composite design In Table 4 3 the levels of independent variables and coded identifications are given The input operating conditions and the measured mean particle size as response are presented in Table 4 4

Postulation of model

The functional relationship between the response (mean particle size) and the investigated independent variables can be written by the following equation

$$D_{avg} = Cf_d^{\,k} p^l f_f^{\,m} \in' \qquad (4\ 15)$$

where D_{avg} = mean particle size (μm)

f_d = drying air flow rate (m^3/min)

p = atomizing air pressure (Kg_f/cm^2)

f_f = feed flow rate (ml/min) and

C, k, l, and m are the constants and $\in'$ is a random error

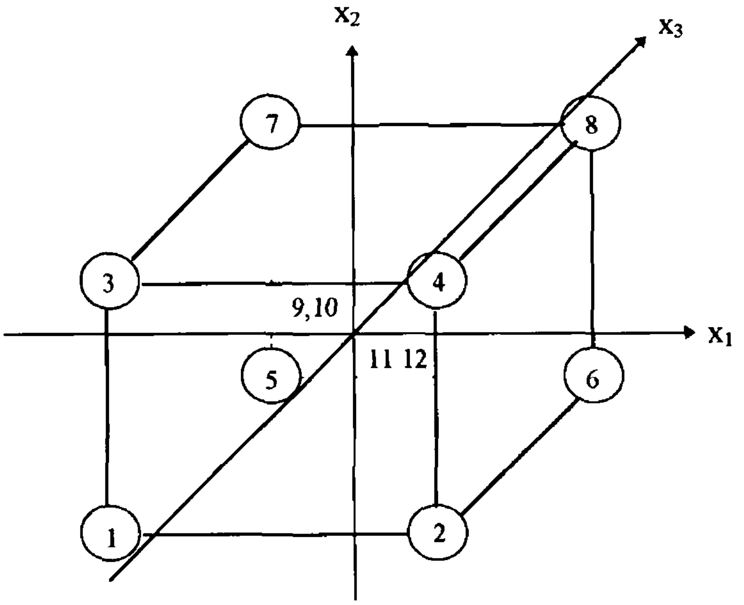

Figure 4.2 2^3 Central composite design for the first order model

Table 4.3 Levels of independent variables

Levels of parameters	Low	Centre	High
Coding	-1	0	+1
Drying air flow rate (m^3/min)	0.6	0.7	0.8
Atomizing air pressure (Kg_f/cm^2)	0.8	1.0	1.2
Feed flow rate (ml/min)	26	30	39

Equation (4.15) can be written in the following logarithmic form

$$\ln D_{avg} = \ln C + K \ln f_d + l \ln p + m \ln f_f + \ln \in' \qquad (4.16)$$

which can be written by the following linear model

$$y = \beta_o x_o + \beta_1 x_1 + \beta_2 x_2 + \beta_3 x_3 + \in \qquad (4.17)$$

where y is the measured mean particle size in the logarithmic scale, while $x_o = 1$ (dummy variables), and $x_1 = \ln f_d$, $x_2 = \ln p$, $x_3 = \ln f_f$, $\in = \ln \in'$ where $\in$ is assumed to be normally distributed uncorrelated random error with zero mean and constant variance, $\beta_o = \ln C$, β_1, β_2, and β_3 are the model parameters The estimated response can be written as

Table 4.4 Experimental conditions and the response

No of run	Drying air flow rate (m^3/min)	Atomizing air pressure (Kg_f/cm^2)	Feed flow rate (ml/min)	Coding			Mean size (µm)
				x_1	x_2	x_3	
1	0 6	0 8	26 0	-1	-1	-1	57 0
2	0 8	0 8	26 0	+1	-1	-1	57 0
3	0 6	1 2	26 0	-1	+1	-1	46 0
4	0 8	1 2	26 0	+1	+1	-1	43 0
5	0 6	0 8	39 0	-1	-1	+1	60 0
6	0 8	0 8	39 0	+1	-1	+1	65 0
7	0 6	1 2	39 0	-1	+1	+1	54 0
8	0 8	1 2	39 0	+1	+1	+1	50 0
9	0 7	1 0	30 0	0	0	0	54 0
10	0 7	1 0	30 0	0	0	0	52 0
11	0 7	1 0	30 0	0	0	0	55 0
12	0 7	1 0	30 0	0	0	0	53 0

$$\hat{y} = y - \in = b_o x_o + b_1 x_1 + b_2 x_2 + b_3 x_3 \qquad (4\ 18)$$

where $\hat{y}$ is the estimated response, b_o, b_1, b_2, and b_3 are the estimates of β_1, β_2, and β_3 respectively The values of b are to be estimated by least square method from the following relationship

$$b = \left(X^T X\right)^{-1} X^T Y \qquad (4\ 19)$$

where, X is the calculation matrix, X^T is the transpose of X, X^TX is the variance matrix, $(X^TX)^{1}$ is the co-variance matrix which is the inverse of X^TX and Y is the matrix of response in logarithmic scale

The transforming equations corresponding to each of the independent variables are

$$x_1 = \frac{\ln f_d - \ln 0\,7}{\ln 0\,8 - \ln 0\,7} \qquad (4\ 20)$$

$$x_2 = \frac{\ln p - \ln 1\,0}{\ln 1\,2 - \ln 1\,0} \qquad (4\ 21)$$

$$x_3 = \frac{\ln f_f - \ln 30}{\ln 39 - \ln 30} \qquad (4\ 22)$$

The developed model for the mean particle size stands as

$$\hat{y} = 3\,98 - 0\,00875x_1 - 0\,107x_2 + 0\,0611x_3 \qquad (4\ 23)$$

Solving equation (4 20), (4 21), (4 22), and (4 23) the developed model can be presented as

$$D_{avg} = 23\,67 f_d^{-0\,066} p^{-0\,587} f_f^{\,0\,233} \qquad (4\ 24)$$

The equation is valid in the following range of the drying air flow rate, atomizing air pressure, and the feed flow rate

$0\ 6 \le f_d \le 0\ 8$ m^3/min

$0\ 8 \le p \le 1\ 2$ Kg$_f$/cm^2

$26 \le f_f \le 39$ ml/min

Reliability of the model

Due to the experimental error $\in'$, the estimated mean particle size is subjected to uncertainty Hence the precision of the model can be estimated by calculating variance and the confidence intervals which are presented in Tables 4 5 and 4 6 respectively

Table 4.5 Analysis of variance for the first order model

Source	Sum of squares	Mean squares	degrees of freedom	F_{cal}	F_{tab}
Zero-order term	190 112661	190 113	1	326166 49	9 01
First-order term	0 1242985	0 041433	3	71 08	
Lack of fit	0 010002	0 0020000	5	3 432	
Pure error	0 001749	0 0005828	3		
Total	190 2487				

The ratio of lack of fit to pure error is 3 432 while for 95% confidence interval the tabulated F-statistic with $v_{5\ 3}$ is 9 01 In addition to that the same confidence intervals are found to be narrow Therefore, the model can be conveniently considered to be adequate

The model as given in equation (4 24) indicates that the mean particle size of the spray dried granules decreases with the increase of the drying air flow rate and the atomizing air pressure, whereas the trend is reversed with the feed flow rate Higher feed flow rate leads to an increase in the mean particle size However, the dominating factors on the response are atomizing air pressure and the feed flow rate as evident from the magnitude of the exponents

Table 4.6 95% confidence intervals for the model

$(\hat{y} = 3.98 - 0.00875x_1 - 0.107x_2 + 0.0611x_3)$

No of run	D_{avg}	y	$\hat{y}$	$\hat{D}_{avg}$	$\hat{y}$		$\hat{D}_{avg}$	
					Lower	Upper	Lower	Upper
1	57.0	4.043	4.088	59.62	4.0104	4.1656	55.28	63.96
2	57.0	4.043	4.069	58.50	3.9914	4.1466	54.16	62.84
3	46.0	3.828	3.849	46.99	3.7714	3.9266	42.65	51.33
4	43.0	3.761	3.831	46.11	3.7534	3.9086	41.77	50.45
5	60.0	4.094	4.182	65.53	4.1044	4.2596	61.19	69.87
6	65.0	4.174	4.163	64.30	4.0854	4.2406	59.96	68.64
7	54.0	3.989	3.945	51.65	3.8674	4.0226	47.31	55.99
8	50.0	3.912	3.925	50.68	3.8474	4.006	46.34	55.02
9	54.0	3.989	3.980	53.53	3.9024	4.0576	49.19	57.87
10	52.0	3.951	3.980	53.53	3.9024	4.0576	49.19	57.87
11	55.0	4.007	3.980	53.53	3.9024	4.0576	49.19	57.87
12	53.0	3.970	3.980	53.53	3.9024	4.0576	49.19	57.87

4.5.3 Electrical Characteristics

A two level half factorial design was applied to estimate the main and interacting effects of the spray drying variables on the electrical properties of the varistor. The feed flow rate, the atomizing air pressure, and the drying air outlet temperature were considered as the independent variables. Whereas, nominal voltage, wattloss, clamping ratio, non-linear exponent, and energy absorption capability were taken as dependent variables. In Table 4.7 the arrangement of the input data and the corresponding responses are presented. The main and interactive effects were evaluated and given in Table 4.8. It is noticeable from the analysis that the spray drying variables do not have any significant effect on the wattloss, clamp ratio, and non-linear coefficient or exponent, α. The nominal voltage is largely influenced by both the atomizing air pressure and the feed flow rate and it increases with an increase of the atomizing air pressure and a decrease of the feed flow rate An increase in the atomizing air pressure and a decrease in the feed flow rate will result in finer atomization which can consequently enhance the nominal voltage

Table 4 7 Data for 2^3 half factorial design and responses on electrical properties

No of run	Atom air pressure (psi)	Feed flow rate (ml/min)	Drying air outlet temp °C	Nominal voltage (Volt/cm)	Watt-loss (W cm^{3})	Clamp ratio	Non-linear co-efficient	Energy (J cm^{3})
1	(-)10	(-)71	(+)130	2081	0 012	1 73	25 15	330
2	(+)40	(-)71	(-)115	2150	0 01	1 73	25 25	358
3	(-)10	(+)258	(-)115	2054	0 011	1 74	24 95	418
4	(+)40	(+)258	(+)130	2090	0 011	1 74	25 07	391

The interactive effect of the atomizing air pressure and the feed flow rate was also found to be significant for the nominal voltage

Table 4 8 Main and interactive effects of spray drying variables on electrical properties

Main and interactive effects	Nominal voltage (Volt/cm)	Wattoss (W cm^{3})	Clamp ratio	Non-linear co-efficient	Energy (J cm^{3})
Atomizing air pressure (1)	52 5	-0 001	0 00	0 11	0 50
Feed flow rate (2)	-43 5	0 00	0 01	0 19	60 5
Interaction (12)	-16 5	0 001	0 00	0 01	-27 5

The energy absorption capability of the varistor is significantly influenced by the feed flow rate The change of the feed flow rate from lower to a higher level has resulted in an enhancement of the energy absorption capability However, the interacting effect of the atomizing air pressure and the feed flow rate is not negligible At lower level of the atomizing air pressure the effect of the change of feed flow rate is more prominent than at the higher level of atomizing air pressure

4 6 BINDER SYSTEMS

The influence of the two input parameters, the content of binder and solid concentration on the powder characteristics and the electrical properties was studied The physical powder properties were bulk, tap, granule, and green densities, mean particle size, and green strength of the compacted discs The electrical properties such as the nominal voltage, non-linear co-efficient, wattloss, and the energy absorption capability were measured The strength of the green and the fired discs was measured by diametral compression test The Weibull parameters were determined to test the repeatability of the strength

4 6.1 Powder Characteristics

Extensive study was conducted to evaluate the effect of the binder and their blends Initially a comparative evaluation between the conventional and the latex binder was performed Several latex binders were chosen for initial experiment On the basis of the powder characteristics the best binder was selected Enhanced powder characteristics were observed with the use of the latex binder, Ltx C Therefore, a two level factorial design was chosen to optimize the concentration of the binder and the solid in the slurry In Table 4 9 the level of the binder and the solid, its code name, and the corresponding responses and in Table 4 10 the main and interactive effects are presented

The analysis indicates that the bulk, tap, granule, and green densities, and the flowability are mainly influenced by the solid level in the slurry The positive value of the effects demonstrates that the properties will be enhanced with the increased solid concentration Whereas, the mean particle size will be significantly influenced by the binder

Table 4 9 2^2 factorial design and the responses on the powder characteristics with different level of binder and solid content

Input parameters		Responses						
Level of binder (%)	Level of solid (%)	Bulk density (gm/cc)	Tap density (gm/cc)	Granule density (gm/cc)	Mean size (µm)	Green density (gm/cc)	Flow rate (gm/sec)	Green strength (MPa)
(-)1 0	(-)72	1 76	2 05	3 06	66 0	3 439	1 27	0 875
(+)1 6	(-)72	1 66	1 92	2 80	66 0	3 439	1 30	0 988
(-)1 0	(+)80	1 88	2 10	3 17	73 0	3 570	1 58	1 07
(+)1 6	(+)80	1 86	2 09	3 15	61 0	3 570	1 43	1 49

In addition to that the interactive effects of the binder and the solid were also observed The negative value of the analysis indicates that the lower level of the binder will increase the mean particle size The interactive effects of the binder and the solid concentrations are diagramatically presented in Figure 4 3 At the lower level of the solid concentration, the increase of the binder content did not affect the mean particle size, but at higher level, the mean particle size is reduced by 12 µm with the increase of the binder content

Table 4 10 The main and interactive effects on the powder characteristics

Main and interacting effects	Responses						
	Mean size (µm)	Bulk density (gm/cc)	Tap density (gm/cc)	Granule density (gm/cc)	Green density (gm/cc)	Flow rate (gm/sec)	Green strength (MPa)
Binder	-6 0	-0 06	-0 07	-0 14	0 00	-0 06	0 27
Solid	1 0	0 16	0 11	0 23	0 13	0 22	0 35
Interaction	-6 0	0 04	0 06	0 12	0 00	-0 08	0 15

This is attributable to the deflocculating nature of the binder which caused the viscosity to drop and the consequent finer atomization produces the smaller droplets

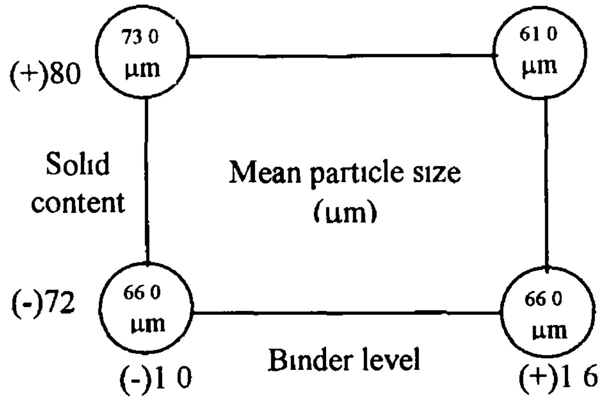

Figure 4.3 The interaction of the binder and the solid content on the mean particle size

The green strength of the discs was influenced by both the binder and the solid concentration The interacting effect was also found to be significant which is shown diagramatically in Figure 4 4

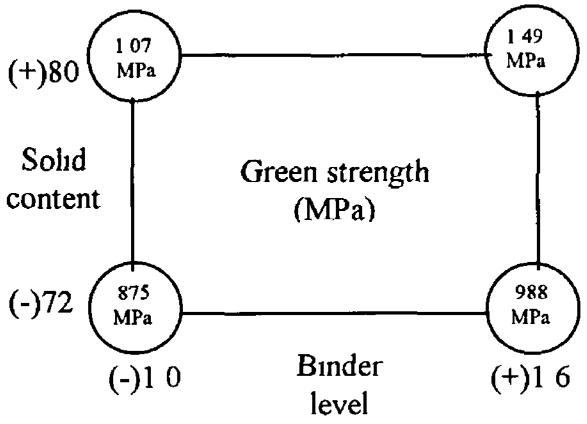

Figure 4 4 The interaction of the binder and the solid content on the green strength

At a lower solid concentration, the change of binder from the lower to a higher level has increased the green strength by 0 113 MPa but at a higher solid concentration, the change has resulted in an increase of the green strength of 0 42 MPa Therefore, the effects of different variables on the green strength can be summarized as follows

(i) The main function of the binder is to enhance the green strength which increases with the higher percentage of the binder

(ii) The higher percentage of the solid in the slurry increases the volume fraction of the solid in the powder, thereby, raising the green strength

(iii) Due to the deflocculating nature of the binder, the higher level of binder at higher solid content results in finer atomization Consequently, the fraction of the fine particles and the volume fraction of solid in the powder increases leading to the higher green strength

4 6 2 Estimation of Weibull Parameters by Fracture Strength

The formation of a green compact body is a major processing operation for the manufacturing of ceramic The strength of the green body is a crucial factor not only for proper handling but also for avoiding the introduction of any further flaws through sintering The green body may have a range of flaw sizes, resulting in a corresponding variation of green strength Empirical or deterministic design approaches may not be adequate in such a case, rather, a probabilistic approach which takes into account the flaw distribution in the material can be more useful The most popular means of characterizing the flaw distribution is by the Weibull approach, a brief description of which has already been given in earlier sections of this chapter

In order to study the effect of the binder on the strength of the ceramic body, 17 0 mm diameter discs were produced in the Carver Laboratory press, by adopting the uniaxial double action compaction technique Ten discs were pressed for each powder, of which five samples were used for the green strength and the rest were sintered to evaluate the fired strength The tensile strength measured by the diametral compression test in MPa was used to calculate the probability of failure using Weibull theory of the strength of brittle materials Figures 4 5 to 4 10 show the Weibull distribution for the green and fired compacts containing different types and levels of the binder, and different solid concentration The plots were used to determine the Weibull modulus, *m* and the normalizing stress, σ_o The calculated values of *m* and σ_o are summarized in Table 4 11

Table 4.11 Values of Weibull constants

Disc	Weibull	Coded identification of binder										
type	const	Ltx A	Ltx B	Ltx C	Ltx D	Ltx E	PVA	Ltx C1	Ltx C2	Ltx C3	Ltx C4	Ltx C5
Green	σ_o	0 85	0 86	0 96	1 0	1 50	0 81	0 92	1 02	1 02	1 03	1 50
Green	m	24 7	55 6	19 6	39 2	20 3	16 8	7 7	15 3	25 3	23 4	40 5
Fired	σ_o	25 8	26 6	24 8	17 3	20 1	24 5	27 3	21 2	26 1	22 0	23 7
Fired	m	2 44	3 80	4 88	5 16	4 12	3 2	1 98	2 68	6 90	3 44	3 56

4.6.3 Electrical Properties

The variation of the electrical properties of the varistor due to the change of the binder level and the solid concentration was evaluated with the binder Ltx C In Table 4 12 the input parameters with their level, and code and the corresponding results of the investigation are given

Table 4 12 Responses on the electrical properties for Latex binder Ltx C

Test level (%)		Nominal voltage (volt/cm)	Clamp ratio	Non-linear co-efficient (α)	Energy (J cm^{3})	Wattloss (watt)	
Binder	Solid					Before shot	After shot
(-)1 0	(-)72	2333	1 66	27 29	265	0 025	0 029
(+)1 6	(-)72	2397	1 65	27 70	246	0 020	0 026
(-)1 0	(+)80	2350	1 63	28 44	274	0 023	0 044
(+)1 6	(+)80	2378	1 64	28 10	267	0 016	0 033

The effects of different independent parameters on the response are summarized in Table 4 13 The analysis of the result revealed that the nominal voltage was mainly affected by the binder A higher level of binder led to an increase of the nominal voltage The solid concentration did not exhibit any significant effect

Table 4 13 Main and interacting effects on the electrical properties of varistors

Main and interacting effects	Nominal voltage (Volt/cm)	Clamp ratio	Non-linear co-efficient (α)	Energy (J cm^{3})	Wattloss (watt)	
					Before shot	After shot
Binder	46 0	0	0 035	-13 0	-0 006	-0 007
Solid	-1 0	0 02	0 775	15 0	-0 003	0 011
Interactions	-18 0	0 01	-0 0375	6 0	-0 001	-0 004

No such effect of the binder and the solid concentrations was observed on the clamp ratio and wattloss before HASD test, while the wattloss after HASD test is mainly influenced by the solid level The effect of the solid level on the non-linear co-efficient is also significant Higher solid concentration is found to lead to more varistor degradation Higher binder level appears to improve the leakage characteristics The energy absorption capability is dependent on both the binder and solid levels The powder processed with lower binder and higher solid concentrations can generate varistors of increased energy absorption capability

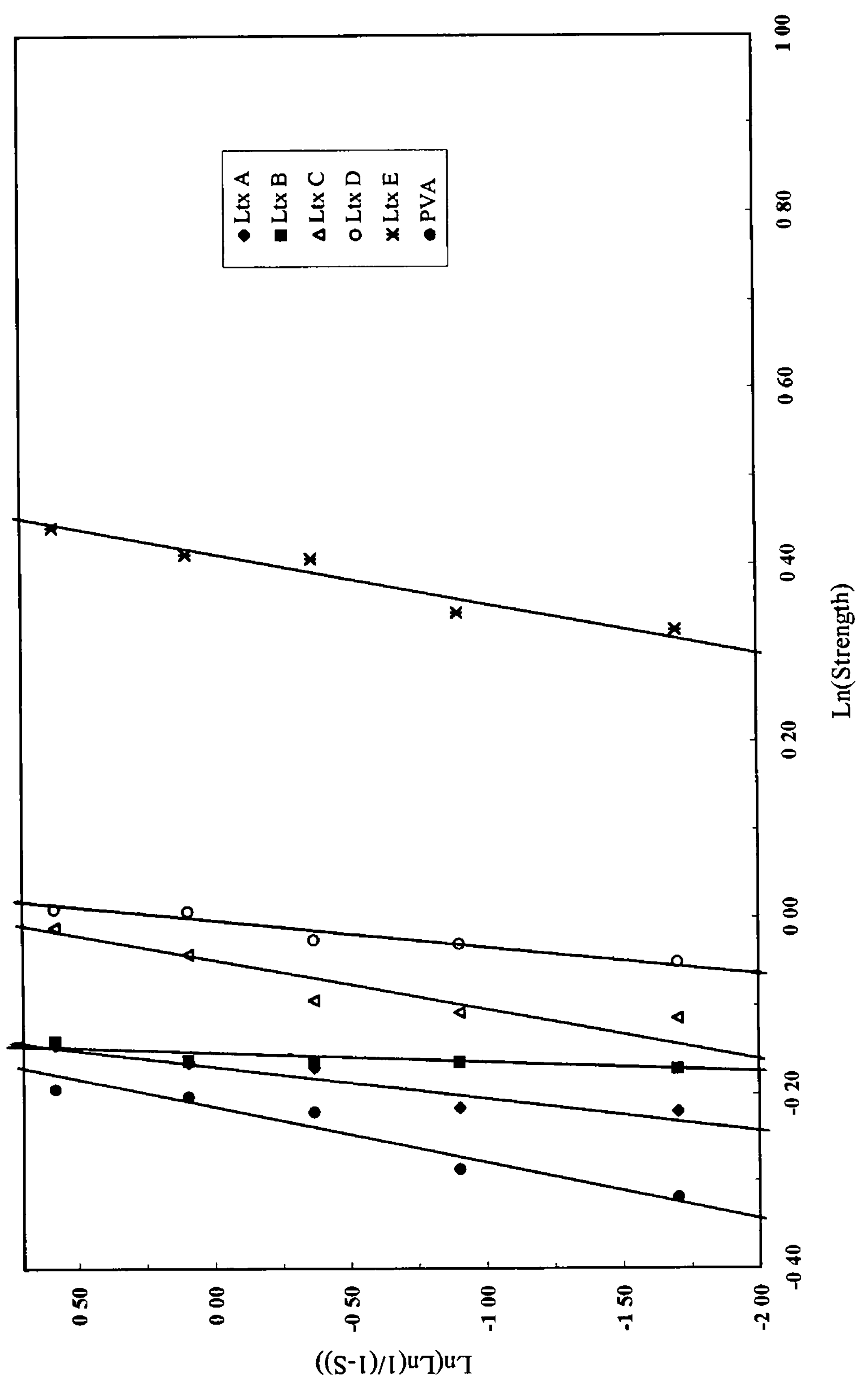

Figure 4 5 Weibull plot of green strength of discs with different binder systems

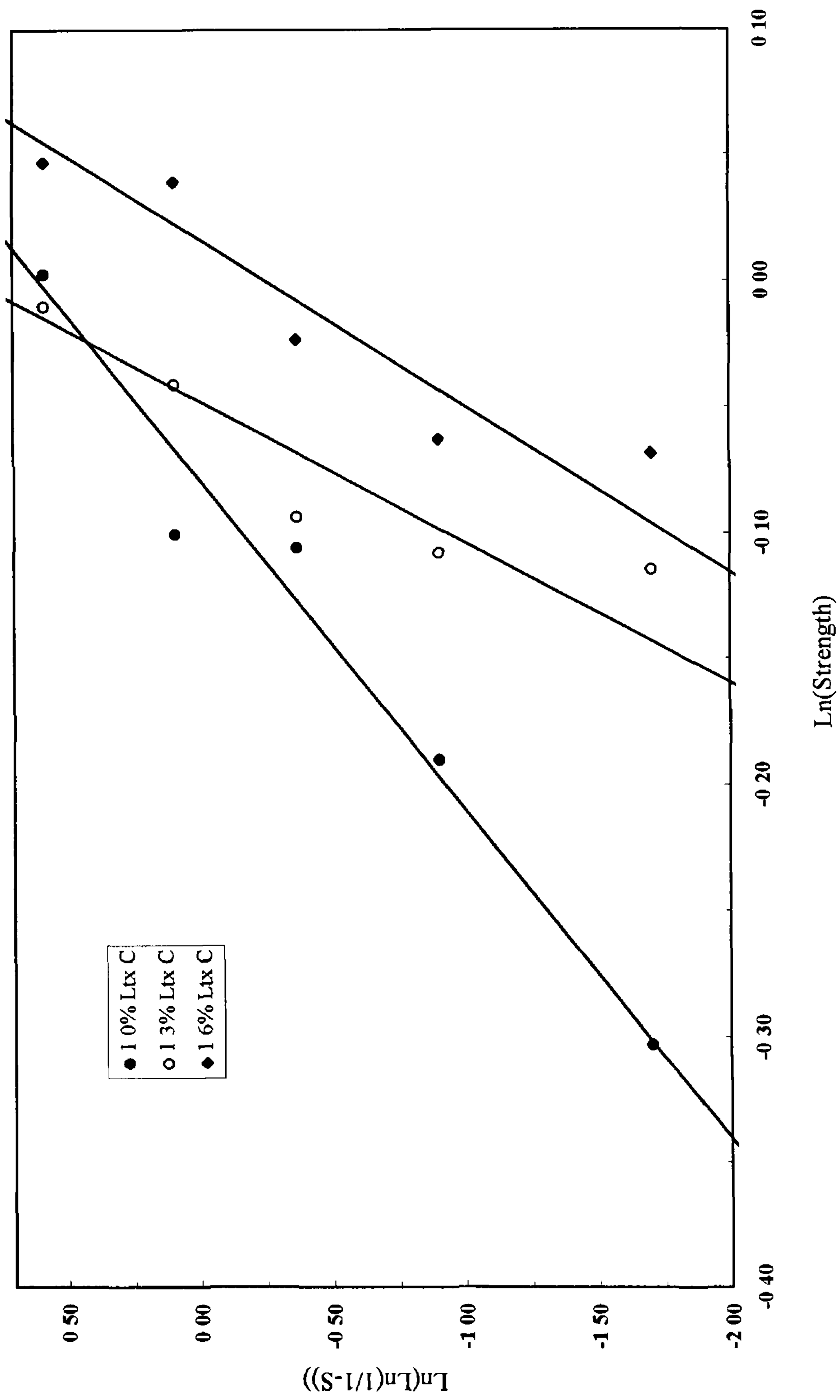

Figure 4.6 Weibull plot of green strength of discs with different levels of binder at lower solid concentration

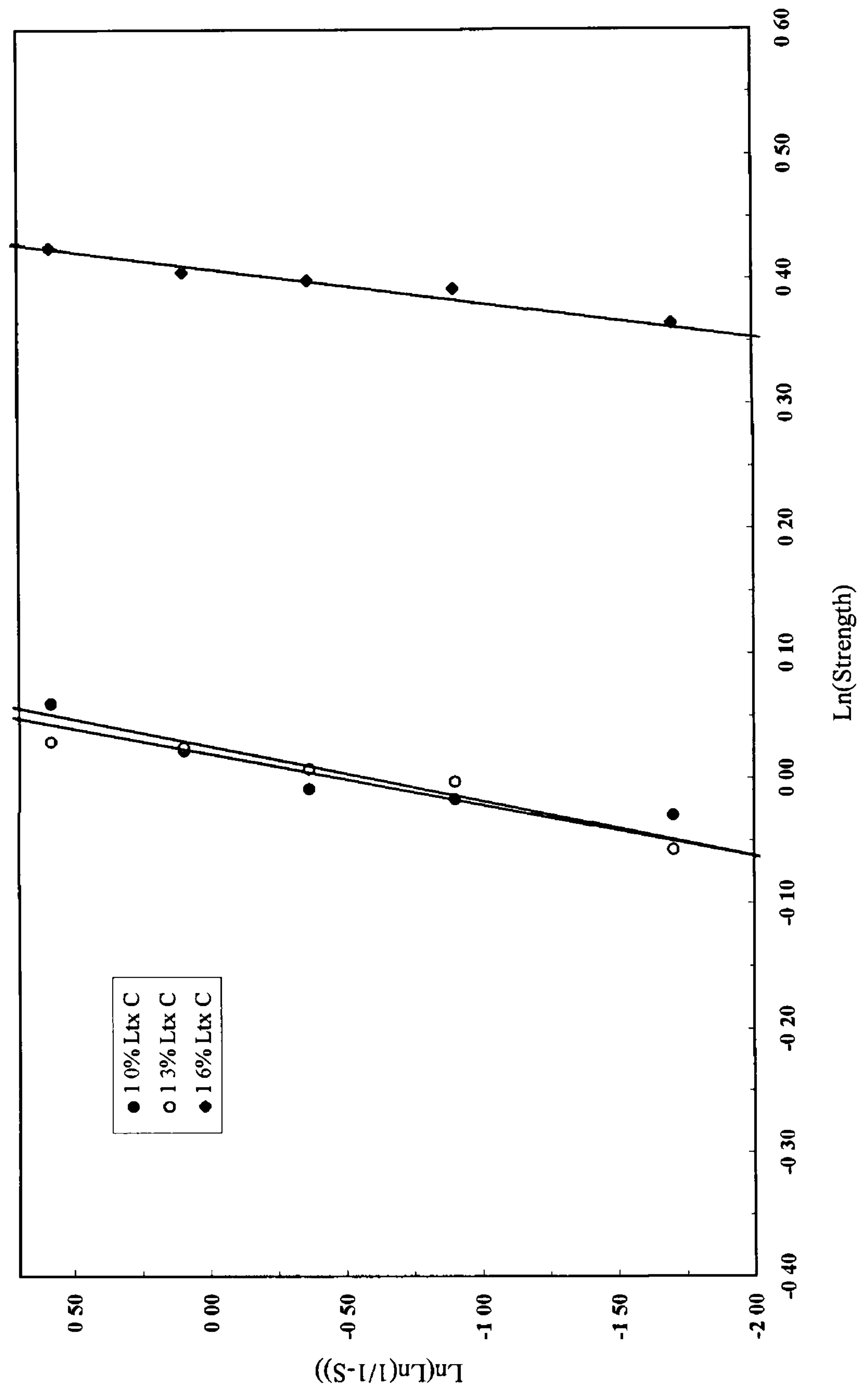

Figure 4.7 Weibull plot of green strength of discs with different levels of binder at higher solid concentration

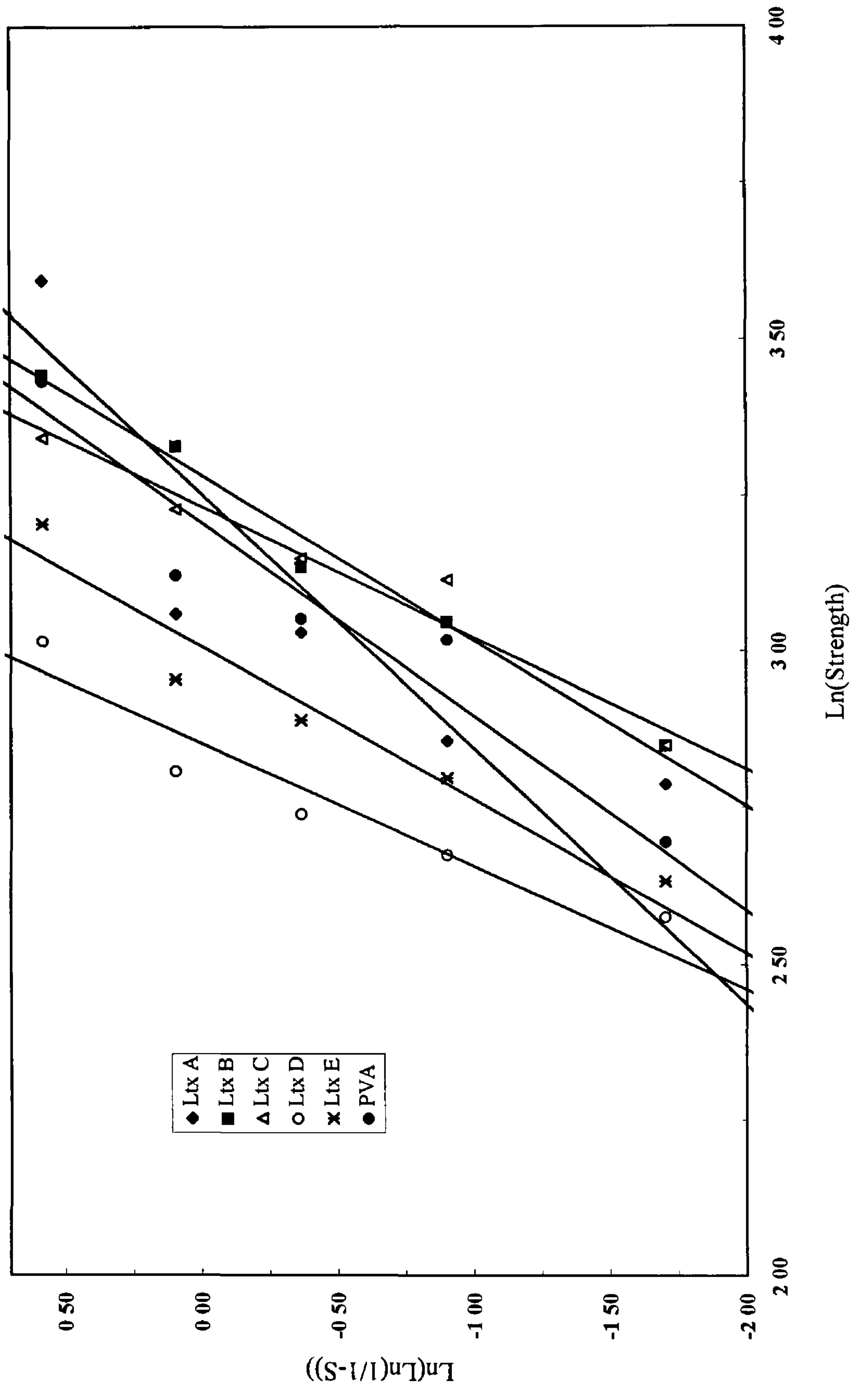

Figure 4.8 Weibull plot of fired strength of discs with different binder systems

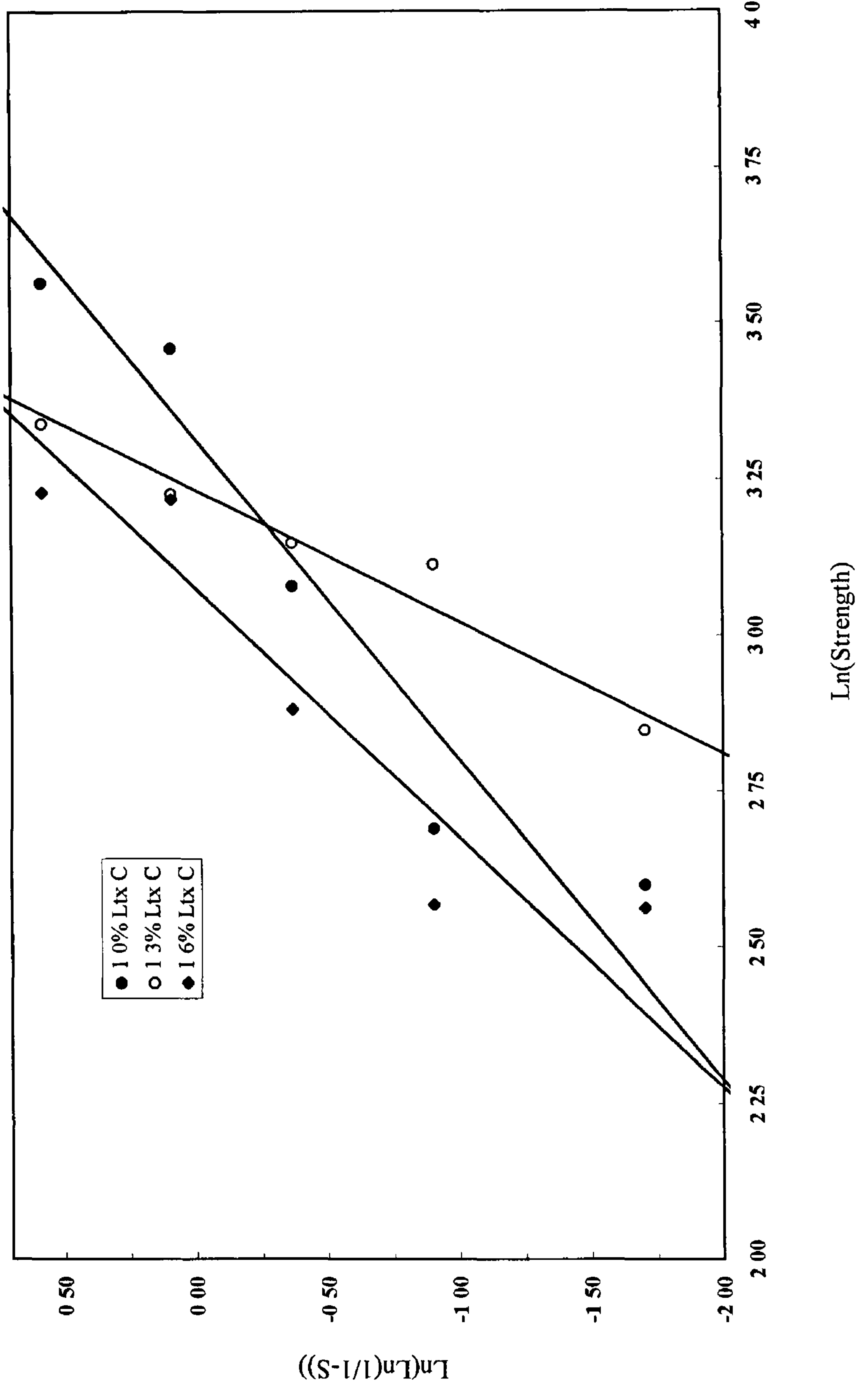

Figure 4 9 Weibull plot of fired strength of discs with different levels of binder at lower solid concentration

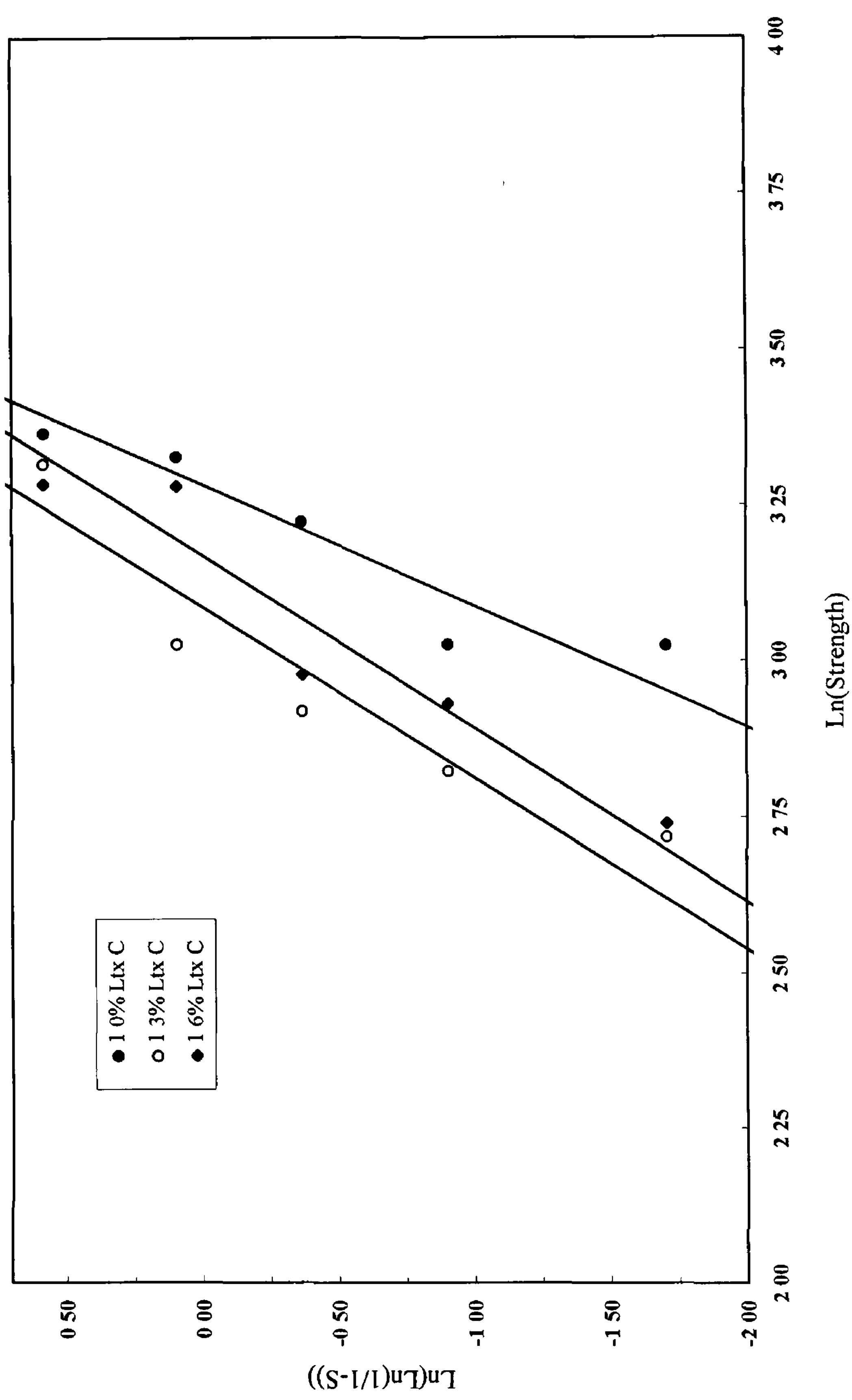

Figure 4.10 Weibull plot of fired strength of discs with different levels of binder at higher solid concentration

Chapter 5

RESULTS AND DISCUSSIONS

5.1 INTRODUCTION

The characteristics of the metal oxide varistor powder, the physical properties of the green and fired discs made thereof, and the electrical performance of the varistors were investigated The primary aim was to correlate the powder processing parameters with the resultant electrical properties of the varistor The input variables were mainly the spray drying conditions, different types of binders and their concentration, and particle size fractions of powder In a separate study the effect of the glass thickness on the varistor performance was assessed by evaluating the energy absorption capability A few samples were microstructurally analyzed using scanning electron microscopy

5.2 SPRAY DRYING PARAMETERS

The influence of the drying parameters on the powder as well as on the electrical performance was studied for both the laboratory and pilot scale dryers The results obtained are outlined in the following sections

5 2 1 Laboratory Scale Dryer

In the laboratory scale spray dryer the effect of three input parameters such as the drying air, feed flow rate and the atomizing air pressure was investigated The measured characteristics were the bulk and tap densities, percent yield, particle shape, the mean particle size, specific

Table 5.1 Characteristics of powder produced through various run conditions of the laboratory spray dryer

No of run	Bulk density (gm/cc)	Tap density (gm/cc)	Mean particle size (µm)	Specific surface area (m^2/gm)	Moisture content (%)	Percent yield
1	1.8	2.2	51.0	1.6	0.1	82.0
2	1.8	2.1	45.5	1.8	0.1	84.0
3	1.8	2.2	78.0	1.6	0.3	42.4
4	1.7	2.1	45.0	1.9	0.2	85.6
5	1.6	2.1	55.0	1.7	0.3	83.3
6	1.9	2.2	50.0	1.6	0.4	76.8
7	1.8	2.2	43.0	1.7	0.3	86.7
8	2.0	2.3	60.0	1.1	0.3	74.5
9	2.0	2.3	57.0	1.1	0.2	80.1
10	1.9	2.2	60.0	1.6	0.3	80.5
11	1.8	2.2	48.0	1.8	0.2	83.4
12	1.8	2.1	46.0	1.2	0.3	88.0
13	1.8	2.2	54.0	0.9	0.4	86.8
14	1.8	2.2	52.0	1.0	0.3	84.6
15	1.8	2.1	48.0	1.2	0.3	85.5
16	1.9	2.3	65.0	0.9	0.4	78.4
17	1.8	2.2	57.0	1.0	0.2	81.9
18	1.9	2.2	62.0	0.8	0.4	79.6
19	1.9	2.2	54.5	1.0	0.3	82.6
20	1.9	2.2	50.2	1.2	0.3	87.4
21	1.9	2.2	58.0	1.1	0.3	78.1
22	1.9	2.2	55.0	1.3	0.2	88.1
23	1.9	2.2	60.5	1.1	0.5	78.7
24*	1.8	2.2	51.0	1.2	0.2	79.8
25*	1.9	2.2	61.5	1.3	0.3	86.7
26*	1.8	2.2	47.0	1.3	0.1	90.1
27*	1.9	2.2	64.0	1.2	0.2	87.4
std	1.6	1.9	41.0	1.4	0.17	-

surface area, moisture content, flowability, and the compressibility of the powder, and the green and fired densities of the discs The powder characteristics are presented in Table 5 1 The bulk and tap densities, mean particle size, flowability, and the moisture content were influenced by the spray drying conditions The low level of the atomizing air pressure and a high rate in the feed flow led to an increase in bulk and tap densities, and the mean particle size Under such a condition a certain combination of the fine and coarse particles is achieved in the powder which helps to yield a higher bulk density[106] The particle size distributions for the optimized run condition of the laboratory scale dryer and the production dryer are given in Figures 5 1 and 5 2 respectively The effect of the three input parameters is elaborated below

Drying air flow rate

The effect of the drying air flow rate on the percent yield of the powder is shown in Figure 5 3 The yield was abated with an increase in the drying air flow rate The very small pulverulent particles could not be collected by the cyclone as they were exhausted through the passage of the aspirator With increased drying air flow rate additional pulverulent particles would be lost through the process

The mean particle size was also increased with an increase in the drying air flow rate as illustrated in Figure 5 4 More fine particles were exhausted with the higher drying air flow rate, leaving coarser particles which in turn resulted in an increase in the mean particle size

The compressibility of the powder was slightly affected by the drying air flow rate as delineated in Figure 5 5 Better compressibility of the powder was obtained at lower drying air flow rate The outlet temperature of the drying air was raised with an increase in the drying air flow rate In general a higher outlet temperature is found to be detrimental for compaction if the powder contains heat sensitive binder under co-current flow condition[81,107]

The impact of the change of the drying air flow rate on the green as well as on the fired density of the discs is shown in Figure 5 6 As expected the green density followed the same trend as the compressibility The change in the fired density of the discs produced from the powder with the changing drying air flow rate did not exhibit any significant difference But in general the higher green density led to an insignificant but higher fired density

Atomizing air pressure

The effect of the atomizing air pressure on the yield of powder is illustrated in Figure 5 7 The percent yield was higher with an increase in the atomizing air pressure More pressure led to finer atomization by producing smaller droplets from the slurry As a consequence moisture evaporated quickly from the smaller droplets resulting in less adhesion of particles on the dryer walls

The average particle size dropped as the atomizing air pressure was increased from 0 8 to 1 0 Kg_f/cm^2 as illustrated in Figure 5 8 However, further increase in the atomizing air pressure did not reduce the mean particle size Nearly complete atomization took place at about 1 0 Kg_f/cm^2 This happened as a result of the limitation of dual fluid atomization

As presented in Figure 5 9 the compressibility was higher for the powder spray dried at lower atomizing air pressure With the decrease in the atomizing air pressure, larger droplets were produced which led

to coarse particles with a broader distribution This type of distribution has less electrostatic charge and exhibits better packing quality[107]
The variation of the green and fired densities with the atomizing air pressure is shown in Figure 5 10 The green density exhibited the same trend as the compressibility, i e the pressed discs with higher density was obtained with the powder produced at lower atomizing air pressure The fired density of the discs was not found to be significantly influenced by the atomizing air pressure

Feed flow rate

The effect of the feed flow rate on the yield of powder and the mean particle size is illustrated in Figures 5 3, 5 4, 5 7, and 5 8 With an increase in the feed flow rate the mean particle size was raised but the percent yield was decreased In the spray dryer as the feed flow rate increases, a larger volume of slurry passes through the nozzle for a constant drying air flow rate and atomizing air pressure condition Larger droplets are produced as less pressure is imparted on the slurry resulting in an increase in the mean particle size

The compressibility of the powder was greater for higher feed flow rate as illustrated in Figure 5 11 More moisture was retained within the particles with an increase in feed flow rate This disrupted the bonding structure of the binder present, reduced the hardness and acted as a plasticizer and the powder became more deformable[78]

The compressibility of the powder with other better characteristics like bulk and tap densities was compared with the powder of standard production process It is clearly evident from Figure 5 12 that the compressibility of the optimized run is significantly higher The feature of better compressibility is attributable to the following observations

(i) The moisture content in the powder plays an important role In the optimized run this content was higher than that in the standard powder Higher level of moisture has plasticizing effect on the powder making it more deformable

(ii) The mean particle size of the powder produced through the optimized run was greater than that of the standard process It is quite likely that higher mean size with increased percentage of coarse has led to achieve a more compressible powder

Particle shape

Scanning electron micrographs for the powder of run 4, 8, and the standard process powder are shown in Figure 5 13 The particles have a single large pore (donut shape) for both the run 4 and 8 This feature is very common for a small dryer having parallel flow systems The residence time is relatively short for this type of dryer The diffusional flow of vapour at the later stage of drying is mainly a function of residence time The particles do not get enough time to allow the water vapour to flow from their centres, and the "donut" shape is formed as a result of the presence of the water vapour at the centre

It is generally thought that "donut" shaped particles have lower bulk density But the data presented in Table 5 1 shows higher bulk and tap densities for both runs as compared to the standard process powder This implies that the single large pore is filled up by the smaller particles and the powder has either higher packing efficiency or that the density of each of the particles is higher In a two fluid nozzle the feed slurry has less chance of aeration prior to or after spray drying So the presence of air voids within the particles is minimized, leading to an increase in density of the granules

Specific surface area

The specific surface area is dependent on the particle size, its distribution and shape Spray dried particles are usually spherical in shape and specific surface area is inversely related to the mean size But the data obtained and presented in Table 5 1 are not strictly supportive of this trend This may be attributable to the percentage of fine, coarse and the inter and intra particle pores within the powder

Flowability

The free flowing nature of the powder is mainly a function of the particle size and its distribution, the surface condition and the moisture present in the powder The powders obtained using the laboratory scale dryer had a wide distribution and the mean size was greater than 40 μm but they did not exhibit any flowability Perhaps the powder was cohesive in nature For a restraining flowability (i) the moisture, (ii) electrostatic charging, and (iii) υan der Waal forces are the bonding mechanisms Significant cohesive effect due to υan dèr Waal forces will be dominating, when the particle size is less than 1 μm But the presence of more adsorbed moisture can cause cohesiveness even at a nominal size of about 80 μm

Electrical characteristics

The powders from the selected runs in the smaller spray dryer (depending on the powder characteristics) were used to fabricate varistors The run condition of the powder with which the varistor was fabricated, together with the clamp ratio, non-linear co-efficient, and wattloss is presented in Table 5 2 The effect of the spray drying variables is not highly significant for the electrical properties like clamp ratio, and wattloss The non-linear co-efficient of the varistor in the pre-breakdown region at a current density of 0 006 to 0 6 mA/cm^2 was very high for some run condition of the spray dryer The value was also found to be higher for the varistor from the standard powder for the same current density The reason of this higher value could not be identified

Nominal voltage

The nominal voltage was found to be influenced by both the drying air flow rate and the atomizing air pressure as presented in Figures 5 14 and 5 15 The nominal voltage is a function of grain number per unit length and the voltage drop at each grain The voltage drop at each grain also depends on the type of junction and the bias direction It is high when the electron travels from the ZnO grain towards intergranular layer but low when the electron travels from the intergranular layer to ZnO grain[17]

Table 5.2 Varistor fabrication condition and performance characteristics for the smaller spray dryer

Operating conditions of the dryer			Non-linear co-efficient @ 0 01-1 mA	Wattloss X 10^3 (W cm^3)	Clamp ratio @ 1 mA-100A
Drying air flow rate (m^3/min)	Atomizing air pressure (Kg$_f$/cm^2)	Feed flow rate (ml/min)			
0 6	0 8	26 0	14 86	4 751	1 36
0 6	0 8	39 0	14 40	5 206	1 36
0 6	1 0	39 0	13 33	5 337	1 43
0 7	1 0	39 0	14 38	5 026	1 35
0 8	1 0	39 0	68 93	5 923	1 38
0 6	1 2	39 0	58 97	6 090	1 38
Std cond	Std cond	Std cond	59 38	8 851	1 36

5.2.2 Pilot Scale Dryer

The effect of the three input parameters such as the atomizing air pressure, feed flow rate, and the drying air outlet temperature was studied The run conditions are given in chapter 2 The investigation consists of the powder properties and electrical performance The observed powder characteristics are presented in Table 5 3 which include bulk and tap densities, mean particle size, moisture content, flowability, angle of repose, green and fired densities, and the green strength

The mean particle size was significantly influenced by the atomizing air pressure and the feed flow rate An increase in the feed flow rate and a decrease in the atomizing air pressure resulted in higher mean particle size of the powder The particle size distribution for the optimized run is given in Figure 5 16 Within the operating level the effect on the bulk and tap densities was only nominal However, the trend for the tap density is the same as the mean particle size of the powder i e higher tap density was obtained by increasing the feed flow rate and decreasing the atomizing air pressure

All of the powders from the pilot scale dryer exhibited flowability except run 4 as summarized in Table 5 3 The powder prepared under this condition had a higher fraction of fine particles It is obvious that the interparticle friction became greater than the gravitational forces and prevented the flow completely

Table 5 3 Characteristics of powder produced through various run conditions of the pilot spray dryer

No of run	Bulk density (gm/cc)	Tap density (gm/cc)	Mean particle size (μm)	Moisture content (%)	Flow-ability (gm/sec)	Angle of repose (°)	Green density (gm/cc)	Fired density (gm/cc)
1	1 83	2 114	58	0 083	1 440	32 47	3 36	5 58
2	1 81	2 120	68	0 124	1 500	31 83	3 40	5 58
3	1 81	2 104	57	0 072	0 855	32 56	3 36	5 57
4	1 80	2 100	54	0 039	0	-	3 35	5 58
5	1 83	2 130	61	0 12	1 320	32 00	3 38	5 57
Cont	1 81	2 070	54	0 062	1 260	31 76	3 34	5 56

The green strength of the discs was measured for the compacted discs using the powder under different run conditions The results are presented in Figure 5 17 The highest strength was observed for the standard condition, while, the run condition 2 gave the lowest Under run condition 2 more moisture was retained within the powder due to the higher feed flow and lower atomizing air pressure This can be explained with the phenomenon that the presence of water molecules disrupts the bonding structure of the PVA binder, softens the binder and acts as a plasticizer which tends to reduce the strength[78]

Electrical characteristics

Varistors were fabricated using the powder from all the six run conditions of the dryer to estimate the effect on the electrical performance The investigation includes I-V characterization, and energy absorption capability The degradation behaviour of the varistor with the application of long pulse wave was evaluated The microstructure was also examined using scanning electron microscope

Nominal voltage

The nominal voltage of varistors fabricated from the powder produced through the pilot scale dryer is shown in Figure 5 18 The lowest value was obtained with powder from run 2 and the highest with run 4 which was even higher than that of the standard condition In general spray drying generates spherical powder with a wide particle size distribution The change in the variables causes the percentage of the fine and the coarse particles to vary As observed in run 2, a broad distribution with a higher percentage of coarse results in higher packing efficiency The higher packing efficiency has an important role in sintering For zinc oxide varistors liquid phase sintering occurs due to the presence of bismuth oxide The initial feature of this mechanism is associated with the formation of liquid and rearrangement of particles due to the capillary force The rapid densification at the earlier stage is due to the capillary force exerted by the wetting liquid on the solid particles[108 110] In the second stage, the higher packing density and smaller pore size lead to a higher average curvature in the neck regions between the particles, thereby raising the average driving force for sintering In the final stage, the formation of solid skeleton prevents further diffusion through the grain boundaries and consequently the grain grows Higher growth in grain size ultimately reduces the nominal voltage of the varistors The mean grain size calculated from SEM photograph was also found to be higher for the run condition 2

Wattloss, Clamp Ratio, and Non-linear Co-efficient

The wattloss of varistor for different run conditions is plotted in Figure 5.19. This was higher for runs 1 and 2 before the application of high amplitude short duration pulses. But the degradation was more for run 2 after the application of high amplitude short duration pulses of current 65 KA. Wattloss is dependent on the leakage current, which is the function of barrier height, donor density, and average voltage drop in each grain. The nominal voltage was lower for this condition as mentioned before. So the higher wattloss may be attributable to the higher donor density and lower barrier height[87,89]. It is also suggested by Bowen and Avella[30] that the larger grain may lead to an increased density of leakage current.

Table 5.4 Clamp ratio and non-linear co-efficient of the varistors from the pilot scale dryer

No of run	Clamp ratio		Non-linear co-efficient	
	0.3 mA-5 mA	5 mA-5 KA	0.3 mA-1 mA	1mA-5 mA
1	1.32	1.73	7.64	13.86
2	1.34	1.74	7.00	13.77
3	1.35	1.74	6.66	13.98
4	1.32	1.73	7.35	14.48
5	1.34	1.73	6.72	14.10
Control	1.33	1.73	7.04	14.51

The clamp ratio and the non-linear co-efficient are summarized in Table 5.4. There was no significant differences for both the pre-breakdown and breakdown region.

Energy absorption capability

The energy absorption capability of the varistors made with powders processed under various spray drying conditions is illustrated in Figure

5 20 Significant influence of the variables was observed on the energy absorption capability On the basis of the initial failure the performance can be said to be lower for both runs 1 and 4, and higher for run 5 The failure commenced at about 150 J cm^{3} for both runs 1 and 4 However, in statistics, neither the lowest nor the highest value is well accepted parameter for comparing the distribution The mean or the median can be considered to evaluate the performance The mean ± standard deviation value of the varistors are presented in Figure 5 21 The values were higher for both runs 2 and 5 The higher energy absorption capability for the runs 2 and 5 cannot be readily explained The moisture content in the powder and the mean particle size were higher for these run conditions Perhaps, the increased amount of moisture and higher mean particle size had some form of positive influence during sintering which ultimately led to the enhanced performance The lower value of the standard error (±10) for energy absorption refers to the significance of the difference from one run to another

Degradation under low amplitude long duration impulse test

Degradation under low amplitude long duration impulse (LA-LD) test was estimated by measuring the wattloss after each cycle of the destruction test The varistor was cooled down before measuring the wattloss after the classification of energy in each cycle The wattloss value obtained by the Wattloss High Temperature Tester after each cycle is presented in Figure 5 22 No significant degradation, that is, the rise in wattloss was observed up to the energy level of 259 J cm^{3} The difference in wattloss within this level is due to the variation of the ambient temperature

Microstructure analysis

For microstructural analysis the samples were prepared by taking a piece approximately from the same location of the varistors prepared from the powders of all the six run conditions Therefore, the SEM photographs should give an idea, but may not be the actual picture of the microstructure of the whole varistor The microstructure comprised of the secondary emission image (SEI) and back scattered electron image (BEI) is presented in Figures 5 23 (a, b), 5 24 (a, b), 5 25(a, b), 5 26 (a, b), 5 27 (a, b), and 5 28 (a, b) for the run conditions 1, 2, 3, 4, 5, and the standard operating condition respectively The SEI photographs show the topography for a particular location, whereas the BEI shows the presence of different phases The phases are evenly distributed for each condition Twinning is also evident for all the cells

The mean grain size was determined from the SEM photographs by the line count method[111,112] using the formula $\bar{d} = 156\bar{L}$ where $\bar{L}$ is the average grain boundary intercept length and determined by drawing random test lines super imposed over a large number of grains in the plain of polish There was variation in the grain size and the average size was 13 μm for run number 1 as presented in Figure 5 23(a, b) The average grain size was 16 μm for run number 2 as delineated in Figure 5 24 (a, b) For the run number 3 the grain size had a mean value of 11 μm as given in Figure 5 25 (a, b) The grain size had an average value of 10 μm in case of run number 4 as shown in Figure 5 26 (a, b) The average value is 14 μm for the run number 5 as presented in Figure 5 27 (a, b) The average grain size was 14 μm for the standard condition as given in Figure 5 28 (a, b) The porosity was found to be intergranular and it was not evenly distributed for all the run conditions The pore number was found to be higher in the standard condition

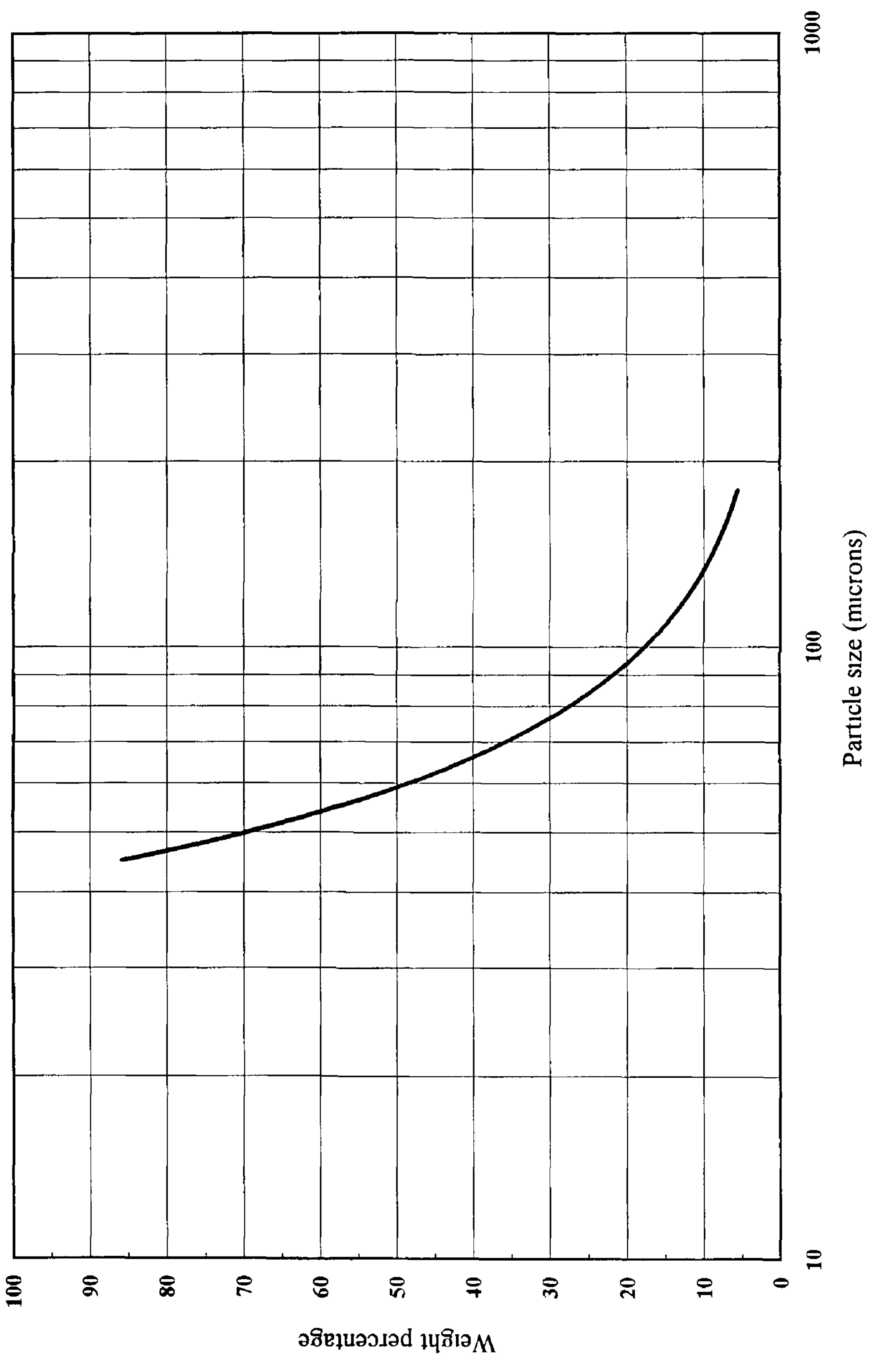

Figure 5.1 Particle size distribution of the powder produced through the optimized run of the laboratory scale dryer

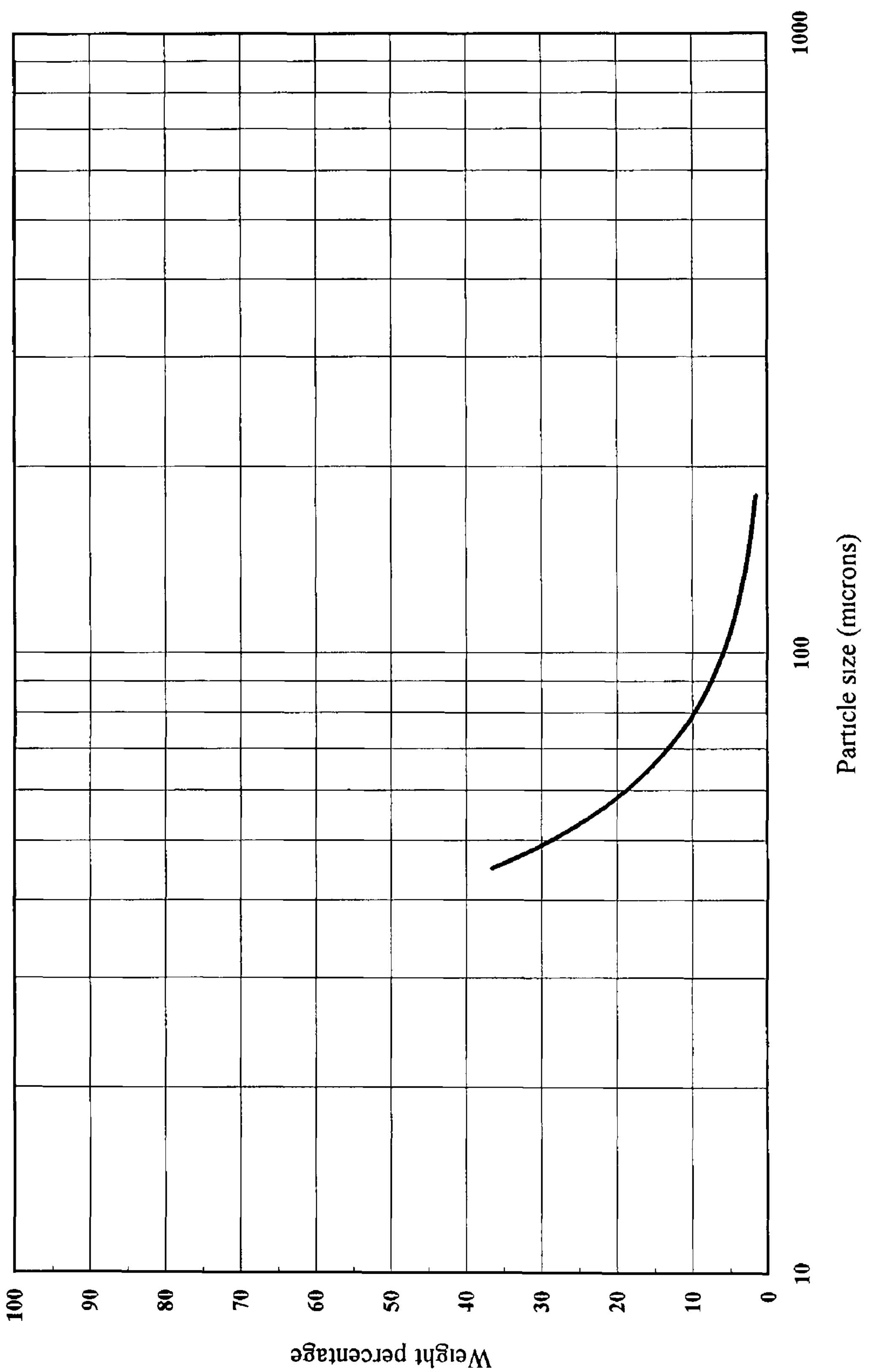

Figure 5 2 Particle size distribution of the powder produced through the production scale dryer

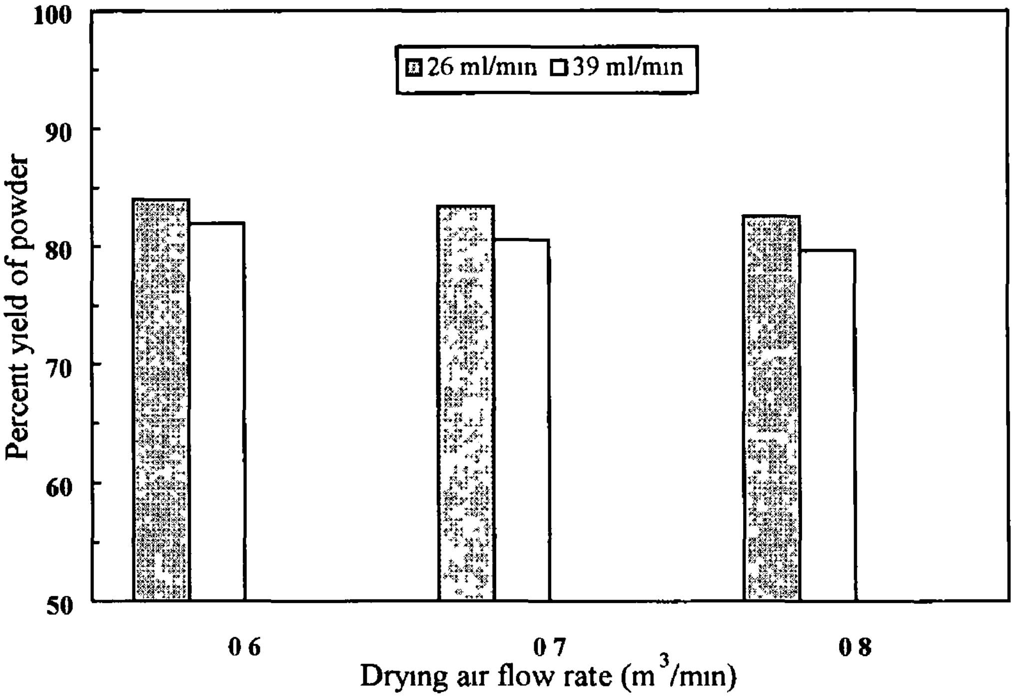

Figure 5 3 Effect of drying air flow rate on percent yield of spray dried powder

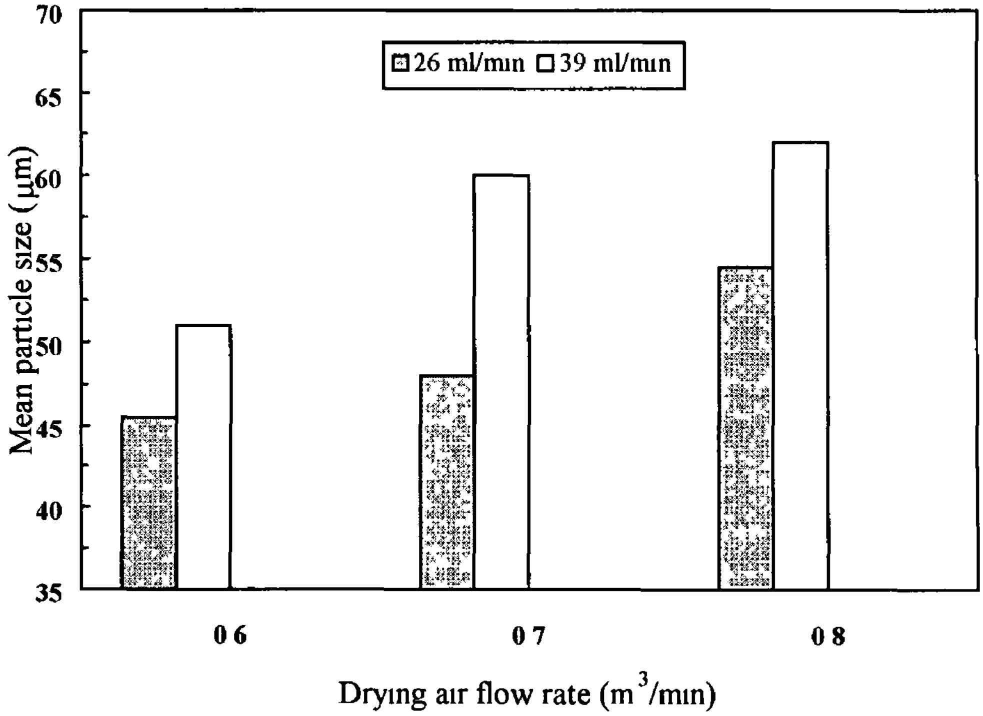

Figure 5.4 Effect of drying air flow rate on the mean particle size of spray dried powder

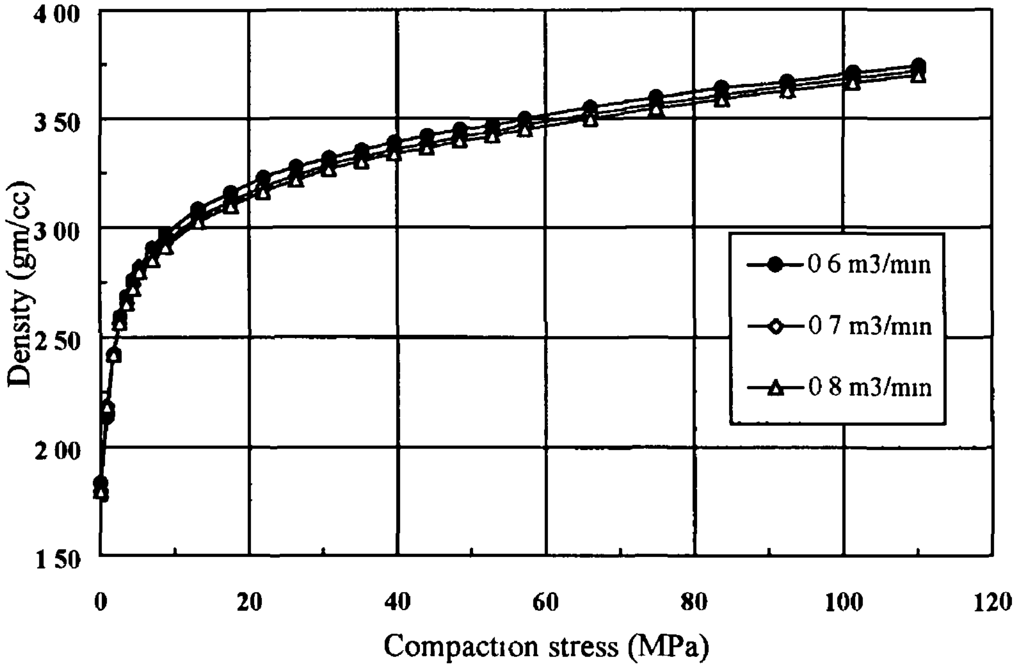

Figure 5 5 Compressibility of powder under various drying air flow rate

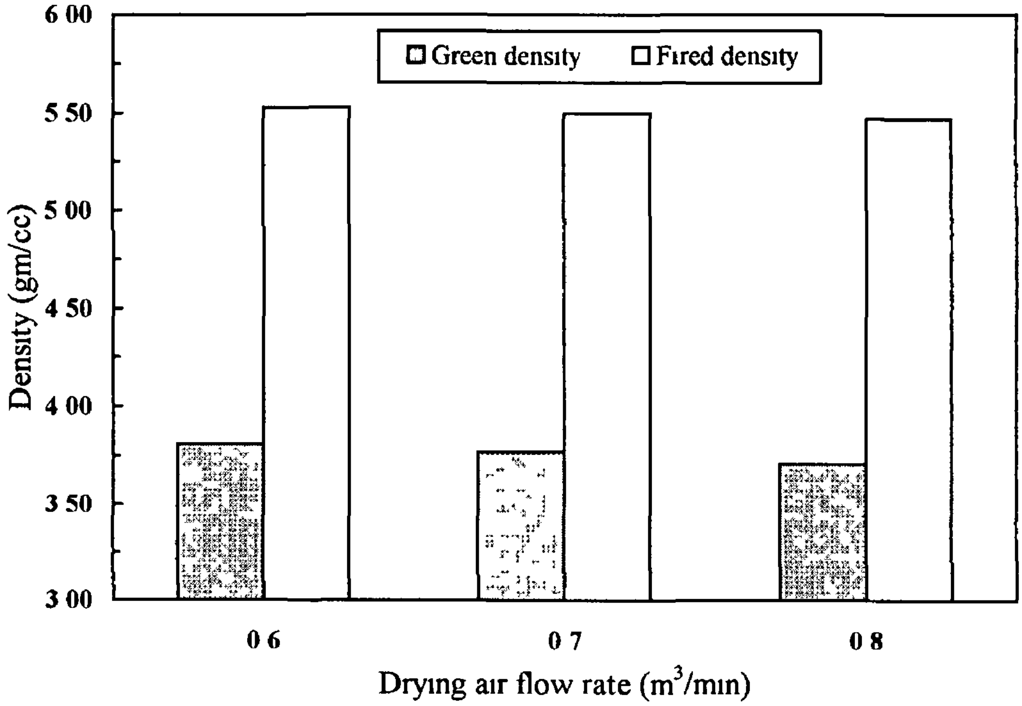

Figure 5 6 Effect of drying air flow rate on density of discs

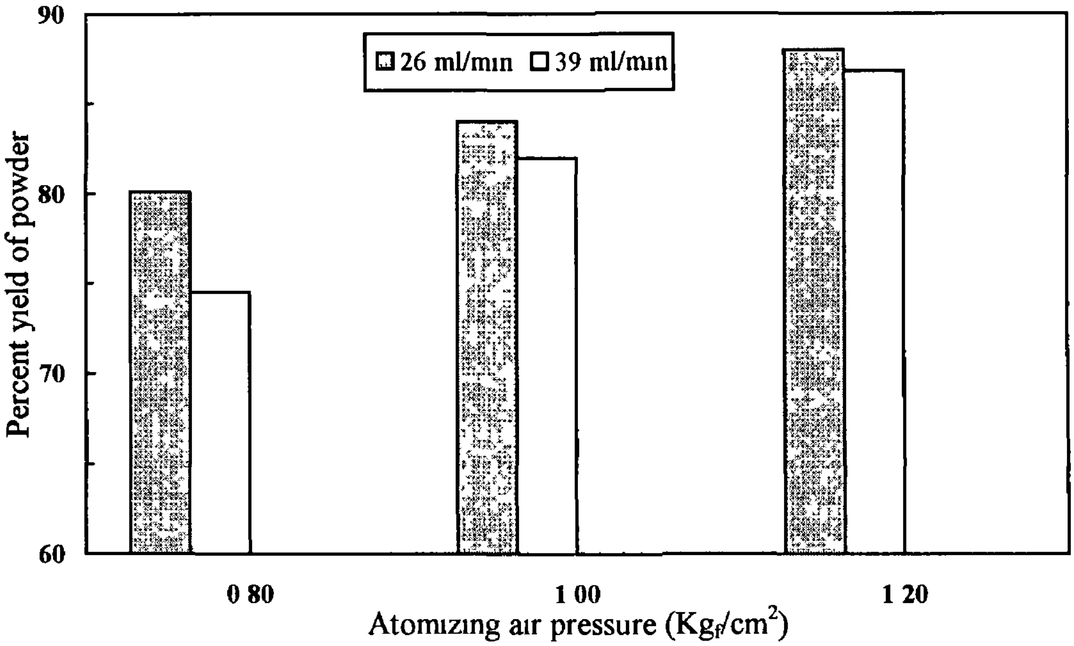

Figure 5 7 Effect of atomizing air pressure on percent yield of powder

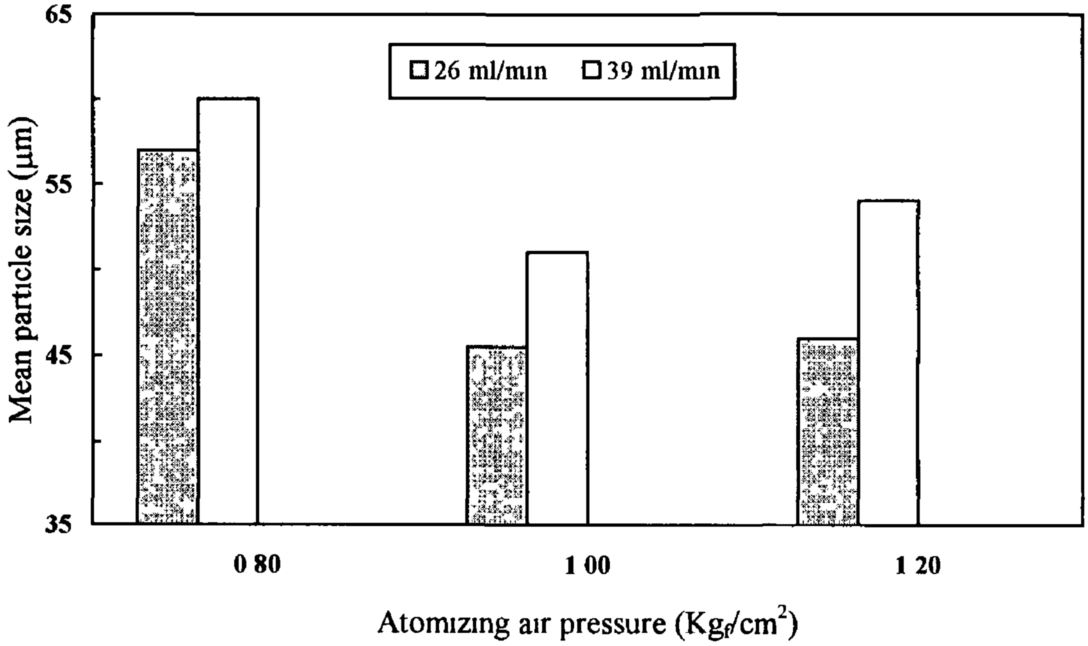

Figure 5.8 Effect of the atomizing air pressure on mean particle size of powder

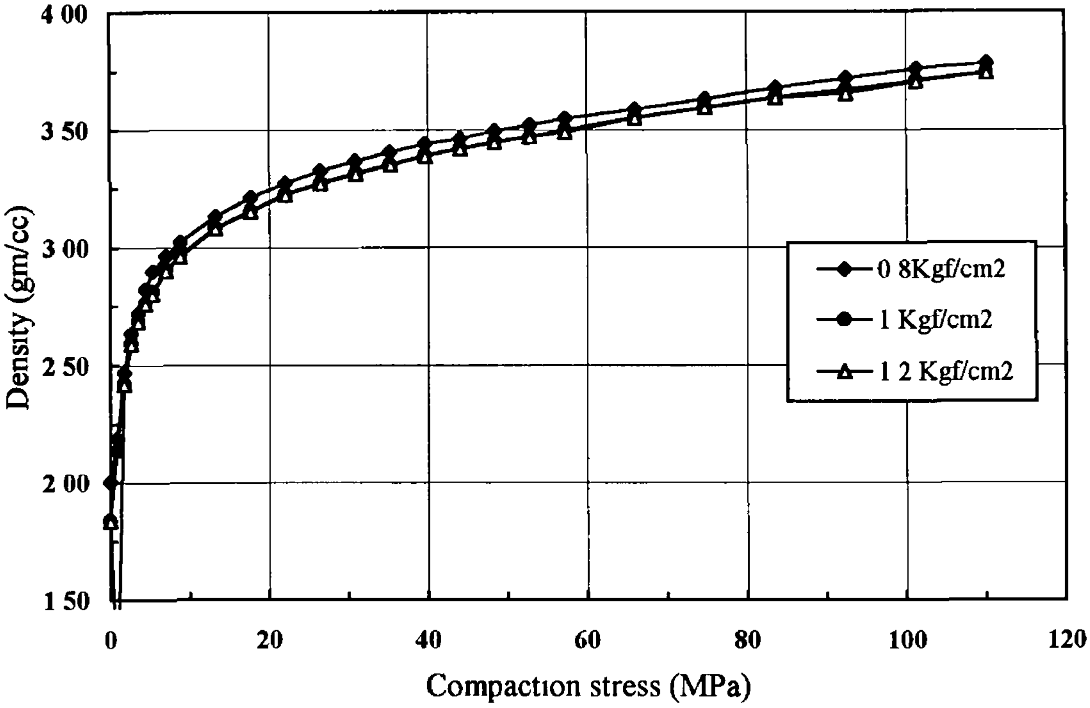

Figure 5 9 Compressibility of powder produced under different atomizing air pressure

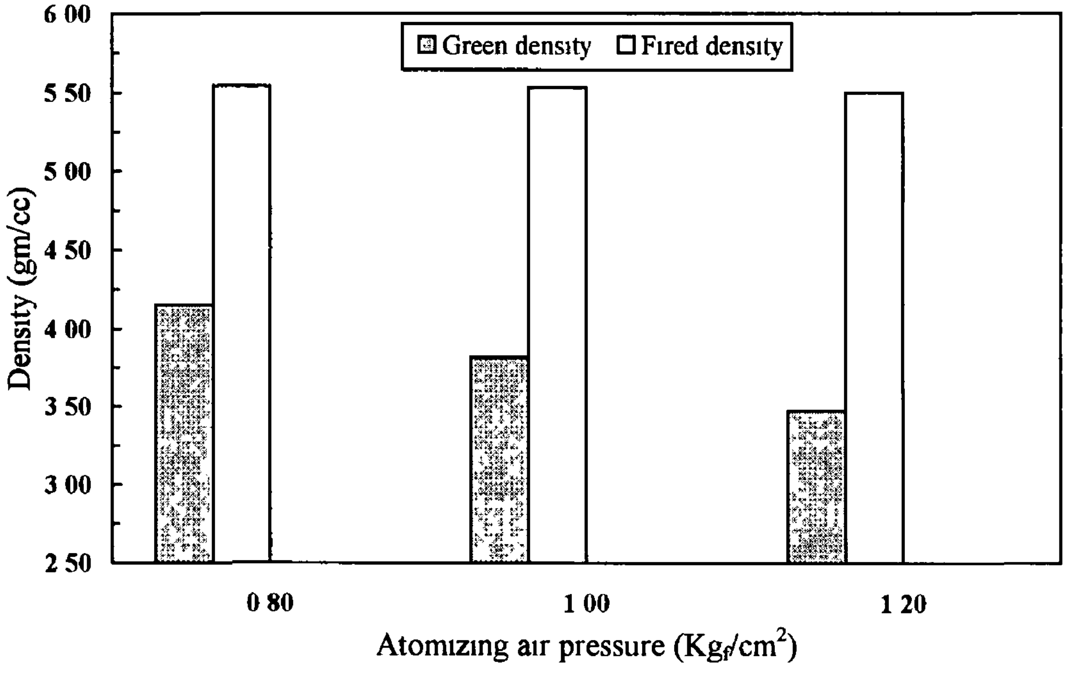

Figure 5.10 Effect of atomizing air pressure on the density of the discs

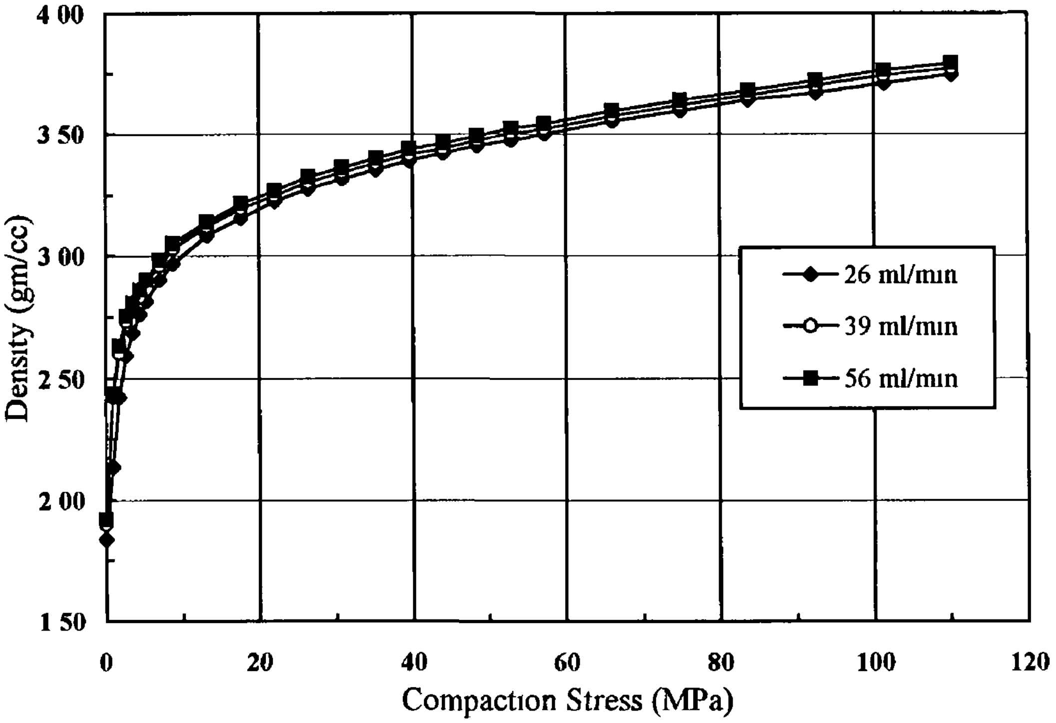

Figure 5 11 Compressibility of powder produced under different feed flow rate

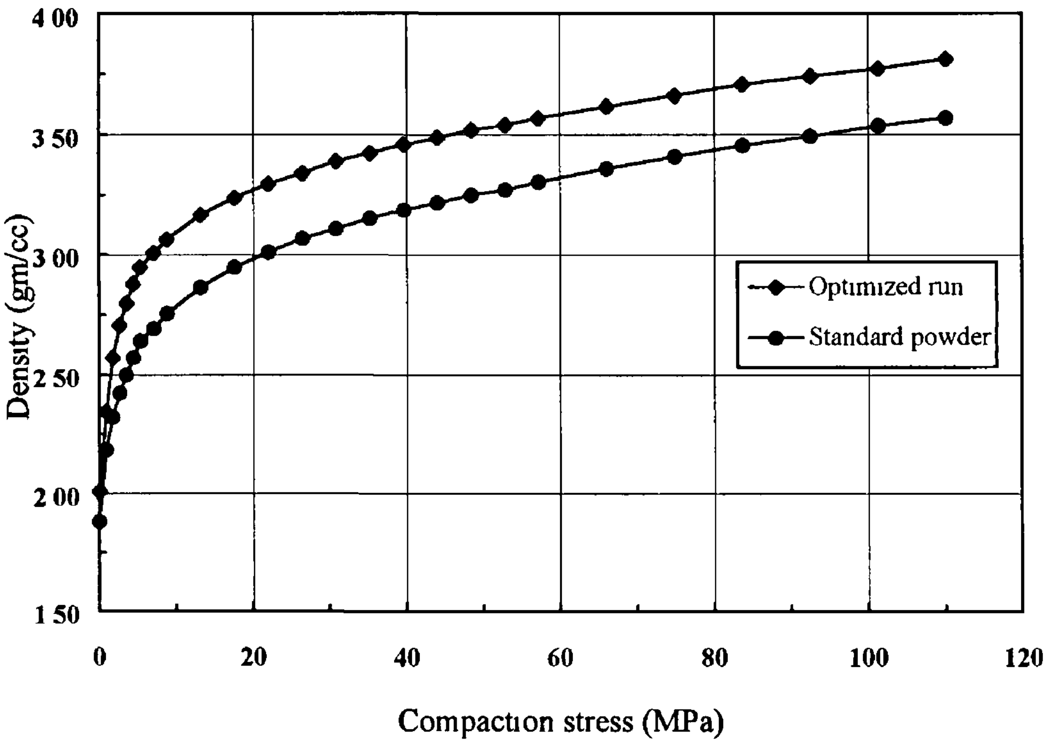

Figure 5 12 Compressibiliy of powders produced through the optimized run and the standard production condition

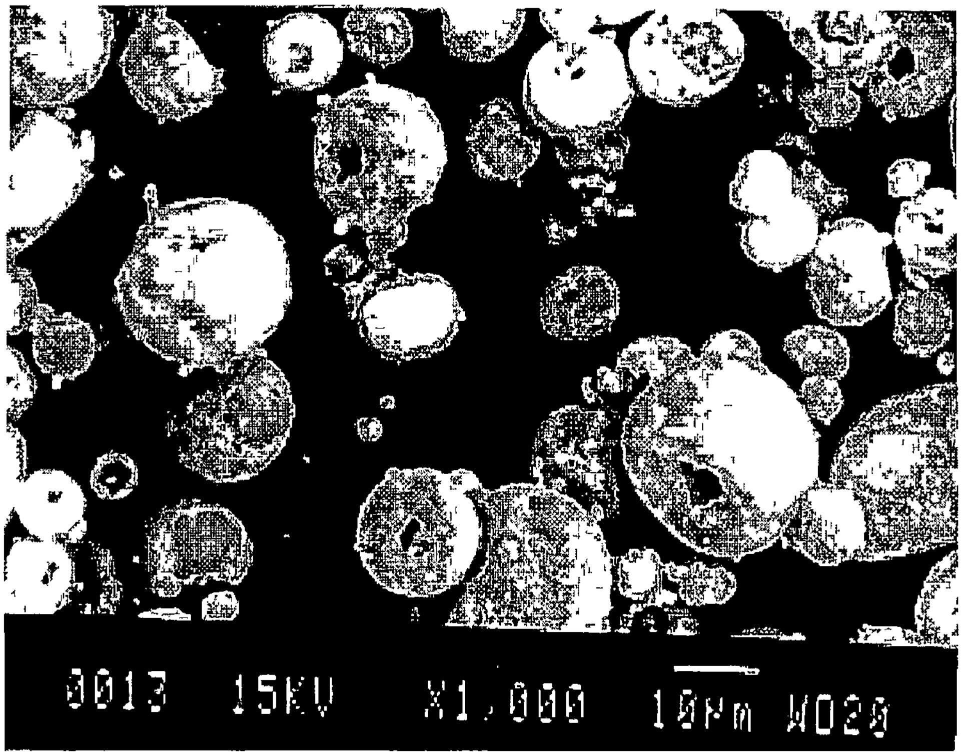

A

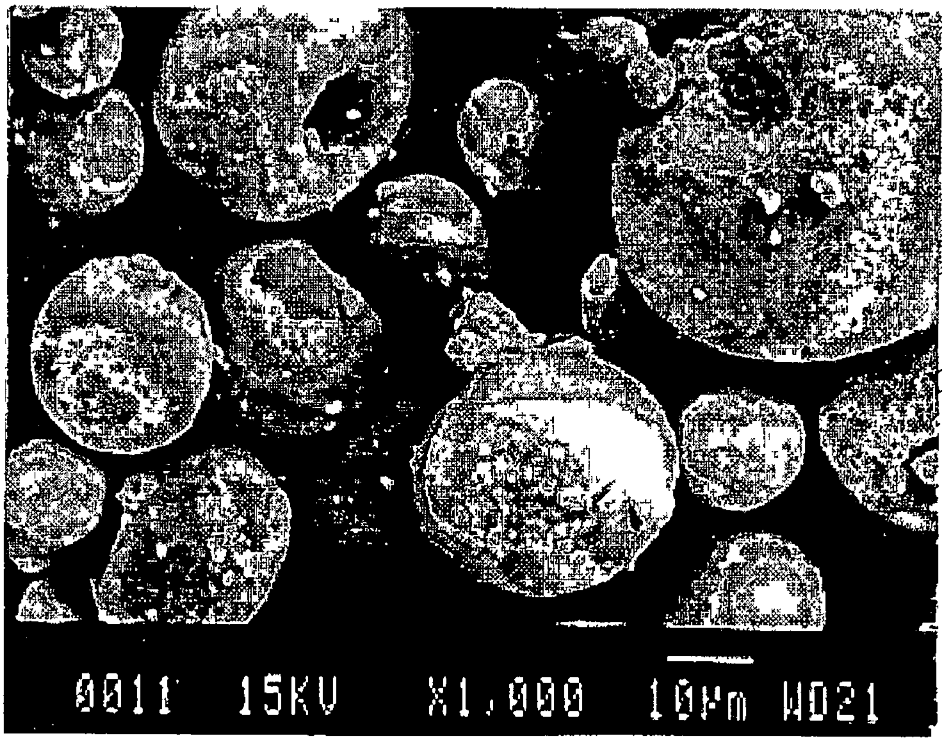

B

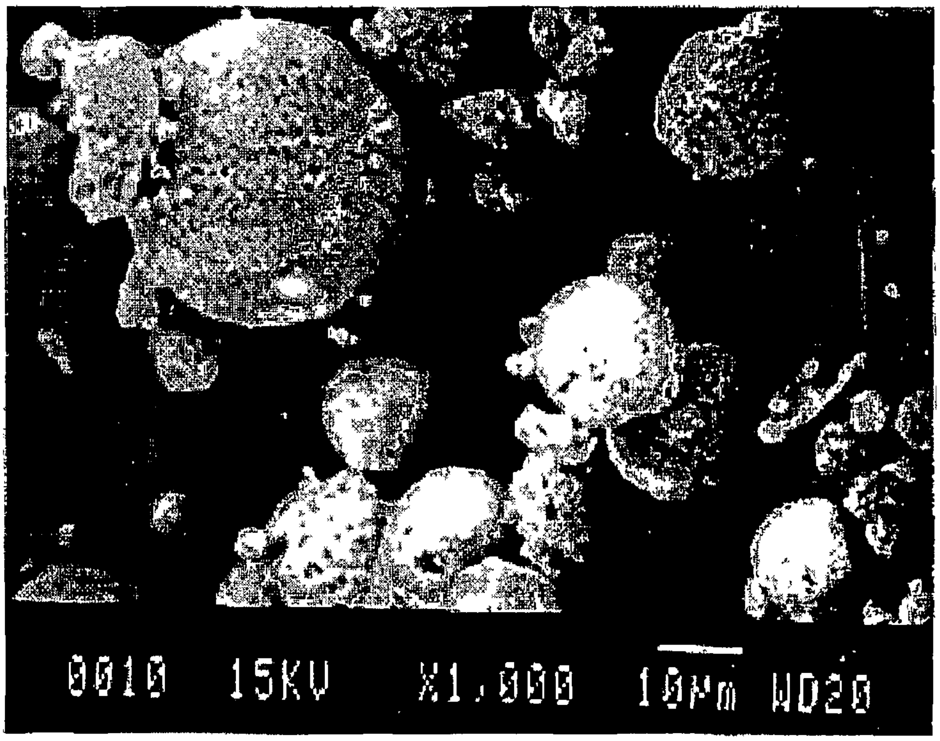

C

Figure 5 13 Scanning electron micrographs of spray dried powders (A) Run 4 (B) Run 8 and (C) Standard Powder

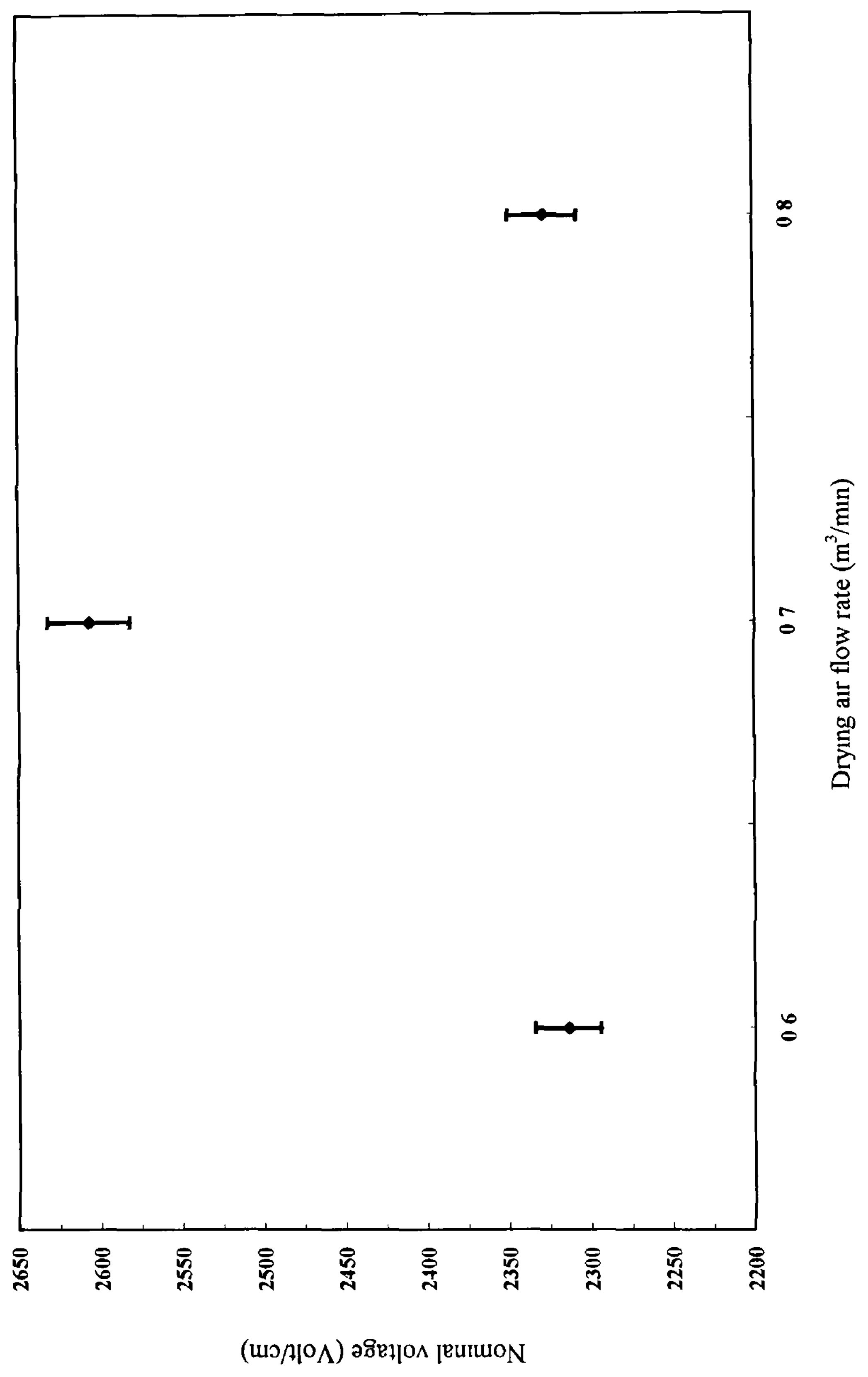

Figure 5 14 Nominal voltage of varistors from the powder produced under different set condition of drying air flow rate of the laboratory scale dryer

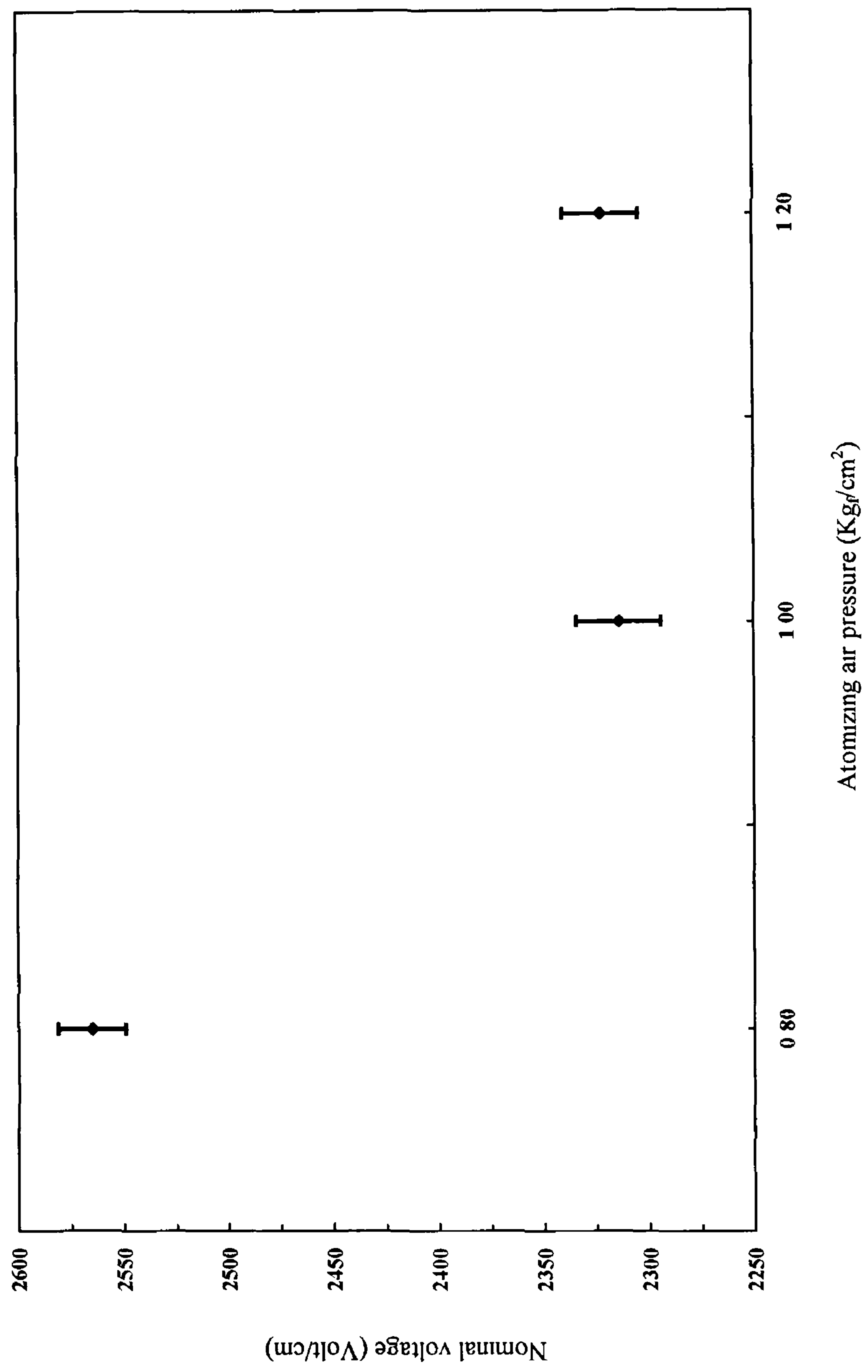

Figure 5 15 Nominal voltage of varistors from the powder produced under different set condition of atomizing air pressure of the laboratory scale dryer

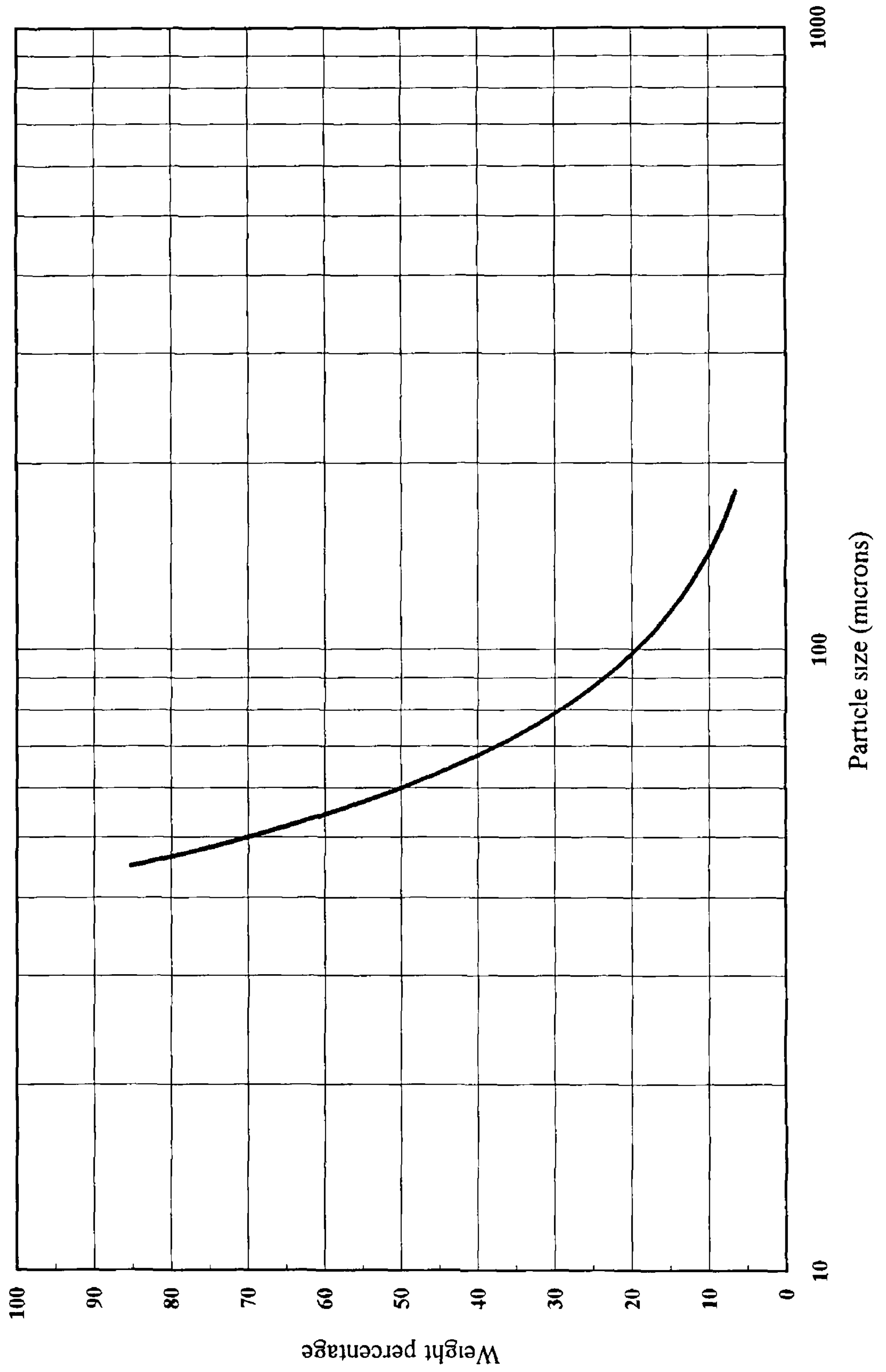

Figure 5 16 Particle size distribution of the powder produced through optimized operating condition of the pilot scale dryer

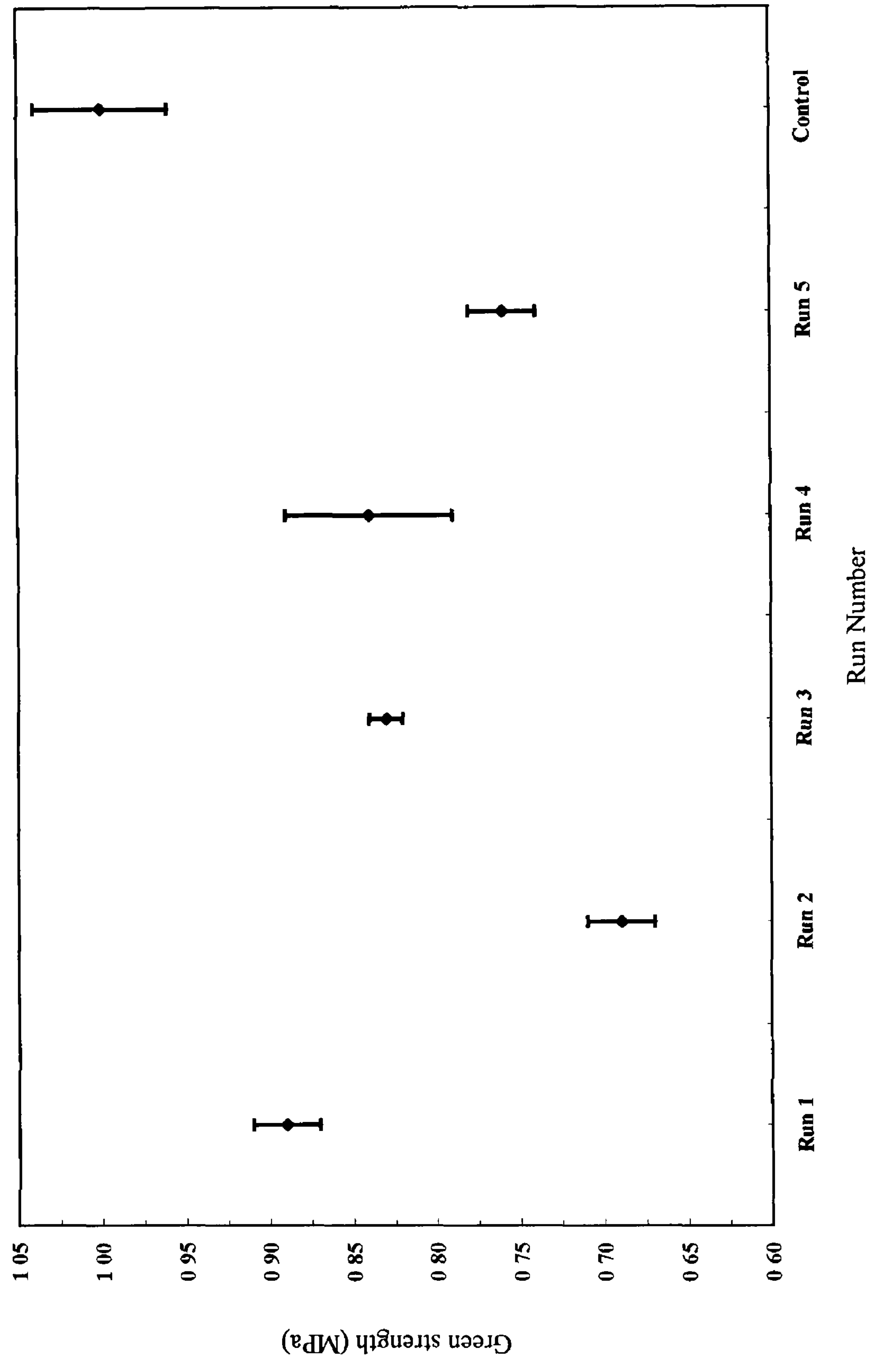

Figure 5 17 Green strength of the discs from the powder produced under different operating conditions of the pilot scale dryer

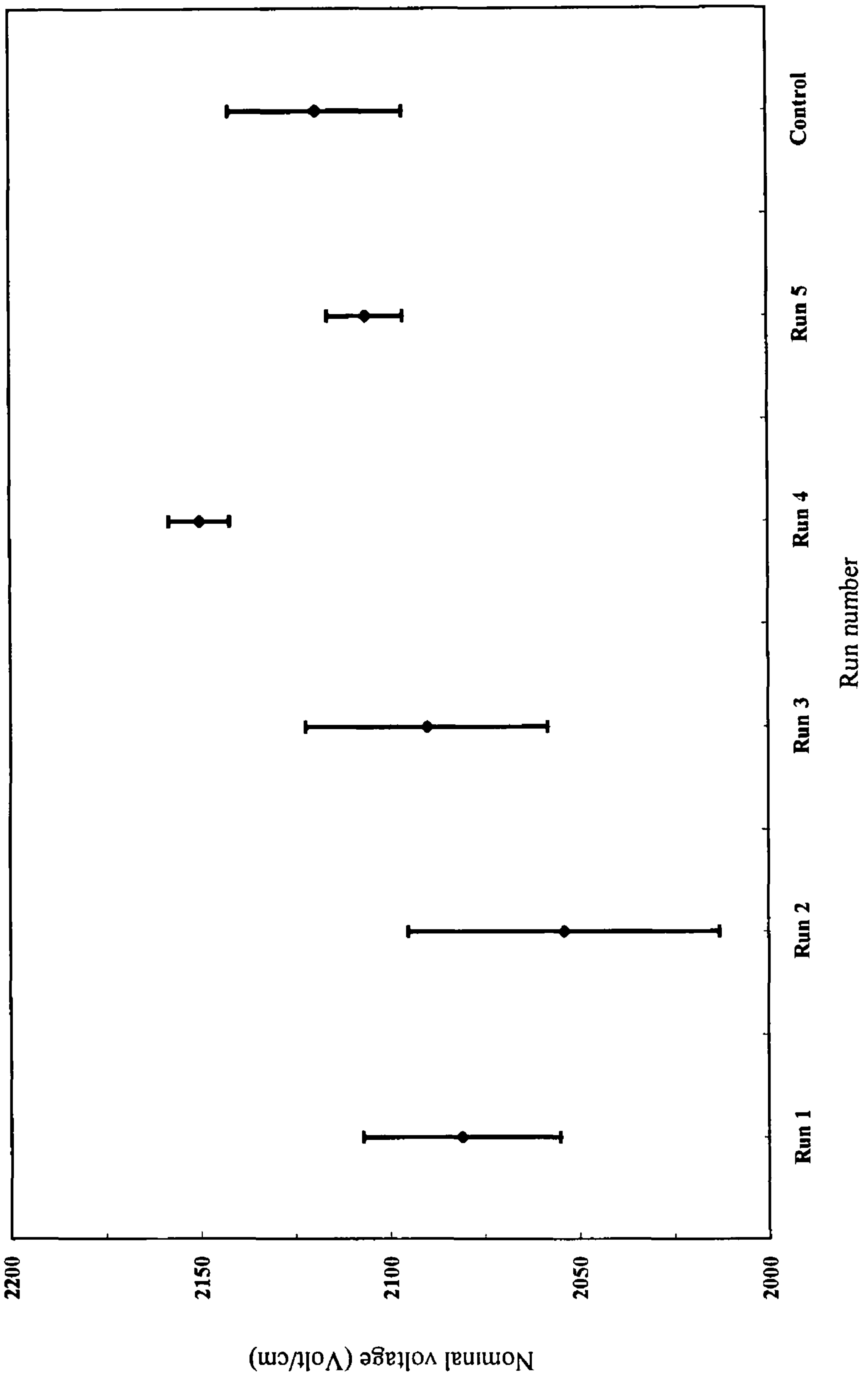

Figure 5.18 Nominal voltage of varistors from the powder produced under different operating conditions of the pilot scale dryer

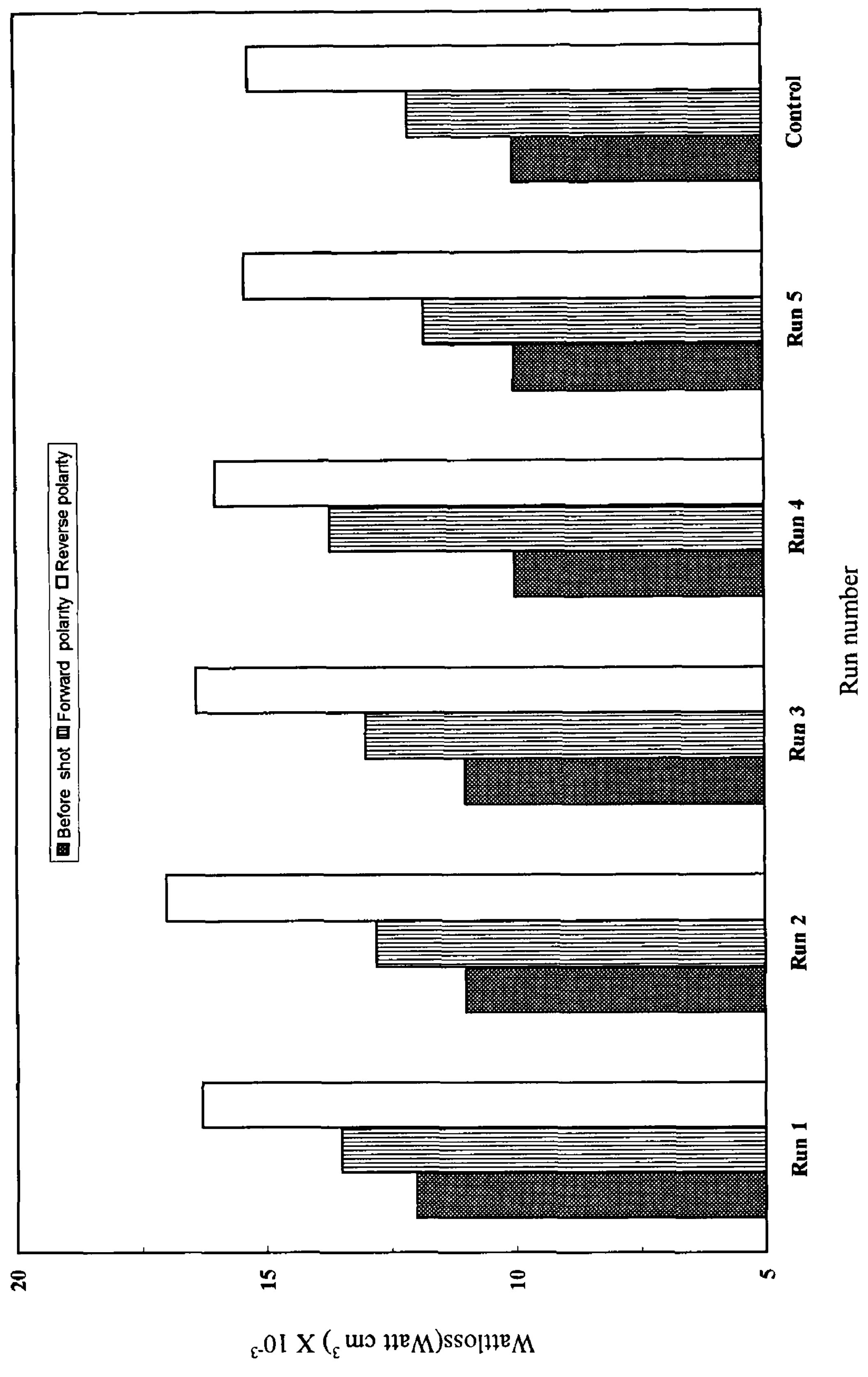

Figure 5 19 Wattloss of varistors from the powder produced under different operating conditions of the pilot scale dryer

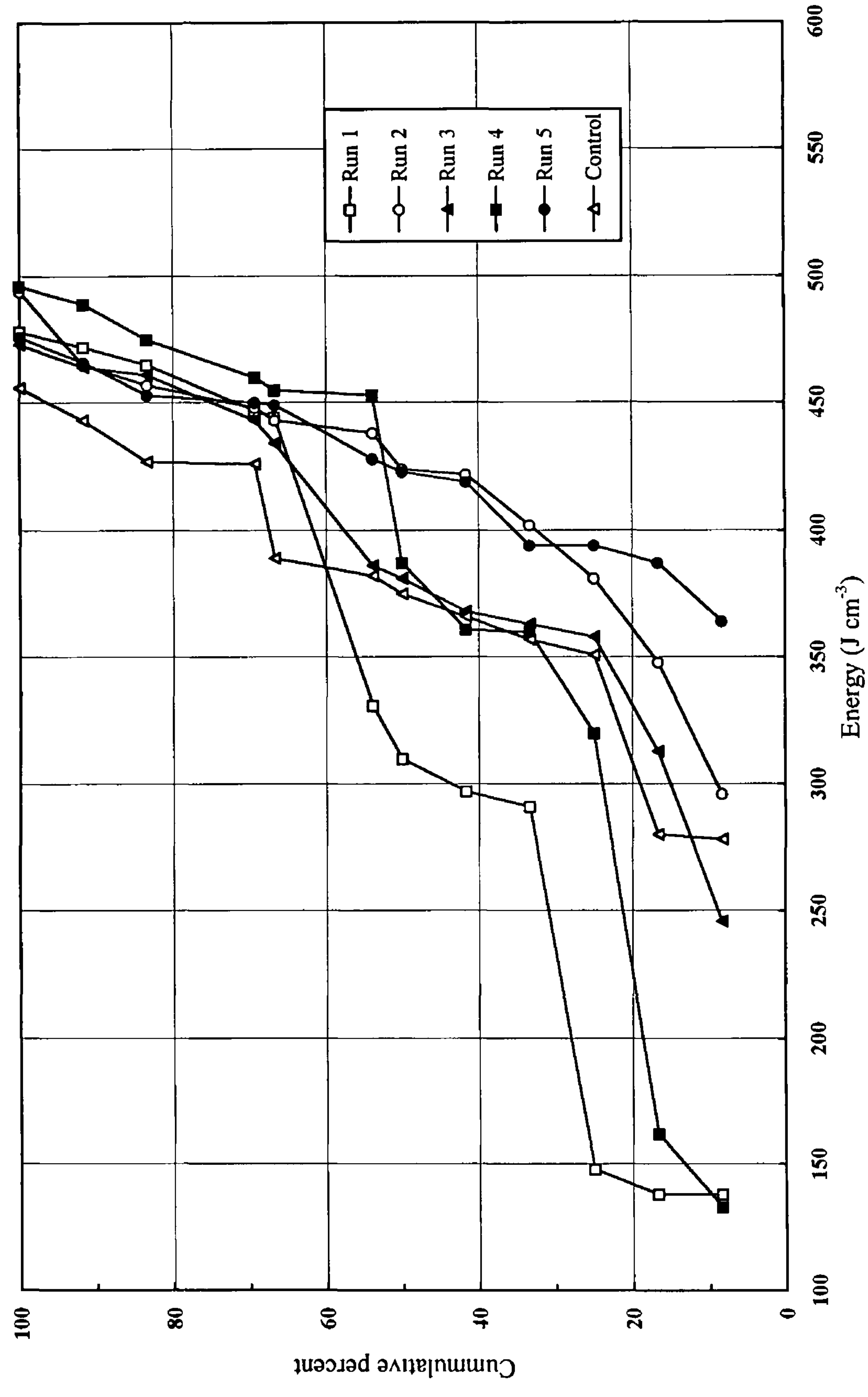

Figure 5 20 Energy absorption capability of the varistors from the powder produced under different operating conditions of the pilot scale dryer

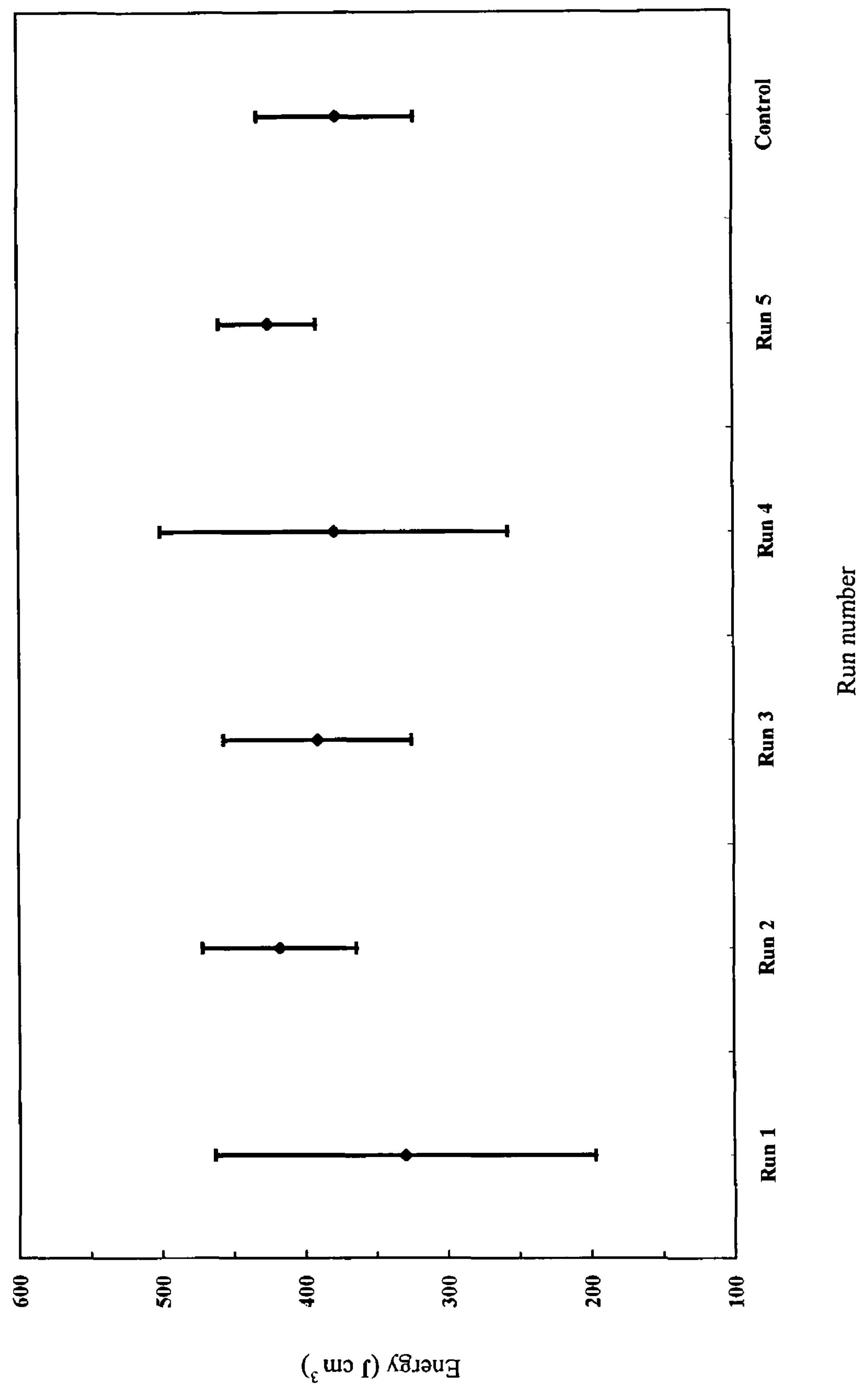

Figure 5.21 The mean value of energy with ± standard error of varistors from the powder produced under different operating conditions of the pilot scale dryer

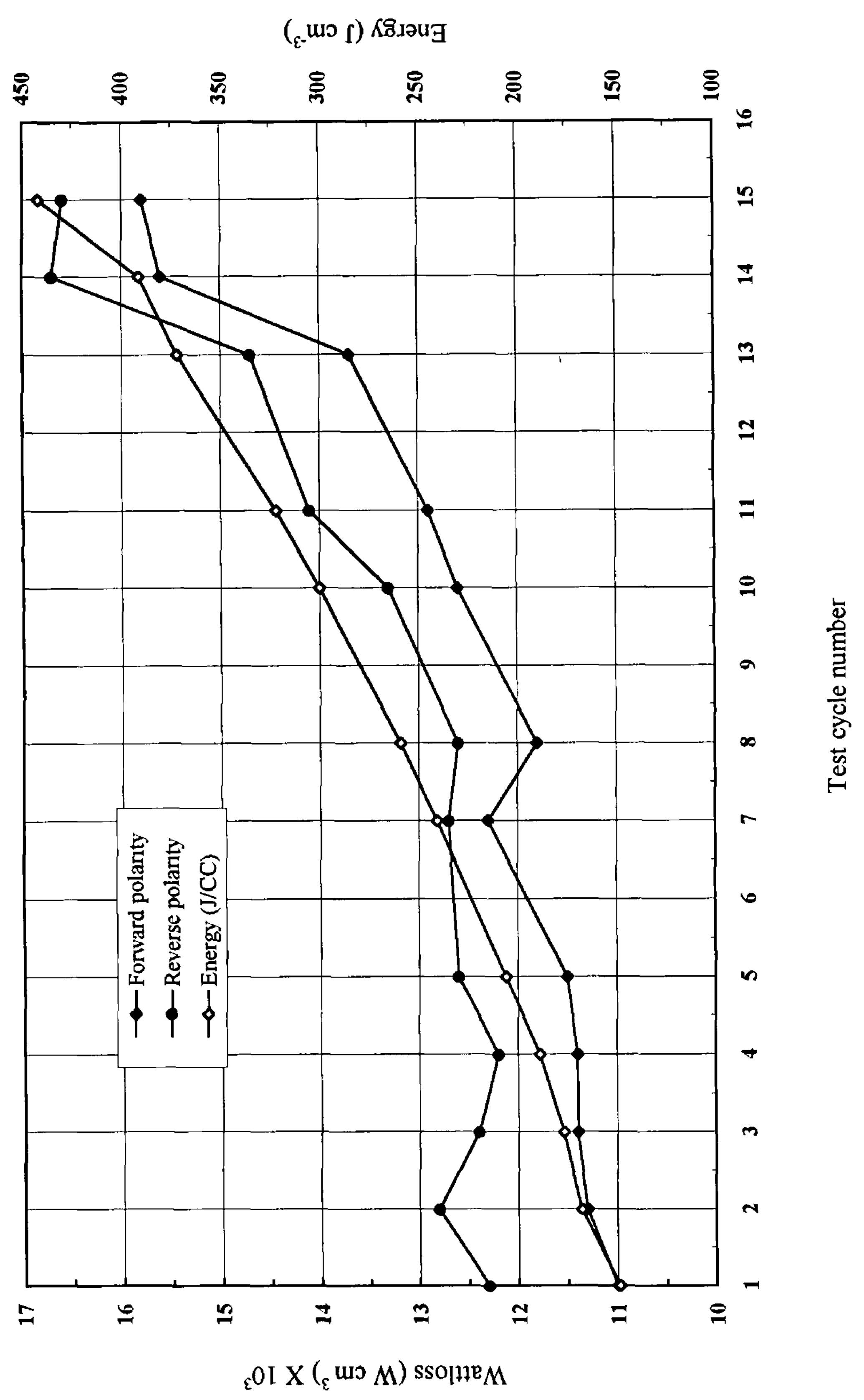

Figure 5 22 Degradation of varistors with the injection of long pulse from the powder produced under different operating conditions of the pilot scale dryer

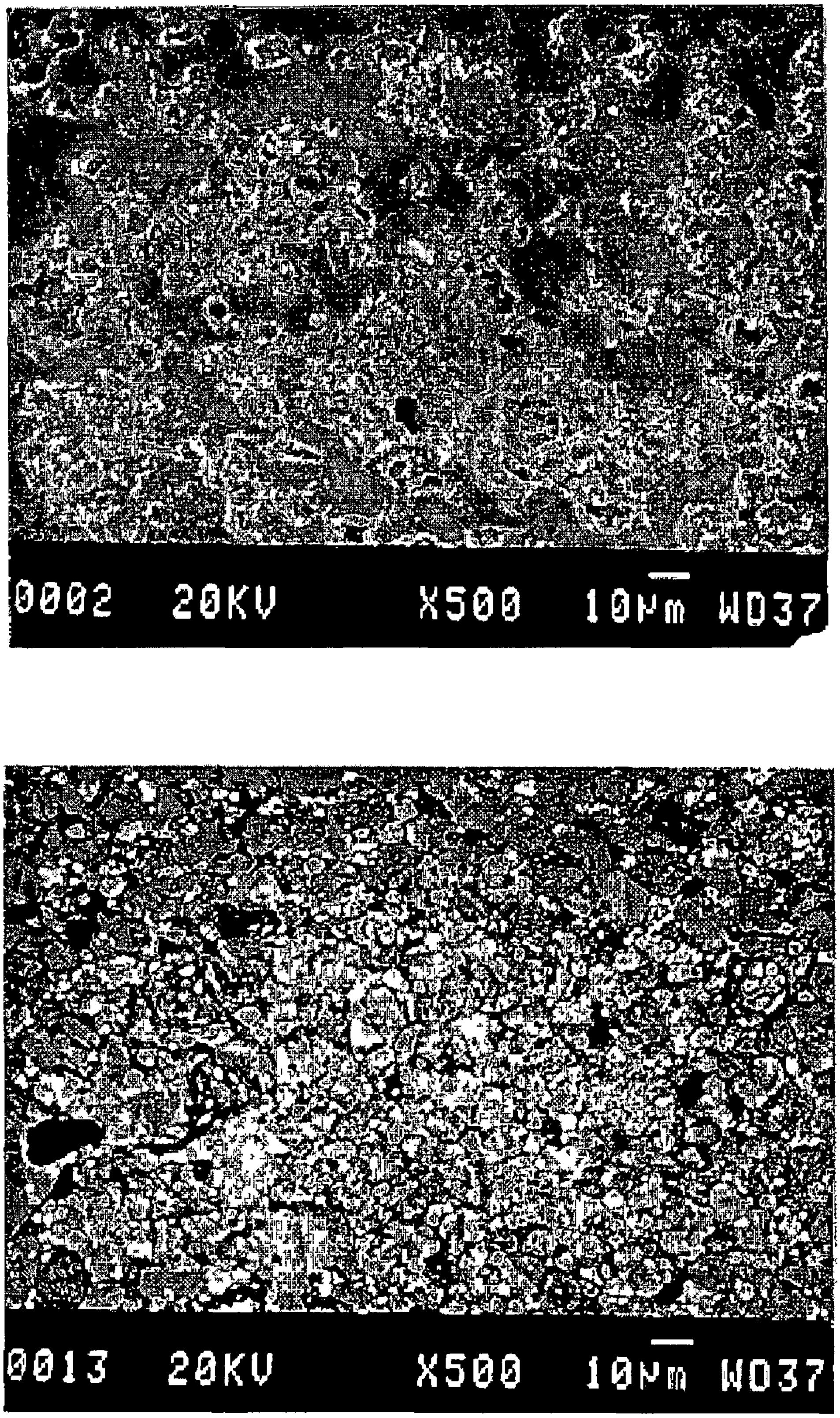

Figure 5 23 SEM photographs of varistors made from powder produced under the run condition 1 of the pilot scale dryer

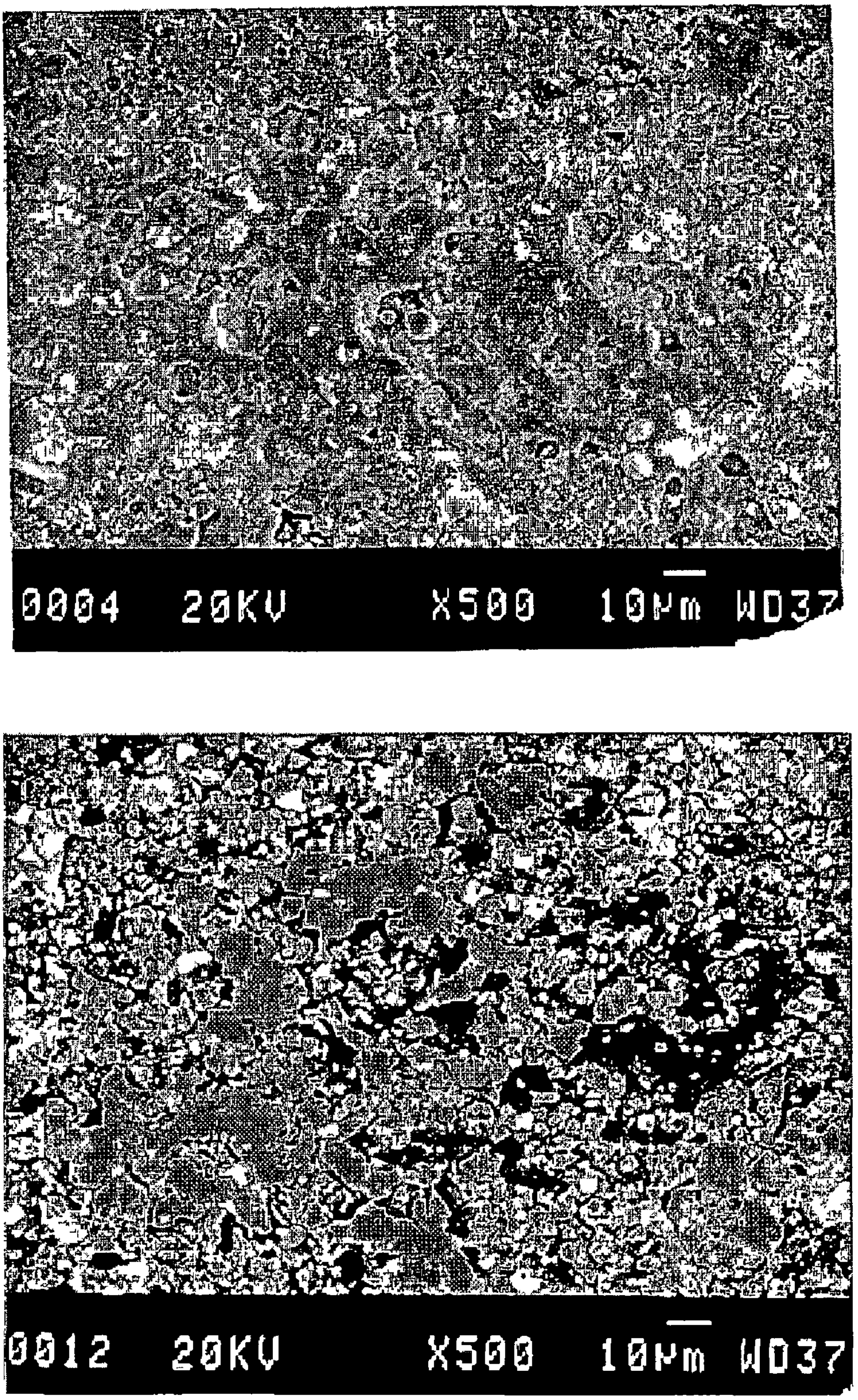

Figure 5 24 SEM photographs of varistors made from the powder produced under the run condition 2 of the pilot scale dryer

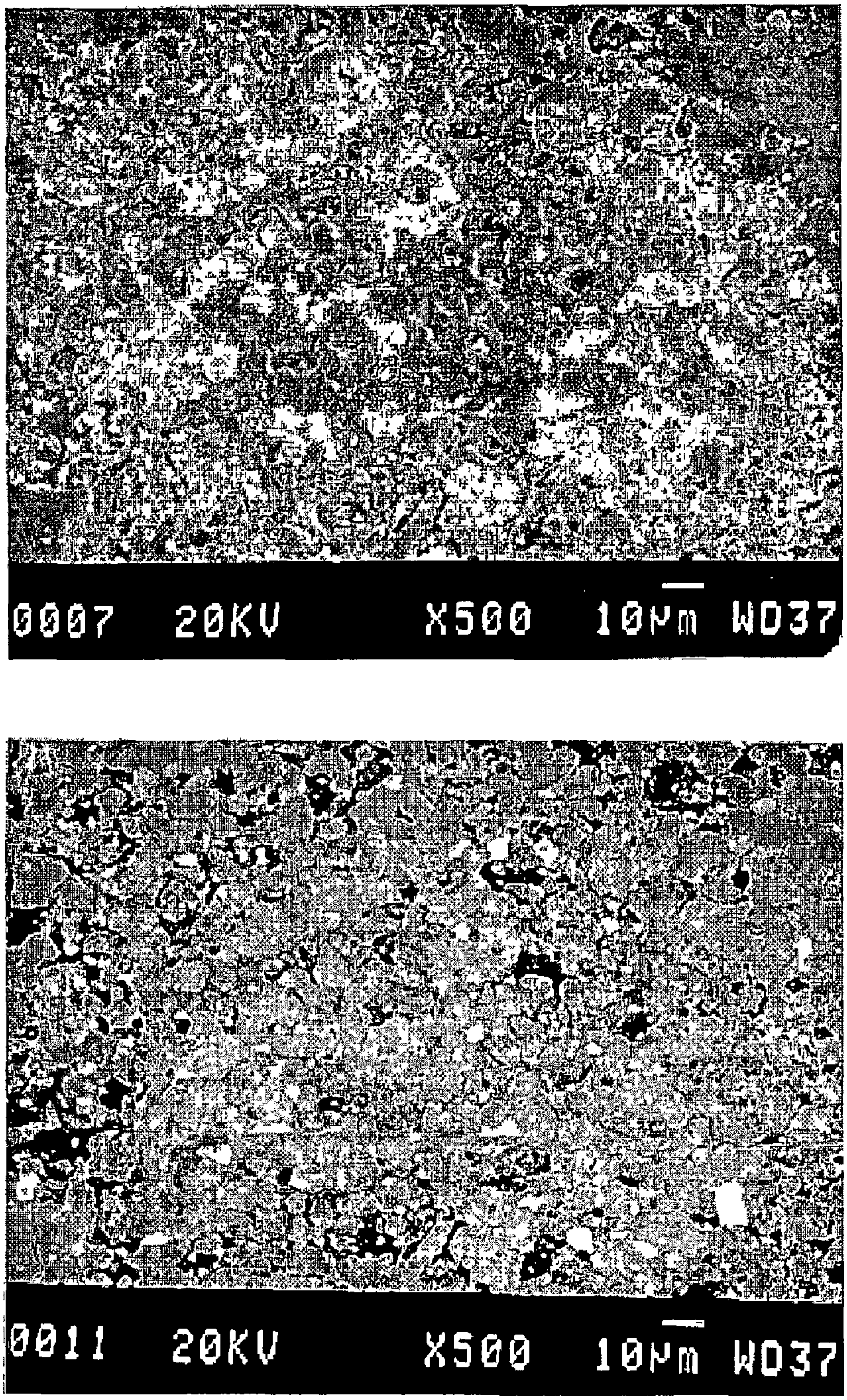

Figure 5 25 SEM photographs of varistors made from the powder produced under the run condition 3 of the pilot scale dryer

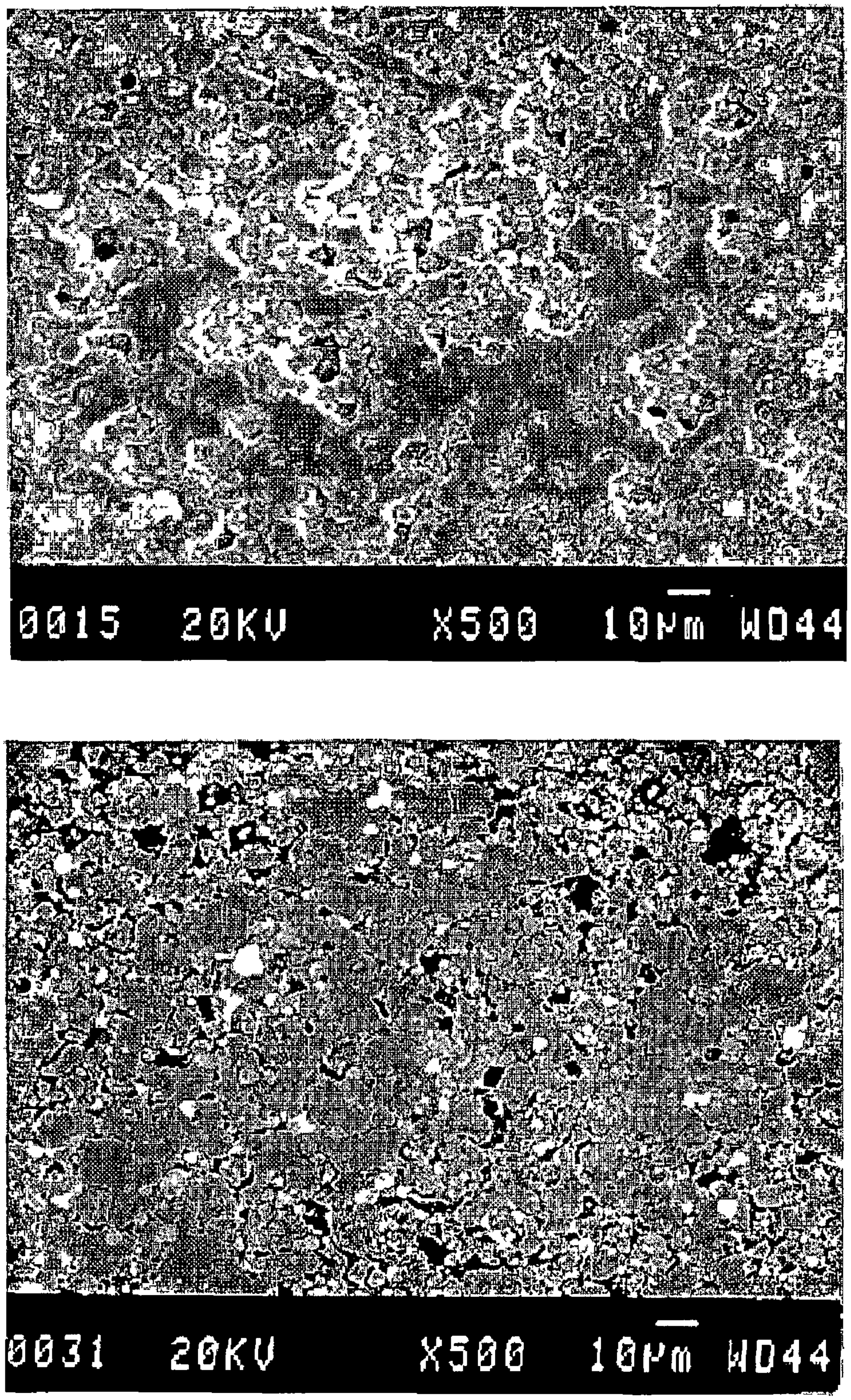

Figure 5 26 SEM photographs of varistors made from the powder produced under the run condition 4 of the pilot scale dryer

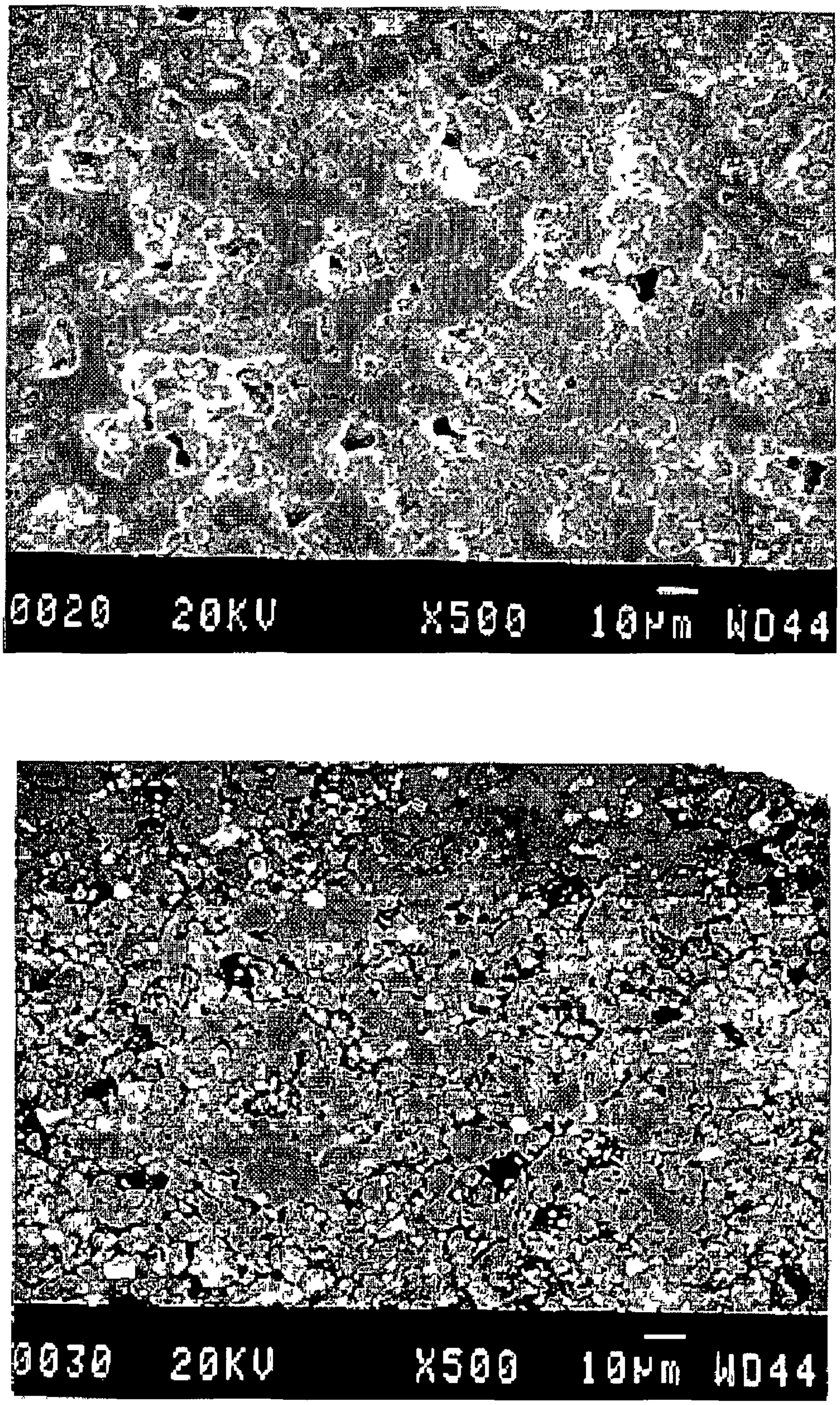

Figure 5 27 SEM photographs of varistors made from the powder produced under the run condition 5 of the pilot scale dryer

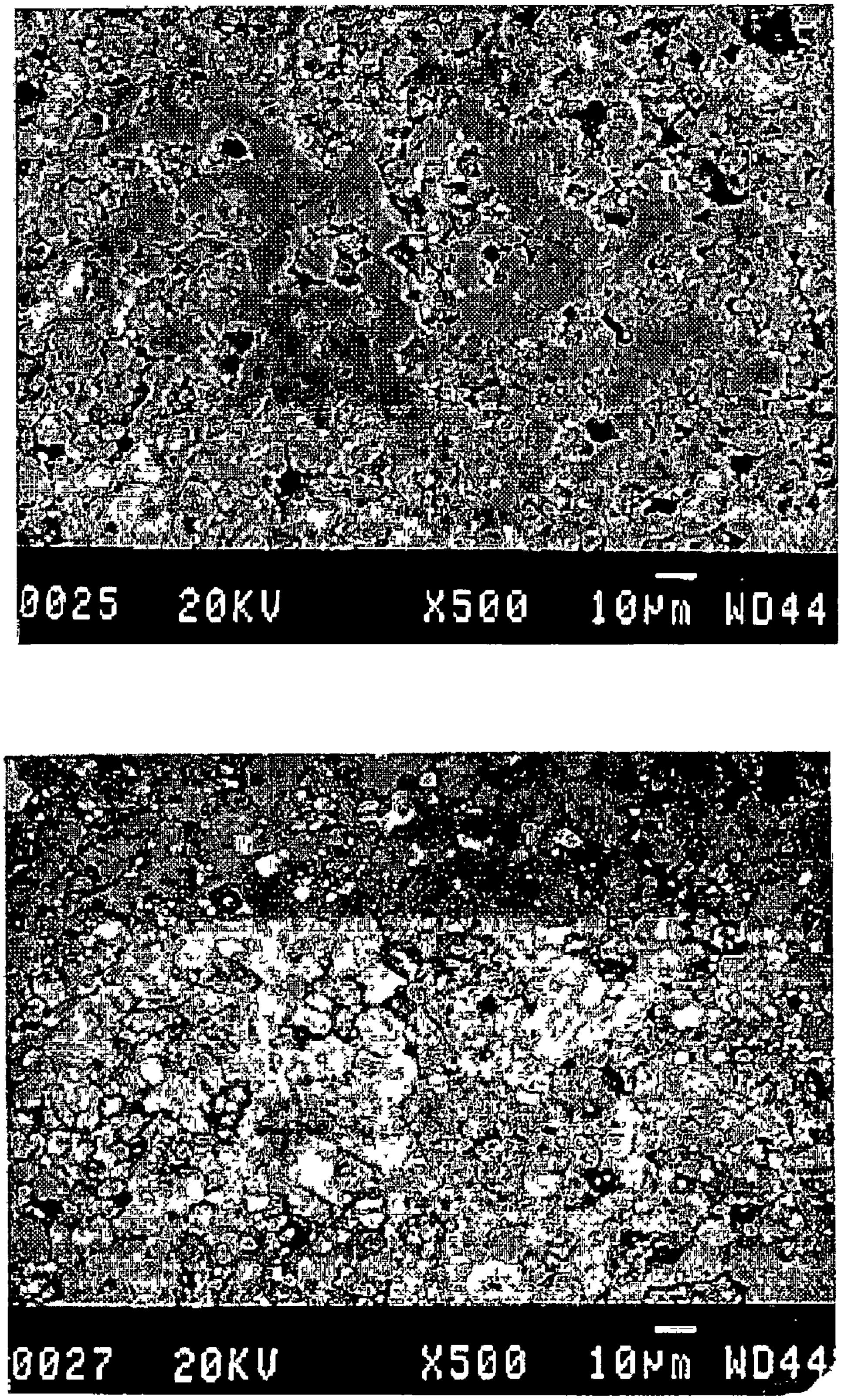

Figure 5 28 SEM photographs of varistors made from the powder produced under standard operating condition of the pilot scale dryer

5.3 BINDER SYSTEMS

5.3 1 Physical Property of Binder

The analysis with the new binder systems was performed by evaluating the physical properties of the binder, its effect on the slurry, the powder produced, and the electrical performance of the discs fabricated using those powders The pH of the emulsion latex binders was measured and found to be within the range of 6 5-10 It is known that the negatively charged polymer particles are stable over a wide pH range of 2 5-10 5, without being counter charged[66 113] and can provide better dispersion of the raw materials in water This is evident from the data presented in Table 5 5 Lower slurry viscosity for the same solid content was obtained with the latex binders Ltx A and Ltx C The lowest being achieved with the Ltx C The pseudoplastic nature of the binder Ltx C made it more attractive, by fulfilling the primary requirement of a binder to be used for spraying a slurry Furthermore, this binder also appeared to have a deflocculating nature as evident from the reduction in viscosity with the increase in binder content

5 3 2 Powder Characteristics

The characteristics of the powder with different binders, their level, and solid concentrations are presented in Table 5 6 The mean granule size was found to be dependent on the binder type and the slurry viscosity Under the same spray drying conditions, with the binder Ltx C, a low slurry viscosity obtained at lower level of solid content primarily produced the smaller particles As mentioned by Smith[53] the low viscosity of the slurry can consequently reduce the thermal efficiency of the spray dryer which can cause particles sticking to the drying chamber wall or to themselves

Table 5 5 Viscosity of binders and slurry at room temperature with spindle 1

Binder type	Binder as received		Slurry	
	rpm	Viscosity (CP)	rpm	Viscosity (CP)
Ltx A	100	68 8	100	52 0
	50	51 2	50	43 2
	20	48 0	20	36 0
Ltx C	100	167 2	100	49 6
	50	174 4	50	40 0
	20	184 0	20	36 0
Ltx E	100	73 6	100	53 6
	50	60 8	50	40 0
	20	56 0	20	24 0
PVA Soln	100	55 2	100	53 6
	50	40 0	50	41 6
	20	28 0	20	40 0

However, the latter can manifest itself by an increase of "satellites" (fines sticking to the large particles) which in turn lead to an increase of the average particle size

The bulk, tap, and granule densities of the powder processed with two latex binders, Ltx A and Ltx C are higher compared to those obtained with the polyvinyl alcohol as the binder Although all of the powders had a wide size distribution, there was a difference in the percent of fine and coarse particles Therefore, the higher bulk density is the result of particle packing efficiency presumably due to the difference in coarse and fine particles in the powder

The flowability of the powder was improved with the binder Ltx C indicating reduced interparticle frictional force The increase in the binder content from 1 0% to 1 3% (Ltx C1 and Ltx C) did not affect the bulk, tap, and granule densities But the increase in the solid content has led to enhanced bulk, tap, and granule densities for all the three binder concentrations as evident from the comparison in Table 5 6 of the effects between Ltx C1 and Ltx C3, Ltx C and Ltx C4, Ltx C2 and Ltx C5

Table 5.6 Viscosity of slurry and characteristics of powder prepared with different binder systems

Binder type	Slurry Viscosity (CP)	Mean size (µm)	Density (gm/cc)			Flow rate (gm/sec)	Angle of repose (°)	Moisture content (%)
			Bulk	Tap	Granule			
Ltx A	52 00	48 00	1 77	2 04	3 11	1 13	27 55	0 04
Ltx B	56 00	56 00	1 71	2 00	3 02	0 66	32 58	0 01
Ltx C	49 60	62 00	1 77	2 04	3 06	1 33	26 65	0 02
Ltx D	55 20	72 00	1 69	1 94	2 85	0 83	32 43	0 03
Ltx E	53 60	88 00	1 74	1 99	2 90	1 34	30 91	0 01
PVA	53 60	56 00	1 69	1 99	2 96	0 96	30 01	0 02
Ltx C1	50 40	66 00	1 76	2 05	3 06	1 27	28 07	0 02
Ltx C2	48 80	66 00	1 66	1 92	2 80	1 30	27 74	0 003
Ltx C3	116 80	73 00	1 88	2 10	3 17	1 58	28 48	0 04
Ltx C4	110 40	53 00	1 88	2 08	3 16	1 46	30 81	0 01
Ltx C5	107 20	61 00	1 86	2 09	3 15	1 43	30 76	0 02

Compressibility

The compressibility of powders with different binder systems are illustrated in Figure 5 29 The compressibility of the powder increases rapidly at the beginning of the compaction stress and then it starts to slow down at higher stress The sharp increase in the curve is due to the particle rearrangement, whereby the particles try to occupy the smallest place The particle packing efficiency is very important in this early stage As the pressure increases gradually, deformation and fracture of the particles start and this led to further rearrangement In the final stage, the densification depends on the elastic compression of the material No difference in compressibility was observed for the powder produced from the PVA and latex binders of up to 5 MPa But after this pressure level the powders with Ltx C and Ltx D exhibited better compressibility than the powder with polyvinyl alcohol At lower concentration of the solid, the increase of the binder level from 1 0% to 1 3 % increased the compressibility but a further rise in the binder level lowered it as shown in Figure 5 30 This low compressibility seems to be due to the pores within the particles generated by the slurry with low viscosity as inferred from Table 5 6 and the lower deformability caused by the higher strength of the particles with higher binder level Whereas, at higher solid concentration, the compressibility has decreased with the increase of the binder level from 1 0% to 1 3 %, and a further rise in the binder level did not lower it as depicted in figure 5 31 The higher compressibility at the lower binder level can be attributed to the deflocculating nature of the binder The increase in the solid content raised the viscosity to such a level that the atomization resulted in an increase of percent of coarse particles There was also subsequent reduction in pores within the particles as evident from higher granule density, thereby, making the powder more compressible

Green density

The variation in the green density of the discs produced applying the same pressure from the powders and containing different types of binders is shown in Figure 5 32 Higher green density is obtained for the powder with both the Ltx C and Ltx D Though the bulk, tap, and granule densities were poorer with Ltx D, the lower glass transition temperature and higher plasticizing effect due to the addition of a plasticizer made it more deformable, thereby, achieving higher green density similar to that for the powder with Ltx C At lower solid content, the change in the binder level from 1 0% to 1 3% increased the green density of the discs but a further rise in binder level lowered the density as shown in Figure 5 33 The green density had the same trend as compressibility But at higher solid content, the low and high levels of binder had a consistently higher green density

Green strength

The effect of the binder on the green strength of the discs is illustrated in Figure 5 34 There is a wide variation in the green strength, being lowest with the PVA and highest with the Ltx E All of the discs with the latex binder were found to have higher green strength than that of the PVA The measured strength was also analyzed by Weibull Fracture Theory as described in Chapter 4 The normalizing stress (σ_o), calculated from plot *ln (ln (1/1-S))* versus *ln (σ)* had the similar trend like the green strength, that is, the value is higher for the samples prepared with the latex binders and the highest being obtained with the Ltx E However, the Weibull modulus, (m), summarized in Table 4 11 had a higher value with Ltx B, indicating less scattering in strength The latex binders contain carboxylic acid group and the presence of interchain hydrogen bonding within the group is responsible for polymer to ceramic and polymer to polymer bonding This type of bonding is not found with the PVA and it is assumed that this type of bonding will provide more strength[66 67]

The increase in the binder content, therefore, increases the green strength Further enhancement in the green strength was achieved when the discs were made from the powder with a higher percentage of solid in the slurries as shown in Figure 5 35 The percentage of the fine particles and the granule density of powder were higher at higher levels of solid content as can be seen from the data presented in Table 5 6 The increase in green the strength is supported by Rampf[77] in that the strength of the discs would be increased by the higher percentage of the fine and volume fraction of the solid within the powder

Fired density

The fired density of the discs sintered in the same pot kiln with the same temperature profile is presented in Figure 5 36 Higher fired density is obtained with both the Ltx C and Ltx D and it is almost the same as the discs with the binder PVA Densification during sintering is a complex phenomena In general it is believed that a higher green density will lead to a higher fired density But the densification mechanism of zinc oxide varistor is liquid phase sintering There are three stages in this process (i) the first stage-solubility and rearrangement, (ii) intermediate stage-solution reprecipitation, and (iii) the last stage-solid state controlled sintering The rearrangement at the first stage is the function of capillary force of the liquid, the contact angle between the solid and the liquid, and solid-solid separation Higher green density, that is, less solid-solid separation is not favourable for better rearrangement In the later stage, diffusion mechanism is the dominating factor, which can cause the pore to shrink or grow It is established that if the pores co-ordinate with particles fewer than the critical number then they disappear spontaneously[74] The pore closure also depends on the dihedral angle which is the ratio of the external surface energy to the grain boundary energy

The variation in the fired density with the change in the binder level at various solid concentrations is illustrated in Figure 5 37 At lower solid content, the change in the binder level from 1 0% to 1 3% increased the fired density but further rise in the binder level did not increase the density any more However, for a higher solid content in the slurry, the low level of binder exhibited the highest fired density

Shrinkage

The shrinkage of the fired discs with the different latex binder systems are plotted in Figure 5 38 for a standard level of binder and solid concentration Both the radial and axial shrinkage were found to be less for Ltx C and Ltx D in comparison to PVA The magnitude of shrinkage is dependent on the green density and it is obvious that the highly dense discs will undergo minimum shrinkage to attain a particular fired density The axial shrinkage was found to be lower than the radial shrinkage for all the cases

The influence of binder level on shrinkage of the fired discs at lower level of solid concentration is presented in Figure 5 39 Shrinkage was less at 1 3% of binder compared to that observed at two other levels But, at higher solid concentration the effect was found to be the reverse Less shrinkage was observed for 1 0% and 1 6% binder level as shown in Figure 5 40

Fired strength

The influence of the binder on the strength of the fired discs are demonstrated in Figure 5 41 There are a wide variation in strength and the highest being obtained with Ltx B The strength of the fired discs with Ltx C was higher than that of PVA The consistency of the strength was also higher than that of Ltx B, as can be seen by the lower standard deviation and higher Weibull modulus, (m) (Table 4 11)

The fired strength was changed significantly with the variation in the level of binder Ltx C at lower solid concentration as shown in Figure 5 42 The higher strength was obtained at 1 3% binder level with a low value of standard error While, the higher solid concentration at 1 0%

binder level enhanced the fired strength as illustrated in Figure 5 43 Moreover, the Weibull modulus, (m) and normalizing stress, (σ_o) were found to be higher for the same condition The higher fired strength might be related to higher green density, as it is thought that a highly dense green body would introduce less flaws in the fired body

5.3 3 Electrical Characteristics

The useful varistor parameters such as nominal voltage, wattloss, clamp ratio, non-linear exponent, energy absorption capability were evaluated for the varistors prepared from powder with different binder systems Nominal voltage was found to be significantly influenced by the type of binder present in the powder The low slurry viscosity with binder Ltx C resulted in finer atomization As a result smaller particles were produced which consequently raised the number of grains Non-linear co-efficient and clamp ratio were also improved for the varistors made from powder containing Ltx C The influence of binder, its level and solid concentration had influence on the energy absorption capability of varistor

I-V curves

The I-V curves of the varistors made from the powder containing different binder systems are presented in Figure 5 44 The curves were shifted slightly toward the left for the varistors when fabricated from the powder with Ltx C and Ltx E The varistors with other latex binders did not show any significant difference from the conventional one The I-V curves of the varistors with Ltx C with different binder level, at lower and higher solid concentrations are shown in Figures 5 45 and 5 46 The curves moved towards the left at higher binder level for both the low and high solid contents The possible explanation of this behaviour can be given by the binder remnant ash and its composition ICP analysis of the ash is tabulated in Table 5 7

Table 5.7 ICP analysis of ash for different binder systems

Element present	Binder type with percentage of ash content			
	Ltx A (0 43)	Ltx C (0 50)	Ltx E (0 21)	PVA (0 17)
Sodium (ppm)	194 38	606 71	167 7	290 6
Calcium (ppm)	3 6667	7 7400	1 4100	-
Copper (ppm)	1 2222	0 8600	0 126	ND
Aluminum (ppm)	2 2957	1 0522	ND	ND
Iron (ppm)	2 5385	1 6923	ND	4 6
Zinc (ppm)	0 5164	1 0901	-	-

The main component of the ash is sodium and its amount is high for the Ltx C binder The sodium atom acts as an amphoteric dopant[114] which can occupy both the lattice and interstitial sites of ZnO grains The presence of sodium up to a certain extent in ppm level can help to reduce the grain boundary resistivity and to shift the curve towards the left

Nominal voltage

The nominal voltage at a current density of 0 61 mA/cm^2 is illustrated in Figure 5 47 The powder processed with Ltx E gave the highest value But the influence of Ltx C is quite high in comparison to the PVA The change in the nominal voltage with the variation in binder level at different solid concentrations is given in Figure 5 48 The value decreased for the change of the binder level from 1 0% to 1 3% but rose again at 1 6% binder level for both the low or high solid concentrations The deflocculating nature of the binder Ltx C caused finer atomization As a result, smaller particles were produced which increased the grain number during firing, and consequently raised the nominal voltage

Wattloss

The wattloss is presented in Table 5 8 for varistors made from the powder with different binder systems The wattloss before the application of the high amplitude short duration pulses was low with Ltx C This may be due to the sodium, the presence of which in ppm up to a certain amount can reduce grain boundary resistivity and thereby, the joule heating

However, after the application of the high amplitude short duration pulses, the higher wattloss was obtained for the varistor made with powder having a lower level of binder Ltx C and higher solid concentration in the slurry, that is, with Ltx C3 Due to the use of lower level of binder Ltx C less sodium was incorporated into the varistor by firing It is mentioned by Gupta[112] that the presence of sodium up to a certain extent can occupy the position of interstitial zinc ion in the depletion layer and can promote the stability of the device

Clamp ratio

The clamp ratio was not significantly affected by the binder systems as seen in Table 5 8 But, a lower value was obtained with Ltx C and Ltx E both in the pre-breakdown and breakdown regions With the Ltx C2, that is, the higher level of binder Ltx C at lower solid has resulted in a further reduction in clamp ratio It is anticipated that the lower clamp ratio is due to sodium incorporated by the binder within the varistor Sodium acts as a donor and it can decrease the grain resistivity at higher current density and lower the clamp ratio However, the lowest clamp was obtained with Ltx C3, that is, at high solid concentration and a lower level of binder Ltx C This may be attributable to the larger grain size which can reduce the clamp voltage[30]

Table 5 8 Wattloss of varistor produced from powder with different binder systems

Binder in varistor powder	Wattloss X 10^3 (W cm^{3})			Clamp ratio	
	Before shot	After shot		@ 50 µA-1 mA	@1 mA-1 KA
		Forward polarity	Reverse polarity		
Ltx A	16 0	15 0	17 0	1 17	1 68
Ltx B	14 0	17 0	17 0	1 16	1 68
Ltx C	12 0	16 0	17 0	1 14	1 66
Ltx D	15 0	15 0	16 0	1 15	1 67
Ltx E	13 0	14 0	15 0	1 14	1 66
PVA	15 0	18 0	19 0	1 16	1 67
Ltx C1	14 0	15 0	17 0	1 15	1 66
Ltx C2	11 0	14 0	15 0	1 12	1 65
Ltx C3	13 0	25 0	25 0	1 08	1 63
Ltx C4	14 0	15 0	15 0	1 14	1 68
Ltx C5	11 0	14 0	14 0	1 06	1 64

Non-linear co-efficient

The non-linear co-efficient of varistors produced from the powder with different binder systems is shown in Figure 5 49 A high exponent was obtained with Ltx C But it increased further with a high level of Ltx C and a low solid concentration in the slurry The highest exponent (α) was obtained with Ltx C at a lower level of binder and higher solid concentration as illustrated in Figure 5 50 The trend is the same as the clamp ratio, as the lower clamp results in higher non-linear co-efficient

Energy absorption capability

The energy absorption capability of the varistors made from the powder with different binder systems is illustrated in Figure 5 51 There was no significant difference in the energy absorption capability among the varistors produced from the powder containing latex and conventional binder But the performance was poor with the Ltx C The binder, Ltx C, showed enhanced performance in terms of the powder characteristics as well as the electrical properties like wattloss, clamp ratio, non-linear co-efficient, and nominal voltage etc as discussed earlier The reason for the poor performance in terms of energy is not clear

The presence of either a lower or a higher level of Ltx C resulted in almost the same energy absorption capability as the conventional one as shown in Figure 5 52 However, it was much more consistent with Ltx C3, that is, at low level of Ltx C and high solid concentration in the slurry as given in Figure 5 53 The consistency can be attributed to the presence of less flaws in the fired body as interpreted from the Weibull modulus, m (Table 4 11) for fired strength The failure mode was predominantly by electrical puncture for the varistor with all the binder systems

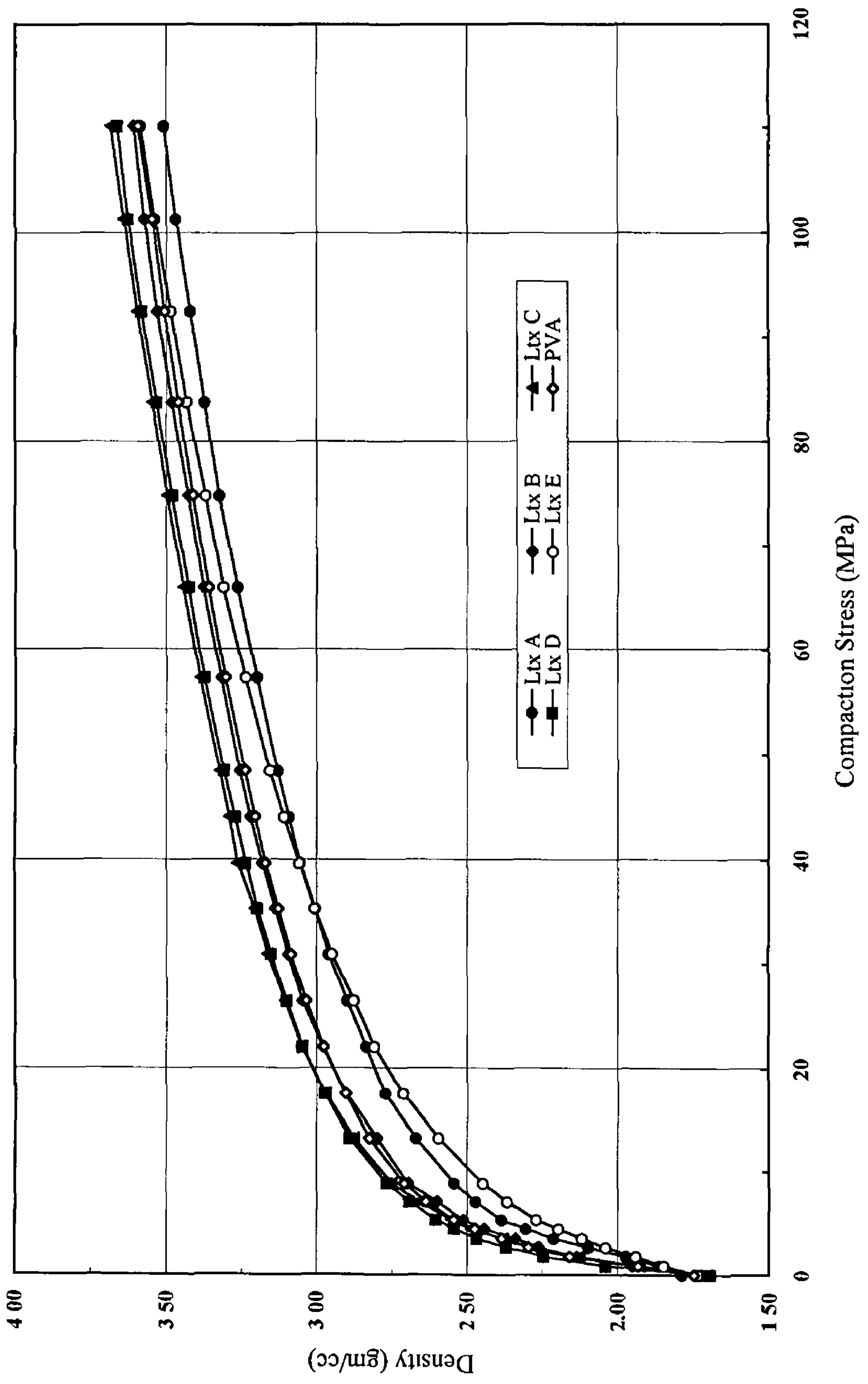

Figure 5 29 Compressibility of the powders with different binder systems

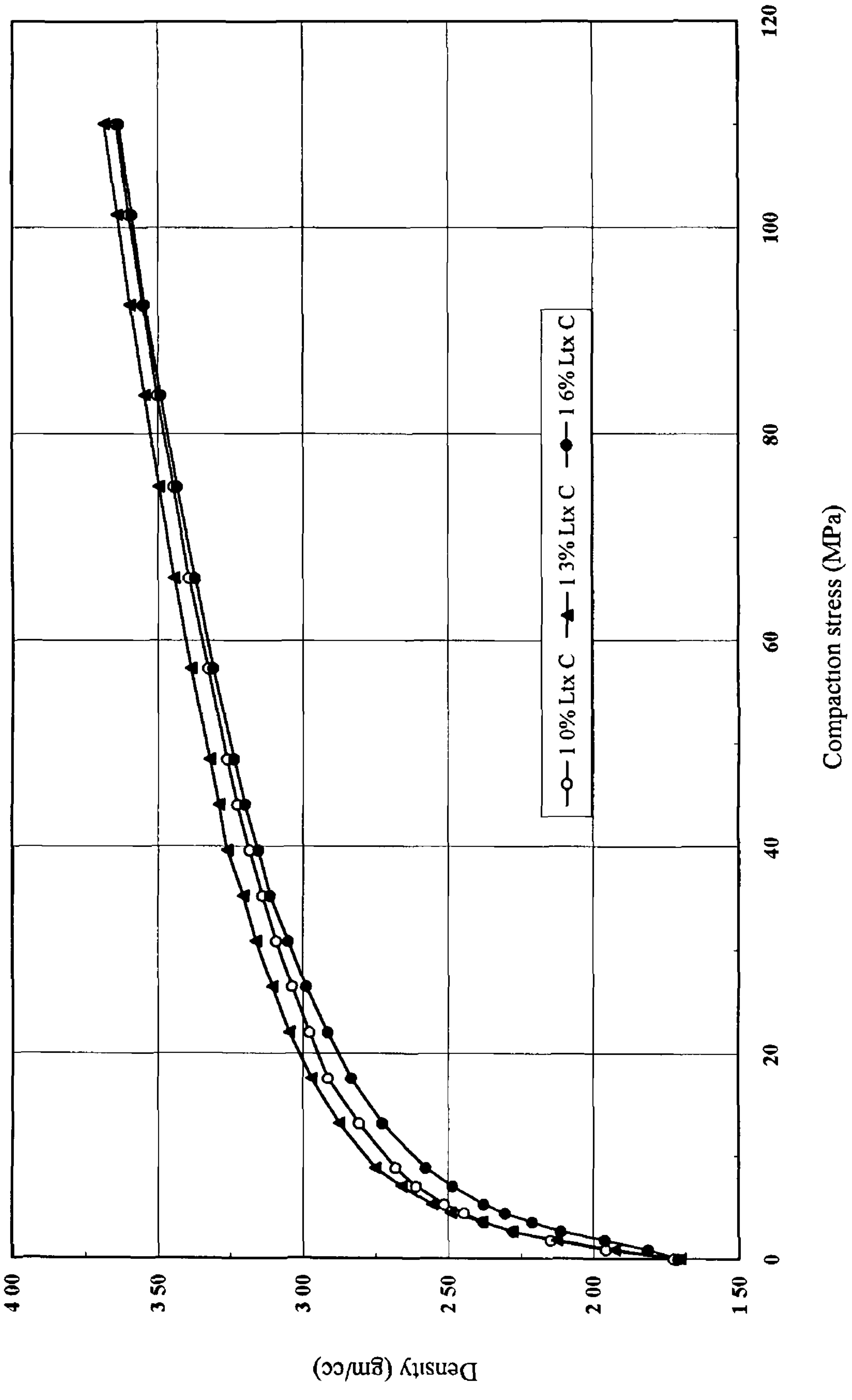

Figure 5.30 Compressibility of the powders with different levels of binder at lower solid concentration

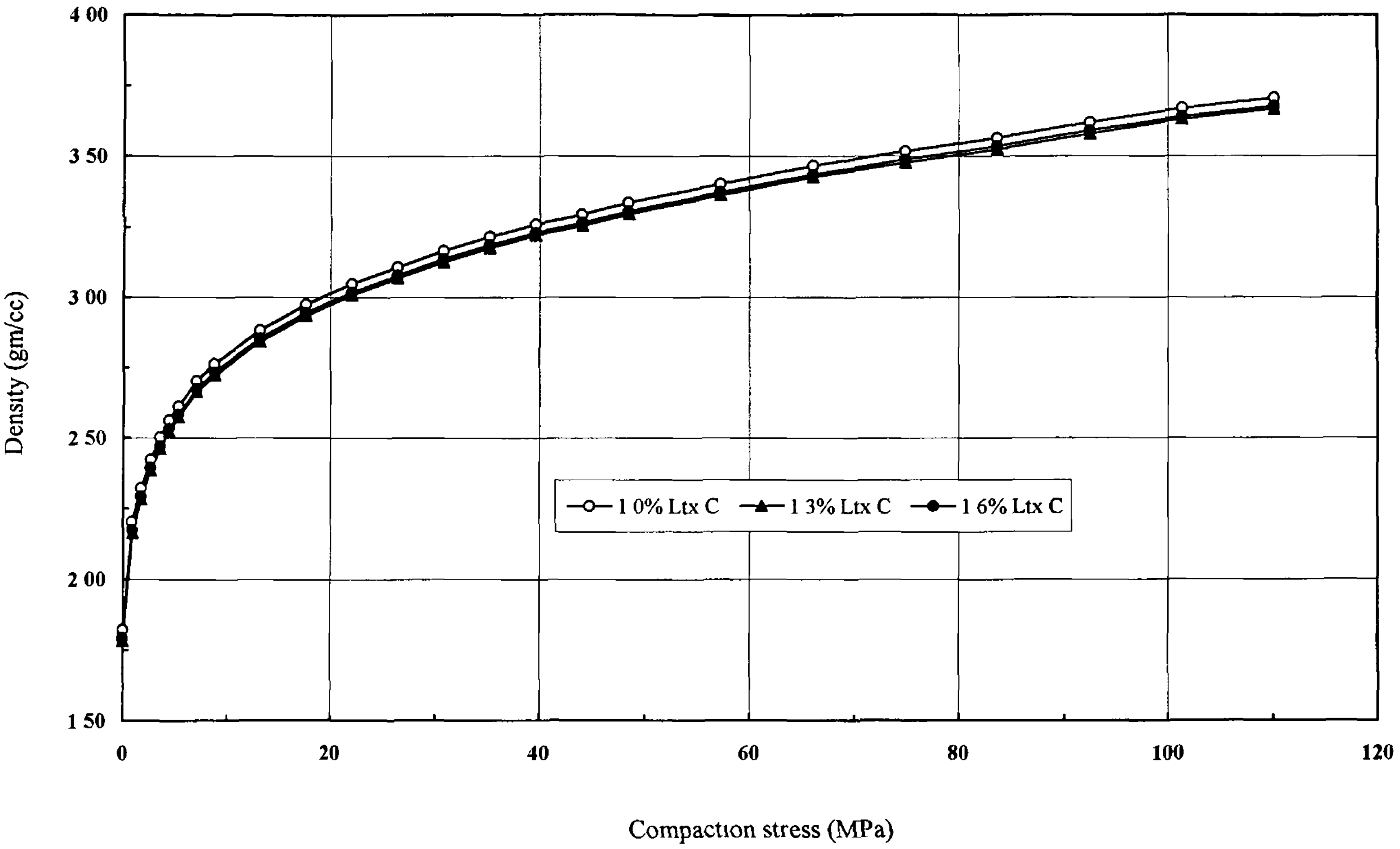

Figure 5.31 Compressibility of the powders with different levels of binder at higher solid concentration

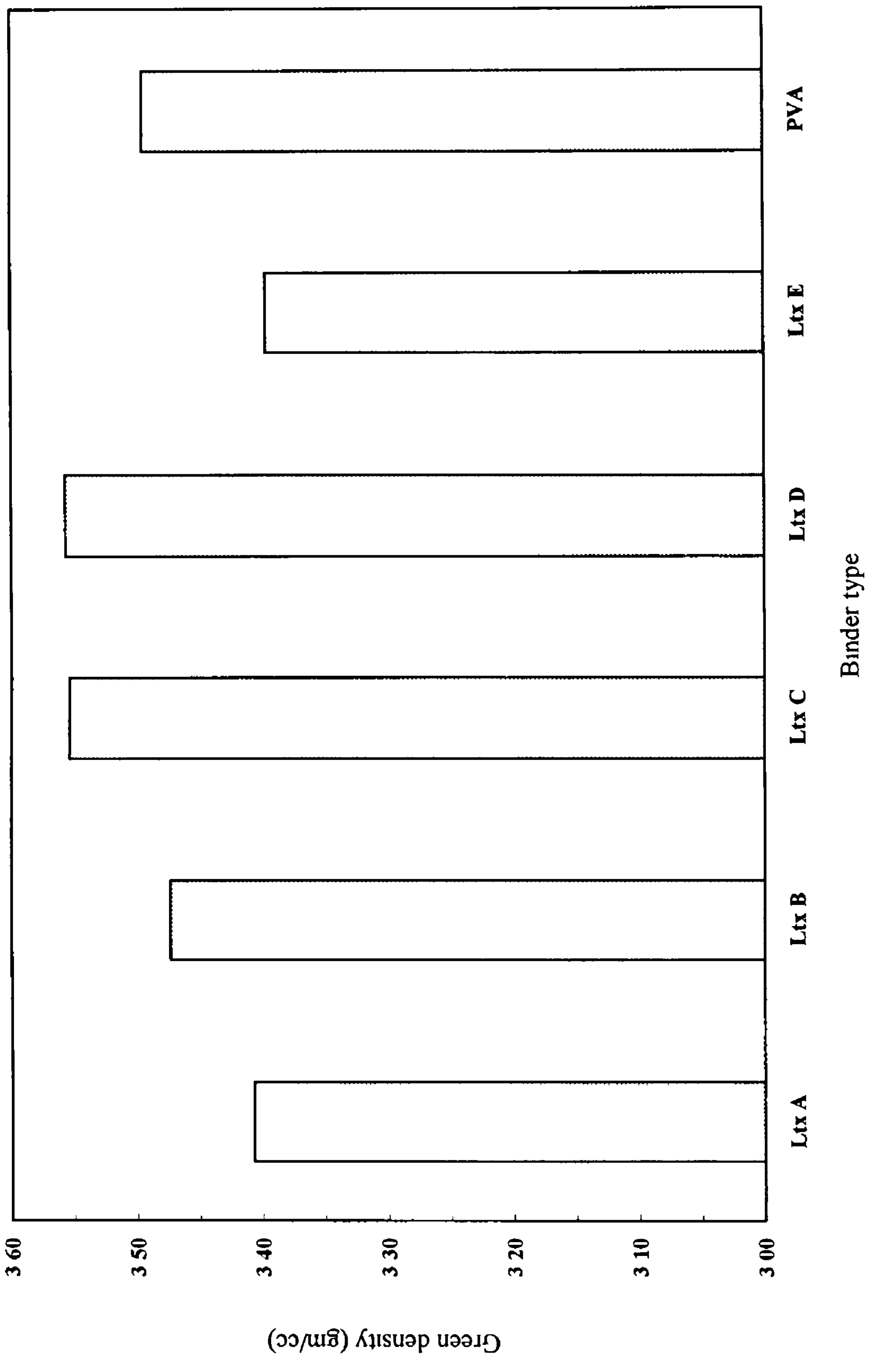

Figure 5.32 Green density of the discs produced from the powders with different binder systems

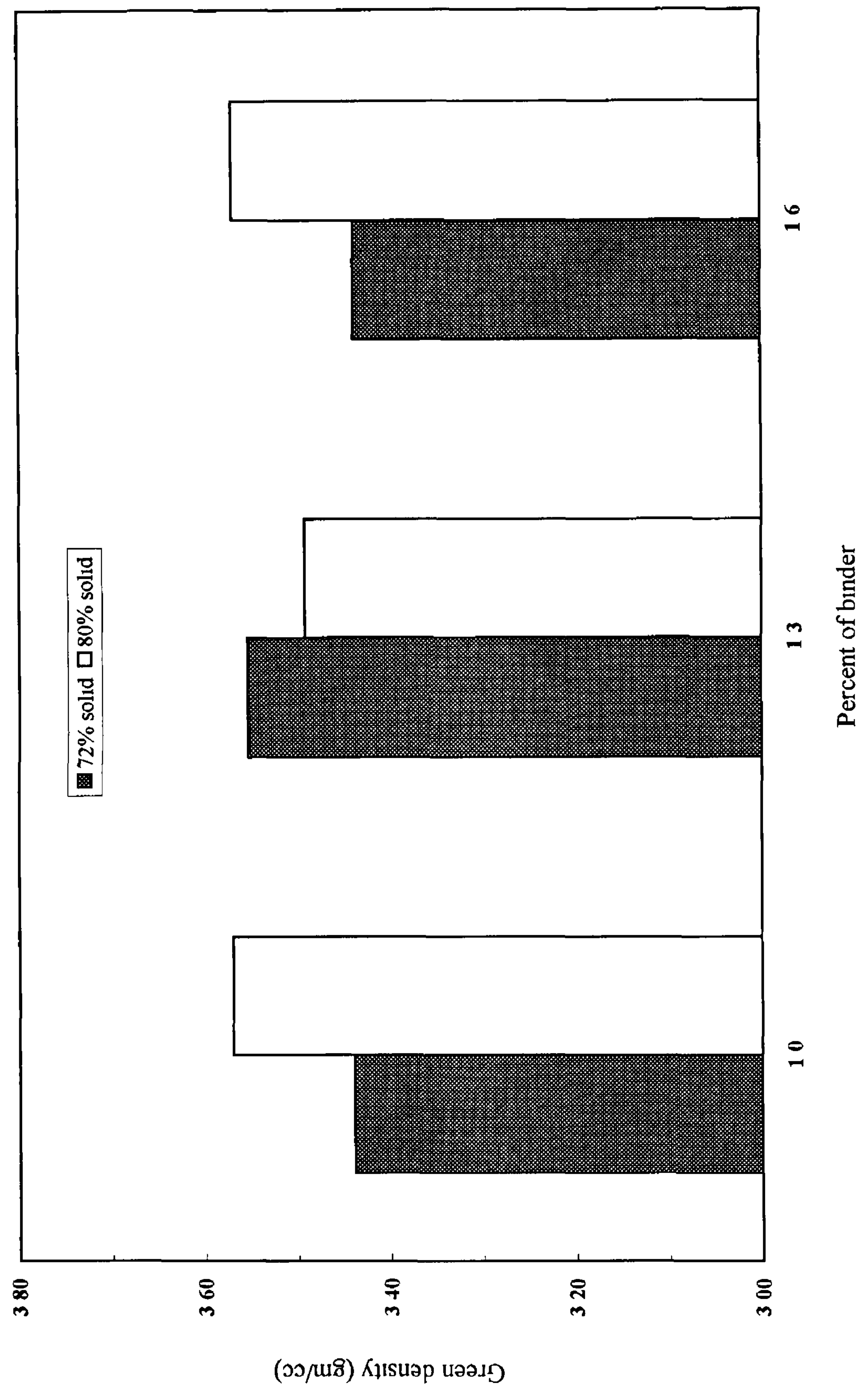

Figure 5.33 Green density of the discs produced from the powders at various levels of binder with different solid concentrations

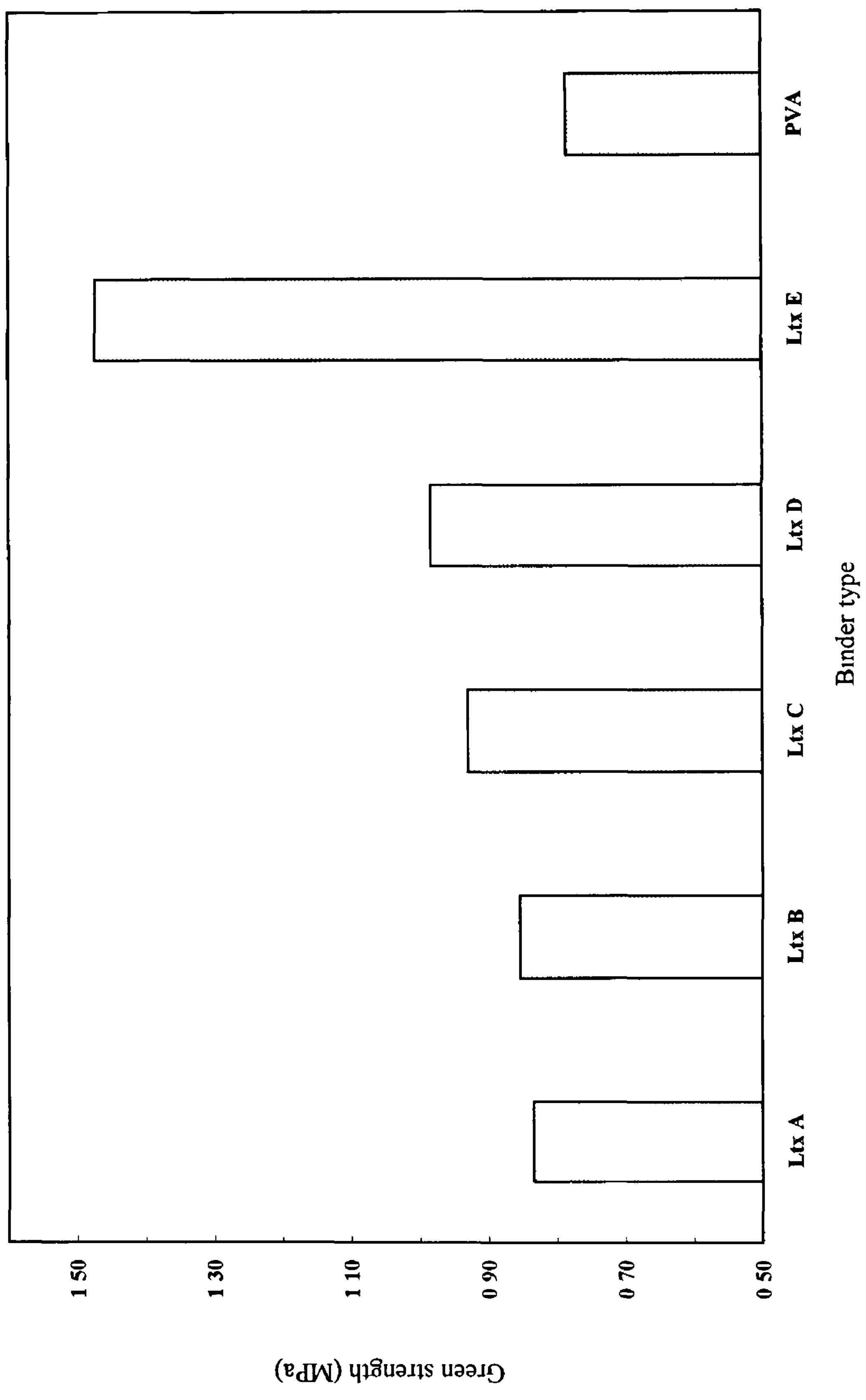

Figure 5.34 Green strength of the discs produced from the powders with different binder systems

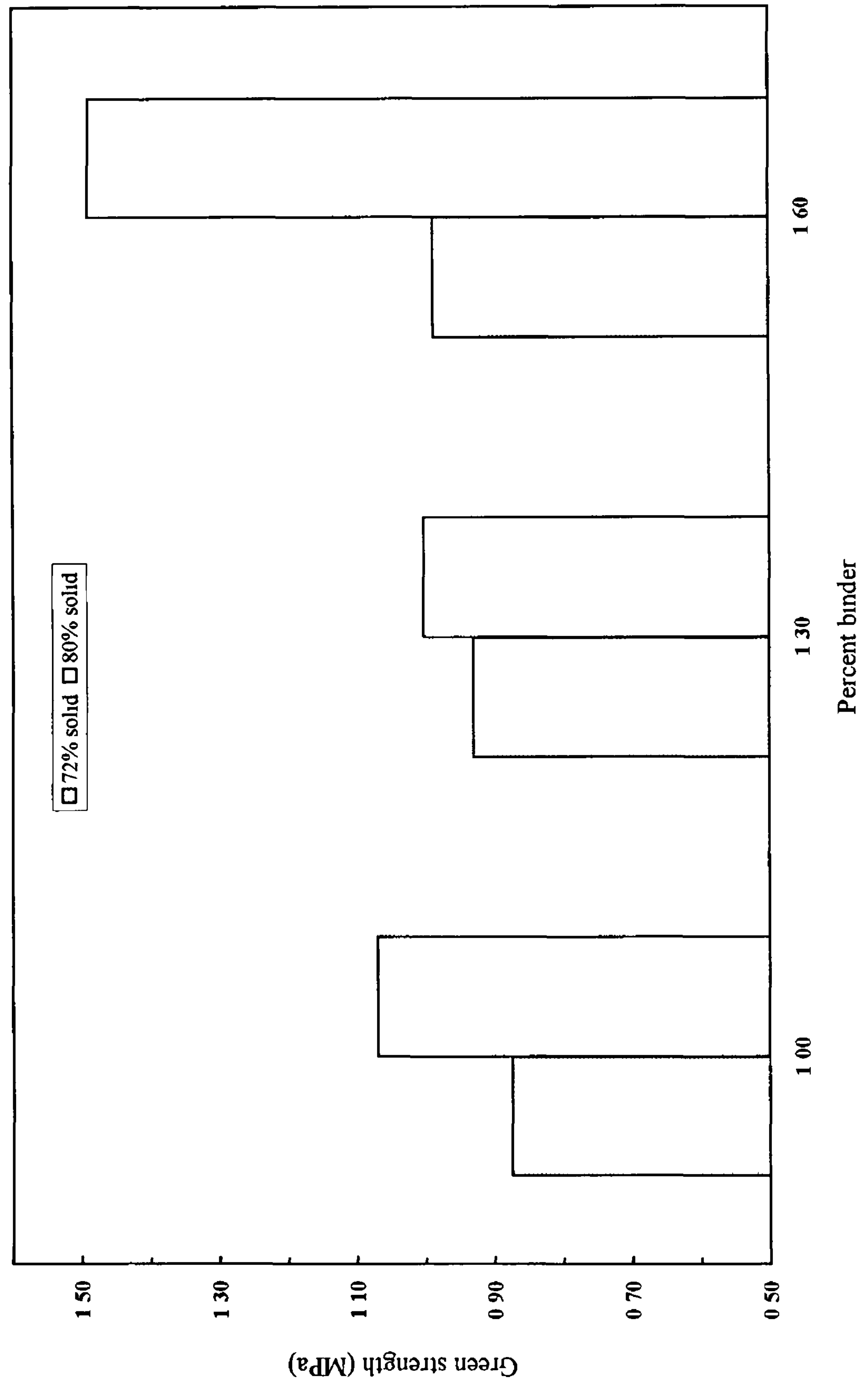

Figure 5 35 Green strength of the discs produced from the powders at various levels of binder with different solid concentrations

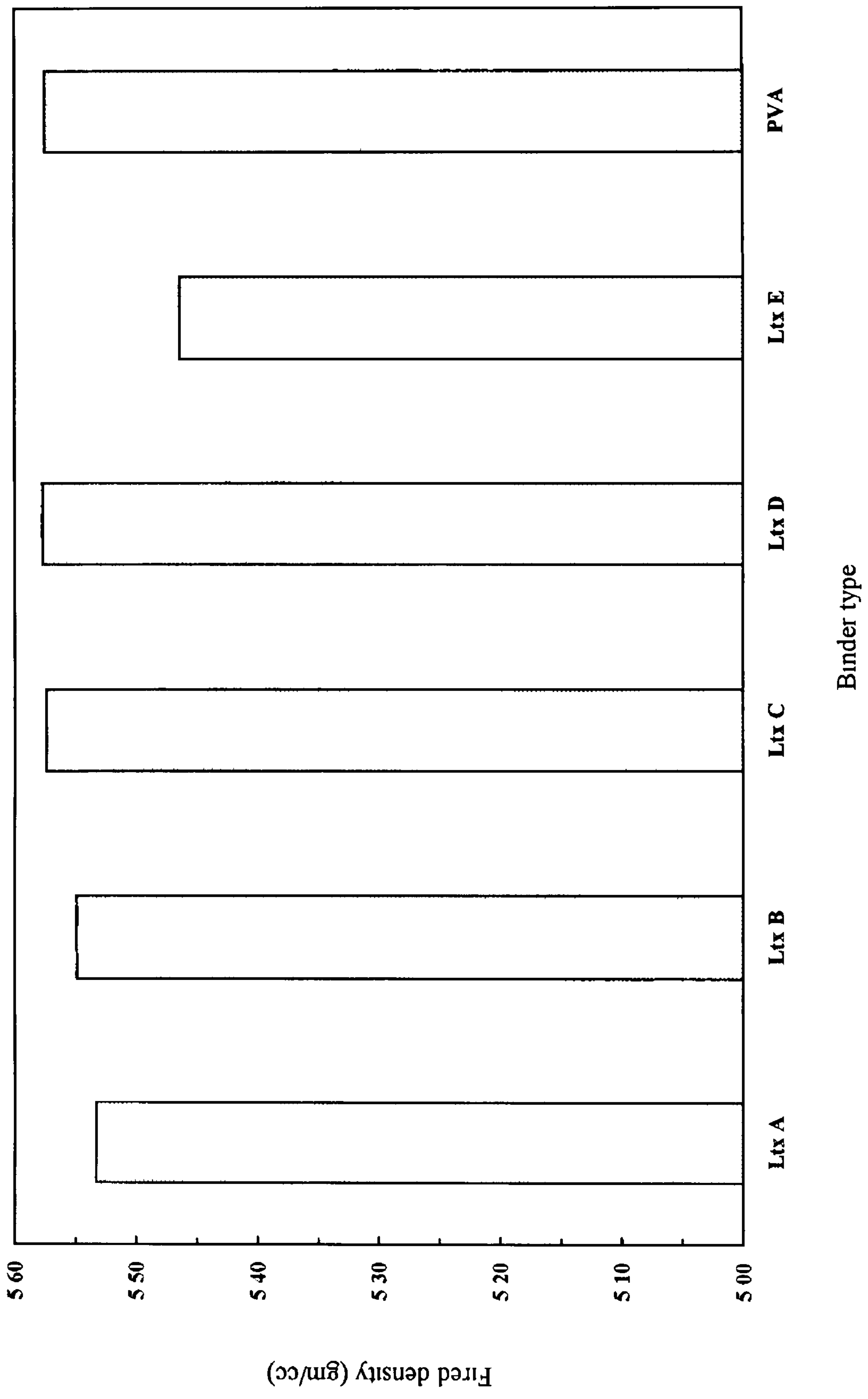

Figure 5.36 Fired density of the discs produced from the powders with different binder systems

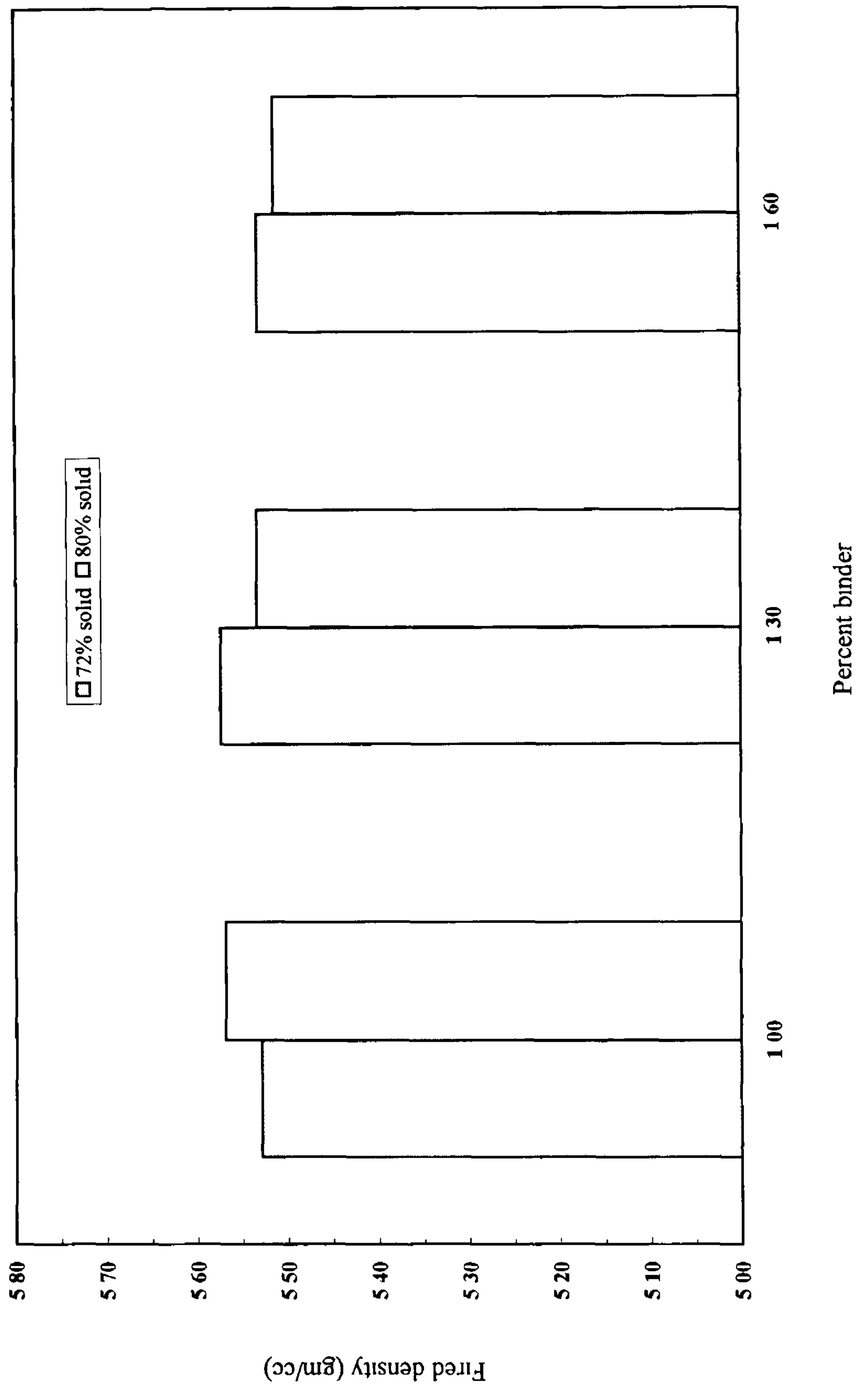

Figure 5.37 Fired density of the discs produced from the powders at various levels of binder with different solid concentrations

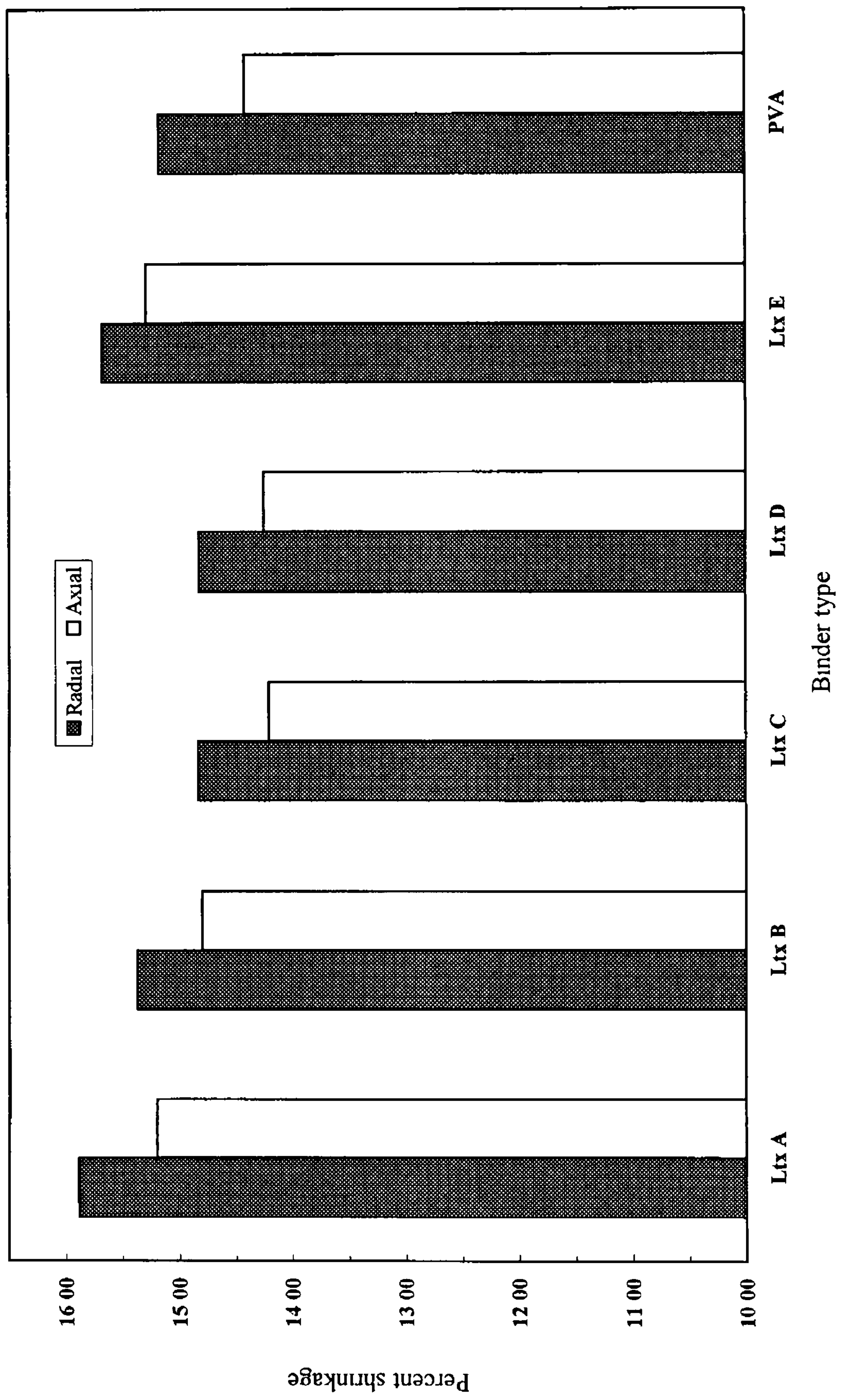

Figure 5.38 Shrinkage of the fired discs produced from the powders with different binder systems

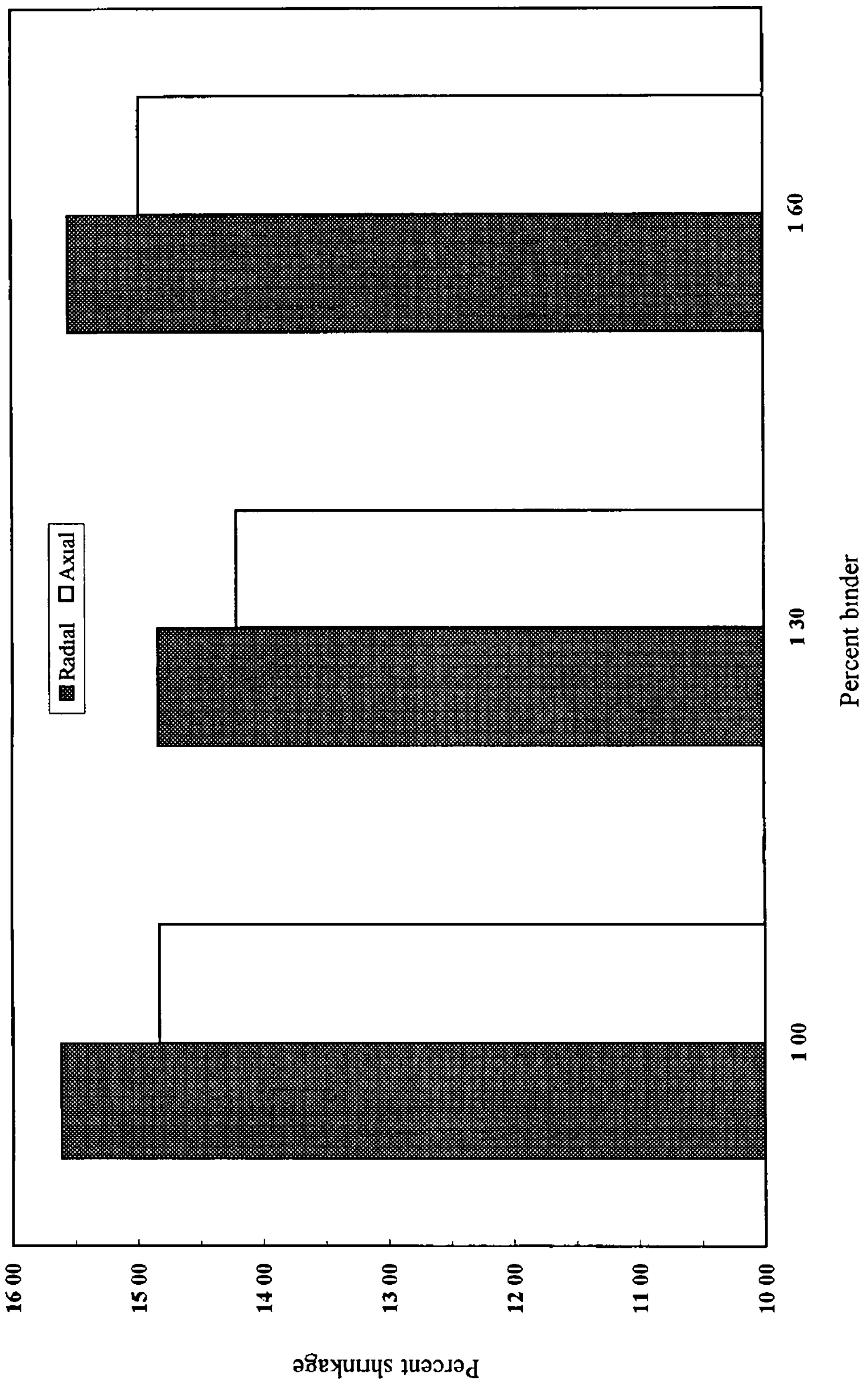

Figure 5 39 Shrinkage of the fired discs produced from the powders with different levels of binder at lower solid concentration

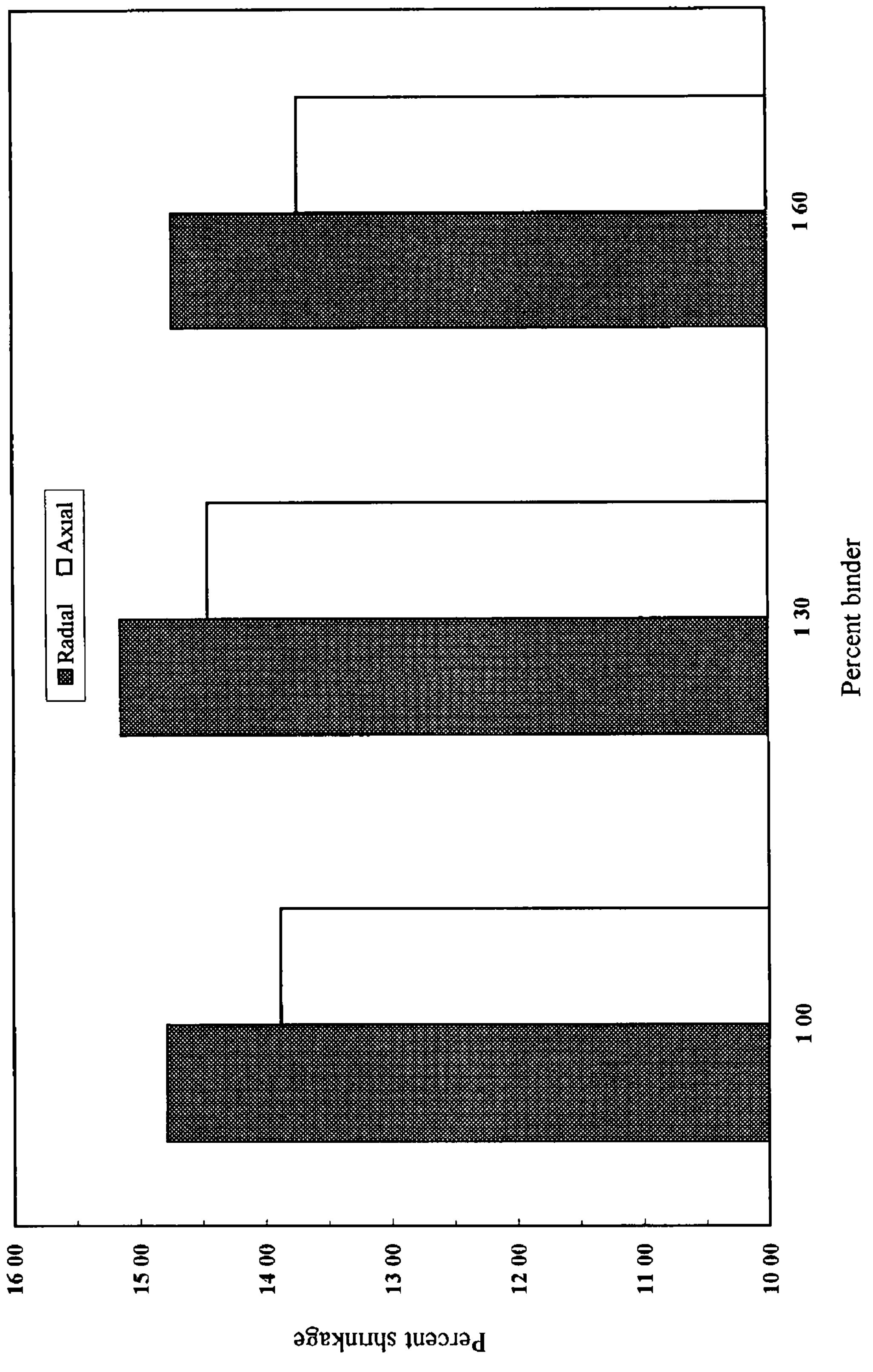

Figure 5.40 Shrinkage of the fired discs produced from the powders with different levels of binder at higher solid concentration

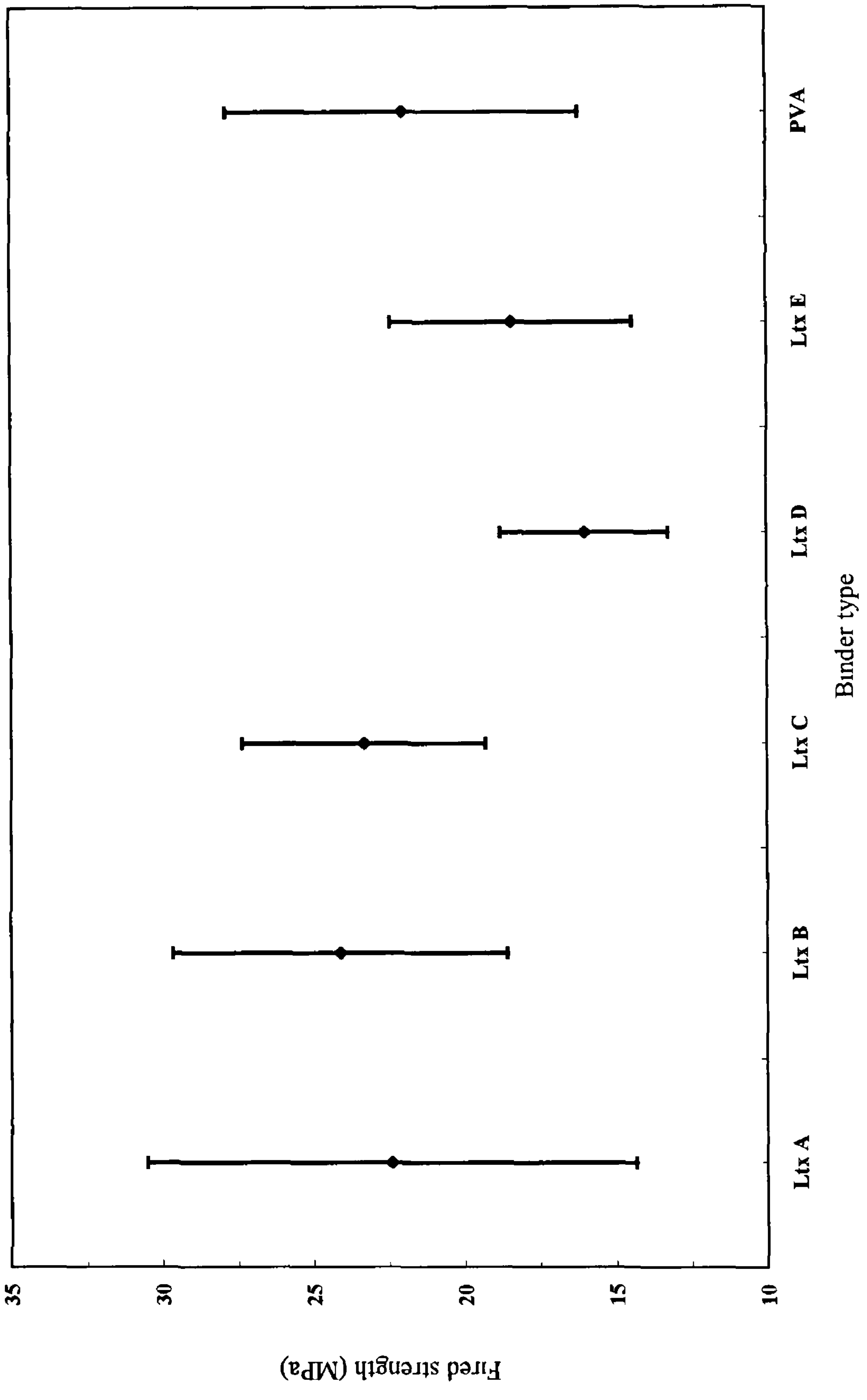

Figure 5 41 Fired strength of the discs produced from the powders with different binder systems

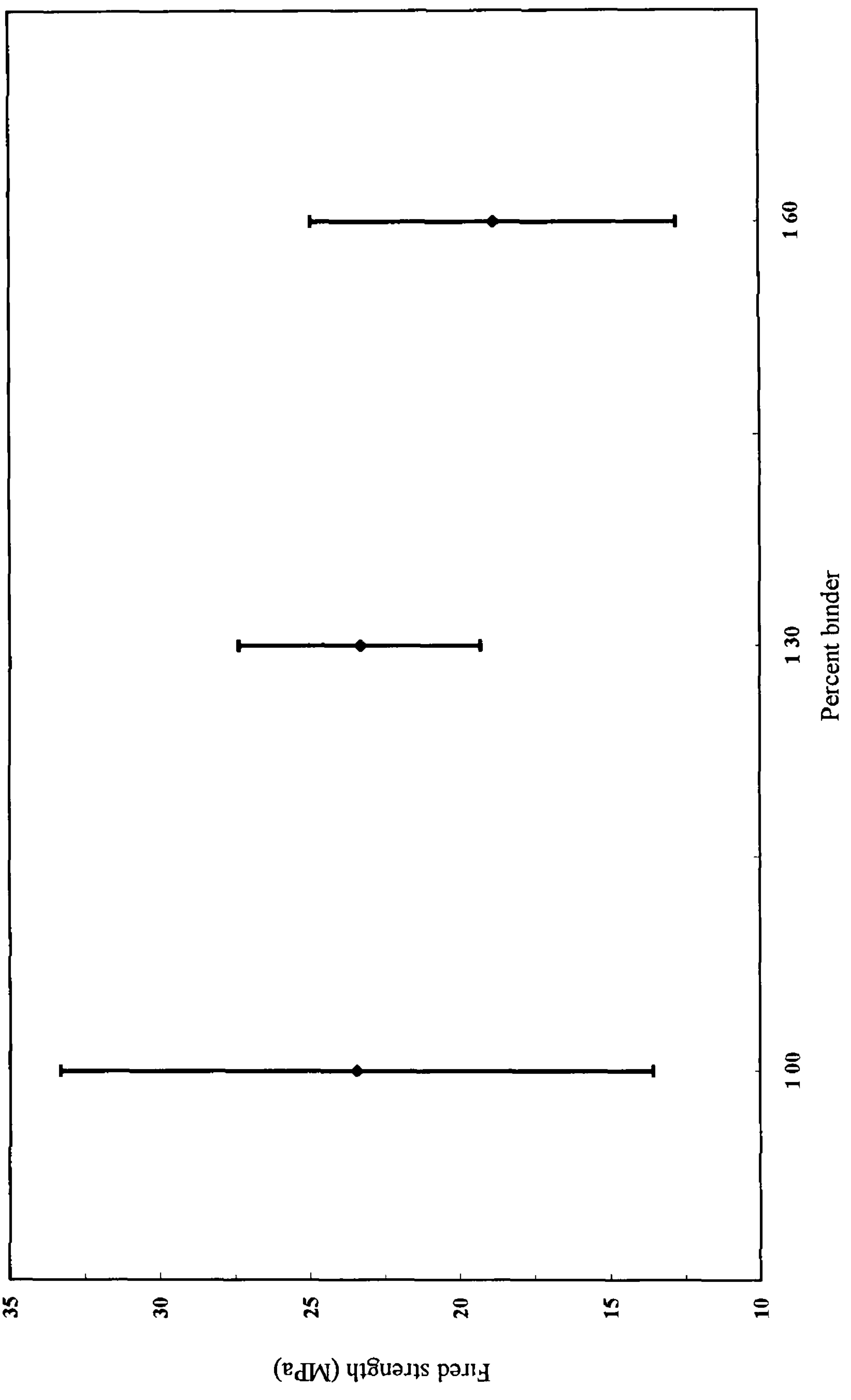

Figure 5 42 Fired strength of the discs produced from the powders with different levels of binder at lower solid concentration

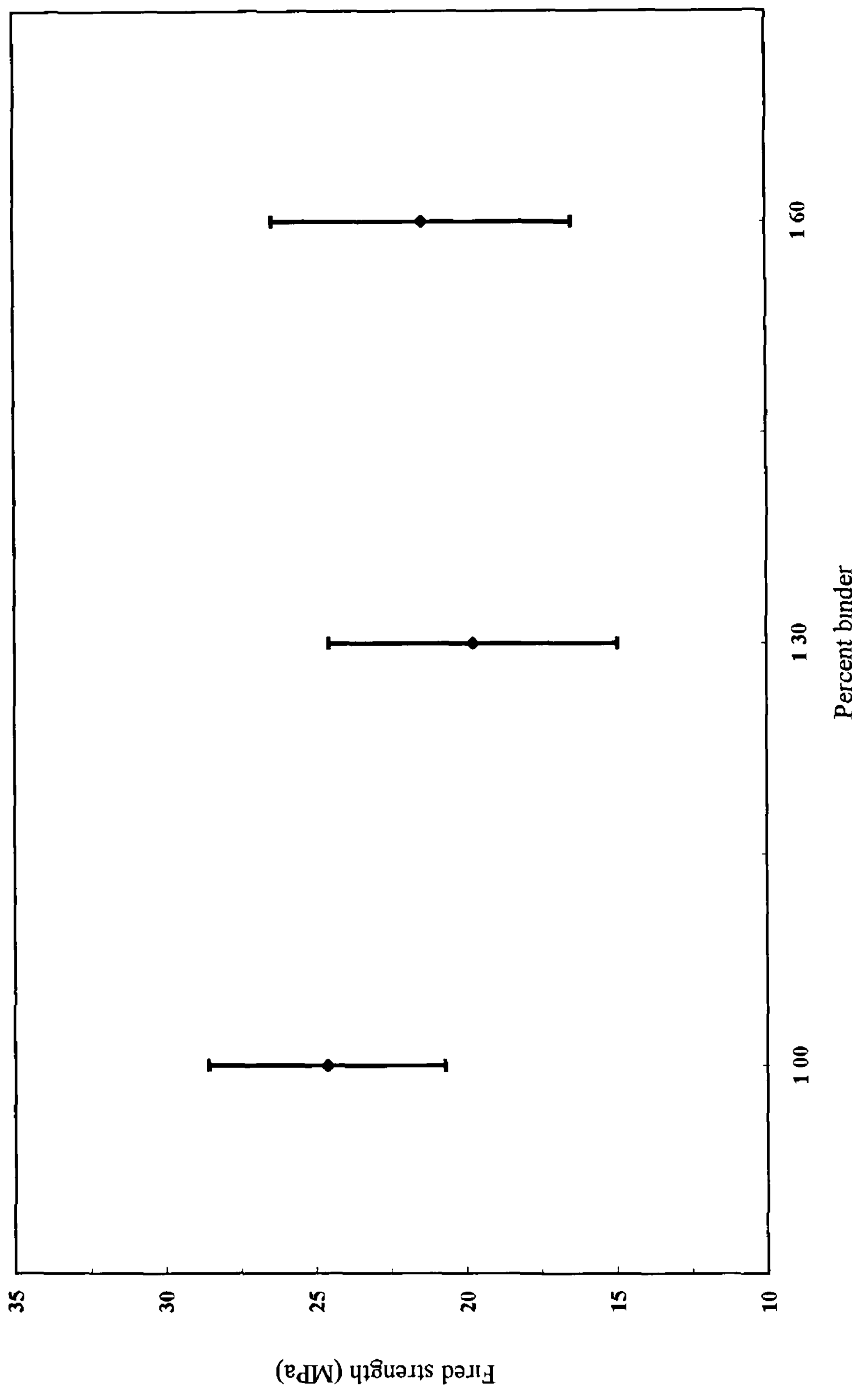

Figure 5 43 Fired strength of the discs produced from the powders with different levels of binder at higher solid concentration

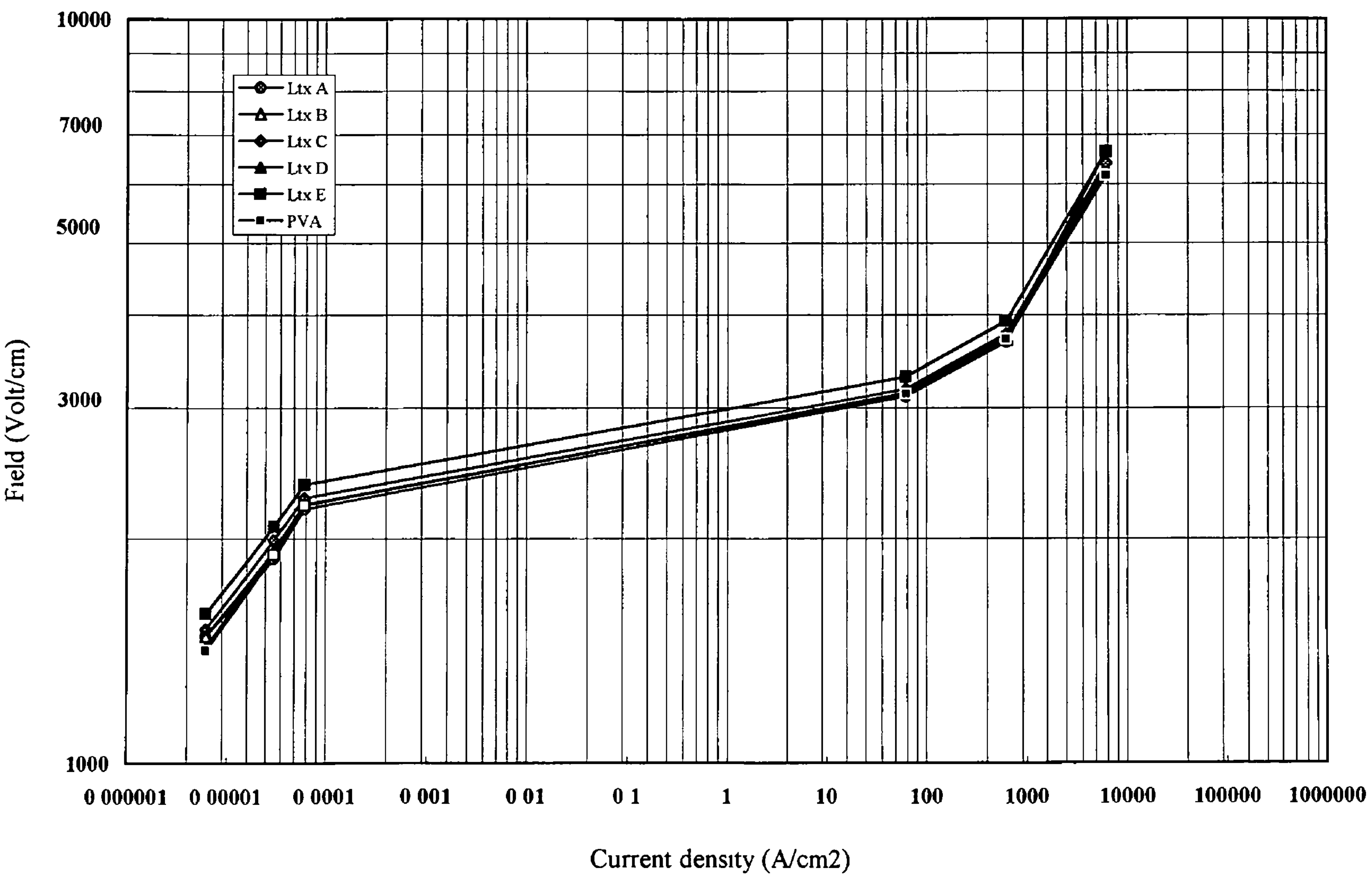

Figure 5 44 I-V curves of the varistors produced from the powders containing different binder systems

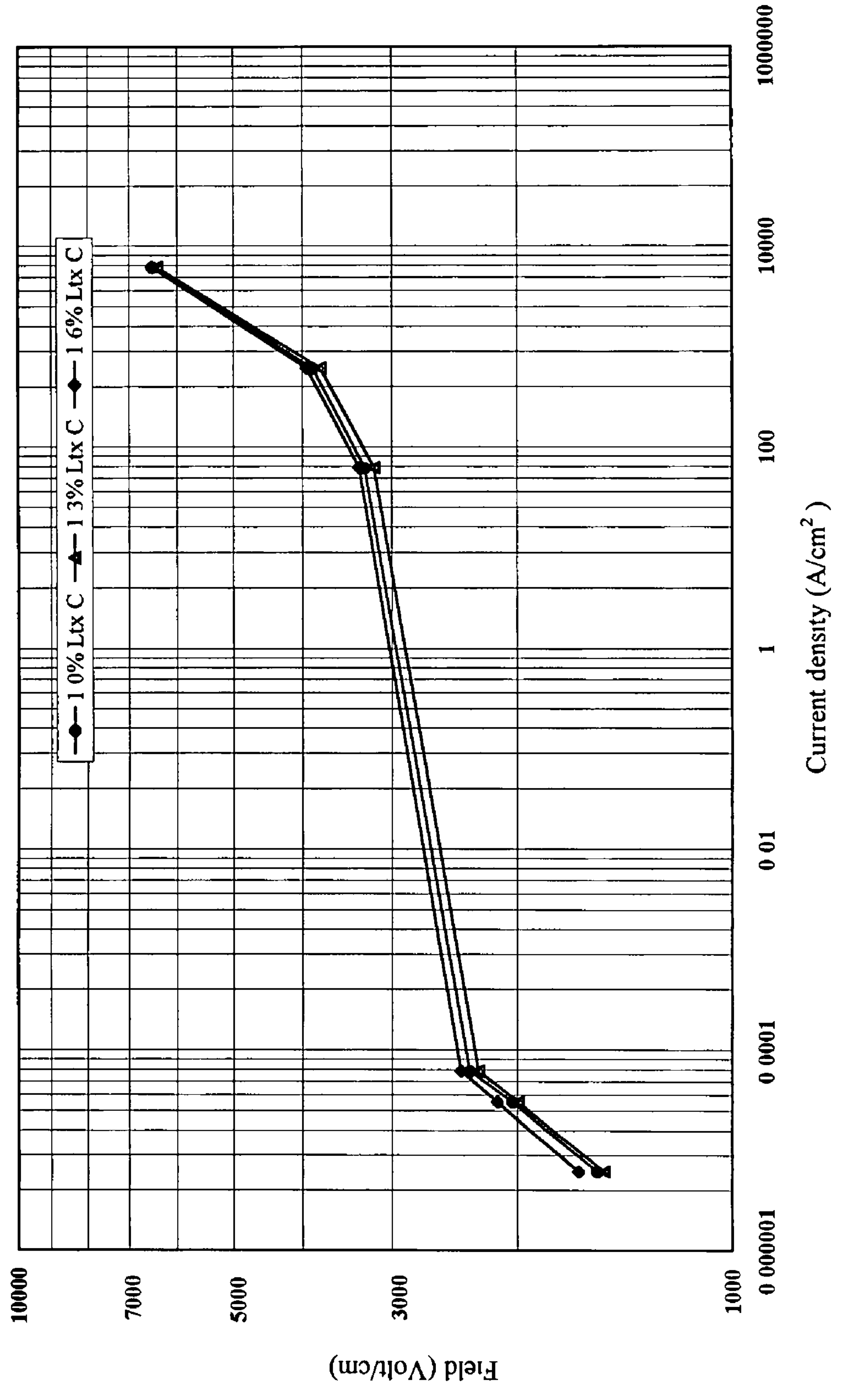

Figure 5 45 I-V curves of the varistors produced from the powders containing different levels of binder at lower solid concentration

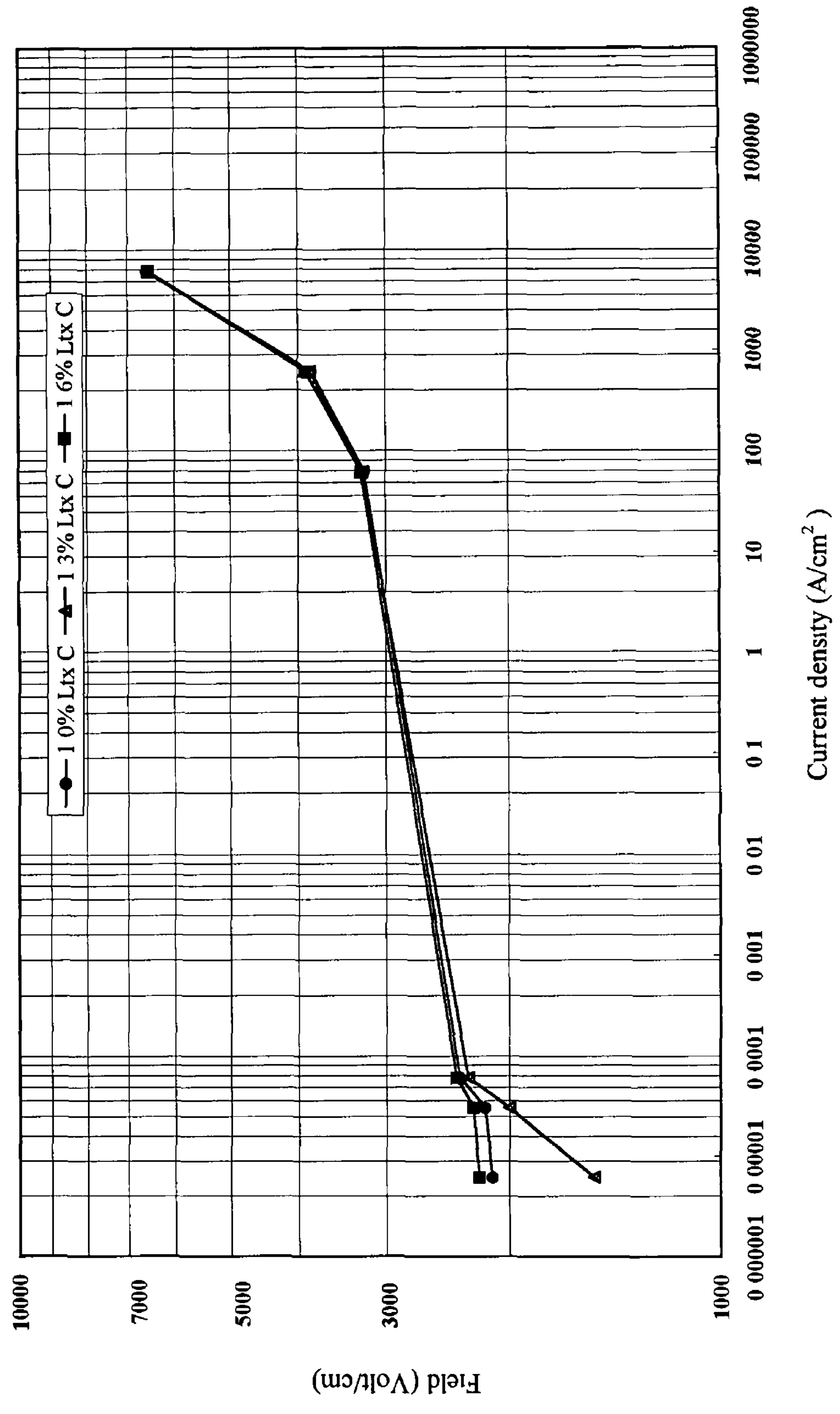

Figure 5 46 I-V curves of the varistors produced from the powders containing different levels of binder at higher solid concentration

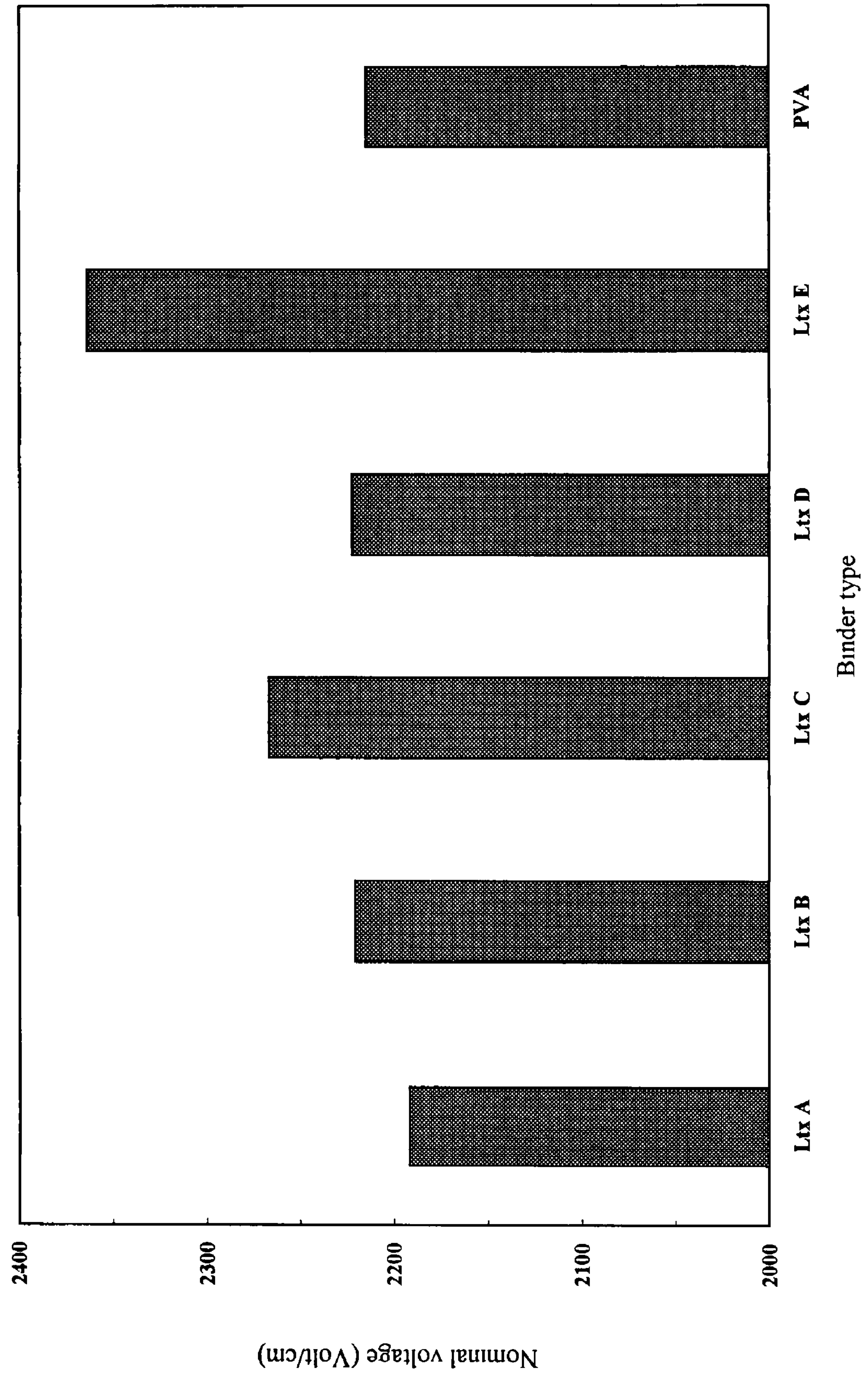

Figure 5 47 Nominal voltage of the varistors produced from the powders containing different binder systems

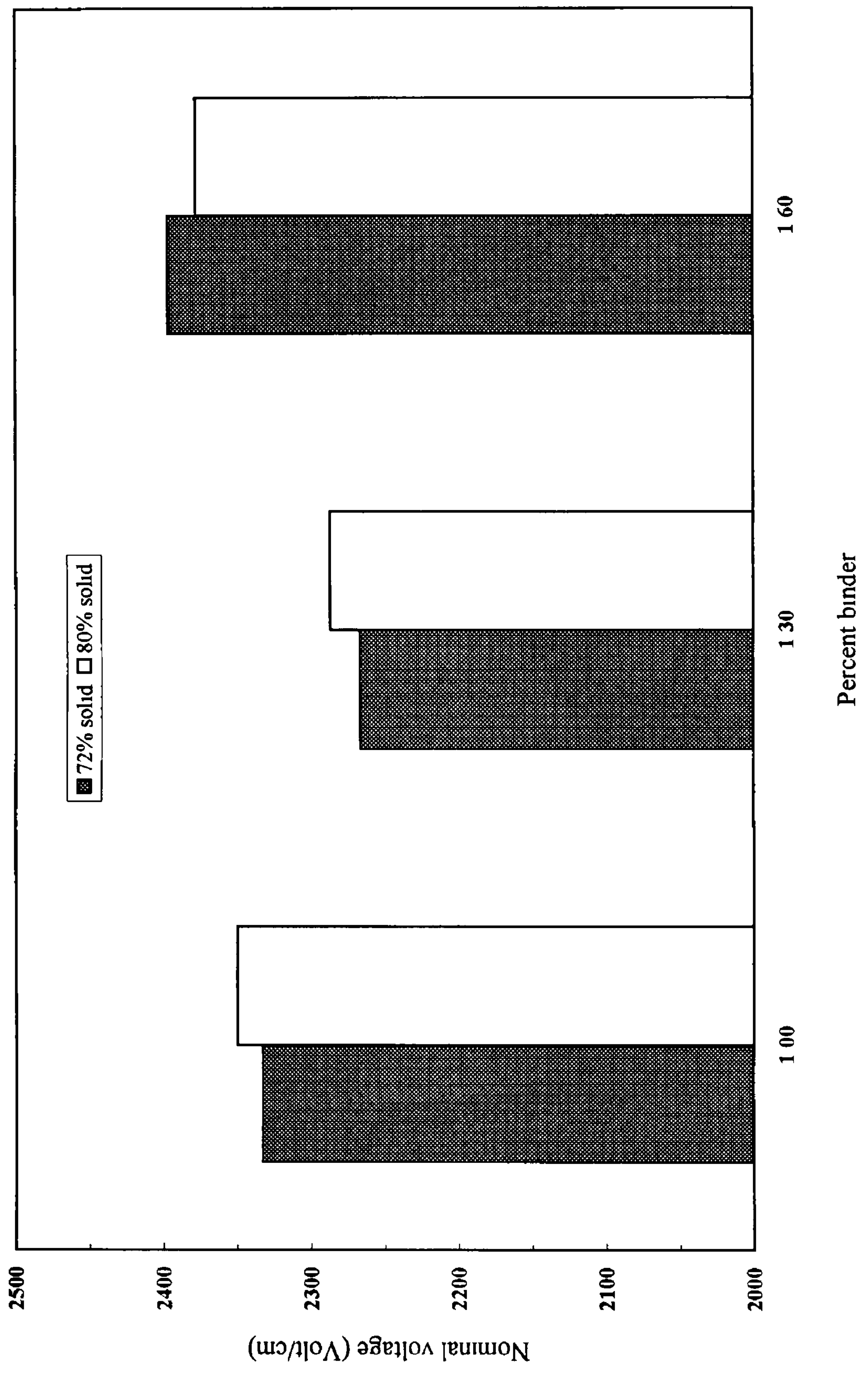

Figure 5.48 Nominal voltage of the varistors produced from the powders containing different levels of binder at various solid concentrations

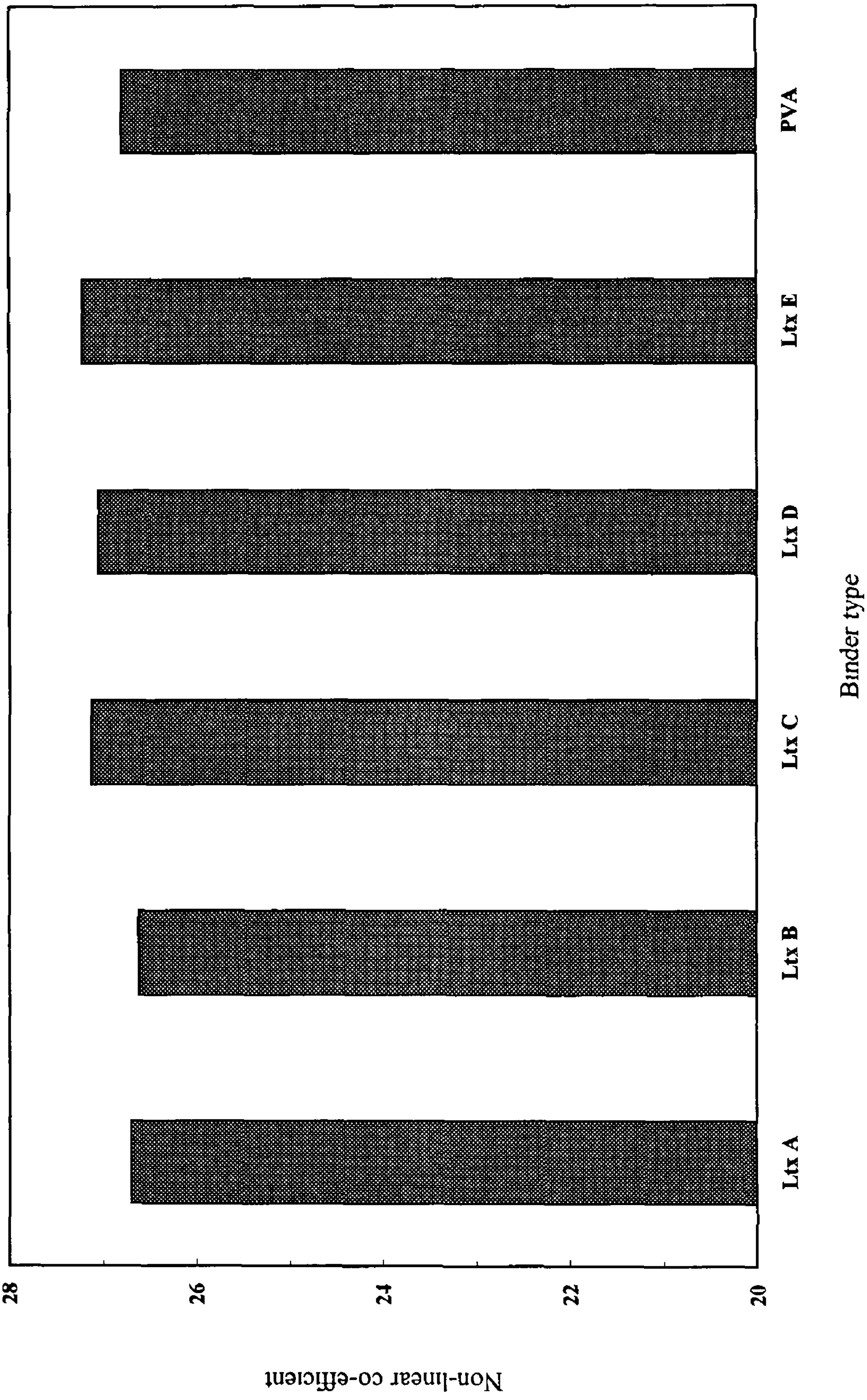

Figure 5 49 Non-linear co-efficient of the varistors produced from the powders containing different binder systems

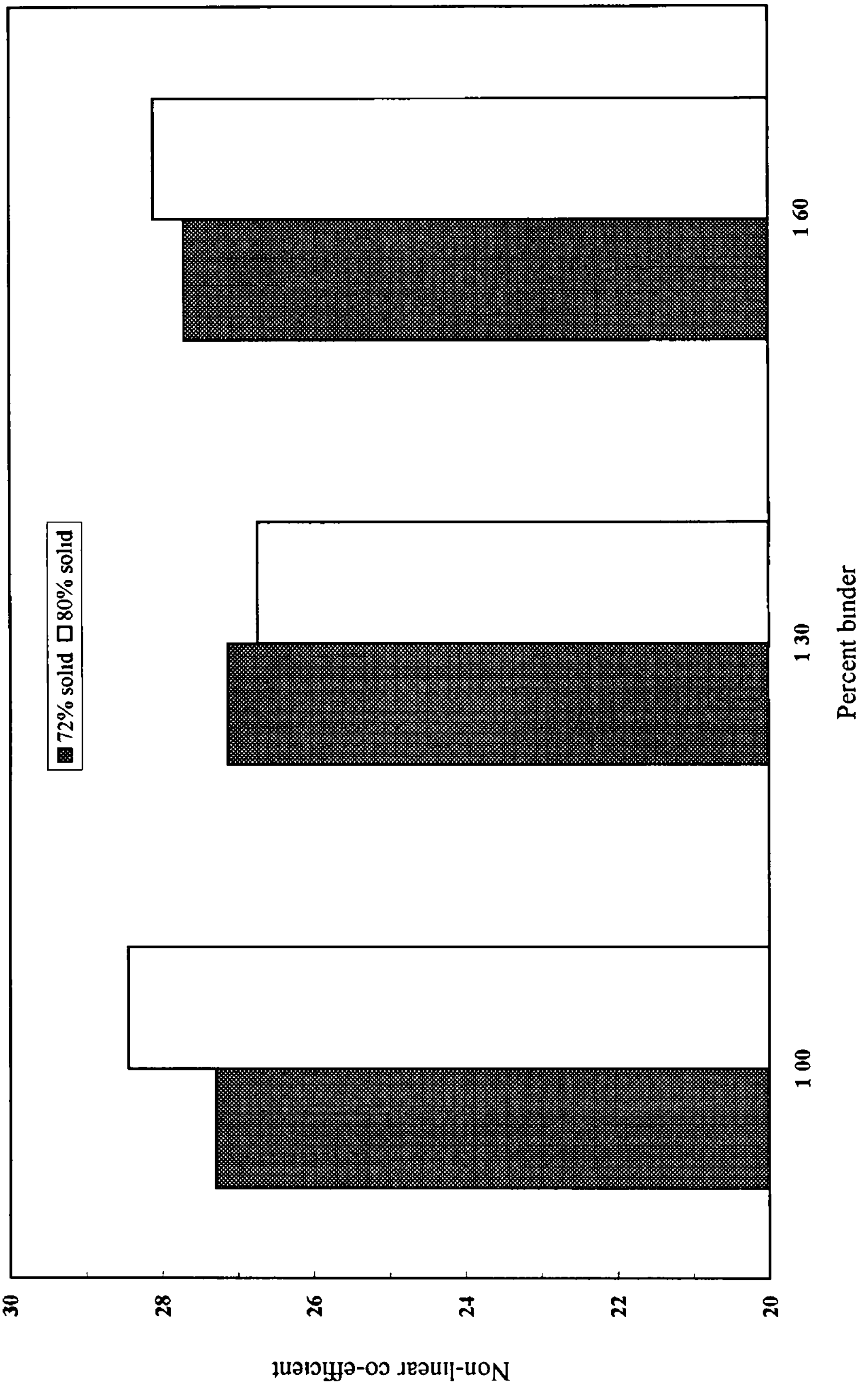

Figure 5.50 Non-linear co-efficient of the varistors produced from the powders containing different levels of binder at various solid concentrations

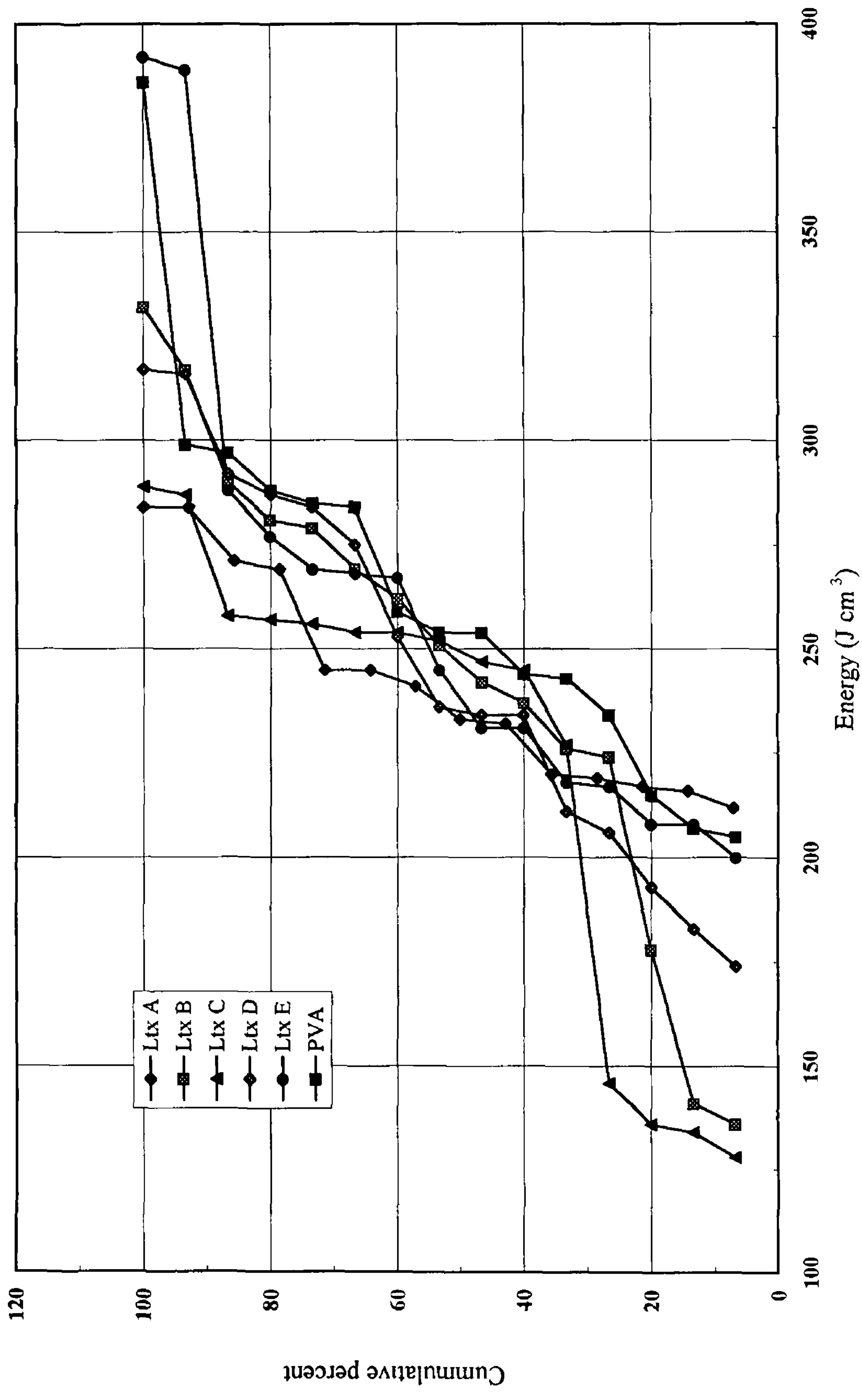

Figure 5 51 Energy absorption capability of the varistors produced from the powders containing different binder systems

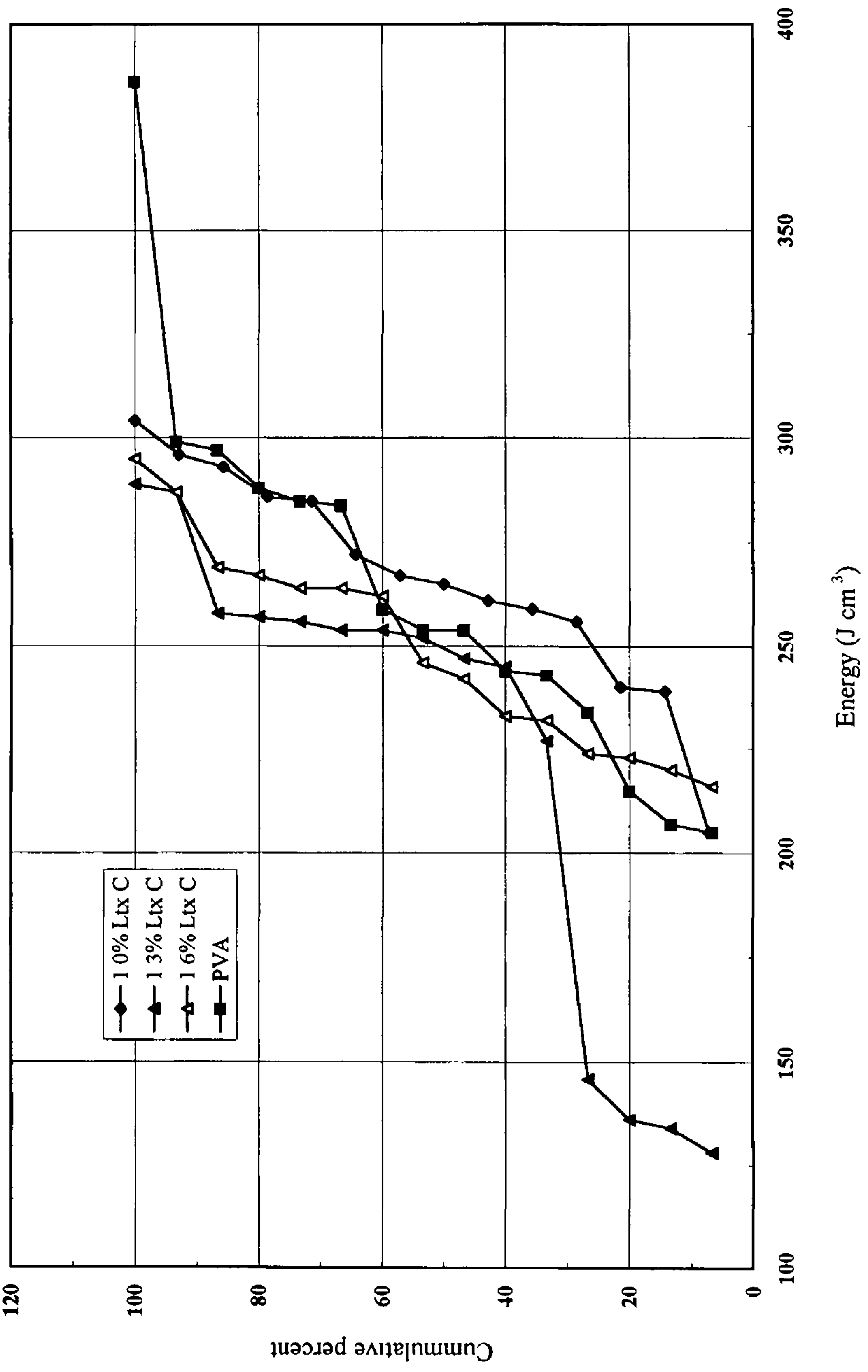

Figure 5 52 Energy absorption capability of the varistors produced from the powders containing different levels of binder at lower solid concentration

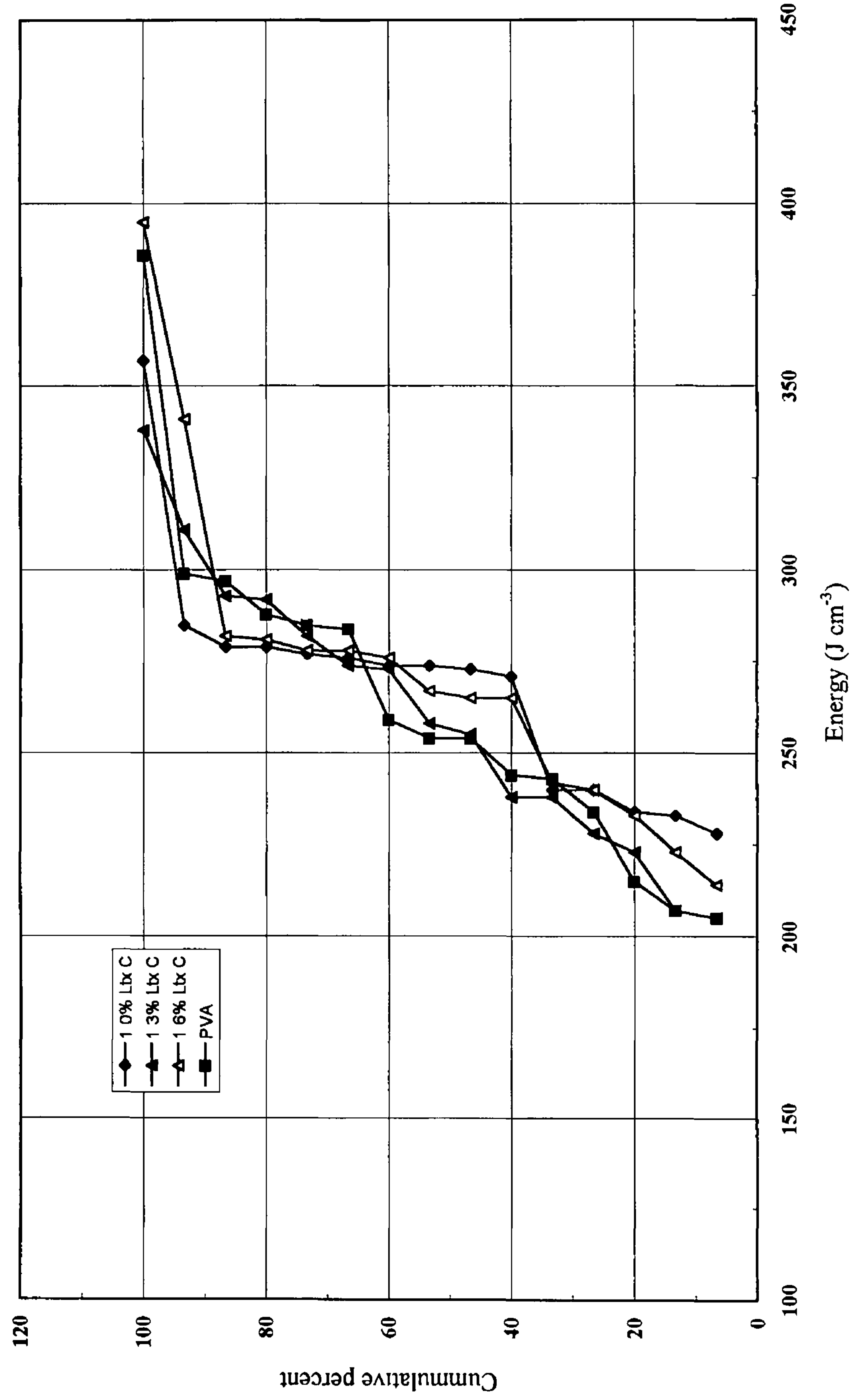

Figure 5 53 Energy absorption capability of the varistors produced from the powders containing different levels of binder at higher solid concentration

5.4 PARTICLE SIZE FRACTION

The influence of particle size fraction on the physical as well as on the electrical properties was analyzed The investigation on the physical property was limited to the evaluation of the green density and the green strength, and the fired density It should be mentioned here that the powder with fine particles did not perform well in compaction Excessive frictional effects were primarily responsible

5 4 1 Physical Characteristics

The physical characteristics of discs prepared from the powder with narrow distribution of different size ranges and the standard one are presented in Table 5 9 The values within the parenthesis are the standard error The green and fired densities did not show any appreciable difference but these are highest for cell D which had particles smaller than 45 µm The enhanced fired density with the smaller particles was achieved as a result of the higher capillary pressure exerted by the liquid formed during sintering The total surface energy was also higher for smaller particles due to the small radius of curvature Both the capillary pressure and the surface energy provide more driving energy for densification

Table 5 9 Characteristics of discs produced from powder with different narrow size range

Powder type	Green density (gm/cc)	Fired density (gm/cc)	Green strength (MPa)
Cell A	3 380 ± (0 03)	5 60 ± (0 011)	0 89 ± (0 01)
Cell B	3 387 ± (0 01)	5 60 ± (0 014)	0 91 ± (0 02)
Cell C	3 332 ± (0 02)	5 58 ± (0 028)	0 92 ± (0 03)
Cell D	3 389 ± (0 04)	5 62 ± (0 015)	0 76 ± (0 03)
Standard	3 334 ± (0 03)	5 59 ± (0 020)	0 91 ± (0 03)

The green strength was the lowest with cell D, while it was almost the same for all the other cells including the standard one According to Rampf's theory[77] higher green strength was thought to be obtained from the discs produced from the powder containing smaller particles However, it is envisaged that due to the frictional effect the packing of the particles was not effective which reduced the strength

5.4.2 Electrical Characteristics

The electrical properties were evaluated for the varistors fabricated from the powder of different size ranges including the standard distribution The clamp ratio, non-linear co-efficient (α), and wattloss are summarized in Table 5 10

Table 5.10 Clamp ratio, non-linear co-efficient, and wattloss for varistor fabricated with different size fractions of powder

Cell ident for varistor from powder of diff size range	Clamp ratio	Non-linear co-efficient (α)	Wattloss (W cm^{3})		
	@ 5mA-5KA	@ 1mA-5mA	Before shot	After shot	
				Forward polarity	Reverse polarity
Cell A	1 693	15 041	0 010	0 011	0 013
Cell B	1 694	14 682	0 009	0 012	0 015
Cell C	1 692	14 498	0 009	0 011	0 013
Cell D	1 702	14 189	0 012	0 012	0 015
Standard	1 696	14 175	0 009	0 011	0 014

The clamp ratio, and α did not change significantly for different cells The clamp ratio was slightly higher and non-linear co-efficient was lower for cell D The wattloss before the application of the high amplitude short duration pulses of peak current 65 KA was found to be slightly higher for the same cell But after the application of the high current pulses, increment in wattloss was minimum for cell D making it comparable with varistors from all other cells

Nominal voltage

The nominal voltage of the varistor produced from the powder having different size ranges is plotted in Figure 5 54 The lowest nominal voltage was achieved for cell A and the highest for cell D The effect of the particle size is clearly evident from the plot as cell A was composed of coarser particles and cell D of finer particles It can be inferred that the coarser spray dried granules lead to bigger grains after sintering leading to lower nominal voltage The finer granules generate smaller grains after firing

Energy absorption capability

The energy absorption capability of varistors prepared from the powder containing particles of different size ranges is illustrated in figure 5 55 It is evident that the energy withstanding capability is low for cell D The other fractions composed of coarse, medium, and wide distribution of particles do not exhibit any noticeable difference It can be said from the data presented in Table 5 9 that the green body is less homogeneous for the cell D The inhomogeneity of the discs in the green state might be intensified further by firing Hence, the varistor failed at a very low level of injected energy

The failure mode of varistors by the destruction testing is presented in Table 5 11 It is noticeable from Table 5 11 that the failure happened mainly by flashover and by combined flashover and pinhole

The variance analysis for cell D and the standard one was carried out considering the energy absorption capability as the response and is presented in Table 5.12.

Table 5.11 Failure pattern during "strength to destruction" testing of varistors produced from powder with different size fraction

Cell identification	Sample size	Failure mode			
		Pinhole (ph)	Flashover (fo)	ph+fo	ph+crack
Cell A	16	3	5	8	-
Cell B	11	2	5	3	1
Cell C	15	2	5	8	-
Cell D	6	3	2	1	-
Standard	15	1	8	6	-

Table 5.12 Analysis of variance for particle size fraction samples

Source of variation	Sum of squares	Degrees of freedom	Mean squares	F_{cal}	F_{tab}
Treatments	92107	1	92107	5.18	4.38
Error	337710	19	17774		
Total	429817	20			

The calculated F-statistic at 95% confidence interval was higher than F_{tab} at $\nu_{1,19}$. Therefore, it can be said that the particle size fraction exhibited a significant influence on the energy absorption capability of the varistors.

5.5 PASSIVATION THICKNESS

The glass thickness plays an important role in varistor performance. The influence of glass thickness on the varistors performance was assessed by evaluating the energy absorption capability. The cummulative plot of the energy absorption capability of the varistors with different glass thicknesses is presented in Figure 5 56 and the mean energy with standard error is illustrated in Figure 5 57 The standard amount of glass taken as the minimum level in the experiment had shown inferior performance and the varistors started to fail at a very low energy level Nevertheless, the heaviest coating did not exhibit the best energy absorption capability

The coating of glass acts as an insulator and resists heat transfer The effect is more obvious in the second and the third shot in the energy test The heavier coating acts as higher insulator and does not dissipate heat as effectively as the lower thickness Thus, the high temperature in the ceramics makes it more vulnerable to failure This feature is supported by the fact that the discs with the thicker coating failed through the ceramic and most of the discs failed by electrical puncture as presented in Table 5 13 It was also noticed from Figure 5 56 that for the best cell, 47% of the discs survived after 400 J cm ^{3}

Table 5.13 Failure mode of varistors with different glass coatings during “strength to destruction” test

Glass thickness (µm)	Sample size	Failure mode						
		Inter-face	PH	FO	Rupture	Interface + fo	Interface + ph	PH+FO
110	15	8	3	-	-	3	-	1
220	15	3	4	-	4	3	-	1
340	14	-	8	-	2	2	-	2

The mode of failure with various glass thicknesses was also catagorized and illustrated in Figure 5 58 It is clear from the figure that the increase of glass thicknesses has shifted the failure More than 85% of the varistors failed through the ceramic coated with the thicker passivation coating compared to 27% in the case of the thin coating

The variance analysis of the energy of varistors with different glass thicknesses is given in Table 5 14 At 95% confidence interval the tabulated F-statistic at $V_{2\ 41}$ is less than F_{cal} Hence, the glass thickness had a significant influence on the energy absorption capability of the varistor

Table 5.14 Analysis of variance for the energy absorption capability of varistor with various glass thicknesses

Source of variation	Sum of Squares	Degrees of freedom	Mean squares	F_{cal}	F_{tab}
Treatment	225721	2	112861	9 858	3 234
Error	469384	41	11448		
Total	695105	43			

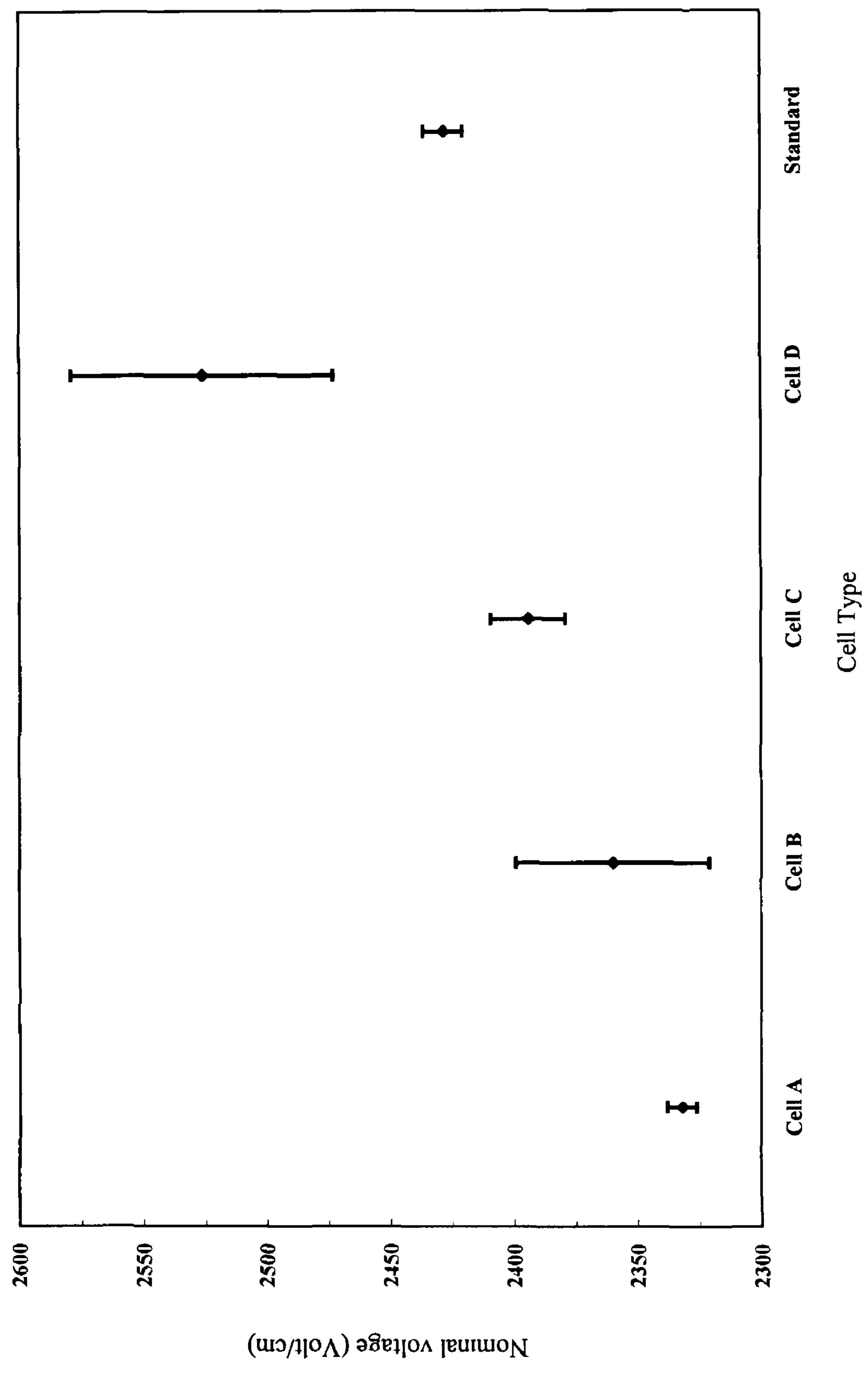

Figure 5 54 Nominal voltage of varistors produced from the powders with different size fractions

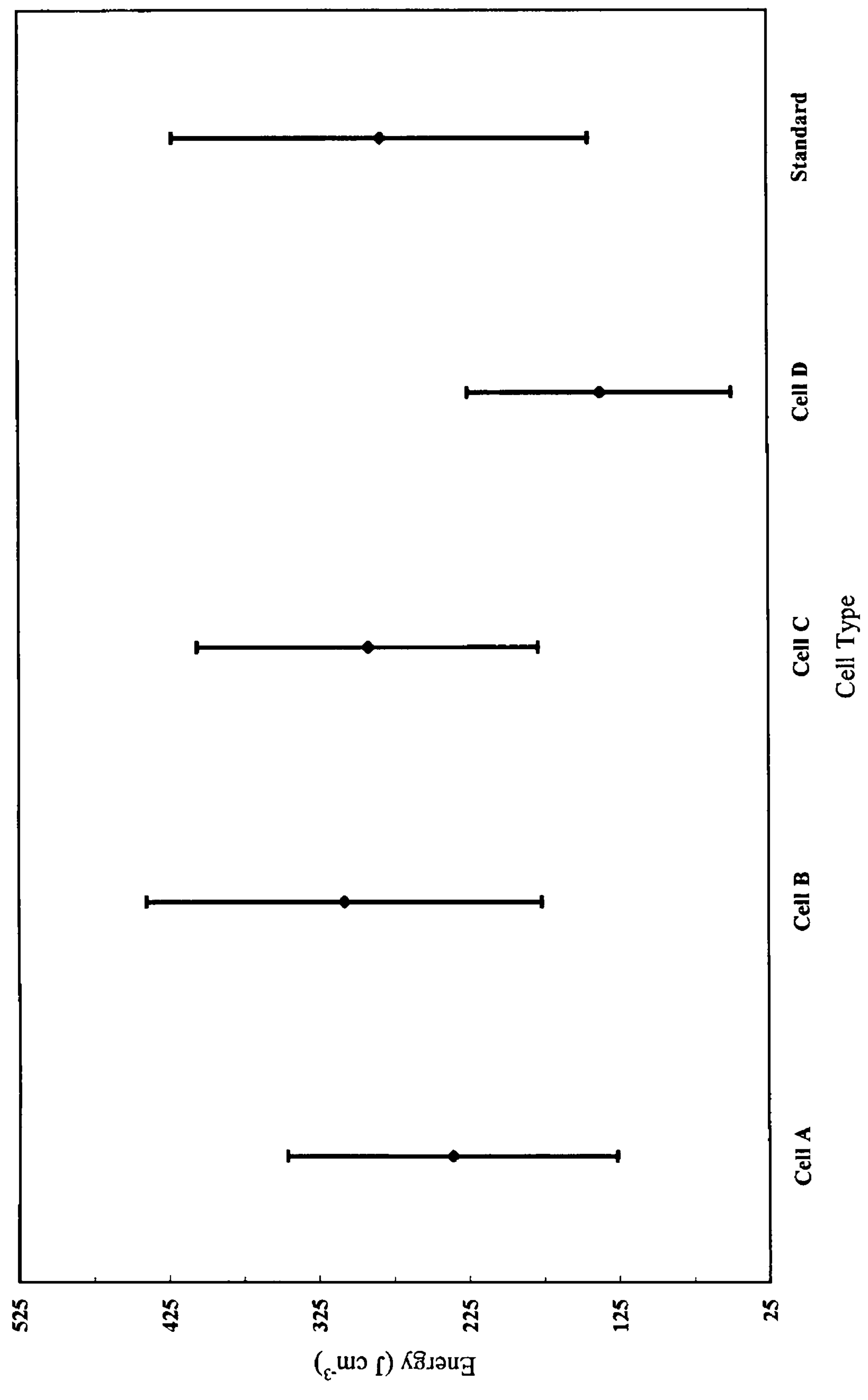

Figure 5 55 Energy absorption capability of varistors produced from the powders with different size fractions

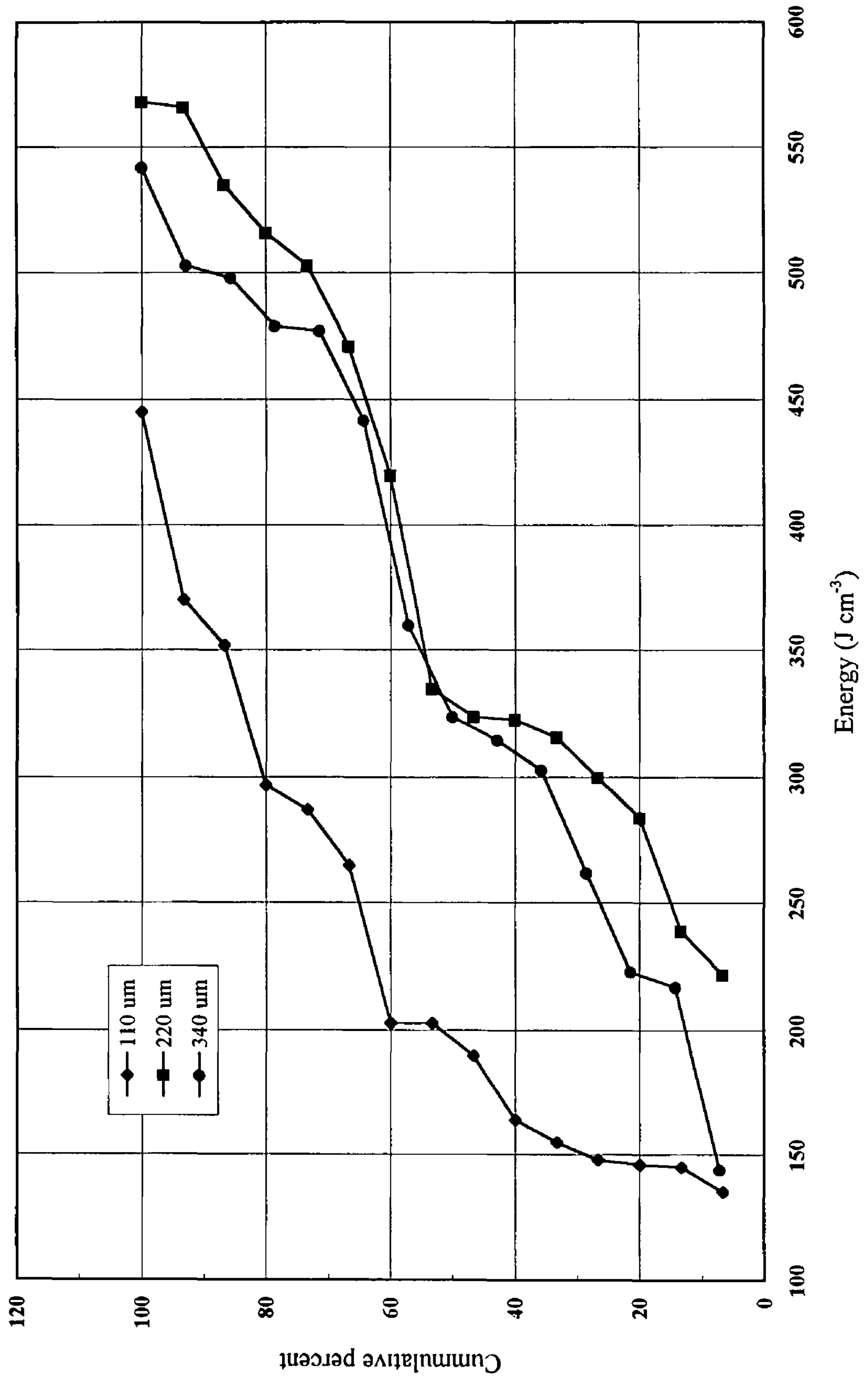

Figure 5 56 Energy absorption capability of varistors having different glass thicknesses

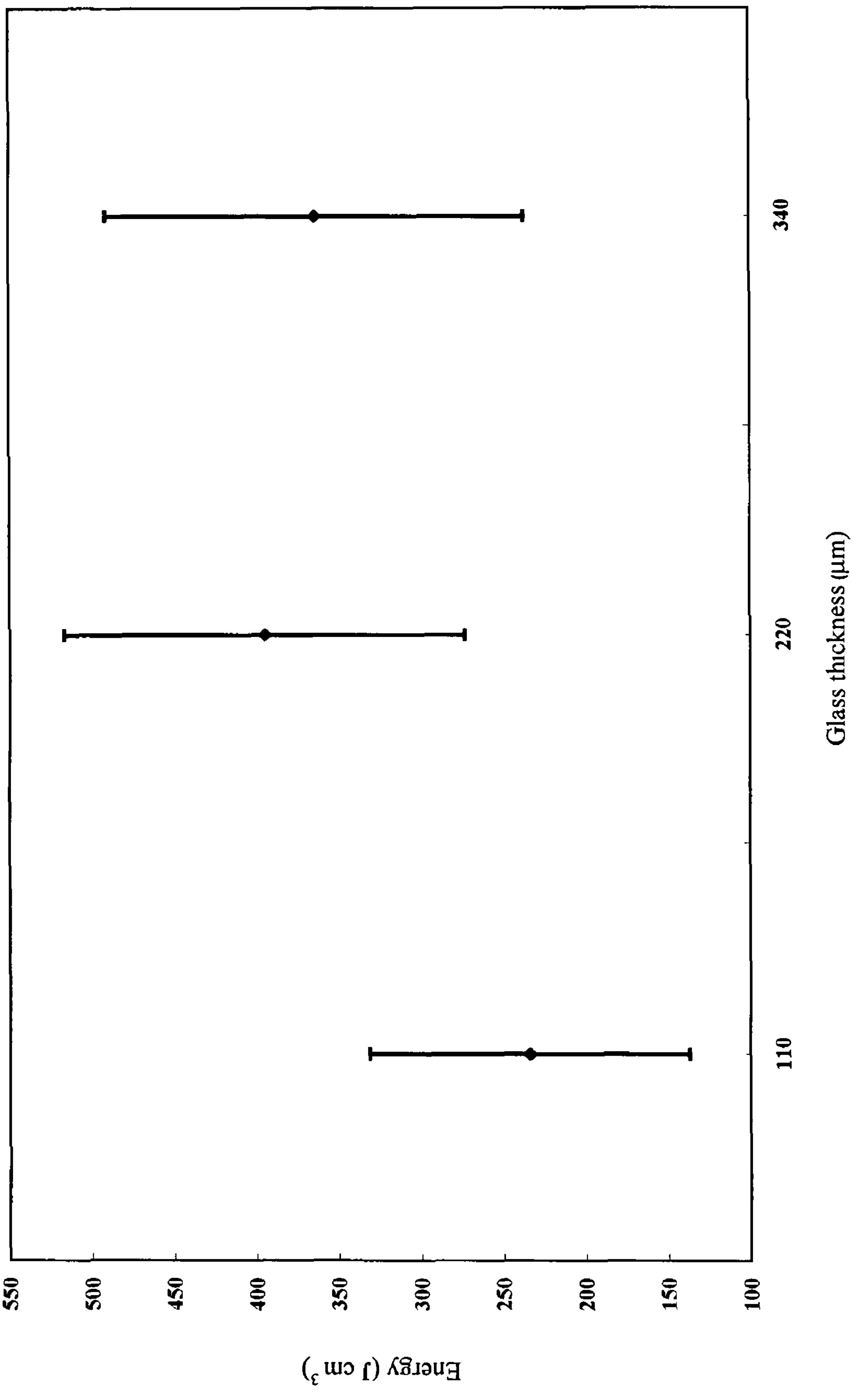

Figure 5 57 Mean value of the energy absorption capability with ± standard deviation of the varistors having different glass thicknesses

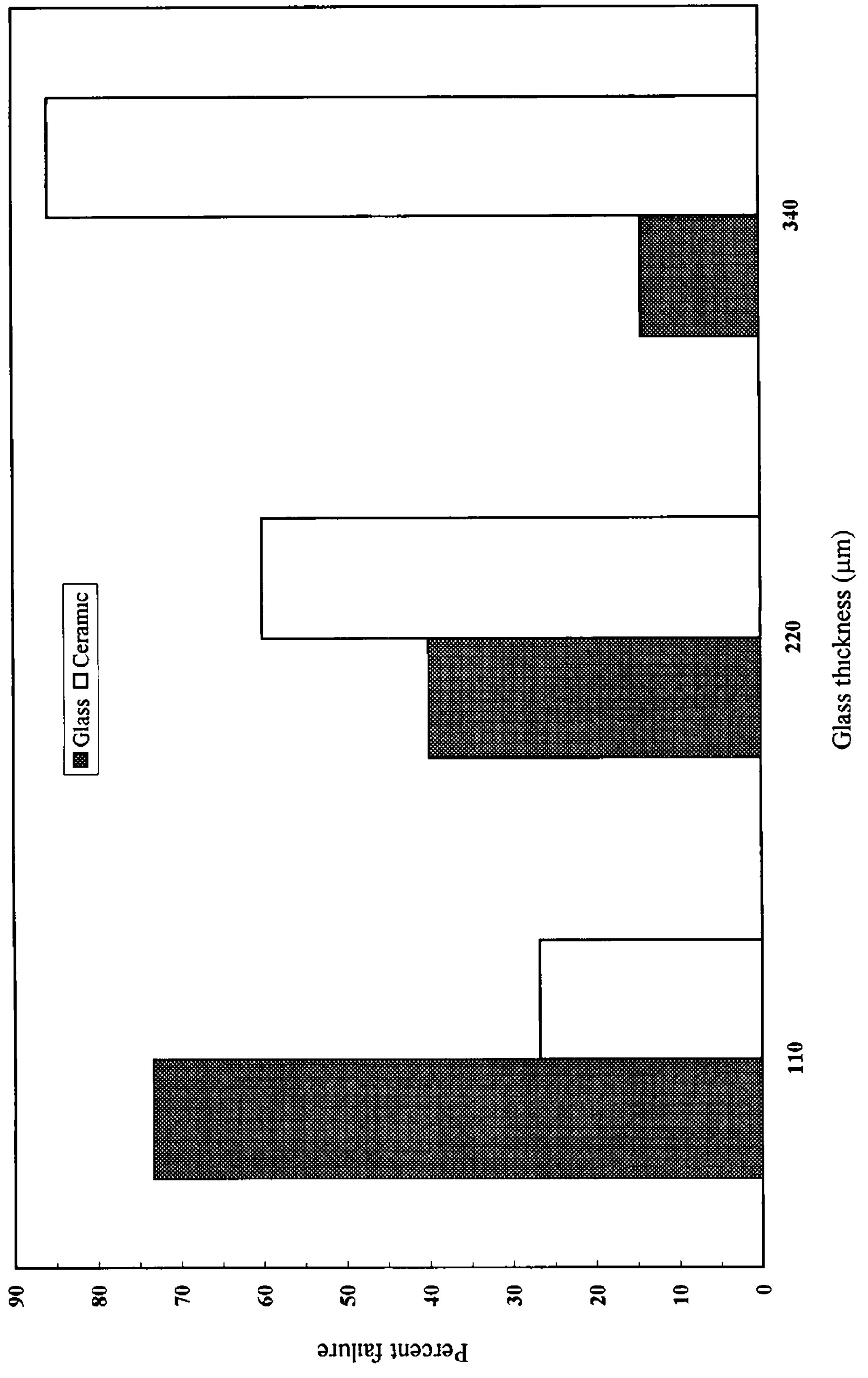

Figure 5.58 Failure mode of the varistors during destruction testing having different glass thicknesses

Chapter 6

CONCLUSIONS AND RECOMMENDATIONS

6 1 CONCLUSIONS

The remarks concluded here are based on the results of the experiments conducted under specified conditions

6 1 1 Laboratory Scale Spray Dryer

By changing the spray drying conditions higher bulk and tap densities were achieved compared to the standard production line powder

The moisture content in the powder was increased with an increase in feed flow rate

Compressibility of the powder was found to be higher compared to the standard powder The powder with a higher percentage of coarse particles is expected to show better compressibility This category of powder was produced by increasing the feed flow rate and decreasing both the atomizing air pressure and the drying air flow rate

A larger mean particle size was obtained by increasing the feed flow rate and decreasing atomizing air pressure A strong interactive effect of the atomizing air pressure and drying air flow was also observed on the mean particle size

Neither the powder from the smaller dryer nor the standard process powder exhibited any flowability due to the presence of higher moisture content in the former and increased percentage of fine particles in the latter

The nominal voltage of the varistor was also influenced by the spray drying conditions A higher nominal voltage was achieved for the varistor when produced from the powder at higher level of feed flow rate, and lower level of atomizing air pressure and the drying air flow rate

Depending on the analysis of the powder characteristics as well as the electrical properties, the optimized condition of the laboratory scale dryer can be regarded as follows

Operating parameters	**Optimized condition**
Feed flow rate	39 0 (ml/min)
Atomizing air pressure	0 8 (Kg_f/cm^2)
Drying air flow rate	0 6 (m^3/min)

6.1.2 Pilot Scale Spray Dryer

The mean particle size was significantly influenced by the feed flow rate and the atomizing air pressure The increase in feed flow rate and a decrease in atomizing air pressure led to an increase in the mean particle size The moisture content was also found to be higher for the same operating condition

A high level of atomizing air pressure and a low level of feed flow rate resulted in powder without any flowability While for the reverse operating condition, that is, a low level of atomizing air pressure and a high level of feed flow rate, significantly increased the flowability of the powder

The powder with the higher mean size led to an increase in green density of the disc pressed under equal load However, the higher green density of the compacts achieved by changing the spray drying conditions did not exhibit the higher green strength

The influence of spray drying variables on powder characteristics was translated into varistor performance Varistors fabricated from the powder containing higher fraction of fine particles increased the nominal voltage due to the smaller grain size in the sintered ceramic body

Degradation behaviour of powder was also influenced depending upon the powder used Varistors made from the powder containing the higher fraction of coarse degraded remarkably after application of high amplitude short duration pulse

The energy absorption capability of the varistor was found to be significantly influenced by the powder used There is a certain level of combination in fine and coarse particles in the powder which was helpful for energy absorption capability

Depending on the analysis of the powder characteristics as well as the electrical properties, the optimized condition of the pilot scale dryer can be regarded as follows

Operating parameters	Optimized condition
Atomizing air pressure	10 0 (psi)
Feed flow rate	172 0 (ml/min)
Drying air outlet temperature	127 0 (°C)

6.1.3 Binder Systems

The powder characteristics like the bulk, tap, and granule densities, compressibility, flowability, the frictional effect of the particles, the green density of the discs were measured for the powder produced from the slurry containing a fixed level of binder and solid Enhanced powder characteristics and higher green density were obtained with the Ltx C binder than that of the conventional binder PVA

The powder produced from the slurry containing lower level of the binder Ltx C and the higher level of the solid resulted in further enhancement of bulk, tap, granule densities, green density of the discs, compressibility, flowability, and reduced the frictional effect within the particles

The higher green strength was obtained when the powder was produced from the slurry containing a higher level of the binder Ltx C and the solid However, the strength of the fired discs was higher, as fabricated from the powder containing a low level of the binder Ltx C and a high level of the solid

The nominal voltage of the varistor prepared from the powder with the Ltx C was higher A further increase in value was obtained when prepared from powder containing a higher level of Ltx C Both the low and the high concentration of solid exhibited the same trend

The wattloss of the varistor was found to be less when fabricated from the powder processed with the Ltx C binder A further decrease in wattloss was achieved as the varistor was produced from the powder with a higher level of the binder and the solid

The clamping efficiency and the non-linear co-efficient were also improved for the varistor made from powder with the Ltx C Further enhancement of the properties were achieved as the percentage of the binder was decreased and the solid level was increased in the powder

The powder processed from the slurry containing a lower level of binder and a higher level of solid could generate varistor with consistent energy absorption capability

Investigating and analyzing all of the properties of the powder produced through the new binder systems and considering the performance of varistor made thereof, the most suitable binder, its level, and solid concentration in the slurry can be assigned as follows

Binder type	**Level of binder in slurry**	**Level of solid in slurry**
Ltx C	1 0%	80%

6 1 4 Particle Size Fraction

Regarding the parameters studied with different size fractions of powder it can be said that it had insignificant influence on the physical properties of the discs and the performance of varistor Though there was a high frictional effect with the fine fractions, but it could produce discs with higher green density in comparison to a widely distributed standard powder However, a reduction in the green strength was achieved The fired density was also higher for the fine fraction of powder

The particle size fractions had a significant influence on the nominal voltage and energy absorption capability of the varistor A higher nominal voltage was obtained when the varistor was prepared with the fine fraction of powder Degradation of the varistors made from the fine fraction of the powder was found to be less after the application of the high amplitude short duration pulses Nonetheless, the energy absorption capability was degraded severely

Hence on the basis of physical characterization and evaluation of the electrical performance it can be said that the powder with a wide distribution is more suitable for the fabrication of zinc oxide varistor

6.1.5 Passivation Thickness

The effect of passivation thickness on varistor performance was evaluated on the basis of energy absorption capability Significant influence of glass thickness on energy absorption capability left the scope of optimizing the amount of glass to be used for passivating Neither too low nor too high amount of passivating material is favourable for varistor performance Initial failure was prevented by applying glass material of thickness 220 μm and the survival of a larger number of discs above 500 J cm^{-3} was also increased

6.2 THESIS CONTRIBUTION

- By changing the spray dryer operating conditions powders with enhanced characteristics in terms of the bulk and the tap densities, and compressibility was achieved

- Effect of spray drying parameters was observed on the electrical properties
- The optimum operating condition was identified by evaluating the electrical characteristics
- Evaluation of a new organic binder was performed
- Compared to the conventional binder, superior performance was observed with the new binder
- Efficiency of the spray dryer was increased due to the increase of the solid content in the slurry with the new binder
- The cost effectiveness of the process was improved due to the use of low level of the new binder
- Positive effect on the electrical properties of the varistor made from the powder processed with the new binder was observed
- Influence of particle size fraction on the physical and electrical properties of the varistor discs was assessed
- The effect of glass thickness on energy absorption capability was evaluated

6 3 RECOMMENDATIONS

6.3.1 Spray Drying Parameters

The higher density of the green body can be utilized to reduce the sintering time through the use of rate controlled sintering The effect of a reduction of the sintering time on the varistor performance can be studied considering wattloss, clamp ratio, high current performance, and energy absorption capability

The optimization of the spray drying variables was carried out in the laboratory and pilot scale spray dryers The optimum condition of the smaller dryer cannot be applied directly to the production dryer However, on the basis of the knowledge gained through the pilot scale dryer, some trial run can be carried out in the production scale to optimize the operating conditions

The optimum condition of the varistor powder can also be applied to the production of other powder like multilayer and radial products

6.3.2 Binder Systems

The study with the latex binders was accomplished in the pilot scale Hence manufacturing in the production scale is recommended to be carried out

A more detailed analysis, regarding the percentage of the Ltx C binder and the solid level in the slurry to be used is necessary before implementation The study includes clamp ratio, degradation with time, high amplitude short duration (HASD) performance, energy absorption capability etc

Very high green strength was obtained for the discs prepared from powder containing Ltx E The electrical performance of the varistors made from powder with Ltx E was also found to be better than the powder containing the conventional binder A more elaborate study with different percentage of binder Ltx E is recommended to be done on the basis of physical characteristics and electrical performance

All of the electrical evaluation was carried out with varistors of non standard size Hence evaluation with the standard size is needed before implementation

The new binder may have the potential use in other varistor products like multilayer and radial products etc Hence investigation is recommended to be carried out in the processing of those powders

6 3.3 Particle Size Fractions

The analysis of powder with different size fractions did not show any significant difference between the standard distribution and narrowly distribution coarse fractions But the discs from the fine fraction of powder had high green density However, difficulty was faced with the fine fraction during pressing due to high frictional effect The use of a lubricant, can reduce the frictional effect and thereby, facilitate the production of the fired disc with a high density

If nominal voltage of varistor is of prime importance, the varistor from fine fraction of powder can increase it substantially

But, considering all of the physical and electrical properties, a wide distribution of powder is recommended for the fabrication of zinc oxide varistors

6 3.4 Passivation Thickness

The influence of glass thicknesses on varistor performance was assessed only in terms of energy absorption capability However, the effect of glass thicknesses due to the application of high amplitude short duration pulses (HASD) was not estimated The higher survival rate during this testing is a very important criteria in the use of varistor Hence further evaluation on the basis of energy as well as on high amplitude short duration pulses (HASD) performance are recommended to carry out to optimize the passivation thickness

REFERENCES

1 Kalpakjian, S , "Manufacturing Process for Engineering Materials", Addison Wesly Publishing Companies, July, 1985

2 Reed, R S , "Introduction to the Principles of Ceramic Processing", A Wiley Interscience Publication, John Wiley and Sons, 1988

3 Haber, R A and Smith, P A , "Overview of Traditional Ceramics", Engineered Material Handbook, Vol 4, pp 3-14, 1991

4 Craner, D C , "Overview of Technical, Engineering, and Advanced Ceramics, Engineered Materials Handbook, Vol 4, pp 16-20, 1991

5 Losevic, O N , Uskokovic, D et al, "Synthesis of ZnO Based Varistor Precursor Powders by Reaction Spray Process", Chapman and Hall, pp 5211-5217, 1993

6 Gupta, T K , "Application of Zinc Oxide Varistor", J Am Ceram Soc , Vol 73, No 7, pp 1817-1840, 1990

7 Matsuoka, M J , "Progress in Research and Development of Zinc Oxide Varistor", pp 290 in "Advances in Ceramics", Vol 1, Grain Boundary Phenomena in Electronic Ceramics, Ed by L M Levinson and D Hill, Am Ceram Soc , Columbus, OH, 1981

8 Gambino, J P , et al, "Grain Boundary Electronic States in Some Simple ZnO Varistor", J Appl Phys , Vol 61, No 7, April 1, 1987

9 Kingery, W D , "Grain Boundary Phenomena in Electronic Ceramics", in "Advance in Ceramics", Vol 1, pp 1-22, 1981

10 Einzinger, R , "Grain Boundary Properties in ZnO Varistors", in "Advance in Ceramics", pp 359-373, 1981

11 Matsuoka, M J , "Nonohmic Properties of Zinc Oxide Ceramics", Jpn J Appl Phys , Vol 10, pp 736-746, 1971

12 Gupta, T K , "Varistors", Engineered Material Handbook, Vol 4, pp 1150-1155, 1991

13 Lin, J N , Lin, C M , Kao, C C , and Chang, W C , "Electrical Properties and Degradation Phenomena of Glass-Doped ZnO Chip Varistors", Material Science and Engineering, B20, pp 261-265, 1993

14 Teketoshi Takemura, Masahiro Kobayashi, Yoshio Takada and Ken Sato, "Effect of Bismuth Sesquioxide on the Characteristics of ZnO Varistors", J Am Ceram Soc , Vol 65, No 5, pp 430-436, 1986

15 Teketoshi Takemura, Masahiro Kobayashi, Yoshio Takada and Ken Sato, "Effects of Antimony on the Characteristics of ZnO Varistors", J Am Ceram Soc , Vol 70, No 4, pp 237-241, 1987

16 Eda, K , "Electrical Properties of ZnO-Bi_2O_3 Metal Oxide Heterojunction-A Clue of A Role of Intergranular Layer in ZnO Varistors, Elsevier Science Publishing Company Inc , pp 381-392, 1982

17 Ai Bui, Huu Tri Nguyen, and Andreloubiere, "High-Field ZnO Based Varistors", J Phys D Appl Phys , Vol 28, pp 774-782, 1995

18 Levinson, L M , Phillip, H R , "Zinc Oxide Varistor-A Review", Ceramic Bulletin, Vol 65, No 4, pp 639-646, 1986

19 Einzinger, R , "Metal Oxide Varistors", Ann Rev Mater Sci , Vol 17, pp 299 321, 1987

20 Kanai, H and Imai, M , "Effect of SiO_2 and Cr_2O_3 on the Formation Process of ZnO Varistor", J Matre Sci , Vol 23, pp 4379-4382, 1988

21 Miyoshi, T , Maeda, K , Takashi and Yamazaki, T , "Effects of Dopants on the Characteristics of ZnO Varistors", in "Advance in Ceramics", pp 309-315, 1981

22 Driear, J M , Guertin, J P , Sokoly, T O and Hackney, L B , "Effect of Dopant Valance State on the Microstructure of ZnO Varistors", in "Advance in Ceramics", pp 317-329, 1981

23 Ichinose, N and Tanno, Y , "Electrical Properties of ZnO Varistors Containing Metallic Zinc", in "Advance in Ceramics", pp 375-381, 1981

24 Mukae, K and Nagasawa, I , "Effect of Prasueodymium oxide and Donor Concentration in the Grain Boundary Region of ZnO Varistors", in "Advance in Ceramics", Vol 1, pp 331-341, 1981

25 Yano, Y , Takai, Y and Morooka, H , "Interface States in ZnO Varistor with Mn, Co, and Cu Impurities", J Mater Res , Vol 9, No 1, pp 112-118, Jan , 1994

26 Hushouxiang, Wang Shiliang, Xu Yuchun and Li Xingjiao, "Effect of Aluminum Doping on the Electrical Properties of ZnO Varistor", IEEE, Transactions on Components, Hybrids and Manufacturing Technology, Vol Chmt-8, No 4, pp 525-529, December, 1985

27 Gupta, T K , "Effect of Minor Doping on High Current Application of ZnO Varistor", Ferroelectrics, Vol 102, pp 391-396, 1990

28 Fan, J and Freen, R, "Improvement of the Nonlinearity and Degradation Behaviour of ZnO Varistors", Br Ceram Trans Vol 92, No 6, pp 221-226, 1993

29 Gupta, T K , "Donor Doping of Ga in ZnO Varistor Grain Boundary", J Mater Res , Vol 9, No 9, pp 2213-2215, Sep 1, 1994

30 Bowen, L J and Avella, F J , "Microstructure, Electrical Properties, and Failure Prediction in the Low Clamping Voltage ZnO Varistor", J Appl Phys , Vol 54, No 5, pp 2764-2772, May, 1983

31 Gupta, T K , "Influence of Microstructure and Chemistry on the Electrical Characteristics of ZnO Varistor", pp 493-507, in "Tailoring Multiphase and Composite Ceramics", Edited by Tresoler, R E , Messing, G L , Pantino, C G , Newnham, R E , New York, 1986

32 Hamsphire, S , and Coolican, J , "Microstructural Characterization of Zinc Oxide Varistors", in "High Tech Ceramic" Edited by Vincenzini, P , Elsevier Science Publishers, B V , Amsterdam, pp 1833-1840, 1987

33 Sargent, R A , Dunlop, G L and Darveniza, M , "Effects of Multiple Impulse Currents on the Microstructure and the Electrical Properties of Metal Oxide Varistor", IEEE Transactions on Electrical Insulation, Vol 27, No 3, pp 586-592, June, 1992

34 "Transient Voltage Suppressor Devices", Harris Semiconductor, Harris Corporation, USA, 1994

35 Saksaug, E , Burke, J , and Kresge, J , IEEE Transactions on Powder Delivery, Vol 4, No 4, October, 1989

36 Lawless, W N and Gupta, T K , "Thermal Properties of Pure and Varistor ZnO at Low Temperature", J Appl Phys , 60 [2] pp 607-11, 1986

37 Ozawa, J et al , IEEE Transaction on Powder Apparatus and Systems, Vol PAS-102, No 5, May, 1993

38 Amiji, N et al , Advance Ceramic Materials, 1 [3], pp 232-36, 1986

39 Eda, K "Destruction Mechanism of ZnO Varistors Due to High Currents" J Appl Phys 56(10), pp 2948-2955, 15 Nov , 1984

40 Eda, K , Iga, A and Matsuoka, M , Proc Jpn Soc , "Current Creep in Non-ohmic ZnO Ceramics", Jpn , J Appl Phys , 18[5], pp 997-98, 1979

41 Mahan, G D , Levinson, L M and Phillip, H R , "Single Grain Junction Study of ZnO Varistors" Appld Physics, Lett , Vol 33, No 9, Nov 1, pp 830-832, 1978

42 Levine, J D , "Theory of Varistor Electronic Properties" CRC Critical Reviews in Solid State Sciences, November, pp 597-608, 1975

43 Eda, K , Iga, A and Matsuoka, M , "Degradation Mechanism of Non-ohmic Zinc Oxide Ceramics", J Appl Phys 51, 2678, 1980

44 Hower, P L , and Gupta, T K , "A Barrier Model for ZnO Varistors", J Appl Phys 50, 4847, 1979

45 Pike, G E , "Electronic Properties of ZnO Varistors A New Model", in "Grain Boundaries in Semiconductors", Published by Elsevier Publishing Company, pp 369-379, 1982

46 "Design and Use of Spray Dryer", Bowen Engineering Inc , 4th Edition, 1963

47 Master, K , "Spray Drying Handbook", 4th Edition, George Godown, 1985

48 "Uniformly Shaped Particles Produced by Spray Dryer - Maintenance Requirements Low", Bowen Engineering Inc , 4th Edition, 1963

49 Dittman, F W , and Cook, E M , "Analyzing a Spray Dryer", Reprinted Copy from J Chem Engg , January 17, 1977

50 "Spray Drying of Ceramics for Pressing Operations", Bowen Engineering Inc , 4th Edition, 1963

51 "Dryer Handbook", APV Crepaco Inc , Second Edition, 1994

52 Belcher, D W , Smith, D A , and Cook, E M , "Analyzing Dryer with Pshychrometric Chart", Reprinted Copy from J Chem Engg , January, 1977

53 Smith, G , "Operating the Spray Dryer", Adapted from a Presentation at the Joint Fall Meeting of Southeast and Southwest Sections of the American Ceramic Society, Nashville, Tenn , 1992

54 Yamato, Spray Dryer, Model Dl-41, Instruction Manual, Yamato Scientific Co Ltd , Tokyo, Japan

55 Nakamura, N , Nakano, T , Gotoh, S , and Shimotomai, M , "High T_c Oxide Superconductors Prepared by Spray Drying Method", in "Processing and Application of High T_c Super Conductors", Edited by Mayo, W E , The Metallurgical Society, 1988

56 Ching-Fong Chen, Ender Savrun and Ramirez, A F , "Processing and Characterization of High Thermal Conductivity Aluminium Nitride Ceramics" Proc of the Technical Program, Nepcon East, pp 545-58, 11-14 June, 1990

57 Sacks, M D , "Rheological Science in Ceramic Processing", in "Science of Ceramic Chemical Processing", Edited By Hench, L L and Ulrich, D R ,

Department of Material Science and Engineering, Wiely Interscience Publication, pp 522-537, 1989

58 Bast, R , "Organic Additives for Ceramics-An Over View", Vol 92, pp 217-218, 1993

59 Pincus, A G and Shipley, L E , "The Role of Organic Binders in Ceramic Processing", IIT Research Institute, 1969

60 Hoffman, E R , "Importance of Binders in the Spray Dried Press Bodies", 73rd Annual Meeting of the American Ceramic Society, Chicago, April 24, 1971

61 Youshaw, R A and Halloran, J W , "Compaction of Spray Dried Powders", Am Ceram Soc Bull , 61, 227, 1982

62 Levine, S , "Organic (Temporary) Binders for Ceramic Systems", pp 39-42, January, 1960

63 Brewer, J A , Moore, R H and Reed, J S , "Effect of Relative Humidity on the Compaction of Barium Titanate and Manganese Zinc Ferrite Agglomerates Containing Polyvinyl Alcohol", 81st Annul Meeting of the American Ceramic Society, Cincinnati, March 24, 1980

64 Dimilia, R A and Reed, J S , "Dependence of Compaction on the Glass Transition Temperature of the Binder Phase", 83rd Annual Meeting of the Am Cem Soc , Washington, D C , May 5, 1981

65 Nies, C W and Messing, G L , "Effect of Glass Transition Temperature of Polyethylene Glycol-Plasticized Polyvinyl Alcohol on Granule Compaction" 85th Meeting of Am Cerm Soc Chicago, Illions, April 25, 1983

66 Brita Nyberg, Elis Carlstrom, Miahael Persson and Roger Carlsson, "Uniform Distribution of a Pressing Aid", Swedish Institute of Silicate Research, Box 5403, S-402 29, Goteborg, pp 573-80, 1988

67 Kevin Wu, X L and McAnany, W J , "Acrylic Binder for Green Machining", J Am Ceram Soc Vol 74, No 5, May, 1995

68 Walker, W J Jr , Reed, J S and Verma, S K , "Polyethylene Glycol Binders for Ceramics Produced by Compaction of Spray Dried Granules", Ceramic Transaction, Vol 22, 1991

69 Verma, S K , Robson, J H , Walker, W J Jr and Reed, J S , "Amorphous Polyethylene Glycol in Ceramic Powder Processing", 4th International Conference on Ceramic Powder Processing, Nagoya, Japan, March 12-15, 1991

70 Huffine, C L and Bonilla, C F , "Particle Size Effect in the Compression of Powders", A I Ch E Journal, September, Vol 8, No 4, pp 490-93, 1962

71 Evans, A G, "Consideration of Inhomogenity Effects in Sintering", J Am Ceram Society, Vol 65, No 10, pp 497-501, October, 1988

72 German, R M, "Powder Metallurgy Science", Metal Powder Industries Federation, Princenton, New Jersey, 1984

73 Tshoung-Shou Yeh, and Sacks, M D, "Effect of Green Microstrcture on Sintering of Alumina", 90th Annul Meeting and Exposition, Cincinnati, Ohio, May 1-5,1988

74 Lange, F F and Kellett, B, "Influence of Particle Arrangements on Sintering, Proceeding on "Science of Ceramic Chemical Processing", Wiely Interscience Publication

75 "Strength Dependence on Porosity for P/M Compacts", Int J Powder Met Powder Tech Vol 13, No 4, pp 259-71, 1977

76 Duffield A and Grootenhuis, P, J Inst Metals, Vol 87, pp 33, 1959

77 Rumpf, H "Internatinal Symposium on Agglomeration", Edited by Knepper, W A, Interscience, London, pp 379-418, 1962

78 Cutler I B, "Active Powder in Ceramic Processing Before Firing", Edited by Onada, G G and Hunch, L L, A Wiley Interscience Publication, John Wiley and Sons, pp 21-37, 1978

79 Harnby, N, "Mixing of Powder" in "Compaction of Particulate Solids", Post Graduate Student of Powder Metallurgy, University of Bradford, 1980

80 Roger, L K, "Mechanical Consolidation", Herculus Advanced Materials and System Company, Engineered Materials Handbook, Vol 4, ASM International pp 125-129, 1991

81 Boschi, A O And Gilbert, E, "Wet Forming Process as a Potential Solution to Agglomeration Problems" in "Advanced Ceramic Processing Technology", Edited by Binner, G P, Vol 1, 1990

82 Lowed, S and Shields, J E, "Powder Surface Area and Porosity, 2nd Edition, 1979

83 Machead, H, "Compaction of Ceramics" in "Compaction of Particulate Solids", Post Graduate School of Powder Metallurgy, University of Bradford, 1980

84 Dimilia R A, and Reed, J S, "Stress transmission During the Compaction of a Spray Dried Aluminum Powder in a Steel Die", J Am Ceram Soc, USA, Vol 66, No 9, pp 667-72

85 Karim, A N M, Puyane, R, El-Baradie, M and Hashmi, M S J, "Effect of Compactiom Parameters on the Physical Properties of Zinc Oxide Varistor

Discs", Proc of International Conference on "Mechanics of Solids and Material Engineering", pp 286-91, Vol A, 1995

86 Gupta, T K and Straub, W D, "Effect of Annealing on the Leakage Components of the ZnO Varistor II Capacitive Current", J Appl Phys, 68(2), 15 July, 1990

87 Seitz, M A, and Hirthe, R W, "Thermal Runway in Metal Oxide Varistor", in "Grain Boundaries in Semiconductors", Elsevier Science Publishing Company, Inc, Vol 5, pp 405-417, 1982

88 Chiang, Y and Kingery, W D, "Compositional Changes Adjacent to the Grain Boundaries During Electrical Degradation of a ZnO Varistor", J Appl Phys, 53(3), pp 1765-1768, March, 1982

89 Gupta, T K, Carlson, W G and Hall, B O, "Metastable Barrier Voltage in ZnO Varistor", in "Grain Boundaries in Semiconductors", Elsevier Science Publishing Company, Inc, Vol 5, pp 393-398, 1982

90 Takahashi, K, Miyoshi, T, Maeda, K and Yamazaki, T, " Degradation of ZnO Varistors" in "Grain Boundaries in Semiconductors", Elsevier Science Publishing Company, Inc, Vol 5, pp 399-404, 1982

91 Sun, H, Zhang, L, and Yao, X, "Electrical Nonuniformity of Grain Boundaries within ZnO Varistors" J Am Ceram Soc, 76(5), pp 1150-55, 1993

92 Tanaka, J and Hishita, S, "Deep Level Near the Grain Boundary in a Zinc Oxide Varistors Energy Change Due to Electrical Degradation", J Am Ceram Soc, 73(5), pp 1425-28, 1990

93 Shen C, Chen, Y and Wu, L, "The Effect of Antimony Oxide on the Electrical Properties of ZnO Varistors" J Appl Phys, Vol 32, pp 1147-1153, 1993

94 Gupta, T K, Mathur, M P, and Carlson, W G, "Effect of Externally Applied Pressure on ZnO Varistor", J Electron Mater, 6(5), pp 483-97, 1977

95 Montegomery, D C, "Design and Analysis of Experiment", Second edition, John Wiley and Sons, New York, 1984

96 Box, G E P, Haunter, W G, and Haunter, J S, "Statistics for Experiments, "An Introduction to Design, Data Analysis and Model Building" John Wiley and Sons, 1978

97 "Griffith, A A, Proc of the 1st International Congress for Applied Mechanics, Edited by, Biezeno, C B, and Burgers, J M, The Netherlands, pp 55-63, 1924

98 Batdorf, S B and Heimisch, H L Jr, "Weakest Link Theory Reformulated for Arbitrary Fracture Criterion", J Am Ceram Soc, Vol 61, No 7-8, pp 355-358, 1978

99 Richerson, D W, "Modern Ceramic Engineering, Properties, Processing, and Use in Design", Marcel Dekker Inc , 1982

100 Weibull, W , "The Phenomenon of Rupture in Solids", INGVETENSK AKAD HANDL 153 Publ Royal Inst Techn Stockholm

101 Box, G E P , and Wilson, K B , "On the Experimental Attainment of Optimum Condition", J Royal Statistical Society, Vol 13, pp 1-45,1951

102 Wu, S M , "Tool Life Testing Response Surface Methodology", Part I and II, Trans ASME, 86, pp 105-116, 1964

103 Chowdury, I A , and El-Baradie, M A , "Tool-life Prediction Model by Design of Experiments for Turning High Strength Steel (290 BHN), Proc of International Conference on "Advances in Materials and Processing Tech Vol 3, pp 1397- 1404, 1995

104 El-Baradie, M A , "Computer Aided Analysis of Surface Roughness Model for Turning", J Mat Proc Tech , 26, pp 207-216, 1991

105 El-Baradie, M A , "Surface Roughness Model for Turning Grey Cast Iron (154 BHN)", Proc Instn Mech Engrs Vol 207, pp 43-54

106 O'Sullivan, F , "Green Body Process Variables in Uniaxially and Isostatically Pressed Varistor Bodies" M Sc Thesis, The University of Limerick, Ireland, 1990

107 "Spray Drying" Engineered Materials Handbook, Vol 4, ASM International, pp 100-107, 1991

108 Al-Tounsi, A , "Effect of Sintering Parameters on the Mechanical and Physical Properties of the Sintered Formed Material", Ph D Thesis, Dublin City University, 1992

109 German, R M , "Liquid Phase Sintering", Plenum Press, New York, 1985

110 Dey, D and Bradt, R C , "Grain Growth of ZnO During Bi_2O_3 Liquid-phase Sintering" J Am Ceram Soc , 75(9), pp 2529-34, 1992

111 Dettoff, R T and Rhines, F N , "Quantitative Microscopy" Edited by McGraw Hill Book Co , 1968

112 Bai, Shr-Nan and Tseng, Tseng-Yuen, "The Effect of Grain Boundaries on the Electrical Properties of Zinc Oxide Based Varistor", J Elec Matrl Vol 21, No 11, pp 1073-1079, 1992

113 Mikeska, K R , Eng, D C and Cannon, W R , "Dispersion Properties of $BaTiO_3$", Presented at the Annual Meeting of the American Ceramic Society, Cincinnati, Ohio, May, 1985

114 Gupta, T K and Miller, A C , "Improved Stability of the ZnO Varistor Via Donor and Acceptor Doping at the Grain Boundary" J Mater Res 3(4), pp 745-54, Jul/Aug, 1988

APPENDIX A

Calculation for the model of the mean particle size

APPENDIX A

A1. Calculation of the coefficient b

The value of the coefficients “b” of the model was computed by least square method, that is, $b = (X^TX)^{-1} X^Ty$ The matrix of independent variables X for the twelve tests is given below

$$\begin{array}{r|cccc|c}
 & x_o & x_1 & x_2 & x_3 & \text{Trial no} \\
 & 1 & -1 & -1 & -1 & 1 \\
 & 1 & 1 & -1 & -1 & 2 \\
 & 1 & -1 & 1 & -1 & 3 \\
 & 1 & 1 & 1 & -1 & 4 \\
 & 1 & -1 & -1 & 1 & 5 \\
X = & 1 & 1 & -1 & 1 & 6 \\
 & 1 & -1 & 1 & 1 & 7 \\
 & 1 & 1 & 1 & 1 & 8 \\
 & 1 & 0 & 0 & 0 & 9 \\
 & 1 & 0 & 0 & 0 & 10 \\
 & 1 & 0 & 0 & 0 & 11 \\
 & 1 & 0 & 0 & 0 & 12
\end{array}$$

and

$$X^T = \left|\begin{array}{cccccccccccc}
1 & 1 & 1 & 1 & 1 & 1 & 1 & 1 & 1 & 1 & 1 & 1 \\
-1 & 1 & -1 & 1 & -1 & 1 & -1 & 1 & 0 & 0 & 0 & 0 \\
-1 & -1 & 1 & 1 & -1 & -1 & 1 & 1 & 0 & 0 & 0 & 0 \\
-1 & -1 & -1 & -1 & 1 & 1 & 1 & 1 & 0 & 0 & 0 & 0
\end{array}\right|$$

Hence

$$(X^TX) = \begin{vmatrix} 12 & 0 & 0 & 0 \\ 0 & 8 & 0 & 0 \\ 0 & 0 & 8 & 0 \\ 0 & 0 & 0 & 8 \end{vmatrix}$$

and

$$(X^TX)^{-1} = \begin{vmatrix} \frac{1}{12} & 0 & 0 & 0 \\ 0 & \frac{1}{8} & 0 & 0 \\ 0 & 0 & \frac{1}{8} & 0 \\ 0 & 0 & 0 & \frac{1}{8} \end{vmatrix}$$

A2 Calculation of confidence intervals First order model

The error limits for the mean particle size were calculated and the calculation steps are given below

$$\hat{y} \pm t_{\alpha/2df}\sqrt{V(\hat{y})}$$

where

$$V(\hat{y}) = C^{ij} s^2$$

Step 1

Estimated error for variance s^2 based on the residual sum of square S(b) (from Table 4 6 as given in chapter 4) is

$$s^2 = \frac{S(b)}{DF} = \frac{0.0195763}{8} = 0.00247037$$

Step 2

Calculation of the variance-covariance matrix for b is $(X^TX)^{-1}s^2$, where $(X^TX)^{-1}$ is given earlier

Step 3

Calculation of variance. The variance, $V(\hat{y})$, for the mean particle size was calculated considering the eight corner points (trials 1, 2, 3, 4, 5, 6, 7, and 8) as follows

$$\begin{aligned} V(\hat{y}) &= V(b_0 + b_1x_1 + b_2x_2 + b_3x_3) \\ &= V(b_0) + x^2{}_1V(b_1) + x^2{}_2V(b_2) + x^2{}_3V(b_3) \\ &= \left(\frac{1}{12} + \frac{1}{8} + \frac{1}{8} + \frac{1}{8}\right)s^2 \\ &= \left(\frac{11}{24}\right)s^2 \end{aligned}$$

95 percent confidence interval for $\hat{y}$ is

$$\hat{y} \pm t_{df\ \alpha/2}\sqrt{v(\hat{y})}$$

which can be written as follows

$$\hat{y} \pm t_{8\ 0.05/2}\sqrt{\frac{11 \times 0.0195763}{24}} = \hat{y} \pm 2.306\sqrt{\frac{11 \times 0.0195763}{24}} = \hat{y} \pm 0.081$$

A3: Adequacy of the postulated model

In order to perform the analysis of variance, the total sum of the square, $\sum y^2$, is usually divided into contributions due to the "zero-order terms", "first-order terms", "the lack of fit", and "pure error" The sum of square of individual items divided by their respective degrees of freedom give the mean square The mean square of lack of fit can be compared with the mean square of pure error to test the adequacy of the postulated model by using the F distribution

The detailed formulae for the analysis of the variance used in this investigation is given in Table 1, where n_o is the number of central points, n_c the number of corner points, N the total number of experimental points, k is the dimension of design (for 2^3 full factorial design the value of k is 3), y_{ni}, the logarithm of observed responses at the central point with mean $\bar{y}_o$,and *(iy)* the sum of the cross-products of the columns in the X matrix with the column y of observation

Table A1 Formulae for the analysis of variance of the first order model

Source	Sum of square (SS)	Degrees of freedom (DF)
Zero-order term	$\left(\sum_{i=1}^{N} y_i\right)^2 / N = n\bar{y}^2$	1
First-order term	$\sum_{i=1}^{k} b_i (iy)$	k
Lack of fit	By subtraction	n_c-k
Pure error	$\sum_{i=1}^{n_o} (y_{ni} - y_o)^2$	n_o-1
Total	$\sum_{i=1}^{N} y^2_i$	N

APPENDIX B

TGA curve of different types of binders

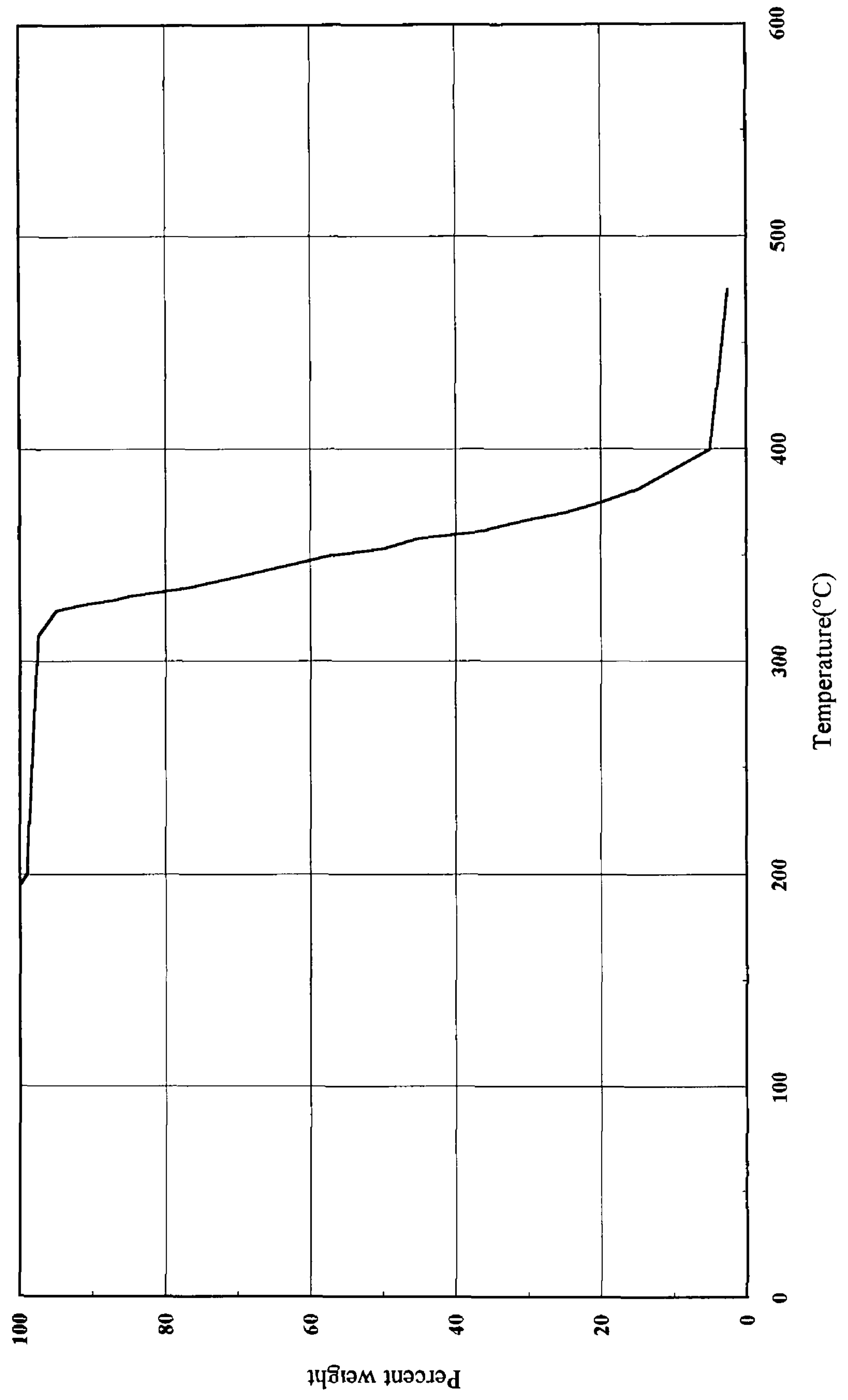

Figure B1 TGA curve for the latex binder Ltx A in the air

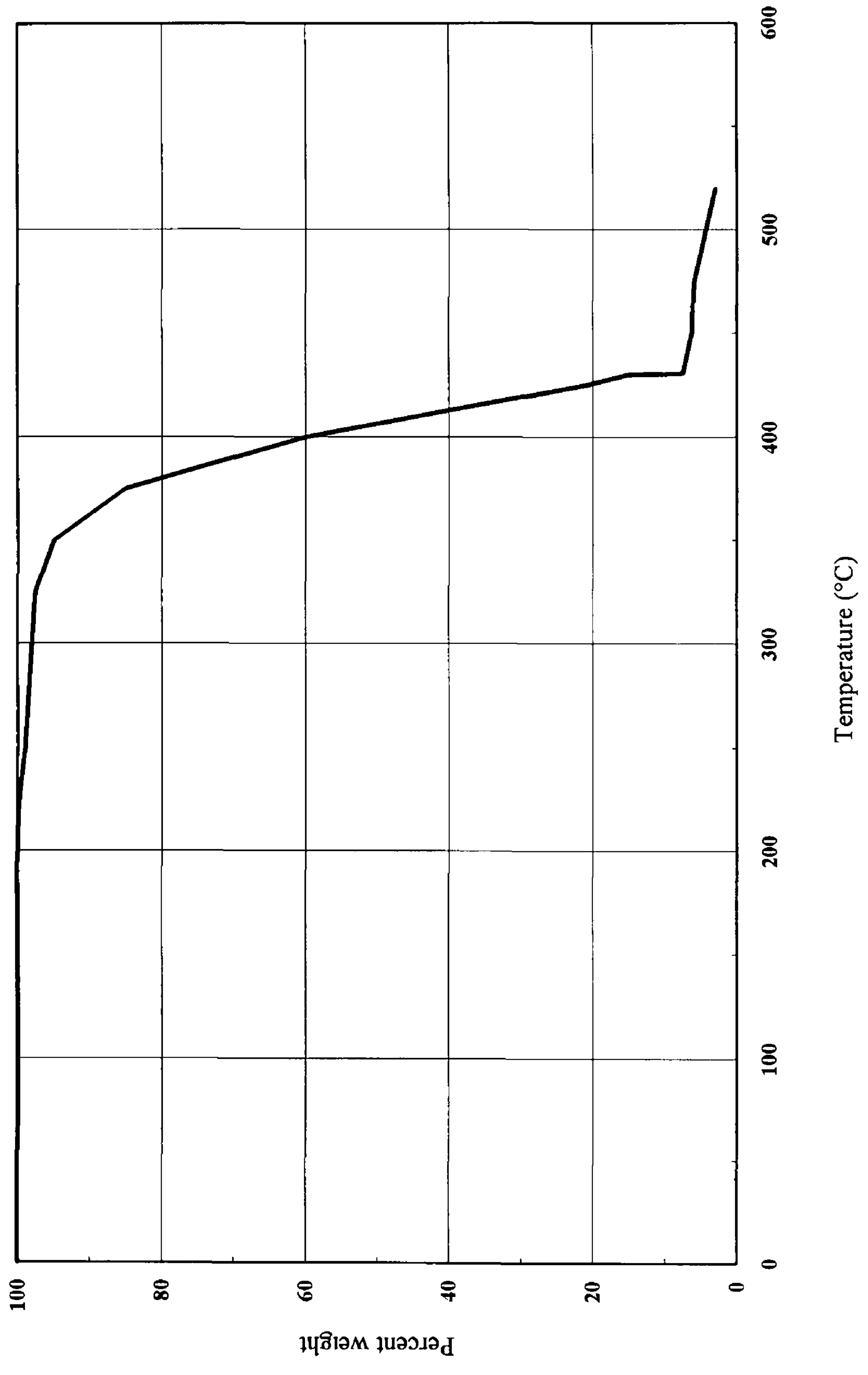

Figure B2 TGA curve for the latex binder Ltx C in the air

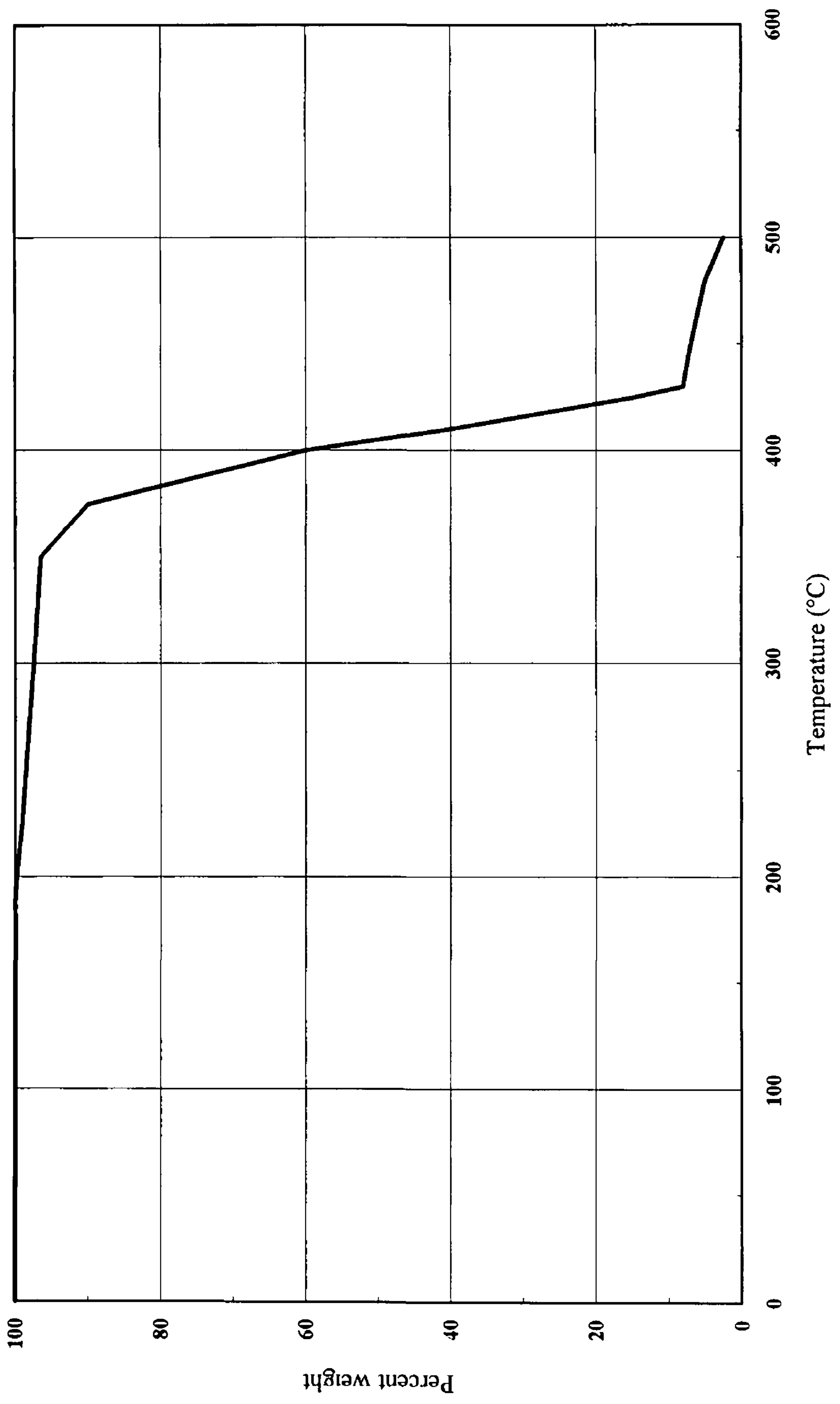

Figure B3 TGA curve for the latex binder Ltx E in the air

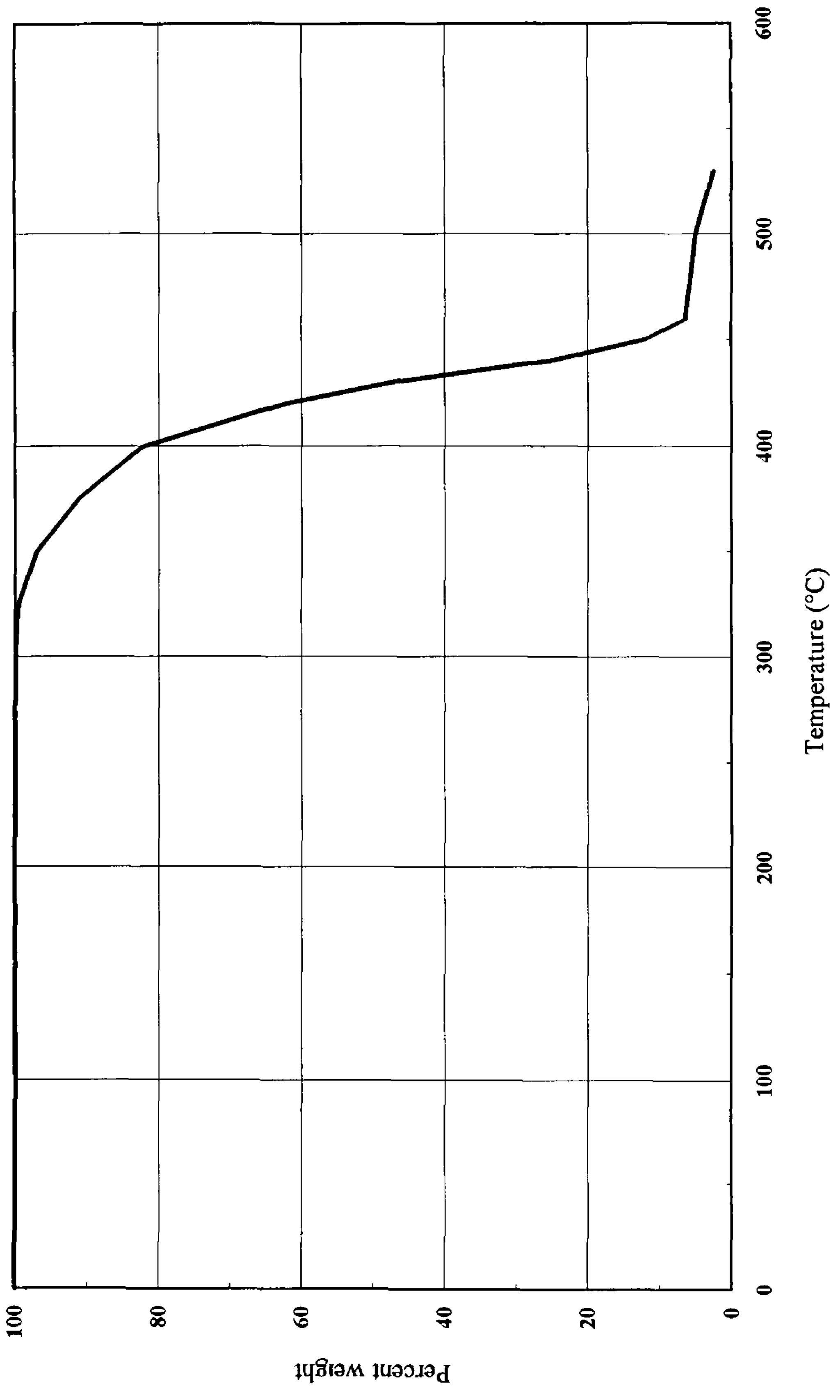

Figure B4 TGA curve for the latex plasticizer in the air

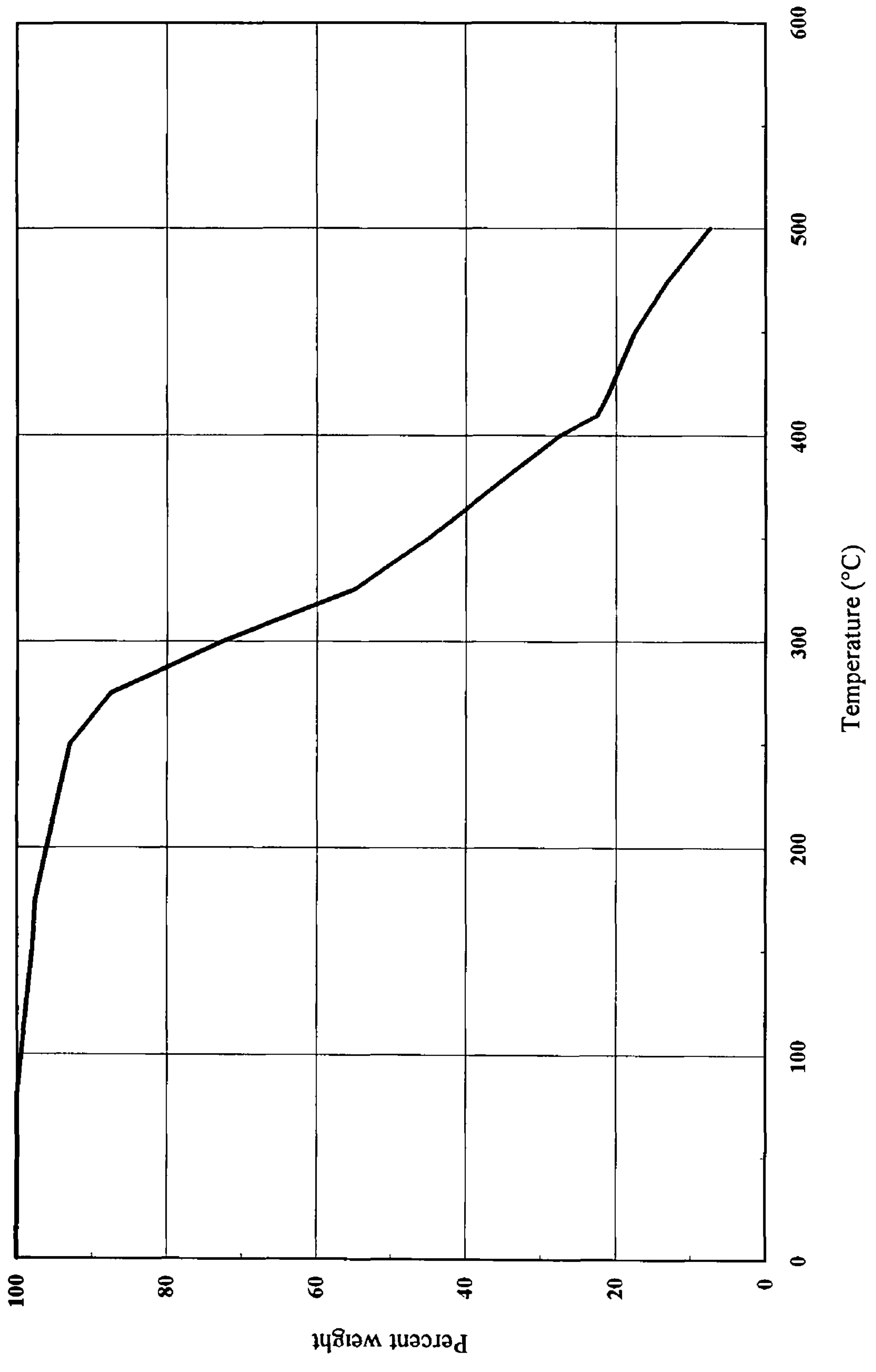

Figure B5 TGA curve for the conventional binder PVA in the air

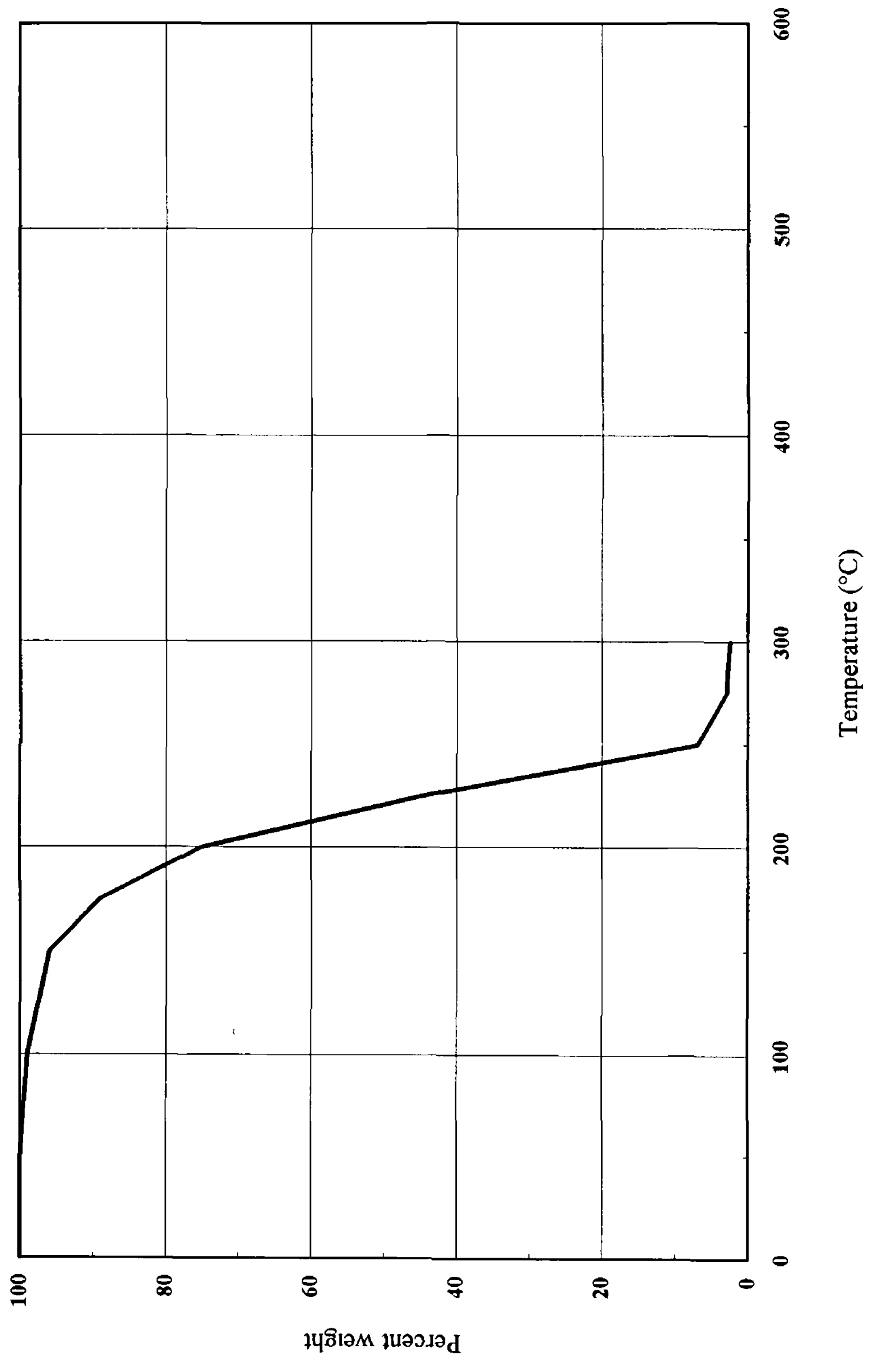

Figure B6 TGA curve for the conventional plasticizer PEG in the air

APPENDIX C

Publications

PUBLICATIONS

[1] S Begum, A Duff, R Puyane and M S J Hashmi, "Evaluation of Latex Binder in the Processing of Electronic Ceramic", in the Proc of International Conference on "Advance Materials and Processing Technology", pp 115-122, Vol 1, 1995

[2] S Begum, R Puyane and M S J Hashmi, "Effect of Spray Drying Variables on the Physical Properties of ZnO Varistor Powder", To be Published

[3] S Begum, R Puyané and M S J Hashmi, "Performance Evaluation of ZnO Varistor by Injecting Pulse of Different Time Duration Produced from Powder Under Changed Spray Drying Conditions", To be Published

[4] S Begum, R Puyane and M S J Hashmi, "Modelling for the Mean Granule Size of Spray Dried ZnO Varistor Powder", To be Published

[5] S Begum, A N M Karim, R Puyane and M S J Hashmi, "Physical Characterization of Varistor Discs Processed with Different Latex Binders", To be Published

[6] S Begum, R Puyane and M S J Hashmi, "Electrical Performance of ZnO Varistor Produced from the Powder Processed by Different Latex Binders", To be Published

[7] S Begum, A N M Karim, R Puyane and M S J Hashmi, "Dependence of Energy Absorption Capability on Passivation Thickness and Degradation of Varistor due to the Injection of Energy", To be Published

[8] S Begum, R Puyane and M S J Hashmi, "Influence of Particle Size Fraction on the Physical and Electrical Characteristics of ZnO Varistor", To be Published